Université de Montréal

Complexes cationiques POCOP de nickel : Synthèse, caractérisation, réactivité et étude catalytique

par

Sébastien Lapointe

Département de Chimie

Faculté des arts et des sciences

Mémoire présenté à la

Faculté des études supérieures et postdoctorales en vue de l'obtention du grade de maître ès sciences (M.Sc.) en chimie

Juin 2016

Résumé

Ce mémoire traite de la chimie des complexes pinceurs de nickel (II) cationiques ayant un ligand de type POCOP. Elle se divise en deux parties. La première traite de la synthèse, de la caractérisation et de la réactivité des complexes cationiques pinceurs de Ni(II) de type POCOP (POCOP = 1,3-bis(phosphinitobenzene), où *C* fait partie d'un cycle benzénique et est lié au métal, et *P* est un ligand phosphoré aussi lié au métal). Ces complexes ont un ligand acétonitrile coordonné au centre métallique et sont du type [(R-POCOP$^{R'}$)Ni(NCMe)][OSO_2CF_3], où R est un substituant du cycle benzénique et R' est un substituant sur le ligand phosphoré (R' = *i*Pr: R = H (**1**), *p*-Me(**2**), *p*-OMe(**3**), *p*-CO_2Me(**4**), *p*-Br(**5**), *m,m*-*t*Bu_2(**6**), *m*-OMe(**7**), *m*-CO_2Me(**8**); R' = *t*-Bu : R = H (**9**), *p*-CO_2Me(**10**)).

Les complexes cationiques sont préparés en faisant réagir le dérivé Ni(II) neutre correspondant R-(POCOP$^{R'}$)Ni-Br avec Ag(OSO_2CF_3) dans l'acétonitrile à température ambiante. L'impact des groupements R et R' du ligand POCOP sur la structure et sur les propriétées électroniques du complexe a été étudié par spectroscopies RMN, UV-VIS et IR, analyse électrochimique, et diffraction des rayons X. Les valeurs de fréquence du lien C≡N (ν(C≡N)) augmentent avec le caractère électroattracteur du complexe, dans l'ordre **7** < **3** ~ **2** ~ **6** < **1** < **5** ~ **8** < **4** et **9** < **10**. Ces résultats sont en accord avec le fait qu'une augmentation du caractère électrophile du centre métallique devrait résulter en une augmentation de la donation σ MeCN→Ni. De plus, les complexes cationiques montrent tous un potentiel d'oxydation Ni(II)/Ni(III) plus élevé que leurs analogues neutres Ni-Br. Ensuite, une étude d'équilibre entre un complexe neutre (R-POCOP$^{R'}$)NiBr et un complexe cationique [(R-POCOP$^{R'}$)Ni(NCMe)][OSO_2CF_3] démontre l'échange facile des ligands MeCN et Br.

La deuxième partie de ce mémoire consiste en deux chapitres. Le premier (Chapitre 3) est une étude structurelle permettant une meilleure compréhension du mécanisme d'hydroamination des oléfines activées promue par les complexes présentés au chapitre 1, suivi de tentatives de synthèse de nouveaux composés POCOP cationiques comportant un ligand amine et nitrile, et de déplacement du groupement amine par un groupement nitrile. Le deuxième chapitre (4) décrit la réactivité et la cinétique de la réaction d'hydroamination et

d’hydroalkoxylation d’oléfines activées, qui permet ainsi de mieux comprendre l’impact des différentes variables du système (groupements R et R’, température, substrats, solvent, etc.) sur la réactivité catalytique.

Mots-clés : nickel (II) cationique, complexes pinceurs, complexes POCOP cationiques de nickel, synthèse, caractérisation, effets électroniques, effets stériques, échange de ligands, oxydation par ferrocène, hydroamination, hydroalkoxylation, études mécanistiques, composés amine, amine, études cinétiques.

Abstract

This thesis describes the chemistry of nickel (II) cationic pincer complexes bearing a POCOP ligand. The content is divided into two parts. The first part (chapter 2) concerns the synthesis, characterization and reactivities of nickel (II) cationic POCOP pincer complexes with an acetonitrile ligand coordinated to the metal center via the nitrile moiety, [(R-POCOP$^{R'}$)Ni(NCMe)][OSO_2CF_3] where R is a ring substituent and R' is a *P*-substituent (R' = *i*Pr : R = H (**1**), *p*-Me(**2**), *p*-OMe(**3**), *p*-CO_2Me(**4**), *p*-Br(**5**), *m,m*-*t*Bu_2(**6**), *m*-OMe(**7**), *m*-CO_2Me(**8**); R' = *t*-Bu : R = H (**9**), *p*-CO_2Me(**10**)). The cationic complexes are synthetized by reacting the neutral nickel (II) bromide derivatives R-(POCOP$^{R'}$)Ni-Br with Ag(OSO_2CF_3) in acetonitrile at room temperature. The impact of R and R' groups of the POCOP ligand on the structure and electronic proprieties of the complexes has been studied by NMR, UV-Vis and IR spectroscopy, as well as by single crystal x-ray diffraction studies and cyclic voltammetry measurements. The observed ν(C≡N) values were found to increase with the increasing electron-withdrawing nature of R, i.e., in the order **7 < 3 ~ 2 ~ 6 < 1 < 5 ~ 8 < 4** and **9 < 10.** This trend is consistent with the anticipation that enhanced electrophilicity of the nickel center should result in an increase in net MeCN→Ni σ-donation. It is also interesting to note that all cationic complexes show a much higher Ni(II)/Ni(III) oxidation potential than their neutral Ni-Br analogues. Following this, an equilibrium study is presented that shows the facile exchange of the MeCN/Br ligands between the charge-neutral and cationic complexes (R-POCOP$^{R'}$)NiBr and [(R-POCOP$^{R'}$)Ni(NCMe)][OSO_2CF_3].

The second part of this thesis consists of two chapters describing, respectively, structural studies that are relevant to our understanding of the mechanism of hydroamination reactions promoted by the title complexes (chapter 3), and reactivity and kinetic studies aimed at understanding the impact of different variables (R and R'; temperature; substrates; solvent; etc.) on the Michael-type hydroamination and hydroalkoxylation of acrylonitrile and its substituted derivatives (chapter 4). Chapter 3 will also discuss the attempted synthesis of new amine and nitrile POCOP cationic and neutral complexes, as well as the facile displacement of the amine moiety by a nitrile.

Keywords : nickel (II), pincer complexes, cationic POCOP nickel complexes, synthesis, characterization, electronic effects, steric effects, ligand exchange, oxidation by ferrocene, hydroamination, hydroalkoxylation, mechanistic investigations, amine complexes, amines, kinetic studies.

Table des matières

Liste des tableaux

Liste des figures

Liste des schémas

Liste des abréviations

appq Quartet apparent (spectroscopie)

Bn Groupement benzyle, CH_2Ph

br Large (spectroscopie)

C_6D_6 Benzène deutéré

calcd Calculé

d Doublet (spectroscopie)

dd Doublet de doublets (spectroscopie)

dh Doublet d'heptuplet (spectroscopie)

DCM Dichlorométhane

Equivs. ou equiv. Équivalents ou équivalent

GC/MS Chromatographie en phase gazeuse couplée à la spectroscopie de masse

^{31}P NMR Spectroscopie RMN du noyeau phosphore (spectroscopie)

^{1}H NMR Spectroscopie RMN du proton (spectroscopie)

^{19}F NMR Spectroscopie RMN du noyeau fluor (spectroscopie)

^{13}C NMR Spectroscopie RMN du noyeau carbone (spectroscopie)

i-Pr Isopropyle

IR Infrarouge (spectroscopie)

Ph Groupement Phényle, C_6H_5

$PC_{sp2}P$ ou PCP 1,3-bis(phosphinobenzene)

$PC_{sp3}P$ 1,5-bis(phosphinopentane)

$POC_{sp2}OP$ ou POCOP 1,3-bis(phosphinitobenzene)

$POC_{sp3}OP$ 1,3-bis(phosphinitopropane)

PIMCOP 3-[2-(phosphanyl)-1H-imidazol-1-yl]phenyl phosphinite

R Groupe générique

RMN Résonnance magnétique nucléaire (spectroscopie)

r.t. Température ambiante

s Singulet (spectroscopie)

t Triplet (spectroscopie)

TON Turn over number

TOF Turn over frenquency

t-Bu Groupement butyle tertiaire

δ Déplacement chimique

Je dédie ce mémoire à mes parents, ma sœur (et mes quatres magnifiques nièces), et à l'homme merveilleux qui partage ma vie. Ces êtres merveilleux m'ont soutenu tout au long de mes études, me permettant ainsi d'avancer de plus en plus chaque jour. Sans la confiance, le support et l'amour inconditionnel qu'ils m'ont donnés chaque jour, je n'aurais jamais osé continuer à la maîtrise et encore moins m'aventurer pour un doctorat au Japon.

Remerciements

Je voudrais remercier, en premier lieu, mon directeur de recherche, Pr. **Davit Zargarian**, pour les efforts soutenus durant toutes les étapes de ma maitrîse, et surtout durant les périodes d'écritures et de révision des articles. Même quand je le dérangeais durant ses vacances, il ne disait rien et m'aidais à terminer d'écrire nos articles. Il a donné beaucoup de son temps pour me permettre de mieux comprendre et d'avancer, et pour ça je lui serais toujours reconnaissant. Il m'a aussi poussé pour que je continue mes études, et sans lui je ne serai pas où je suis.

Je voudrais aussi remercier **Boris Vabre** puisqu'il m'a soutenu, supervisé et a répondu aux questions que je lui ai posées, qui souvent n'étaient pas du plus haut calibre, en plus d'être un bon ami et de m'avoir guidé au début de ma maîtrise mais aussi jusqu'à la fin.

Je voudrais remercier **Jean-Philippe Cloutier**, **Laurent Dubrulle**, Dr. **Jingjun Hao**, **Loïc Mangin** et les autres membres du groupe qui m'ont aidé, d'une manière ou d'une autre, à mieux comprendre certains points pas toujours clairs de ma chimie, d'avoir participé et contribué aux multiples réunions de groupe, rendant ainsi mon expérience à la maîtrise beaucoup plus intéressante.

Je voudrais tout spécialement remercier **Michel Simard** et **Francine Bélanger** pour avoir répondu aux milliers de questions de cristallographie que j'avais, et d'avoir fait grandir ma passion pour cette technique d'analyse. Ils ont un cœur énorme et leurs conseils sont toujours à point et ont toujours été la bienvenue. Je voudrais aussi remercier **Elena Nadezhina** pour les multiplies analyses élémentaires, et pour son grand sourire et sa joie de vivre qui ont illuminés mes (nos) journées. Merci à Antoine Hamel et Cédric Malveau de l'équipe RMN.

Merci à Pr. **Christian Reber**, Pr. **Frank Schaper**, Pr. **André Beauchamp** et Pr. **Gary Hanan** pour leur soutien lors de l'écriture de lettres de recommendation, pour les discussions sur des points plus précis de ma recherche et sur la cristallographie, ainsi qu'à leurs groupes de recherche respectifs pour les multiples discussions de nos réunions inorganiques.

Enfin, je voudrais remercier mes nombreux collègues et ami(e)s que j'ai eu la chance de côtoyer durant mes études, et qui m'ont permis de continuer d'avancer jusqu'où je suis maintenant en me donnant des conseils, en prêtant une oreille à mes soucis et en étant tout simplement là.

Chapitre 1: Introduction

1.1 Catalyseurs et chimie verte

La chimie des complexes organométalliques de métaux de transition a vu une croissance dans les deux dernières décennies,[1] notamment grâce à la découverte de catalyseurs très actifs dans plusieurs types de réactions d'importance industrielle, tels que les couplages C-C [2] et C-X (X = H, Halogènes, OTf…), l'hydrogénation assymétrique[3] et de transfert,[4] les réactions de type Suzuki,[5] Sonogashira[6] ou encore l'application de catalyseurs dans la conversion de biomasse.[7] Toutefois, l'application industrielle des complexes organométalliques vis-à-vis de ces réactions n'est pas encore totalement au point puisque, la plupart du temps, ces réactions sont faites dans des conditions de hautes pressions et de hautes températures et souvent sous forme de catalyse hétérogène. Plusieurs déchets de combustion et des sous-produits de réactions sont produits lors de ces procédés industriels. Ceux-ci sont très souvent difficiles à récupérer où à réutiliser et lorsqu'il est possible de le faire, ces procédés sont souvent coûteux. L'un des déchets les plus importants des procédés chimiques industriels est le CO_2 produit lors des réactions de combustion. Le CO_2 affecte directement la pollution atmosphérique et contribue de façon très importante à l'effet de serre. Depuis l'an 2000, l'émission mondiale de CO_2 par habitant a augmenté de façon importante, passant de 4.1 tonnes par habitant en 2000 à 4.7 tonnes en 2008 puis à 4.9 tonnes en 2011.[8] Cette augmentation importante est le reflet de la nécessité grandissante d'améliorer les procédés industriels actuels en procédés moins dommageables pour l'environnement.

Grâce à une sensibilisation importante de notre société aux problèmes environnementaux grandissants, un nouveau domaine de la chimie est né, la chimie dite « verte », qui a pour but de réduire l'impact environnemental des procédés chimiques. Ainsi, plusieurs chercheurs et plusieurs industries se sont tournés vers l'utilisation de catalyseurs nécessitant moins d'étapes de préparation et utilisant des réactifs plus verts et biodégradables, en plus de se tourner vers les métaux plus abondants tels que le nickel, le cobalt, le fer et le cuivre, entre autres. En plus d'être plus abordables et verts, les catalyseurs utilisant ces métaux deviennent de plus en plus concurrentiels envers ceux utilisant des métaux nobles grâce à l'affinement des propriétés

électroniques et stériques des ligands. En effet, une génération de chercheurs du domaine de la chimie organométallique se sont intéressés et s'intéressent toujours au design du ligand et de leurs multiples propriétés électroniques et stériques, et espèrent ainsi améliorer les procédés industriels actuels.

C'est dans cette vision que notre groupe de recherche, ainsi que plusieurs autres, s'est penché sur la chimie du nickel en tant que métal peu dispendieux et vert.

1.2 Historique et applications des complexes pinceurs

Les ligands de type multidentate ou chélatant sont réputés pour offrir stabilité et rigidité autour du centre métallique. Il existe plusieurs types de ligands chélatants, mais les ligands tridendates chélatants, dit de type « pince » se démarquent par leur grande rigidité et stabilité. Lors de leur découverte en 1976 par les groupes de Shaw[9] et Van Koten[10] et durant plusieurs années par la suite, les ligands de type pinceur ont été majoritairement utilisés pour stabiliser des complexes métalliques et pour offrir un site de réaction accessible. Le premier exemple de ligand de type pinceur découvert par Coulton et Shaw en 1976[9] ([2,6-Bis[(di-tert-butylphosphino)methyl]phenyl] ; $PCP^{t\text{-}Bu}$) , et puis par van Koten[10] ([2,6-bis[(dimethylamino)methyl]phenyl]]; NCN^{Me}) dans la même année (**Figure 1.1**).

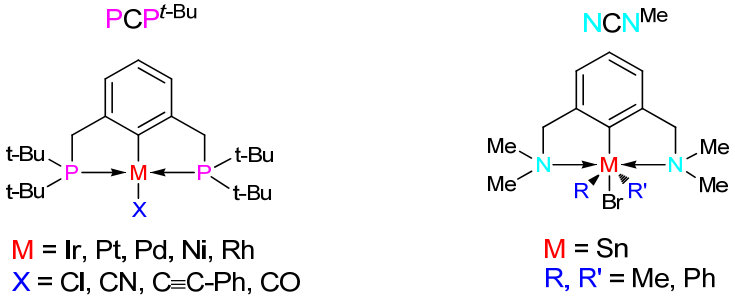

Figure 1.1 Ligands pinceurs PCPt-Bu et NCNMe

Les ligands pinceurs sont la plupart du temps composés d'un squellette aromatique ou aliphatique contenant ou non des substituants sur le cycle aromatique ou la chaine aliphatique.

De plus, le squelette peut contenir plus d'un cycle aromatique et peut contenir des fonctions amines primaires ou secondaires, des fonctions thio ou oxo, ou encore des fonctions phosphorées, entre autres (**Figure 1.2**). Les ligands pinceurs sont souvent reliés au métal de façon tridentate où deux site donneurs neutres (tels que PR_2, NR_2, …) sont en *trans* et le troisième site (souvent un carbone) est orthogonal, ce qui favorise une géométrie proche du plan-carré pour les métaux d^8 (Ni^{II}, Rh^{I}, Ir^{I}, Pd^{II}, Pt^{II}) ou pyramidale à base carrée (octaèdrique est aussi possible) pour les métaux d^6 (Ru^{II}, Rh^{III}, Ir^{III}, Ni^{III}). Ces géométries stabilisent la liaison σ M-C, ce qui explique en partie la grande stabilité thermique et la résistance à l'air et à l'humidité de ces composés, qui peuvent être gardés en solution pour une longue durée sans décomposition. De plus, la modification des groupements directement liés au métal influence souvent de façon importante les propriétés du centre métallique, et sont très souvent la cible première de modifications pour obtenir de nouvelles propriétés. Toutefois, ce ne sont pas les seuls sites qui peuvent être modifiés, et récemment, certains groupe de recherche se sont penchés sur la corrélation entre la modification des groupes distants du métal (groupement en position *méta* ou *para* sur le squelette aromatique, par exemple) et les propriétés électroniques et structurales diverses de celui-ci.[11]

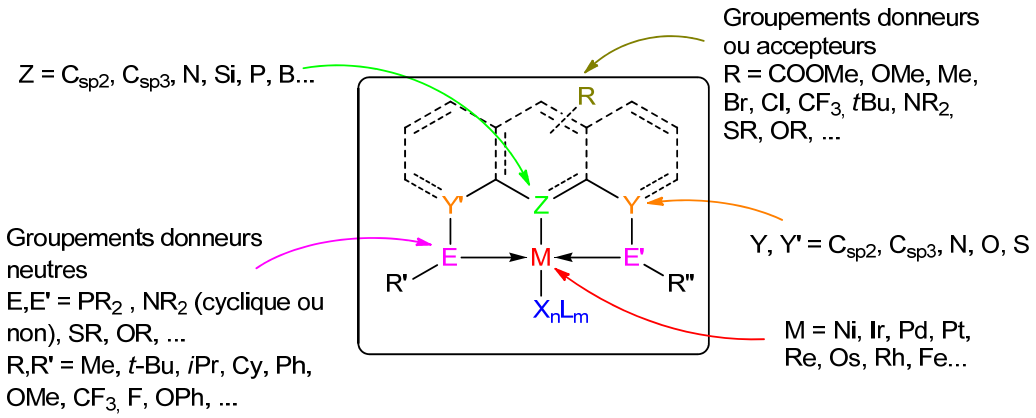

Figure 1.2 Schéma général des complexes pinceurs ou « pincer-like »

Plusieurs types de ligands pinceurs ont étés développés dans les 20 dernières années (**Figure 1.3**) par des groupes pionniers de la chimie des pinceurs et ont permis au domaine de

s'agrandir, soit par la multitude de possibilité de modulation du squelette ou encore par la variété d'applications et de réactivités possible de ces ligands.

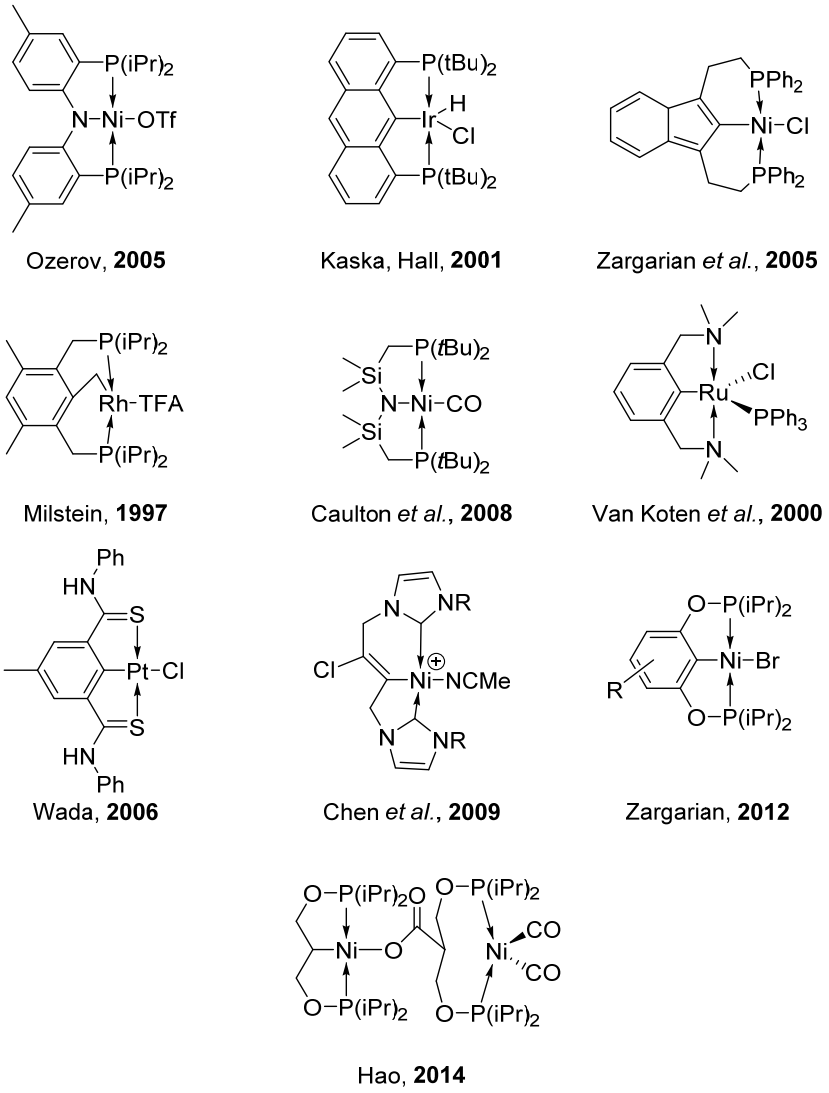

Figure 1.3 Exemple de complexes pinceurs et « pincer-like »[11b, 12]

Les pinceurs sont d'un intérêt particulier pour les chimistes organiciens et inorganiciens puisque beaucoup de ces complexes présentent des réactivités très intéressantes pour des réactions diverses et ont des qualités structurales intéressantes. Les complexes pinceurs démontrent une activité importante dans les réactions d'aldol (réaction avec aldéhydes et isonitriles et couplage réductif d'aldols) (**Figure 1.4**), dans plusieurs types d'addition de Michael (**Figure 1.5**), dans plusieurs réactions de couplages divers (**Figure 1.6**), d'allylation

(**Figure 1.7**), et d'hydrogénation (**Figure 1.8**), entre autres. La grande variété de réactivité des complexes pinceurs et « pincer-like » rend l'utilisation des complexes pinceurs très intéressants pour l'industrie chimique et pour les groupes de recherche organique.

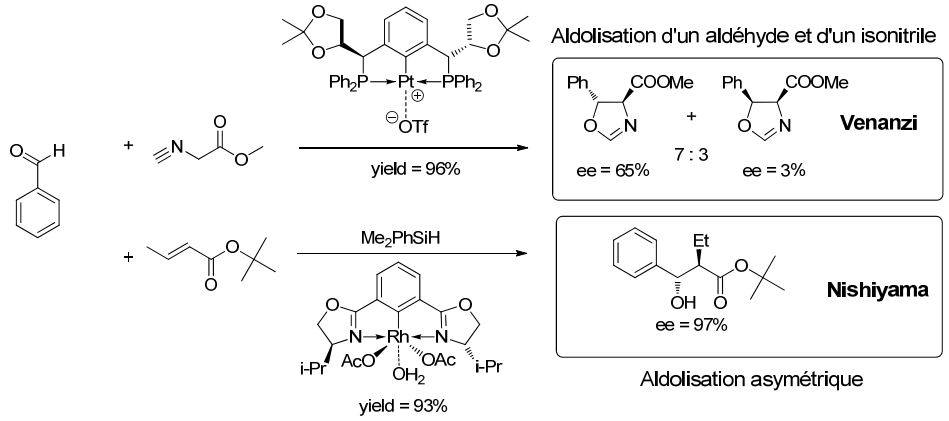

Figure 1.4 Réaction d'aldolisation catalysée par complexe pinceur publié par Venanzi[13] et Nishiyama.[14]

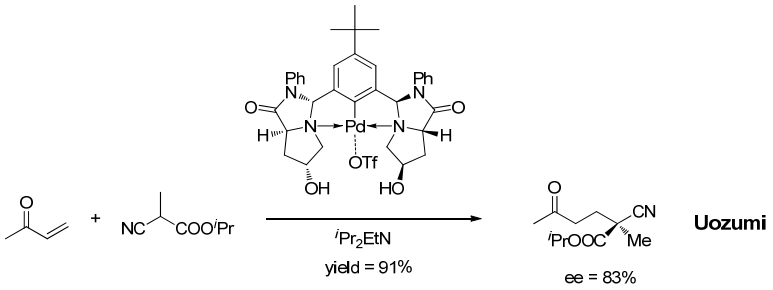

Figure 1.5 Addition de Michael asymétrique catalysée par un complexe pinceur publié par Uozumi.[15]

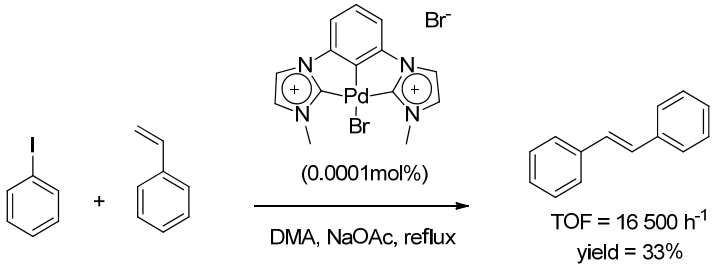

Figure 1.6 Couplage de Heck catalysé par un complexe pinceur de Crabtree.[16]

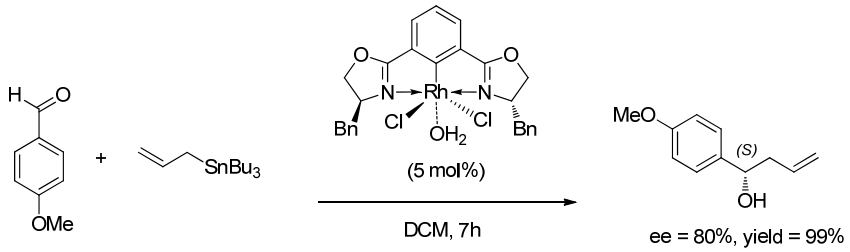

Figure 1.7 Exemple de réaction d'allylation utilisant des catalyseurs pinceurs.[17]

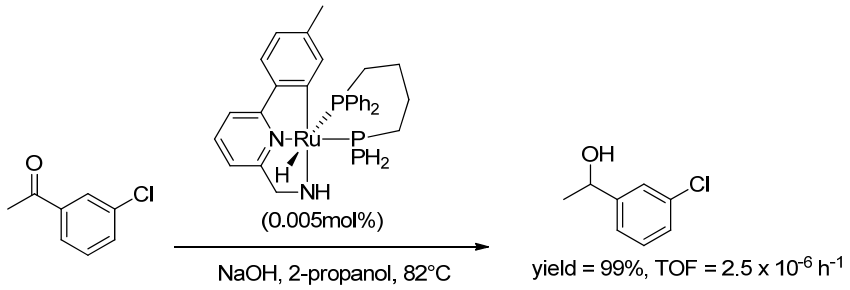

Figure 1.8 Hydrogénation par transfert par un catalyseur pinceur de Rigo.[18]

1.3 Préparation des composés de type pinceur

Plusieurs voies ont étés développées pour la préparation des complexes métalliques pinceurs, et sont toujours utilisées selon le type de métal ou le type de complexe désiré. Toutefois, certaines voies de synthèse, bien qu'attrayante dans les dernières décennies grâce à la facilité de préparation, sont mises de côté pour favoriser les voies nécessitant moins d'étapes et qui sont plus vertes. La plus connue et utilisée de nos jours est la voie d'activation de liens C-H, et les synthèses de type « one-pot » dans des conditions vertes voient leur popularité augmenter de façon considérable. En 1976, Shaw et Moulton[9] ont préparé le premier complexe pinceur par activation du lien C-H aromatique du ligand 1,3-(*t*-$Bu_2PCH_2)_2$-C_6H_4 ($PCHP^{tBu}$) à l'aide du précurseur $NiCl_2.6H_2O$ dans l'éthanol. Fait remarquable, ils ont observé la métallation après seulement quelques minutes à température ambiante. Selon les auteurs, les conditions dépendraient beaucoup de l'encombrement stérique puisque le ligand 1,3$(Et_2PCH_2)_2$-C_6H_4 ($PCHP^{Et}$) moins encombrant démontre une réactivité moindre. Peu de temps après, Venanzi a reporté que l'utilisation d'un ligand ayant des substituants moins encombrant sur les phosphines

tel que le ligand 1,3-$(Ph_2PCH_2)_2$-C_6H_4 ($PCHP^{Ph}$), nécessite que la métallation soit faite dans des conditions beaucoup plus dures (chauffage dans l'éthanol à 60 °C pendant 3 heures puis reflux pour 10 minutes en présence d'une base).[19] Bien que cette voie de synthèse semble attrayante, plusieurs voies alternatives ont étés proposées pour la préparation d'une vaste gamme de composés. Quelques exemples de composés préparés par différentes voies de synthèse sont présentés à la **Figure 1.9**. Ces voies de synthèse sont souvent utilisées pour un certain type de composés pinceurs. Par exemple, pour la plupart des complexes NCN-diamines, la synthèse du complexe nécessite deux étapes distinctes soit la formation du complexe lithié par la réaction du substrat de départ avec un sel de lithium, puis par une transmétallation avec un complexe métallique.[20]

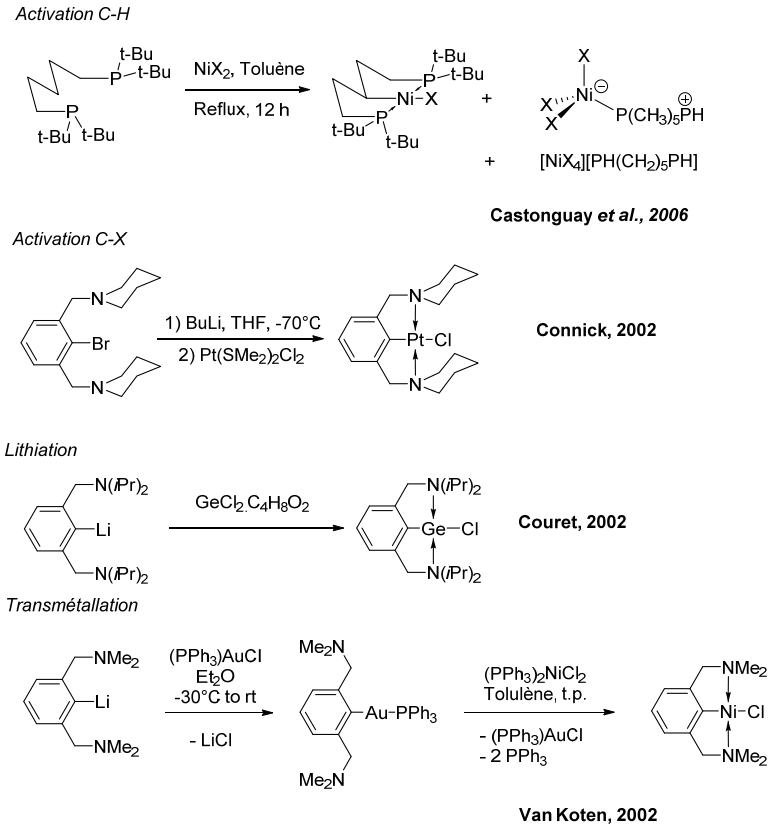

Figure 1.9 Exemples des voies de synthèse possibles pour les complexes pinceurs.[21]

1.4 Complexes de type POCOP

Le premier complexe de type PCP de palladium contenant deux groupements donneurs bis(phosphinite) (POCOP) a été introduit en 2000 par les groupes de Jensen[22] et Bedford.[23] Ils ont montré que ces types de complexes sont de meilleurs catalyseurs dans les réactions de couplage de Heck et de Suzuki. La préparation des complexes POCOP est très similaire à celle des complexes analogues PCP et est peu dispendieuse. Ainsi, plusieurs composés du ligand POCOP (Y-POCOP^{R}, [1,3-$(R_2PO)_2(Y)_nC_6H_{3-n}$]) de différents métaux ont étés préparés et la plupart montrent une activité catalytique plus importante que les dérivés PCP. La présence des oxygènes sur les bras chélatants du ligand POCOP augmente le caractère π-acide du ligand comparativement au ligand PCP, et des analyses électrochimiques indiquent que le ligand POCOP est plus difficile à oxyder que le ligand PCP.[24] Ainsi, le ligand POCOP pourrait être intéressant si l'on désire former des complexes électro-pauvres ou des complexes de métaux de plus bas degrés d'oxydation que ceux avec le ligand PCP, puisqu'il devrait y avoir plus de stabilisation électronique du métal.

1.4.1 Préparation des ligands et complexes métalliques de type POCOP

Quelques voies de préparation des complexes POCOP sont utilisées, la plus connue étant l'activation du lien C-H (cyclométallation) puisqu'elle est la méthode la plus directe de métallation et ne nécessite pas de préfonctionnalisation du ligand. Toutefois, la métallation par activation C-H nécessite la préparation d'un précurseur phosphoré qui est souvent sensible à l'air et à l'humidité, ce qui rend difficile l'isolation et la conservation du précurseur non métallé. Il est toutefois possible de résoudre le problème en utilisant l'activation C-H et la cyclométallation dans une réaction one-pot, telle que celle démontrée par notre groupe dans une publication récente,[25] pour les complexes $POC_{sp2}OP$ de nickel. Dans ce cas, la chlorophosphine est ajoutée sur le ligand dérivé du résorcinol, qui produit deux molécules de HCl. Le nickel métallique sera oxydé par les deux molécules de HCl libérées pour former $NiCl_2$ et qui réagira pour faire la cyclométallation (**Figure 1.10**).

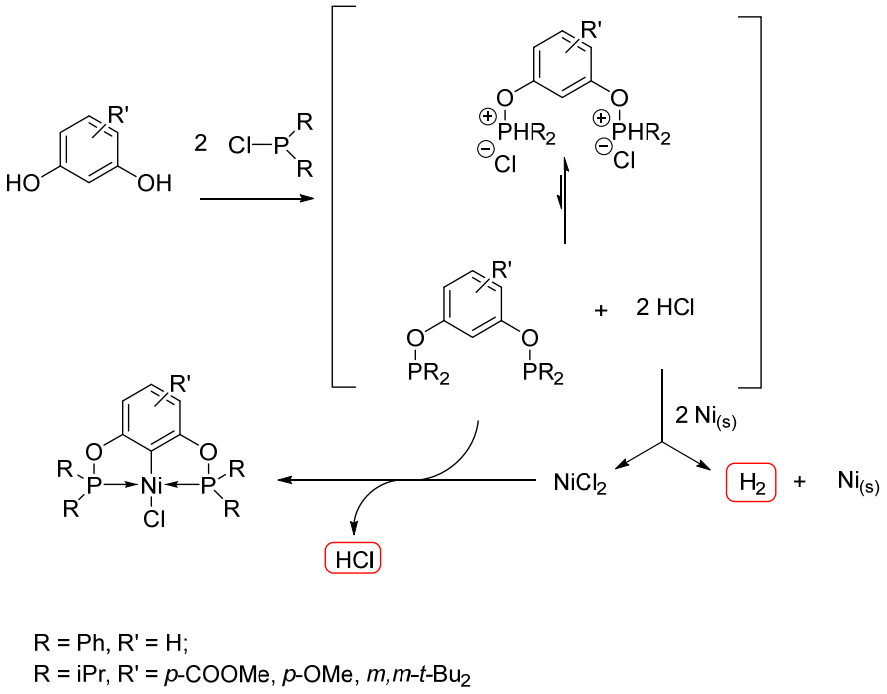

Figure 1.10 Schéma réactionnel possible pour formation POCOP-Ni-Cl par réaction « one-pot ».[25]

Une deuxième voie de synthèse, l'addition électrophile (méthode d'introduction du ligand plutôt que d'introduction du métal), développée en 2006 par Kimura et Uozumi[26] pour un complexe de palladium, permet de générer un précurseur Pd-diol stable à l'air qui réagit à température ambiante pour former rapidement le complexe pince correspondant (**Figure 1.11**). Toutefois, cette voie n'est pas beaucoup utilisée puisque le coût des produits de départs (dérivé iodure du résorcinol et complexes de métaux à l'état d'oxydation 0 sont relativement plus dispendieux que ceux utilisés dans la voie d'activation C-H et de cyclométallation directe.

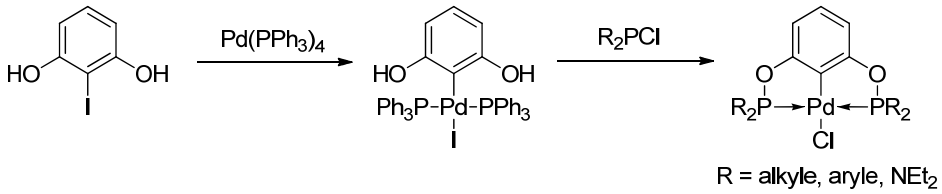

Figure 1.11 Schéma de synthèse d'un complexe pinceur de palladium via la voie d'introduction du ligand.[26]

1.5 Complexes neutres et cationiques POCOP de nickel

La chimie des complexes de nickel a été le sujet de multiples études au cours des 20 dernières années au sein de notre groupe. Les premiers travaux sur des complexes de nickel de notre groupe, il y a déjà maintenant deux décennies, se sont basés sur la chimie des ligands indényles et de leurs réactivités.[27] Toutefois, dans les dernières années, notre groupe a pris une nouvelle direction avec l'augmentation de popularité des complexes pinceurs et la toute nouvelle découverte des ligands de type POCOP. En effet, le premier complexe POCOP de nickel, (POCOP^{Ph})NiCl, a été préparé par le groupe de Morales-Morales en 2006[28] (**Figure 1.12**) puis plusieurs dérivés halogénés, (POCOP^{iPr})Ni-X (X = Cl, Br, I), ont étés reportés peu de temps après par Pandarus *et al.*[24b, 24c] (**Figure 1.12**). Les premiers complexes POC$_{sp3}$OP de nickel (III) ont étés isolés et caractérisés par Pandarus en 2007,[24c] et leur réactivité dans la réaction d'addition de Kharasch de CCl_4 sur des alcènes a été comparée à celle des complexes de nickel (III) de type NCN par van Koten.[29]

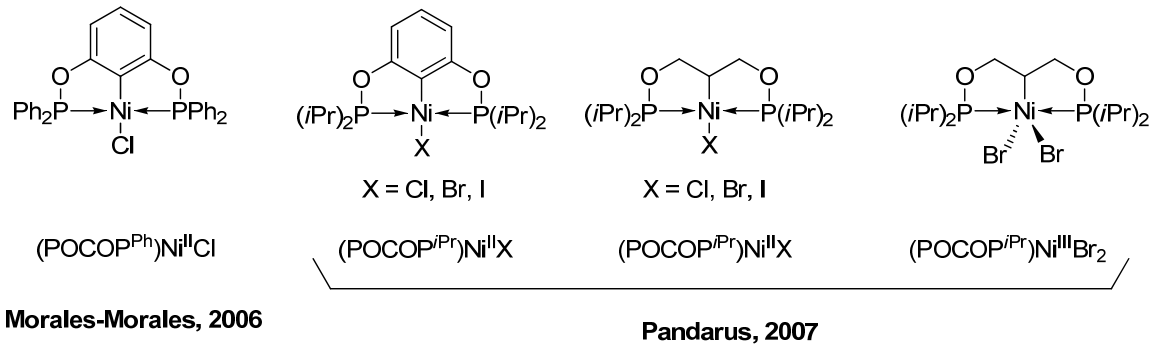

Figure 1.12 Premiers complexes POCOP de nickel (II) et (III) par Pandarus [24b, 24c] et Morales-Morales.[28]

1.5.1 Synthèse des complexes POCOP de nickel cationiques et neutres

Deux voies de synthèse sont utilisées pour la préparation des composés POCOP de nickel par voie d'activation C-H au sein de notre groupe, dépendamment de la nature de l'halogénure lié au nickel. En effet, la première méthode de préparation est une méthode nécessitant l'utilisation d'un précurseur de nickel (II), $NiBr_2L_n$ (L= $NCCH_3$, NC*i*Pr, THF), et nécessite deux étapes soit la préparation du complexe non-métallé POCHOP (Y-POCHOP^{iPr}, 1,3-[OP(*i*Pr)$_2$]$_2$-(Y)$_n$C$_6$H$_{4-n}$) et la réaction de ce ligand avec le précurseur de nickel(II) et permet d'obtenir le complexe avec un ligand brome. La deuxième voie utilisée a été présentée par Vabre[25] en 2013 et est une synthèse one-pot ne nécessitant qu'un dérivé de résorcinol, de 1 à 2 équivalents de nickel métallique et de deux équivalents de chlorodiisopropylphosphine (qui est relativement aisée à préparer en quelques jours incluant la distillation). Le mécanisme de cette réaction est rapidement présenté à la **Figure 1.10**. La réaction peut être faite dans le toluène ou encore l'acétonitrile en chauffant à des températures entre 75 °C et 100 °C, selon le solvant. Les rendements varient de moyens à bons et la réaction peut être appliquée à quelques dérivés du résorcinol. Cette méthode est à la fois verte et peu dispendieuse et ne nécessite pas l'utilisation d'un précurseur toxique. Enfin, le nickel est un métal abordable et disponible en grande quantité et beaucoup moins dispendieux que d'autres métaux couramment utilisés pour la chimie des complexes pinceurs (Pd, Pt, Ir, etc.), ce qui rend la chimie des complexes pinceurs de nickel attrayante pour des applications a plus grande échelle.

1.5.2 Modification du squelette des complexes POCOP, POCN et NCN de nickel

En 2012, Vabre *et al.*[30] ont étudié plusieurs aspects de la métallation des complexes POCOP de nickel, notamment les vitesses relatives de métallation selon la nature des substituants sur le squelette aromatique du ligand. Ils ont ainsi pu déterminer certains aspects influençant la vitesse de métallation tel qu'une diminution de réactivité lorsque des groupements électroattracteurs sont présents sur le ligand et une augmentation lorsque ces groupements sont électrodonneurs. Ainsi, ils ont conclu que la position de ces substituants (*méta* vs *para*

relativement au carbone qui subit une activation C-H) a une influence non négligeable sur la vitesse de métallation. La présence des atomes d'oxygène sur les bras du ligand diminue d'environ six fois la vitesse de métallation, la nature du carbone (sp^2 vs. sp^3) influence grandement la vitesse et enfin des groupements isopropyles sur les phosphines rendent la réaction au moins cent fois plus rapide que des groupements phényles ou tert-butyles. La collaboration avec le professeur Daniel H. Ess de l'université Brigham Young en Utah a permis d'investiguer la métallation des complexes PCP et POCOP par DFT, et a permis de mieux élucider le mécanisme et les différents états de transition possibles pour l'activation C-H et la métallation de ces complexes.

La même année, Vabre et Spasyuk[11b] ont étudié l'effet de substituants toujours sur le squelette aromatique mais plutôt au niveau des effets électroniques et stériques sur le centre métallique plutôt que sur la vitesse de métallation. Entre autres, ils ont confirmé que la nature du substituant en para a un impact direct sur le potentiel redox du complexe. Ils ont aussi remarqué que la position du substituant (méta ou para relatif au carbone métallé) a un impact sur la richesse électronique du système.

Certaines publications de notre groupe se sont basées par contre sur la modification du ligand davantage au niveau des groupes directement liés au nickel, pour obtenir de nouvelles propriétés ou encore pour combiner l'effet de certaines propriétés électroniques. Par exemple, la préparation de complexes de type POCN[31] as permis de combiner la faible richesse électronique du bras phosphoré et la plus grande richesse électronique du bras aminé (**Figure 1.13**). Ce type de composé permet ainsi de stabiliser davantage les états d'oxydation plus élevés du métal, tout en offrant une plus grande stabilité du complexe vis-à-vis de ceux de type NCN. De plus, notre groupe a aussi publié très récemment[32] un nouveau type de ligands asymétriques et spécifiquement préparés pour obtenir cet environnement à la fois pauvre et riche en électrons autour du centre métallique. Ces complexes nommés PIMCOP, PIMIOCOP et NHCCOP[12i] possèdent un caractère à la fois pauvre et riche dû à la combinaison d'un bras O-PR_2 (faible richesse électronique), et d'un bras contenant une fonction amine (plus grande richesse électronique), avec ou sans phosphore (**Figure 1.13**). Ces ligands pourraient permettre d'obtenir des complexes ayant des propriétés intéressantes grâce à la modulation électronique de chacun de ces bras.

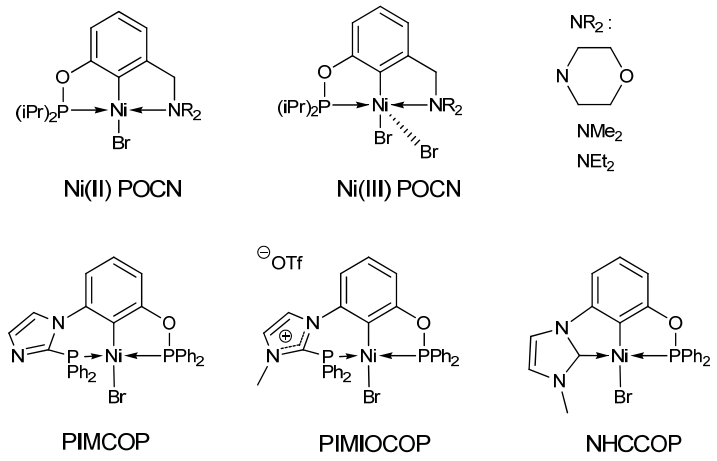

Figure 1.13 Exemples de complexes POCN, PIMCOP, PIMIOCOP et NHCCOP.[12i, 33]

1.5.3 Application catalytique des complexes cationiques POCOP de nickel

Dans le but d'étendre l'analyse des complexes POCOP de nickel, Castonguay[24a] a entrepris la préparation d'un composé cationique POCOP de nickel portant un ligand acétonitrile. Ses études sur la réactivité de l'acrylonitrile envers certaines amines (hydroamination, addition Aza-Michael) par son complexe POCOP cationique montrent une activité de moyenne à bonne, et cette étude a porté Lefèvre,[34] en 2011, à publier une analyse plus large de la catalyse du complexe POCOP cationique envers la même réaction (**Figure 1.14**) et envers l'addition de phénols. Certaines amines et phénols montrent une activité importante, notamment les amines primaires aliphatiques qui, en moins de cinq minutes à la température ambiante, montrent une conversion complète. D'autres amines ou phénols ne sont pas aussi actifs même à 60 °C pendant 24 h. Toutefois, il est intéressant de noter qu'en utilisant le crotonitrile ou le méthacrylonitrile, la seule amine aromatique qui ait réagi est l'aniline, et ce avec de très mauvais rendements même à 60 °C pendant 24 h tandis que pour l'acrylonitrile, la réaction se rendait à complétion en 4h à la température de la pièce.

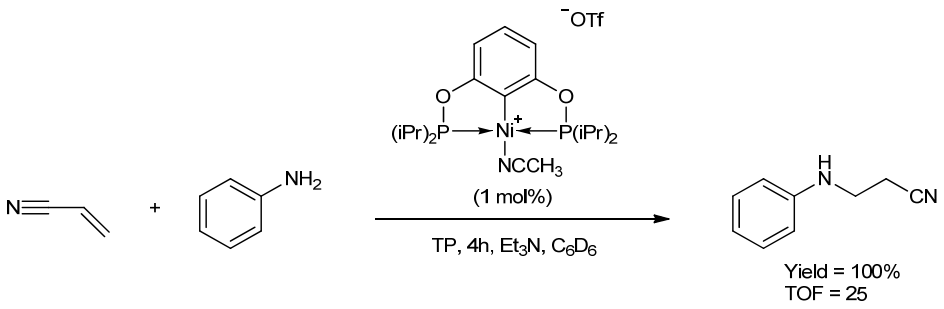

Figure 1.14 Réaction d'hydroamination de l'acrylonitrile par l'aniline.[34]

La réaction d'addition d'Aza-Michael est une des réactions les plus importantes et les plus utilisées en industrie et en laboratoire pour la formation de liens C-N. L'un des avantages de cette réaction est qu'elle est verte, puisqu'elle suit le principe d'économie d'atome, et qu'elle ne produit pas de sous produits. Certains liens C-N ne sont pas toujours faciles à produire, donc il est important d'étudier la diversité des systèmes compatibles, les différentes limites de ces systèmes ainsi que les limites quant aux conditions du milieu, et la variété de groupements qui peuvent être utilisés dans ces systèmes. Dans ce mémoire, nous avons étudié une large gamme de groupements fonctionnels, tout autant sur le substrat que sur le nitrile ainsi que sur le cycle aromatique du ligand POCOP. Ces analyses permettent de dresser une certaine image de l'utilité et de la versatilité du système POCOP cationique de nickel dans ce type de réaction. De plus, nous sommes en mesure d'extrapoler les résultats afin de mieux étudier le mécanisme de la réaction, les effets stériques ainsi qu'électroniques qui permettent de diriger la réaction. Il est important de noter que le mécanisme actuellement proposé[24a] pour l'attaque d'une amine sur un nitrile (hydroamination, voire **Figure 1.15**) par voie d'acide de Lewis est légèrement différent pour notre système puisqu'il semble y avoir une part importante de réactions impliquant le produit d'hydroamination en tant que réactif en compétition avec le substrat de départ. Nous avons aussi étudié en détail plusieurs types de réactions catalytiques tels que l'hydroamination[24a, 35] et l'hydroalkoxylation[35b] de nitriles par des composés POCOP de nickel(II) cationiques ou neutres ou encore la réaction d'addition de type Kharasch de CCl_4 sur des oléfines.[24c, 33]

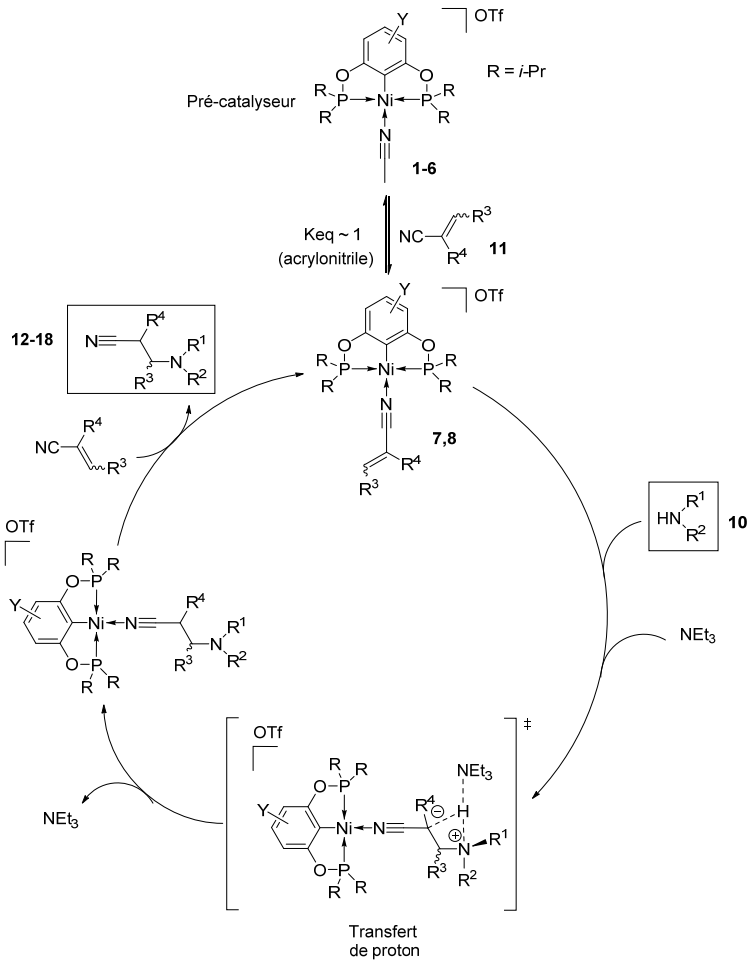

Figure 1.15 Mécanisme proposé d'hydroamination de nitriles adapté de la littérature[24a]

L'utilité de la formation de liens C-N est bien connue, mais il est aussi important de montrer que notre système cationique permet d'utiliser des substrats contenant des groupements hydroxyles, et ainsi de former des liens C-O. Ainsi, nous avons étudiés l'addition de différents alcools aromatiques et aliphatiques sur des nitriles (Hydroalkoxylation) dont le mécanisme proposé est différent de celui d'hydroamination des nitriles.[35b] Bien que moins attrayante puisqu'elle requiert des substrats plus toxique et qu'elle est moins utilisée dans les dernières années, Pandarus[16c] et Spasyuk[25] ont aussi étudiés la réaction d'addition de type Kharasch de CCl_4 sur des oléfines.

Notes spéciales sur la contribution du co-auteur

Le chapitre suivant contient l'apport substantiel et suffisant de Boris Vabre pour lui atribuer le rôle de co-auteur de ce manuscript. Boris Vabre a procédé à l'acquisition de données structurales (données de diffraction des rayons X) d'une partie importante des composés présentés dans le chapitre 2 (5 des 7 structures, nottamment les structures des composés **2** à **6**). Il a choisi les cristaux, collecté les données et finalisé les structures des composés **2** à **6**. Il n'a pas contribué à l'écriture ni à la révision du manuscript, mais à contribué à beaucoup de discussions et d'idées.

Chapitre 2: POCOP-Type Pincer Complexes of Nickel: Synthesis, Characterization, and Ligand Exchange Reactivities of New Cationic Acetonitrile Adducts

Article 1

Sébastien Lapointe,[†] Boris Vabre[‡] and Davit Zargarian[†]

[†] Département de chimie, Université de Montréal, Montréal (Québec), Canada H3C 3J7

[‡] Present address: Department of Chemistry, Texas A&M University, College Station, Texas 77843-3255, United States

Reprinted (adapted) with permission from Lapointe, S.; Vabre, B.; Zargarian, D. *Organometallics* **2015**, *34* (14), 3520-3531.

2.1 Abstract

This report describes the synthesis, characterization, and ligand exchange studies of a family of cationic acetonitrile adducts of nickel featuring resorcinol-based, pincer-type POCOP ligands. The compounds [(R-POCOP$^{R'}$)Ni(NCMe)][OSO_2CF_3] (R-POCOP$^{R'}$ = 2,6-(R'_2PO)$_2$($R_nC_6H_{3-n}$); R' = *i*-Pr : R = H (**1**), *p*-Me (**2**), *p*-OMe (**3**), *p*-CO_2Me (**4**), *p*-Br (**5**), *m,m*-*t*-Bu_2 (**6**), *m*-OMe (**7**), *m*-CO_2Me (**8**); R' = *t*-Bu : R = H (**9**), *p*-CO_2Me (**10**)) were prepared in 80-93% yields by reacting the corresponding charge-neutral bromo derivatives with Ag(OSO_2CF_3) in acetonitrile. The impact of the R- and R'-substituents on electronics and structures of **1-10** have been probed by NMR, UV-vis and IR spectra, X-ray crystallography, and cyclic voltammetry measurements. The observed ν(C≡N) values were found to increase with the increasing electron-withdrawing nature of R, i.e., in the order **7** < **3** ~ **2** ~ **6** < **1** < **5** ~ **8** < **4** and **9** < **10**. This trend is consistent with the anticipation that enhanced electrophilicity of the nickel center should result in an increase in net MeCN→Ni σ–donation. That this transfer of electron density from acetonitrile to the nickel center does not adequately counteract the impact of electron-withdrawing substituents was evident from the measured redox potentials: the MeO_2C-substituted cations showed the highest oxidation potentials. Moreover, all cationic adducts showed greater oxidation potentials compared with their corresponding charge-neutral bromo precursors. Equilibrium studies conducted with selected [(R-POCOP$^{R'}$)Ni(NCMe)][OSO_2CF_3] and (R-POCOP$^{R'}$)NiBr (R' = *i*Pr) have confirmed facile MeCN/Br exchange between these derivatives, and show that the cationic adducts are stabilized with MeO-POCOP, whereas the charge-neutral bromo species are stabilized with MeO_2C-POCOP. The potential implications of these findings for the catalytic reactivities of the title cationic complexes have been discussed.

2.2 Introduction

The pioneering studies begun in the 1970's by groups of Shaw[36] and van Koten[10] laid the foundation for what later came to be known as pincer chemistry.[37] Over the nearly four decades since, researchers have combined old and new ligand types with various d- and p-block elements

to synthesize numerous pincer complexes and explore their reactivities and physical properties. These developments have been captured in a number of authoritative review articles.[38]

Nickel complexes were among the early pincer derivatives introduced by Shaw and van Koten, but it was only over the past decade that organonickel pincer chemistry experienced major developments. The introduction of many different families of pincer nickel complexes (PCP,[12c, 39] $POC_{sp2}OP$,[25, 40] $POC_{sp3}OP$,[12j, 24c, 41] POCN,[31, 42] PNP,[12e, 43] NNN,[44] etc.[12i]) has led to exciting developments that have been reviewed recently.[38e, 45] Among these, resorcinol-based POCOP-Ni systems have proven particularly popular due to the facile synthesis of variously substituted ligands and their complexes (via C-H nickelation),[24b, 24c, 25, 40c] as well as the interesting catalytic transformations these compounds promote.[24a, 35b, 46]

We have initiated a systematic study aimed at mapping out the impact of differently-substituted, resorcinol-derived POCOP ligands on structures and electronic properties of their cationic Ni-acetonitrile adducts. Thus, we have reported on the influence of *P*- and aromatic ring-substituents on C-H nickelation rates, structures, and redox potentials of charge-neutral complexes (R-$POCOP^{R'}$)NiBr.[11b, 30, 47] Analogous studies have been reported by other groups on POCOP complexes of Ir and Pt.[48] These reports have inspired us to study the impact of *P*- and aromatic ring-substituents on the structures and electronic properties of cationic adducts featuring POCOP ligands. Reported herein are the syntheses, spectroscopic and structural studies, redox potential measurements, and ligand exchange reactivities of the cationic acetonitrile adducts [(R-$POCOP^{R'}$)Ni(NCMe)][OSO_2CF_3] where R and R' represent, respectively, various substituents on the resorcinol aromatic ring (H, *p*-Me, *p*-OMe, *p*-CO_2Me, *p*-Br, *m*-OMe, *m*-CO_2Me, *m,m*-*t*-Bu_2) and *P*-substituents (*i*-Pr, *t*-Bu). Given the importance of this family of complexes in a number of interesting catalytic reactivities,[24a, 24c, 34] we hope that the results of our study will provide a basis for tuning the reactivities of [(R-$POCOP^{R'}$)Ni(L)][OSO_2CF_3] for different catalytic applications.

2.3 Results and Discussion

2.3.1 Synthesis of [(R-POCOP$^{R'}$)Ni(NCMe)][OSO_2CF_3]

The target cationic complexes were prepared by treating the charge-neutral bromo derivatives (R-POCOP$^{R'}$)NiBr with 1.2 equiv of AgOTf in dry acetonitrile under nitrogen and in the absence of light (**Scheme 2.1**). The charge-neutral bromide precursors used in these syntheses were, in turn, obtained from the rt reaction of the preligands R-POC^{H}OP with $NiBr_2(NCMe)_2$ in the presence of 1.2 equiv of NEt_3. It should be noted that all but one of these precursors are known species that have been reported previously;[11b] the only new bromide derivative, (*p*-Br-POCOP$^{R'}$)NiBr (R' = *i*Pr, **5'**), was prepared in the same manner as its counterparts **1'-4'** using the new preligand *p*-Br-POC^{H}OP. The latter was prepared by phosphorylation of 5-bromo-resorcinol (**Scheme 2.1**), which was itself obtained from acidic hydrolysis of 3,5-dimethoxybromobenzene using a modified literature procedure.[49]

Scheme 2.1. General Synthetic Scheme for Complexes **1-10**

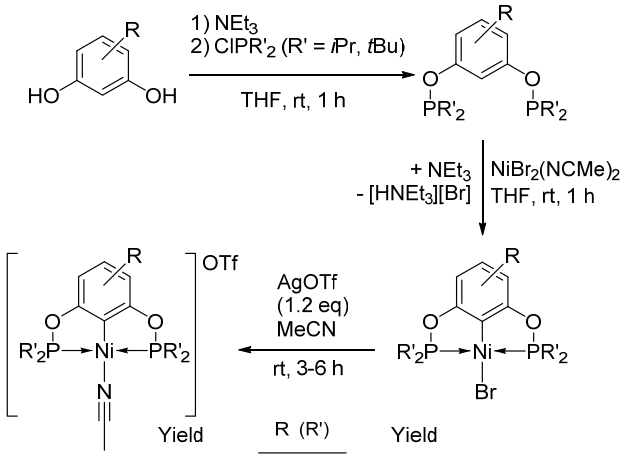

The work-up procedure for the cationic complexes consisted of cannula filtration of the final reaction mixture, followed by a second filtration through a short Celite plug to remove AgBr and furnish the target complexes as yellow powders in 80-93% yield. These cationic adducts proved to be less stable than their bromo precursors: storing analytically pure samples in the drybox (without protection from ambient light) led to a gradual color change from yellow to dark green. Eluting a CH_2Cl_2 suspension of these post-decomposition green solids through a short Celite column left a black residue on top of the column and furnished the desired cationic complexes in analytically pure form. Storing the purified samples under inert atmosphere inside a -37 °C freezer circumvented further decomposition.

The title cationic adducts as well as the new bromo derivative **5'** were characterized by spectroscopy (NMR, IR, and UV-vis) and cyclic voltammetry. Single-crystal X-ray diffraction studies were also carried out for complexes **5'**, **2-6**, **9**, and **10**; single crystals suitable for diffraction studies could not be obtained for complexes **7** and **8**, whereas the solid state structure of the parent cation **1** has been reported previously.[24b] The solid state structures are discussed below, followed by the results of the spectroscopic studies and electrochemical analyses.

2.3.2 Solid state structures

Table I lists the most pertinent structural parameters for the complexes that were subjected to X-ray diffraction studies, and Figures 2.1-2.3 show a side view of the molecular diagrams of adducts **4**, **6**, and **10**; the molecular diagrams for the remaining four complexes, the front view of the molecular diagrams of complexes **4**, **6** and **10** as well as the details of the diffraction studies are given in Figures A2.1-2.8 and Tables A2.1-2.2 (See « Annexe pour chapitre 2 »).

The nickel center in all complexes adopts a square planar geometry that displays slight distortions due, primarily, to the small bite angle of the POCOP ligands: P-Ni-P ~ 163-165°. The displacement of the nickel atom out of the coordination plane (P_1-N-P_2-C_{ipso}) is either negligible (<0.01 Å) or very minor (0.02-0.05 Å). Another source of notable structural distortion is the C_{ipso}-Ni-N angle, which is more acute in some cases due to the lifting of the acetonitrile moiety out of the coordination plane. For instance, C_{ipso}-Ni-N angles of ca. 170-172° were found in complexes **2** (R = *p*-Me) and **6** (R = *m*,*m*-*t*-Bu_2), in contrast to angles of 175-180° in the remainder of the

complexes; thus, it is difficult to establish with confidence whether these deviations are due to steric or electronic factors.

Table 2.1 Selected bond Distances (Å) and Angles (deg) for cationic adducts 1-10 and charge-neutral complexes **1'-10'**

Complex	Ni-C	Ni-N/Br	N≡C	Ni-P1	Ni-P_2	P_1-Ni-P_2	C-Ni-N/Br
1[a]	1.881(2)	1.874(2)	1.140(3)	2.1683(7)	2.1704(7)	164.38(3)	175.8(1)
2	1.879(3)	1.875(2)	1.142(4)	2.1693(8)	2.1687(7)	163.52(3)	171.7(1)
3	1.884(2)	1.881(2)	1.135(3)	2.1784(5)	2.1747(5)	163.16(2)	176.84(7)
4	1.880(2)	1.879(2)	1.138(2)	2.1698(4)	2.1748(4)	164.45(1)	178.43(6)
5	1.879(3)	1.871(3)	1.145(4)	2.1685(9)	2.171(2)	164.44(4)	176.6(2)
6	1.890(2)	1.875(2)	1.140(2)	2.1785(5)	2.1640(4)	163.79(2)	170.35(6)
9	1.885(2)	1.879(2)	1.140(2)	2.1944(5)	2.1946(5)	163.57(2)	179.02(6)
10	1.881(2)	1.876(2)	1.146(2)	2.1933(4)	2.1922(4)	164.025(1)	178.51(6)
1'[a]	1.885(3)	2.3231(5)		2.1534(8)	2.1422(8)	164.92(4)	178.10(8)
2'[a]	1.882(3)	2.3305(5)		2.1584(4)	2.1584(4)	164.21(3)	180.0(1)
3'[a]	1.877(2)	2.319(1)		2.155(1)	2.152(1)	164.65(2)	178.25(6)
4'[a]	1.872(2)	2.312(1)		2.157(1)	2.159(1)	165.26(2)	179.3(1)
5'	1.877(2)	2.3211(5)		2.1500(7)	2.1467(8)	163.89(3)	178.74(8)
6'[a]	1.892(4)	2.320(1)		2.139(1)	2.143(1)	165.06(5)	179.08(12)
9'[a]	1.887(2)	2.338(2)		2.193(1)	2.189(1)	164.13(3)	179.7(1)
10'[a]	1.877(2)	2.321(1)		2.189(1)	2.194(1)	164.58(3)	178.25(7)

a) Previously reported complexes [11b, 24b]

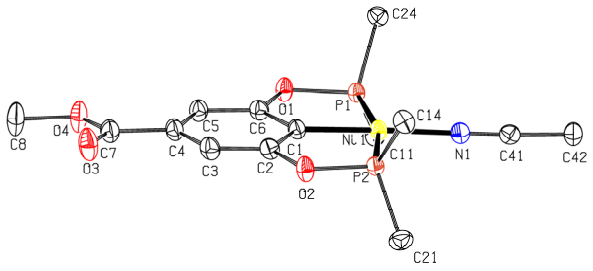

Figure 2.1 Molecular diagram for complex **4.**

Thermal ellipsoids are shown at the 50% probability level. Hydrogens and the *P*-substituents have been removed from this diagram for clarity.

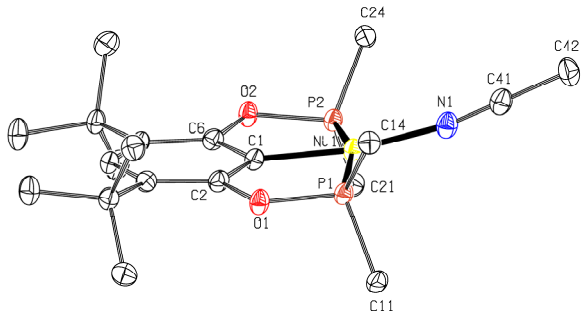

Figure 2.2 Molecular diagram for complex **6.**

Thermal ellipsoids are shown at the 50% probability level. Hydrogens and the *P*-substituents have been removed from this diagram for clarity.

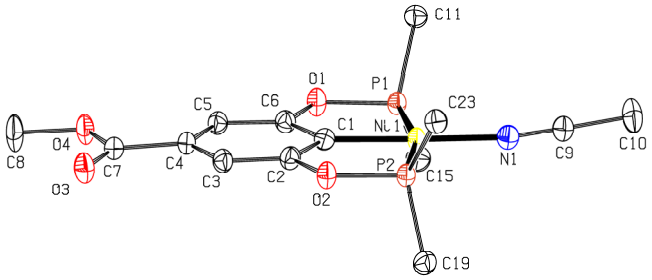

Figure 2.3 Molecular diagram for complex **10.**

Thermal ellipsoids are shown at the 50% probability level. Hydrogens and the *P*-substituents have been removed from this diagram for clarity.

The Ni-P distances show some variations in these compounds. First, the *t*-Bu$_2$P-Ni distances are much longer than their *i*-Pr$_2$P-Ni counterparts, particularly for the charge-neutral bromo derivatives: average of 2.19 Å for *t*-Bu$_2$P complexes vs. 2.15 Å for *i*-Pr$_2$P complexes. Moreover, the cationic adducts display consistently longer Ni-P distances relative to their charge-neutral bromo counterparts, particularly among the *i*-Pr$_2$P derivatives: average of 2.17 vs. 2.15 Å, respectively. Finally, the aromatic ring substituent(s) R appear to have some impact on the *i*-Pr$_2$P-Ni distances (range = 2.139-2.158 Å), whereas this impact is more muted in the cationic adducts (range = 2.168-2.179 Å). The smallest Ni-P distances (ca. 2.14 Å) were found in the bromo complex **6'** featuring the *m,m*-(*t*-Bu)$_2$ substituents; this observation was made previously and has been interpreted elsewhere.[11b] Additional bond distances and angles for cationic adducts reported in **Table 2.1** can be found in **Table A2.3** in « Annexe pour chapitre 2 ».

Most of the remaining Ni-X distances appear to be insensitive to the nature of the ring substituents. Thus, the Ni-C_{ipso} distances are essentially equal in all structures, whether cationic adducts or charge-neutral bromides (1.879(3)-1.890(2) Å). Quite uniform distances were also observed for Ni-N (1.871(3)-1.881(2) Å) and Ni-Br (2.312(1)-2.338(2) Å) bonds. The observed Ni-N and N≡C distances fall closer to the lower values in the range of distances available in the Cambridge Structural Database: ca. 1.88 vs. 1.71-2.51 Å for Ni-N and 1.14 vs. 0.91-1.69 Å for N≡C. The Ni-O distances of 3.9-5.4 Å are very long compared to the corresponding distances in complexes wherein the triflate anion is directly bound to the Ni(II) center (average of 2.05 Å);[50] we conclude that little or no covalent Ni-OSO_2CF_3 interactions are present in our cationic acetonitrile adducts.

2.3.3 IR analyses

The IR spectra recorded using solid samples of the cationic complexes showed the characteristic bands for ν(C≡N) (ca. 2329-2293 cm^{-1}), ν(SO) (ca. 1270, 1030 and 636 cm^{-1}), and ν(CF) (ca. 1135 cm^{-1}) (See **Table A2.4** in «Annexe pour chapitre 2»). Comparing the ν(C≡N) values in various complexes shows a fairly clear correlation between the electronic nature of ring substituents R and the C-N bond strength (**Table 2.2**). For instance, replacing the H at the *para* position of the central ring (with respect to the metalated *i*-C) by the electron withdrawing substituent CO_2Me increases the ν(C≡N) values by 32 cm^{-1} (**1** vs. **4**) or 22 cm^{-1} (**9** vs. **10**). The frequency shift, Δν(C≡N), observed on going from **1** to **5** was +5 cm^{-1}, which shows that the impact of Br is smaller in magnitude but in the same direction as that of CO_2Me.

In the case of adducts bearing the electron releasing substituents *p*-Me and *p*-OMe, the impact on ν(C≡N) was similarly small in magnitude but in the opposite direction: Δν(C≡N) = -3 cm^{-1} in **2** and -4 cm^{-1} in **3**. Moreover, the same types of frequency shift result from substitution at the *m*-position, but in this case the electron releasing substituent OMe leads to a larger impact than its electron withdrawing counterpart CO_2Me: Δν(C≡N) = -13 cm^{-1} in **7** and +6 cm^{-1} in **8**. Finally, the fairly small impact of the two *t*-Bu substituents in adduct **6** (Δν(C≡N) = -3 cm^{-1}) should be interpreted more cautiously, because it likely is a composite of the steric and electronic effects of these substituents.[51]

Table 2.2 ν(C≡N) data for **1-10**, related complexes, and free MeCN

Complex	ν(C≡N) (cm^{-1})	Δν(C≡N) (cm^{-1})[c]
[(H-POCOP$^{i\text{-Pr}}$)Ni(NCMe)][OSO_2CF_3], **1**[a]	2297 (2292)[b]	45 (40)[b]
[(*p*-Me-POCOP$^{i\text{-Pr}}$)Ni(NCMe)][OSO_2CF_3], **2**	2294	42
[(*p*-OMe-POCOP$^{i\text{-Pr}}$)Ni(NCMe)][OSO_2CF_3], **3**	2293	41
[(*p*-CO_2Me-POCOP$^{i\text{-Pr}}$)Ni(NCMe)][OSO_2CF_3], **4**	2329	77
[(*p*-Br-POCOP$^{i\text{-Pr}}$)Ni(NCMe)][OSO_2CF_3], **5**	2302	50
[(*m,m-t*-Bu_2-POCOP$^{i\text{-Pr}}$)Ni(NCMe)][OSO_2CF_3], **6**	2294	42
[(*m*-OMe-POCOP$^{i\text{-Pr}}$)Ni(NCMe)][OSO_2CF_3], **7**	2284	32
[(*m*-CO_2Me-POCOP$^{i\text{-Pr}}$)Ni(NCMe)][OSO_2CF_3], **8**	2303	51
[(H-POCOP$^{t\text{-Bu}}$)Ni(NCMe)][OSO_2CF_3], **9**	2293	41
[(*p*-CO_2Me-POCOP$^{t\text{-Bu}}$)Ni(NCMe)][OSO_2CF_3], **10**	2315	63
[(H-$POC_{sp3}OP^{iPr}$)Ni(NCMe)][OSO_2CF_3] [a]	2284	32
[(H-PCP^{iPr})Ni(NCMe)][BPh_4] [a]	2282	30
[(H-$PC_{sp3}P^{iPr}$)Ni(NCMe)][BPh_4] [a]	2274	22
[(H-POCOP^{Ph})Ni(NCMe)][OSO_2CF_3] [a]	2297	45
[(H-POCOP^{iPr})Ni(NCCH=CH_2)][OSO_2CF_3] [a]	2257	
[(H-$POC_{sp3}OP^{iPr}$)Ni(NCCH=CH_2)][OSO_2CF_3] [a]	2252	

a) Previously reported complexes.[24a, 24b, 35b, 52] b) For complex **1**, the ν(CN) values in parentheses were measured using KBr pellets to provide a comparison to the solid-state ATR measurements used in the discussion. c) Δν(CN) is relative to the free MeCN stretching frequency (2252 cm^{-1}) measured under our experimental conditions.

The observed correlation between ν(C≡N) values and the POCOP ring substituents R can be rationalized in terms of the MO description of bonding in acetonitrile, as follows. Similarly to CO, acetonitrile's HOMO possesses a certain degree of antibonding character with respect to the C≡N bond, such that σ-donation from this HOMO to a Ni-based acceptor orbital should reinforce the C-N bond and increase the value of ν(C≡N).[53] This phenomenon is underlined by the observation that in all the acetonitrile adducts the C≡N stretching frequency is much higher than that of free acetonitrile (2252 cm^{-1}), consistent with a net transfer of charge from acetonitrile to the Ni center.

It follows then that ν(C≡N) values in the adducts examined here should reflect the approximate electron donating character of R-POCOP ligands, those with electron withdrawing

substituents allowing greater MeCN→Ni donation and showing higher ν(C≡N) values, and vice versa. This is reflected in plots of the ν(C≡N) stretching frequencies for complexes **1-10** and the σ_m or σ_p Hammett coefficients for the corresponding ring substituents R (**Figures A2.9-2.11**). Moreover, it stands to reason that the degree of electron donation from RCN to the electrophilic Ni center should be fairly proportional to its degree of activation toward nucleophiles. Hence, ν(C≡N) values can help estimate the degree of nitrile activation toward outer-sphere nucleophilic attacks either at the nitrile carbon, as in amidination,[34, 54] or at the R moiety as in Michael-type hydroamination of acrylonitrile and its substituted derivatives.[24a, 24b, 35b, 55]

The above arguments can be extended to other structural parameters in $[(\text{pincer})\text{Ni}(\text{NCR})]^+$ and their impact on ν(C≡N) values. For instance, changing the ligand backbone from an aromatic to an aliphatic skeleton has a significant effect on ν(C≡N) as seen from the values for **1** (2297 cm^{-1}) and its $POC_{sp3}OP$ counterpart $[(\text{H-POC}_{sp3}\text{OP}^{i\text{Pr}})\text{Ni}(\text{NCMe})][OSO_2CF_3]$ (2284 cm^{-1}).[24b] A similar influence is exerted by the nature of the PR'_2 moiety: replacing the phosphinite moiety by a better net donor phosphine moiety (P-O vs $P\text{-}CH_2$ connections) leads to a significant decrease in ν(C≡N) values from 2297 cm^{-1} in **1** to 2282 cm^{-1} in its PCP analogue $[(\text{H-PCP}^{i\text{Pr}})\text{Ni}(\text{NCMe})][BPh_4]$.[24a] A further decrease in the ν(C≡N) value to 2274 cm^{-1} is observed in the aliphatic $PC_{sp3}P$ analogue $[(\text{H-PC}_{sp3}\text{P})\text{Ni}(\text{NCMe})][BPh_4]$.[24a] These observations are consistent with lower net donation from MeCN to Ni ligated by strong donor ligands.

The influence of *P*-substituents R' on ν(C≡N) values can be discerned from a comparison among the following two series of complexes: $[(\text{H-POCOP}^{\text{Ph}})\text{Ni}(\text{NCMe})][OSO_2CF_3]$ [35b] vs $[(\text{H-POCOP}^{i\text{-Pr}})\text{Ni}(\text{NCMe})][OSO_2CF_3]$ (**1**) vs $[(\text{H-POCOP}^{t\text{-Bu}})\text{Ni}(\text{NCMe})][OSO_2CF_3]$ (**9**); $[(p\text{-}CO_2\text{Me-POCOP}^{i\text{-Pr}})\text{Ni}(\text{NCMe})][OCO_2CF_3]$ (**4**) vs $[(p\text{-}CO_2\text{Me-POCOP}^{t\text{-Bu}})\text{Ni}(\text{NCMe})]$ $[OSO_2CF_3]$ (**10**). This comparison confirms that for both of these series the observed correlation is in line with the anticipated donor strength of the different *P*-substituents, i.e., Ph < *i*-Pr < *t*-Bu for the first series and *i*-Pr < *t*-Bu for the second.[56] On the other hand, the *t*-Bu_2P complexes display the longest Ni-P distances (2.195(1) Å in **9** vs 2.173(1) Å in **1**; 2.1928(8) Å in **10** vs. 2.1723(8) Å in **4**), which should normally lead to poorer orbital overlap between the Ni center and the bulky *t*-Bu_2P moiety, less efficient P→Ni donation, and hence more electrophilic Ni centers in **9** and **10**. However, the opposite scenario is implied by the IR data. We have further probed this issue through cyclic voltammetry measurements and, as will be discussed below, the redox potentials of these

complexes tend to contradict the implications of ν(C≡N) values for adducts **9** and **10**. Furthermore, correlation between the IR data and the C≡N bond length difference as seen by X-ray diffraction of single crystals is not possible because the difference in that bond length between the complexes are all within the range of their esd, and thus are of the same length.

2.3.4 NMR studies

Table A2.5 lists the pertinent ^{31}P, ^{1}H, and ^{13}C NMR data for complexes **1-10**, and the relevant spectra are shown in **Figures A2.13-2.51** . The ^{31}P NMR spectra show a rather narrow chemical shift range, ca. 192-196 ppm for **1-8** and ca. 198-200 ppm for **9** and **10**, indicating that the ring substituents do not influence ^{31}P δ values significantly. To be sure, the electron withdrawing substituents CO_2Me and Br seem to lead to downfield ^{31}P chemical shifts relative to the parent complex **1**, but no clear trend is evident with electron releasing substituents in any of the spectra. The parent compound **1** and its symmetrically substituted analogues **2-6**, **9**, and **10** show a singlet, whereas the unsymmetrical complex **7** shows the anticipated doublet of doublets for the two chemically inequivalent ^{31}P nuclei (see Fig. S37 SI). Complex **8**, the only other compound in the series bearing an unsymmetrically substituted POCOP ligand, shows a ^{31}P singlet instead of the anticipated AB signals (see Fig. S43 in SI); this is presumably because the difference in the chemical shifts of the two inequivalent ^{31}P nuclei is smaller than the resolution of the spectrum. The ^{13}C NMR spectra of **7** and **8** showed ABX signals for the methyne carbon nuclei, giving an apparent dt for **7** and a partially resolved dd for 8. (See **Figures A2.38 and A2.42**)

2.3.5 Absorption spectra

The UV-vis spectra of complexes **1'-10'** and **1-10** were recorded in dry CH_2Cl_2 (ca. 10^{-4} M solutions). The wavelengths and molar absorptivity of all complexes are tabulated in Table S2.6 in SI, and the spectra of complexes **1-10** and **1'**, **3'** and **4'** are shown in Figure 2.4. The low energy bands (370-420 nm) display low intensities and appear fairly indifferent to the nature of ring substituents, implying that they are likely spin-allowed but Laporte-forbidden d-d transitions. Conversely, the bands in the 300-350 nm region that are most affected by the nature of the ring

substituent likely represent π⟶π* transitions. For instance, the λ_{max} for complex **4** bearing the *p*-CO_2Me substituent is at 341 nm, 12-16 nm higher than those of the unsubstituted complex **1** and the complexes **2** and **3** bearing electron releasing substituents. This observation can be rationalized by the fact that electron-withdrawing groups stabilize the charge build-up in the excited state better than would electron-donating groups, thus lowering the π⟶π* transition energy and leading to a red shift.[11b] In other words, ligands bearing the most effective electron-accepting ring-substituent should exhibit lower energy $\pi \longrightarrow \pi^*$ transitions. A similar phenomenon is at work for the MLCT transition in the complexes. As shown in Figure 4 and Table S2.6 in SI, the MLCT transitions of the charge neutral bromide complexes feature molar absorptivities and wavelengths that are very similar to those of cationic acetonitrile adducts.

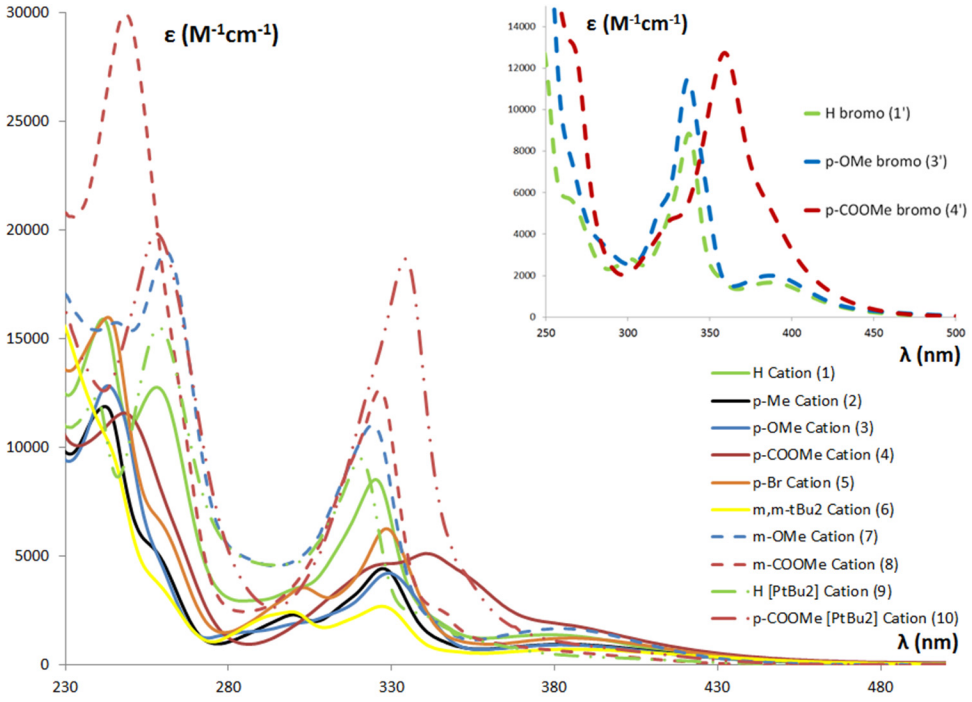

Figure 2.4 UV-Vis spectra of cationic complexes 1-10 in full, dashed and "dash dot dot" lines, and of complexes **1', 3', 4'** in dashed lines for comparison**.**

The spectra were recorded in air, using 10^{-4} M CH_2Cl_2 solutions.

2.3.6 Electrochemical studies

For the cationic adducts under study, another indication of how POCOP ring or *P*-substituents affect the electron density of the Ni center can be extrapolated from their redox potentials. We have conducted cyclic voltammetry measurements on the charge-neutral bromo complexes **1'-10'** and the cationic acetonitrile adducts **1-10** and the results are reported in **Table 2.3**; the cationic adducts are presented in **Figures A2.52-2.63**. Most complexes displayed irreversible oxidation, whereas complexes **3**, **6** and **7** displayed quasi-reversible behavior, presumably because the substituents *m,m*-*t*-Bu_2 and *p*- and *m*-OMe stabilize the Ni center sufficiently to prevent decomposition during the $Ni^{II} \rightarrow Ni^{III}$ oxidation event. The redox potentials obtained from these measurements (calibrated against the Cp_2Fe/Cp_2Fe^+ redox couple) are listed in Table 2.3 and plotted against Hammett coefficients for the *para* and *meta* substituents (**Figure A2.64**).

The electrochemical measurements reveal the following order of oxidation potential for [(R-POCOP$^{R'}$)Ni(NCMe)][OSO_2CF_3] as a function of both ring substituent R and *P*-substituent R' : *p*-CO_2Me [*t*-Bu_2P] (**10**) > H [*t*-Bu_2P] (**9**) > *p*-CO_2Me (**4**) > *m*-CO_2Me (**8**) > *p*-Br (**5**) > H (**1**) > *p*-Me (**2**) > *m,m*-*t*-Bu_2 (**6**) > *m*-OMe (**7**) > *p*-OMe (**3**). If we focus on the *i*-Pr_2P complexes, the observed order of oxidation potentials is consistent with the anticipated electronic impact of the aromatic-ring substituents. This trend shows some similarities to the corresponding tend in ν(C≡N) stretching frequencies (**4** > **8** > **5** > **1** > **2**), but there are also significant differences. The most striking differences between these two trends lie primarily in the positions of the *t*-Bu_2P containing complexes **9** and **10**. It is conceivable that the steric bulk of the *t*-Bu_2P moieties constrains the acetonitrile moiety in a configuration that would reduce orbital overlap of the nitrogen atom with the nickel center, thus lowering the ν(C≡N) values compared to their *i*-Pr_2P analogues.

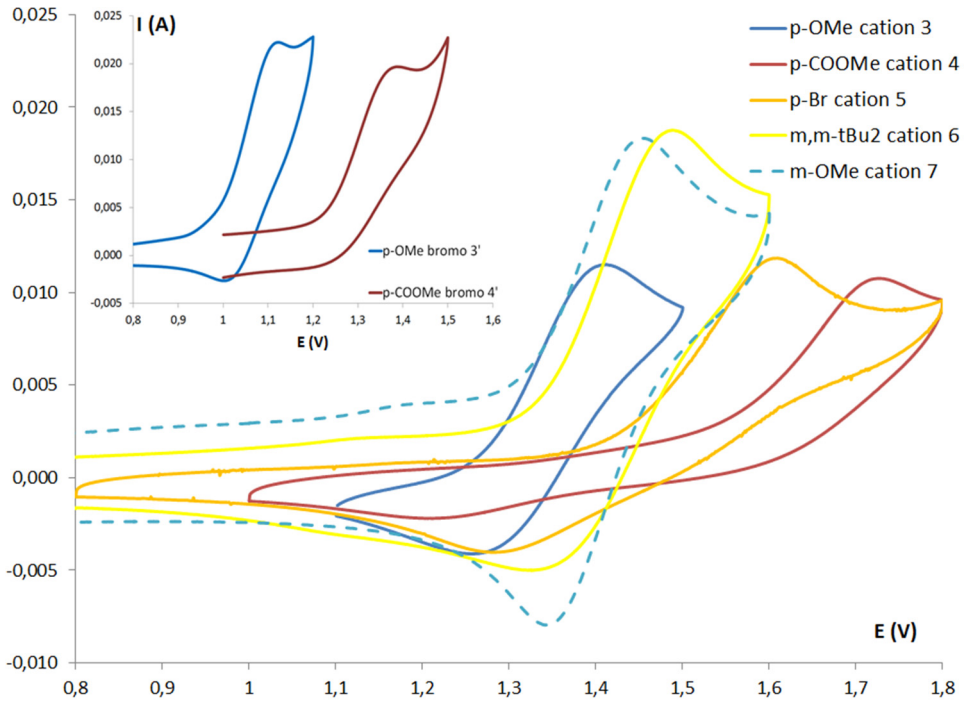

Figure 2.5 Cyclic voltammograms of **3-7, 3'** and **4'.**

The measurements were carried out at 298K using dry CH_2Cl_2 solutions containing equimolar quantities of the given complex and $[Bu_4N][PF_6]$ as electrolyte (10^{-4} M). Prior to beginning the measurements, the samples were purged for 2 min by bubbling a stream of N_2, and a nitrogen atmosphere was maintained over the samples throughout the measurements. A scan rate of 100 mV s^{-1} was used, and the potentials were referenced to the Cp_2Fe/Cp_2Fe^+ redox couple.

Table 2.3 Redox potentials of 1-10 and 1'-10'[a]

Complex	E_{ox} or $E_{1/2}$ (mV)	Complex	E_{ox} or $E_{1/2}$ (mV)
1[b]	1168	1'[b]	817
2	1151	2'[b]	692
3	933 (922)	3'[b]	560 (572)
4	1269	4'[b]	776
5	1159	5'	738
6	1012 (997)	6'[b]	567
7	977 (967)	7'[b]	761 (715)
8	1262	8'[b]	900
9	1298	9'[b]	800 (750)
10	1457	10'[b]	920 (860)

a) $E_{½}$ values are given for quasi-reversible redox couples. See caption of **Figure 2.5** for measurement details. b) Previously reported complexes[24b,11b] for which the redox values were re-measured in the current experimental conditions.

Another insight provided by the oxidation potentials shown in **Table 2.3** pertains to the impact of *P*-substituents on the electronic density of the metal center: the *t*-Bu_2P analogues **9** and **10** have higher oxidation potentials than their *i*-Pr_2P counterparts, implying that among the cationic acetonitrile adducts the supposedly better donor *t*-Bu substituents seem to decrease instead the electron density on the Ni center. A similar phenomenon has been observed in previous studies and has been attributed to the longer Ni-P distances with the sterically larger *t*-Bu_2P moieties.[39h] Inspection of the Ni-P distances in our complexes supports this assertion: the Ni-P(*t*-Bu)$_2$ bond distance is significantly longer than Ni-P(*i*-Pr)$_2$ in every case both for the cationic adducts and the charge-neutral bromo species. On the other hand, this phenomenon appears to be more complex, because the charge-neutral bromo complexes represent a less clear-cut scenario: complexes **10'** and **4'** show the oxidation potential order observed for their cationic analogues, whereas **9'** and **1'** show the opposite order. Evidently, more studies are required to develop a better understanding of this phenomenon.

Finally, the overall charge of the complexes seems to be a significant factor in the oxidation potential of the complexes studied here: all cationic adducts are more difficult to oxidize than their neutral bromo counterparts. We note also that oxidation potential trends are maintained regardless of the overall charge. In the *i*-Pr_2P series, for instance, the same oxidation potential trend is seen with the charge-neutral and cationic complexes bearing the following ring substituents: *p*-CO_2Me > *m*-CO_2Me > H > *p*-Me > *m*-OMe > *p*-OMe. The same is also true for the two remaining cases, *p*-Br > *m,m*-*t*-Bu_2, as well as for the two *t*-Bu_2P complexes (*p*-CO_2Me > H).

2.3.7 Oxydation studies with $FeCp_2$

As alluded to above, the values of redox potentials were calibrated against the redox couple for ferrocene. This was done at the end of the CV measurements by adding $FeCp_2$ to the sample solution and measuring the $FeCp_2/FeCp_2^+$ redox couple under the conditions of the measurement in question. Cyclic voltammograms of complexes **2** and **4** with added $FeCp_2$ are shown in **Figures A2.53 and A2.56**. We were surprised to note a dramatic color change, from pale yellow to black/dark green, upon addition of ferrocene to some of our cationic adducts. The rate of this color change varied from almost instantaneous to over minutes on ca. 10^{-4} M solutions. In addition, the

CV traces of samples containing ferrocene also showed multiple redox features (see for instance **Figures A2.53 and A2.56**). These observations prompted us to investigate the chemical reaction at its origin.

We began our investigation by examining those samples that did not appear to display this color change. Tests showed in fact that the same color change took place instantaneously when $FeCp_2$ was added to more concentrated solutions of these complexes. For instance, addition of 1.0 equiv of $FeCp_2$ to yellow 20-30 $\times$ 10^{-4} M $CDCl_3$ solutions of all cationic adducts (i.e., > 20 times more concentrated than the samples used for CV measurements) led to immediate formation of a dark solution. Analysis of the resulting solution by ^1H NMR showed that the characteristic singlet resonance for the Cp protons of $FeCp_2$ (at 4.17 ppm) was absent from the spectrum. In addition, the spectrum displayed a number of ligand signals as well as a new signal that was very broad ($LW_{1/2}$ ~500 Hz) and showed a variable intensity corresponding to between 4 to 7 protons depending on sample. The chemical shift of this new signal was also quite variable from one sample to another (10-6 ppm region), hinting that it might represent a paramagnetic species. Significantly, no reaction was apparent between the neutral bromide complexes **1'-6'** and one or more equivalents of $FeCp_2$, confirming that the observed reaction takes place with the more electrophilic cationic adducts. These observations seemed to point to a redox interaction taking place between ferrocene and our cationic adducts. Rest potential measurements (undertaken with and without added ferrocene) confirmed the likelihood of the proposed redox reaction (see **Figure A2.65 and Table A2.7**). Another piece of evidence supporting this proposal was furnished by the isolation of the oxidized species from a NMR sample, as follows: slow evaporation of a $CDCl_3$ solution containing the cationic adduct **3** and 2 equiv of ferrocene gave an amorphous green powder containing orange and dark-red crystals that were identified by X-ray crystallography as Cp_2Fe and $[Cp_2Fe][OTf]$, respectively.

The observed oxidation of ferrocene by our cationic Ni(II) complexes requires the concomitant reduction of the latter into charge-neutral, monovalent species; unfortunately, however, we have not succeeded in identifying the monovalent Ni product of the proposed redox reaction. Indeed, the following observation has indicated that the Ni-containing species might in fact be diamagnetic: the amorphous dark green solid obtained from the mixture of **8** and ferrocene showed a new ^{31}P NMR signal ($LW_{½}$ = 217 Hz) ca. 1-2 ppm upfield of the signal for the starting

material.[57] This would rule out the formation of paramagnetic monomers of the type (R-POCOP$^{R'}$)Ni(NCMe). In conclusion, the fate of the Ni-containing species remains obscure at this point, but investigations are in progress to shed more light on this unexpected outcome.

2.3.8 Ligand-exchange studies

Previous reports in the context of Michael-type hydroamination of acrylonitrile promoted by pincer-Ni species have shown that the K_{eq} for the equilibrium [(PCP^{iPr})Ni(NCMe)][BPh$_4$] ⇆ [(PCP^{iPr})Ni(NCCHCH$_2$)][BPh$_4$] is near unity.[39a] This is an important consideration when discussing the mechanism of this catalytic reaction, because both the substrates and products feature nitrile moieties and their competitive binding can have an impact on catalytic turn-over rates. On the other hand, in the context of Ni-catalyzed nitrile amidinations, the in-situ generated amidine products are much more strongly donor ligands relative to nitrile substrates, a phenomenon that can lead to product inhibition, especially during the later phases of the catalytic process. Thus, in cationic adducts [(pincer)NiL][OSO$_2$CF$_3$] the kinetic lability of the Ni-L moiety can influence catalytic turnover rates.

In contrast to the above cases involving the substitution of neutral donors L in [(pincer)NiL][OSO$_2$CF$_3$] by other neutral donors L', little is known about the substitutional lability of the corresponding Ni-X bond in the charge-neutral species (pincer)NiX (X= halides, OR, NR$_2$, etc.). We know, of course, that halide exchange by other halides or pseudo-halides is possible in the presence of excess salts MX', and that this type of exchange is usually more facile in polar solvents. We also know that halides can be displaced by charge-neutral nucleophiles L, but in most cases this is a less facile exchange that normally requires abstracting agent such as Ag^+.

The question arose: what about halide/L exchange involving two complexes, a charge-neutral Ni-halide species and its cationic Ni-L analogue, L$_1$NiX + [L$_2$NiL]$^+$ ⇆ [L$_1$NiL]$^+$ + L$_2$NiX ? Although such ligand X/L exchanges are rarely considered, they can play a potentially important role in ionization of M-X moieties during catalytic reactions, thus affecting catalytic efficacy by creating resting states or dormant species. To shed some light on this issue, we have examined the ionization of the charge-neutral bromo species (R-POCOP^{i-Pr})NiBr in the presence of their cationic acetonitrile adducts [(R-POCOP^{i-Pr})Ni(NCMe)][OSO$_2$CF$_3$], as depicted in **equation 2.1**. An

interesting question to probe is whether the lability of the Ni-Br bond can be modulated by the nature of the POCOP ring substituent R.

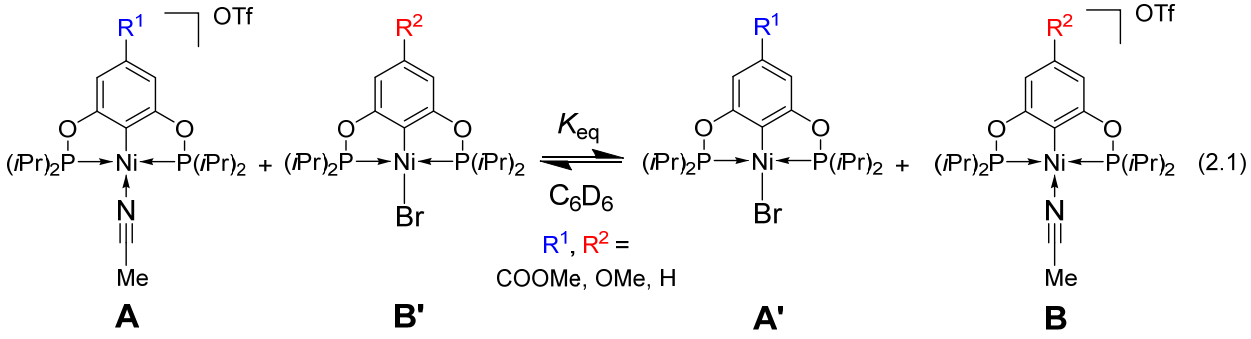

Table 2.4 Equilibrium ligand exchange as per **equation 2.1.**

Entry	**A** (R^1)	**B'** (R^2)	K_{eq} (± 0.1)
1	**1** (H)	**1'** (H)	1.0
2	**4** (*p*-CO_2Me)	**4'** (*p*-CO_2Me)	1.1
3	**3** (*p*-OMe)	**3'** (*p*-OMe)	1.1
4	**3** (*p*-OMe)	**4'** (*p*-CO_2Me)	0.3
5	**4** (*p*-CO_2Me)	**3'** (*p*-OMe)	2.8
6	**4** (*p*-CO_2Me)	**1'** (H)	1.9
7	**1** (H)	**4'** (*p*-CO_2Me)	0.6
8	**1** (H)	**3'** (*p*-OMe)	1.5
9	**3** (p-OMe)	**1'** (H)	0.8

Experimental conditions: 1H NMR spectra were recorded for two equimolar C_6D_6 solutions of A(R^1) and B′(R^2) each containing 2 equiv of dodecane as an internal standard (total volume of each sample: 750 µL). The samples were then combined in one NMR tube and subjected to repeated ^{1}H NMR measurements over a 25 min interval. The K_{eq} values were determined based on the integration of the aromatic region signals with respect to the dodecane signals.

The predicted observation of near unity K_{eq} values obtained for the exchange of precursors **A** and **B'** bearing the same substituents R (**Table 2.4**: entries 1, 2, and 3) served to confirm the reliability of the methodology. Inspection of the remaining data shows that the smallest K_{eq} value is obtained for the exchange of **4'** and **3** (entry 4), i. e., when the bromo species bears an electron-withdrawing substituent R^1 and the cationic adduct bears an electron-donating substituent R^2. Conversely, the largest K_{eq} value is obtained from the exchange of **4** and **3'** (entry 5), i.e., when the cationic adduct bears an electron-withdrawing substituent R^1 and the bromo species bears an electron-donating substituent R^2. These observations can be rationalized by considering that the

more labile acetonitrile moiety should be found in the cationic complex bearing an electron-withdrawing substituent, and vice versa. This explanation is also consistent with the observations that the second largest K_{eq} value involves the exchange of **4** (entry 6), whereas the second smallest K_{eq} value involves the exchange of **4'** (entry 7). Finally, that the exchange of **3'** and **1** (entry 8) results in a greater K_{eq} than that of **1'** and **3** (entry 9) further supports the above rationale.

We put the above rationale to test by studying the exchange of one of our electron-poor POCOP-based cationic adducts against a much more electron-rich charge-neutral bromo species, namely van Koten's (NCN)Ni-Br (**Scheme 2.2**).[58] Exchange of the latter with complex **8** (R^2= *m*-CO_2Me) led to an instantaneous reaction and gave a white precipitate. Analysis of the reaction mixture by ^{31}P NMR and ^{1}H NMR showed that the main product (~82%) was the charge-neutral bromide **8'** (two doublets at 190.43 and 192.12 ppm; J_{PP} = 323 Hz), confirming the facile ligand exchange between the starting materials (See Fig. S66 and S67 in SI). The reaction also generated side-products that displayed two apparent doublets; we believe that the latter represent the two central lines of poorly resolved AB signals, as follows. The first of these side-products displays two poorly resolved signals at 190.3 and 190.2 ppm, similar to the two peaks at 191.137 and 191.225 ppm in Figure S66 in SI; this species (~18% relative intensity) was later identified as the charge neutral triflate species (*m*-CO_2Me-POCOP)Ni-OTf (see below). The other side-product displays two poorly resolved signals at 187.9 and 187.8 ppm (~2% relative intensity) and remains unidentified. The observed white precipitate was identified as the cationic complex [(NCN)Ni(NCMe)][OSO_2CF_3] based on its characteristic ^{1}H NMR signal at 0.66 ppm for the coordinated acetonitrile.[59]

Next we studied another ligand exchange equilibrium involving the bromo complex ($PC_{sp3}P^{i\text{-}Pr}$)Ni-Br, a species for which the oxidation potential is lower than the values recorded for the POCOP systems **1-10**, but higher than that of van Koten's (NCN)Ni-Br. ^{31}P NMR analysis of a 1:1 mixture of ($PC_{sp3}P^{i\text{-}Pr}$)Ni-Br and the cationic adduct **8** showed the rapid establishment of an equilibrium mixture of 5 species, as shown in **Scheme 2.2** (see **Figure A2.68**). The assignment of the ^{31}P signals for (*m*-CO_2Me-POCOP)Ni-OTf was confirmed by adding to the reaction mixture an in-situ generated sample from **8'** and AgOTf, as well as by adding a substoichiometric amount of AgOTf to the reaction mixture, which led to an increase in intensity of two signals for the triflate complexes (See **Figure A2.69** for the **s**pectrum with added AgOTf).[59]

Scheme 2.2 Ligand exchange reaction between **8** and ($PC_{sp3}P$)Ni-Br

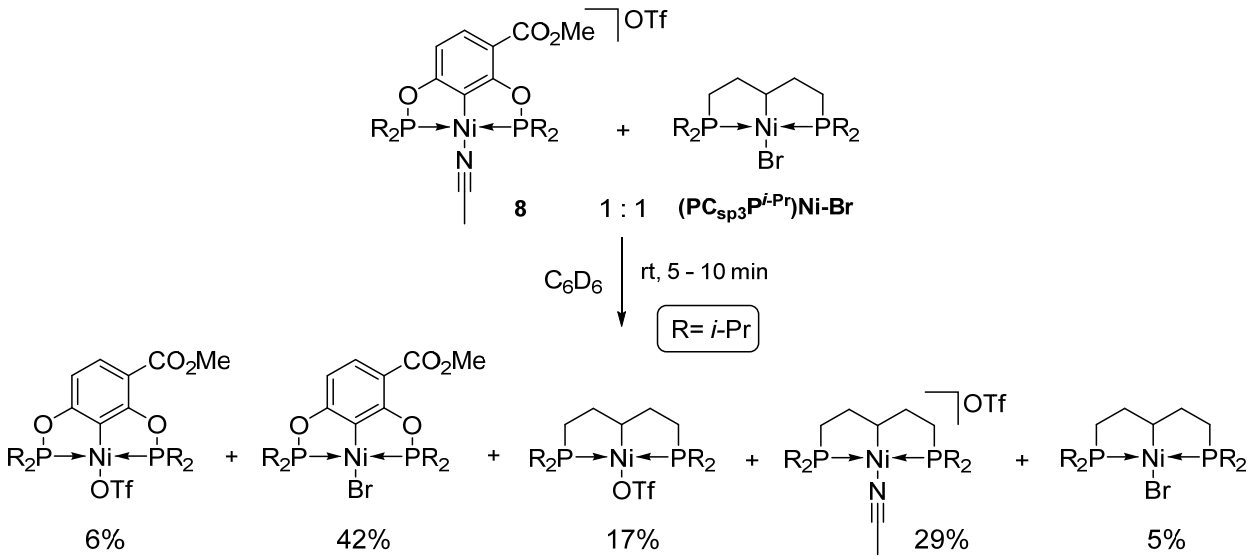

The above observations establish that MeCN/Br^- ligand exchange between (R-POCOP$^{i\text{-}Pr}$)NiBr and [(R'-POCOP$^{i\text{-}Pr}$)Ni(NCMe)][OSO_2CF_3] takes place readily when the difference in the electronic proprieties of the aromatic ring substituents R and R' is relatively small (entries 8 or 9). It is also noteworthy that the ligand exchange occurs in preference over other possible reactions. For instance, no redox reaction took place when we combined a very electron poor complex such as [(*m*-CO_2Me-POCOP$^{i\text{-}Pr}$)Ni(NCMe)][OSO_2CF_3] (**8**) and a very electron-rich complex such as van Koten's (NCN)NiBr. A less electron-rich system also gives the ligand exchange, with two of the species being charge-neutral triflate derivatives.

2.4 Conclusions

This study has resulted in a number of interesting observations regarding the synthesis and stabilities of [(R-POCOP$^{R'}$)Ni(NCMe)][OSO_2CF_3], and has allowed us to study the impact of substituents R and R' on the electrophilicity of the Ni center as reflected in ν(C≡N) values, redox potentials, and K_{eq} values for ligand exchange reactions with charge-neutral bromo complexes. The IR and CV measurements have confirmed the important influence of both *P*- and ring substituents on the electrophilicity of the Ni center in **1-10**. Both parameters show, for instance, that the most electrophilic adducts feature the *p*-CO_2Me substituent, but the redox potentials

indicate that the Ni center ligated by *m*-CO_2Me-POCOP$^{i\text{-Pr}}$ is nearly as electrophilic. Indeed, the two sets of data lead to different conclusions regarding the electron density on Ni in the case of *t*-Bu_2P-based adducts: according to ν(C≡N) values, the Ni center is less electrophilic in [(*p*-CO_2Me-POCOP$^{t\text{-Bu}}$)Ni(NCMe)][OSO_2CF_3] (**10**) compared to its *i*-Pr_2P analogue, i.e., the *t*-Bu_2P moiety is a stronger net donor, whereas the opposite conclusion is suggested by the redox potentials. Of course, the ν(C≡N) values were measured on solid samples, whereas the redox potentials are obtained from solutions; moreover, the fact that the redox events are irreversible in most cases (and certainly for the adducts bearing CO_2Me substituents) require us to treat the implications of the electrochemical data with caution.

The ligand exchange equilibrium studies demonstrated that coordinated acetonitrile ligands can be displaced by bromide and (to a lesser degree) triflate anions, and this substitution is more facile for the more electrophilic Ni center. This result indicates that the catalytic activities of cationic RCN adducts (e.g., acrylonitrile in hydroamination reactions or nitriles in amidination reactions) might be compromised in the presence of halides (used as "additives" in some settings) or other in-situ generated anionic species (e.g., deprotonated amines or alcohols).

Finally, the present study revealed an unexpected side reaction between the cationic acetonitrile adducts and $FeCp_2$, presumably a redox reaction giving what we believe is a trivalent iron product. This intriguing possibility will be the subject of future investigations. We will also probe the catalytic reactivities of the cationic adducts **1-10** for hydroamination of acrylonitrile and its substituted derivatives, as well as for related transformations involving outer-sphere nucleophilic attack on the CN moiety (e.g., amidination and amidation).

2.5 Experimental section

2.5.1 General procedures

Unless otherwise indicated, all manipulations were carried out under a nitrogen atmosphere using standard Schlenk and glovebox techniques. The solvents were dried by passage over activated alumina contained in MBRAUN-SPS systems and analyzed by a Coulorimetric Karl Fischer titrator to acceptable water content. Triethylamine was dried by distillation over CaH_2. The

following reagents and NMR solvents were purchased from Sigma-Aldrich and used without further purification: nickel powder, bromine, ClP(*i*-Pr)$_2$, ClP(*t*-Bu)$_2$, resorcinol, orcinol, 5-methyl-1,3-benzenediol, methyl 3,5-dihydroxybenzoate, methyl 2,4-dihydroxybenzoate, 4,6-di-*tert*-butylresorcinol, ferrocene, silver trifluoromethanesulfonate, C_6D_6 and $CDCl_3$. 5-methoxyresorcinol was purchased from Chemsavers and used as received. 4-Methoxyresorcinol has been synthesized following a published procedure.[60] The precursor bromo complexes **1'-4'** and **6'-10'** were prepared following a previously reported procedure.[11b]

NMR spectra were recorded using the following Bruker spectrometers: AV300, AVII400, and AV500. Chemical shift values are reported in ppm (δ) and referenced internally to the residual solvent signals (^{1}H and ^{13}C: 7.26 and 77.16 ppm for $CDCl_3$; 7.16 and 128.06 ppm for C_6D_6) or externally (^{31}P, H_3PO_4 in D_2O, $\delta = 0$). Coupling constants are reported in Hz. UV/Vis spectra were recorded on a Varian Cary 500i. The IR spectra were recorded on a Bruker Alpha-P FTIR (4000-400 cm^{-1}). The elemental analyses were performed by the Laboratoire d'Analyse Élémentaire, Département de Chimie, Université de Montréal. The absence of certain ^{13}C NMR signals corresponding to quaternary carbons in most spectra (such as N***C***Me or OSO$_2$***C***F$_3$ signals) is common, and are normally hard to detect, unless a very high concentration is used or a higher number of scans is done.

2.5.2 [{2,6-(*i*-Pr$_2$PO)$_2$-4-(Me)C$_6$H$_2$}Ni(NCMe)][OSO$_2$CF$_3$], 2.

To an aluminium-foil covered Schlenk flask containing **2'** (400 mg, 0.810 mmol, 1.00 equiv) in dry acetonitrile (20.0 mL) was added silver triflate (250 mg, 0.972 mmol, 1.20 equiv) at rt. The solution was then agitated for 3 h, filtered to remove the insoluble silver salts, evaporated, and the resulting solids extracted with dichloromethane (10.0 mL) and passed through a short Celite pad to remove the remaining traces of silver salts. Evaporation of the filtrate gave the desired product as a yellow solid (440 mg, 93 %). Single crystals suitable for x-ray diffraction were obtained by slow evaporation in air by layering a $CDCl_3$ solution with hexanes.

^{1}H NMR (400 MHz, $CDCl_3$): δ 1.34 (appq*, ^3J = 7, 12H, P(CHC(C***H***$_3$)$_2$)$_2$), 1.41 (appq, ^vJ = 8, 12H, P(CHC(C***H***$_3$)$_2$)$_2$), 2.23 (s, 3H, C$_{Ar}$C***H***$_3$), 2.42 (s(br), 3H, NCC***H***$_3$), 2.52 (sept, $^3J_{HH}$ = 7, 4H, P(C***H***C(CH$_3$)$_2$)$_4$), 6.28 (s, 2H, (C$_{Ar}$***H***$_{meta}$)$_2$). ^{31}P{^{1}H} NMR (202 MHz, $CDCl_3$) δ : 193.4 (s).

$^{19}F\{^{1}H\}$ NMR (282 MHz, $CDCl_3$): δ -78.06(s). $^{13}C\{^{1}H\}$ NMR (75 MHz, $CDCl_3$): δ 3.91 (s(br), 1C, NC***C***H_3), 16.87 (s, 4C, P(CH(***C***H_3)$_2$)$_2$), 17.68 (vt, $^{v}J_{PC}$ = 3, 4C, P(CH(***C***H_3)$_2$)$_2$), 21.66 (s, 1C, C_{Ar}***C***H_3), 28.52 (vt, $^{v}J_{PC}$ = 12, 4C, P(***C***$H(CH_3)_2)_4$), 107.18 (vt, $^{v}J_{PC}$ = 6, 2C, ***C_{Ar}***H), 142.55 (s, 1C, ***C_{Ar}***CH_3), 168.92 (vt, $^{v}J_{PC}$ = 9, 2C, (***C_{Ar}***$OP)_2$). IR (solid state, cm^{-1}): 636 (SO), 1030 (SO_3), 1141 (CF_3), 1262 (SO_3), 1464 ($C=C^{Ar}$), 1555 ($C=C^{Ar}$), 2294 (C≡N). UV-vis ((CH_2Cl_2, [1x10^{-4}M]); λ_{max}, nm (ε, $Lmol^{-1}cm^{-1}$) : 242 (11878), 300 (2302), 327 (2691), 386 (711). E-chem (NBu_4PF_6, 10^{-4}M in dry CH_2Cl_2, E_{ox} vs. $FeCp_2$): 1151 mV. Elemental analysis was not satisfactory for this complex, because it proved difficult to remove all traces of solvents. * appq refers to an apparent quartet signal resulting from two overlapping virtual triplets.

2.5.3 [{2,6-(*i*-$Pr_2PO)_2$-4-(OMe)C_6H_2}Ni(NCMe)][OSO_2CF_3], 3

The procedure described above for the preparation of **2** was used for this synthesis using **3'** (415 mg, 0.812 mmol, 1.00 equiv). The desired product was obtained as a yellow solid (415 mg, 84 %). Single crystals suitable for x-ray diffraction were obtained by slow evaporation in air of an acetone solution layered with hexanes.

^{1}H NMR (400 MHz, $CDCl_3$): δ 1.35 (appq, ^{v}J = 8, 12H, P(CHC(C***H_3***$)_2)_2$), 1.41 (appq, ^{v}J = 8, 12H, P(CHC(C***H_3***$)_2)_2$), 2.39 (s(br), 3H, NCC***H_3***), 2.52 (sept, $^{3}J_{HH}$ = 8, 4H, P(C***H***$C(CH_3)_2)_4$), 3.73 (s, 3H, OC***H_3***), 6.08 (s, 2H, (C_{Ar}***H_{meta}***$)_2$). $^{31}P\{^{1}H\}$ NMR (121 MHz, $CDCl_3$) δ : 191.6 (s). $^{19}F\{^{1}H\}$ NMR ($CDCl_3$, 282 MHz): δ -77.94 (s). $^{13}C\{^{1}H\}$ NMR (125 MHz, $CDCl_3$): δ 3.98 (s(br), 1C, NC***C***H_3), 16.82 (s, 4C, P(CH(***C***H_3)$_2$)$_4$), 17.61 (s(br), 4C, P(CH(***C***H_3)$_2$)$_2$), 28.52 (vt, $^{v}J_{PC}$ = 12, 4C, P(***C***$H(CH_3)_2)_4$), 55.67 (s, 1C, O***C***H_3), 93.22 (vt, $^{v}J_{PC}$ = 7, 2C, ***C_{Ar}***H), 163.47 (s, 1C, ***C_{Ar}***OCH_3), 169.31 (vt, $^{v}J_{PC}$ = 9, 2C, (***C_{Ar}***$OP)_2$). IR (solid state, cm^{-1}): 636 (SO), 1030 (SO_3), 1140 (CF_3), 1266 (SO_3), 1462 ($C=C^{Ar}$), 1561 ($C=C^{Ar}$), 2293 (C≡N). UV-vis ((CH_2Cl_2, [1x10^{-4}M]); λ_{max}, nm (ε, $Lmol^{-1}cm^{-1}$) : 243 (12834), 299 (1858), 329 (4214), 382 (912). E-chem (NBu_4PF_6, 10^{-4}M in dry CH_2Cl_2, E_{ox} vs. $FeCp_2$ [$E_{1/2}$ vs $FeCp_2$]): 933 mV [922 mV]. Anal. calcd. for $C_{22}H_{36}F_3NNiO_6P_2S$ (620.22): C, 42.60; H, 5.85; N, 2.26; S: 5.17. Found: C, 42.83; H, 5.85; N, 1.97 ; S, 5.20.

2.5.4 [{2,6-(*i*-$Pr_2PO)_2$-4-(CO_2Me)C_6H_2}Ni(II)(NCMe)][OSO_2CF_3], 4

The procedure described above for the preparation of **2** was used for this synthesis using **4'** (204 mg, 0.379 mmol, 1.00 equiv). The desired product was obtained as a yellow solid (189 mg, 81 %). Single crystals suitable for x-ray diffraction were obtained by slow evaporation in air of a dichloromethane solution layered with hexanes.

^{1}H NMR (300 MHz, $CDCl_3$): δ 1.38 (m, 24H, P(CHC(C***H***$_3$)$_2$)$_4$), 2.52 (s, 3H, NCC***H***$_3$), 2.57 (m, 4H, P(C***H***C(CH$_3$)$_2$)$_4$), 3.85 (s, 3H, C(O)OC***H***$_3$), 7.10 (s, 2H, C_{Ar}***H***). ^{31}P{^{1}H} NMR (161 MHz, $CDCl_3$) δ : 196.4 (s). ^{19}F{^{1}H} NMR ($CDCl_3$, 282 MHz): δ -78.17 (s). ^{13}C{^{1}H} NMR (75 MHz, $CDCl_3$): δ 4.18 (s(br), 1C, NC***C***H$_3$), 16.80 (s, 4C, P(CH(***C***H$_3$)$_2$)$_2$), 17.59 (vt, $^{v}J_{PC}$ = 3, 4C, P(CH(***C***H$_3$)$_2$)$_2$), 28.62 (vt, $^{v}J_{PC}$ = 11, 4C, P(***C***H(CH$_3$)$_2$)$_4$), 52.41 (s, 1C, O***C***H$_3$), 106.24 (t, J_{PC} = 7, 1C, ***C$_{ipso}$***Ni), 107.12 (vt, $^{v}J_{PC}$ = 6, 2C, ***C$_{Ar}$***H), 133.30 (s, 1C, ***C$_{Ar}$***C(O)OCH$_3$), 166.22 (s, 1C, C_{Ar}***C***(O)OCH$_3$), 168.85 (vt, $^{v}J_{PC}$ = 9, 2C, (***C$_{Ar}$***OP)$_2$). IR (solid state, cm^{-1}): 635 (SO), 1029 (SO_3), 1140 (CF_3), 1277 (SO_3), 1397 (C=C^{Ar}), 1550 (C=C^{Ar}), 1716 (C=O), 2329 (C≡N). UV-vis ((CH_2Cl_2, [1x10^{-4}M]); λ_{max}, nm (ε, Lmol^{-1}cm^{-1}): 248 (11577), 329 (4791), 341 (5111, 390 (1697). E-chem (NBu_4PF_6, 10^{-4}M in dry CH_2Cl_2, E_{ox} vs. $FeCp_2$): 1269 mV. Anal. calcd. for $C_{23}H_{36}F_3NNiO_7P_2S$ (648.24): C, 42.62; H, 5.60; N, 2.16; S: 4.95. Found: C, 43.10 ; H, 5.71 ; N, 1.98; S, 4.65.

2.5.5 [{2,6-(*i*-Pr$_2$PO)$_2$-4-(Br)C$_6$H$_2$}Ni(NCMe)][OSO$_2$CF$_3$], 5

The procedure described above for the preparation of **2** was used for this synthesis using **5'** (400 mg, 0.716 mmol, 1.00 equiv). The desired product was obtained as a yellow solid (412 mg, 86 %). Crystals suitable for diffraction studies were obtained by slow evaporation in air of a dichloromethane solution layered with hexanes.

^{1}H NMR (500 MHz, $CDCl_3$) : δ 1.32 (appq, ^{v}J = 9, 12H, P(CH(C***H***$_3$)$_2$)$_2$), 1.37 (appq, ^{v}J = 8, 12H, P(CH(C***H***$_3$)$_2$)$_2$), 2.37 (s(br), 3H, NCC***H***$_3$), 2.55 (sept, $^{3}J_{HH}$ = 7, 4H, P(C***H***(CH$_3$)$_2$)$_4$), 6.64 (s, 2H, C_{Ar}***H***). ^{31}P{^{1}H} NMR (161 MHz, $CDCl_3$) δ : 195.7 (s). ^{19}F{^{1}H} NMR (282 MHz, $CDCl_3$): δ -77.79 (s). ^{13}C{^{1}H} NMR (75 MHz, $CDCl_3$): δ 3.84 (s(br), 1C, NC***C***H$_3$), 16.76 (s, 4C, P(CH(***C***H$_3$)$_2$)$_2$), 17.57 (vt, $^{v}J_{PC}$ = 3, 4C, P(CH(***C***H$_3$)$_2$)$_2$), 28.58 (vt, $^{v}J_{PC}$ = 12, 4C, P(***C***H(CH$_3$)$_2$)$_4$), 110.01 (vt, $^{v}J_{PC}$ = 6, 2C, ***C$_{Ar}$***H$_{meta}$), 123.54 (s, 1C, ***C$_{Ar}$***Br), 168.93 (vt, $^{v}J_{PC}$ = 9, 2C, (***C$_{Ar}$***OP)$_2$). IR (solid state, cm^{-1}): 637 (SO), 1032 (SO_3), 1142 (CF_3), 1264 (SO_3), 1466 (C=C^{Ar}), 1554 (C=C^{Ar}), 2302 (C≡N). UV-

vis ((CH_2Cl_2, [1x10^{-4}M]); λ_{max}, nm (ε, Lmol^{-1}cm^{-1}) : 243 (15984), 303 (3547), 328 (6245), 386 (1221). E-chem (NBu_4PF_6, 10^{-4}M in dry CH_2Cl_2, E_{ox} vs. $FeCp_2$): 1159 mV. Anal. calcd. for $C_{24}H_{42}BrNNiO_5P_2S$ (655.08): C, 37.70; H, 4.97; N,2.08; S: 4.79 . Found: C, 37.79; H, 4.93; N, 2.04; S, 4.71.

2.5.6 {2,6-(*i*-Pr$_2$PO)$_2$-4-(Br)C$_6$H$_2$}NiBr, 5'

This compound was prepared by adapting a literature procedure.[49] In a 500 mL round-bottom flask containing 1-bromo-3,5-dimethoxybenzene (6.40 g, 29.5 mmol) was added HBr (100 mL) to which was attached a condenser under nitrogen. The heterogeneous solution was stirred and heated for 24 h at 120 °C. The solution was then cooled and treated with anhydrous $KHCO_3$ until the evolution of CO_2 ceased and a precipitate formed. The precipitate was filtered, washed with water, and dried in vacuum at 80 °C, yielding the known 5-bromoresorcinol as a pale pink solid (4.77 g, 85 %). A dry Schlenk flask charged in the glove box with 5-bromoresorcinol (1.00 g, 5.20 mmol in 50 mL) and chlorodiisopropylphosphine (1.77 mL, 11.1 mmol) was taken out of the box and to the contexts were added dry THF (50.0 mL) triethylamine (1.57 mL, 11.6 mmol). The mixture was stirred for 1 h at rt while the ammonium salt precipitated as a white solid. Evaporation, followed by extraction with dry hexane (50.0 mL) and evaporation gave the crude product as pale yellow oil (1.52 g, ca. 68 %). The ^{31}P NMR spectrum of this material showed it to contain the desired product as the major product, in addition to minor quantities of oxidized phosphines. Reaction of the crude sample of the ligand (1.52 g, ca. 3.61 mmol) with the nickel precursor $NiBr_2(NCCH_3)_2$ (1.30 g, 4.32 mmol) in dry THF (50 mL) and in the presence of dry triethylamine (0.630 mL, 4.69 mmol) gave a dark-green suspension. Stirring for 1 h at rt, followed by evaporation and extraction with dry hexane (50.0 mL) gave brown crystals of the desired product (1.21 g, 60 %) after crystallization in air.

^{1}H NMR (400 MHz, C_6D_6) : δ 1.08 ($_{app.}$q, ^vJ = 7, 12H, P(CH(C***H*****$_3$**)$_2$)$_2$), δ 1.32 (appq, ^vJ = 8, 12H, P(CH(C***H*****$_3$**)$_2$)$_2$), δ 2.16 (sept, $^3J_{HH}$ = 7, 4H, P(C***H***(CH$_3$)$_2$)$_4$), δ 6.80 (s, 2H, C_{Ar}***H***). ^{31}P {^{1}H} NMR (161 MHz, C_6D_6) : δ 190.8(s). ^{13}C{^{1}H} (75 MHz, C_6D_6): δ 16.61 (s, 4C, P(CH(***C***H$_3$)$_2$)$_2$), δ 17.69 (s, 4C, P(CH(***C***H$_3$)$_2$)$_2$), δ 28.24 (vt, $^vJ_{PC}$ = 11, 4C, P(***C***H(CH$_3$)$_2$)$_4$), δ 109.40 (vt, $^vJ_{PC}$ = 6, 1C, ***C$_{Ar}$***H$_{meta}$), δ 121.42 (s, 1C, ***C$_{Ar}$***Br), δ 169.20 (vt, $^vJ_{PC}$ = 10, 2C, (***C$_{Ar}$***OP)$_2$). UV-vis ((CH_2Cl_2, [1x10$^-$

^{4}M]); λ_{max}, nm (ε, mol^{-1}cm^{-2}): 266 (6360), 306 (2900), 341 (13600), 391 (2070). E-chem (NBu_4PF_6, 10^{-4}M in dry CH_2Cl_2, E_{ox} vs. $FeCp_2$): 738 mV. Anal. calcd. for $C_{18}H_{30}Br_2NiO_2P_2$ (558.88 g/mol): C, 38.68; H, 5.41. Found: C, 39.30; H, 5.59.

2.5.7 [{2,6-(*i*-Pr$_2$PO)$_2$-3,5-(*t*-Bu)$_2$C$_6$H}Ni(II)(NCMe)][OSO$_2$CF$_3$], 6

The procedure described above for the preparation of **2** was used for this synthesis using **6'** (407 mg, 0.686 mmol, 1.00 equiv). The desired product was obtained as a yellow solid (410 mg, 87 %). The crystals were obtained by slow evaporation in air of the solid dissolved in acetonitrile.

^{1}H NMR (300 MHz, $CDCl_3$): δ 1.29 (s, 18H, (C_{Ar}(C***H$_3$***)$_3$)$_2$), 1.31-1.42 (m, 24H, P(CHC(C***H$_3$***)$_2$)$_4$), 2.38 (s(br), 3H, NCC***H$_3$***), 2.55 (m(br), 4H, P(C***H***C(CH$_3$)$_2$)$_4$), 7.00 (s, 1H, C_{Ar}***H***). ^{31}P{^{1}H} NMR (161 MHz, $CDCl_3$) δ : 192.9 (s). ^{19}F{^{1}H} NMR ($CDCl_3$, 282 MHz): δ -78.04 (s). ^{13}C{^{1}H} NMR (75 MHz, $CDCl_3$): δ 4.22 (s, 1C, NC***C***H$_3$), 8.94 (s, 1C, N***C***CH$_3$), 16.97 (s, 4C, P(CH(***C***H$_3$)$_2$)$_2$), 17.62 (vt, $^{v}J_{PC}$ = 3, 4C, P(CH(***C***H$_3$)$_2$)$_2$), 28.43 (vt, $^{v}J_{PC}$ = 12, 4C, P(***C***H(CH$_3$)$_2$)$_4$), 29.82 (s, 6C, (C_{Ar}(C(***C***H$_3$)$_3$)$_2$), 34.42 (s, 4C, (C_{Ar}(***C***(CH$_3$)$_3$)$_4$), 126.31 (s, 1C, ***C$_{Ar}$***H), 127.66 (vt, $^{v}J_{PC}$ = 5, 2C, (***C$_{Ar}$***(C(CH$_3$)$_3$))$_2$) 164.36 (vt, $^{v}J_{PC}$ = 11, 2C, (***C$_{Ar}$***OP)$_2$). IR (solid state, cm^{-1}): 636 (SO), 1028 (SO_3), 1143 (CF_3), 1251 (SO_3), 1459 (C=C_{Ar}), 1552 (C=C_{Ar}), 2294 (C≡N). UV-vis (CH_2Cl_2, [1x10^{-4}M]; λ_{max}, nm (ε, Lmol^{-1}cm^{-1})): 299 (2432), 327 (2691), 386 (711). E-chem (NBu_4PF_6, 10^{-4}M in dry CH_2Cl_2, E_{ox} vs. $FeCp_2$ [$E_{1/2}$ vs. $FeCp_2$]): 1012 mV [997 mV]. Anal. calcd. for $C_{29}H_{50}F_3NNiO_5P_2S$ (702.41) : C, 49.59; H, 7.17; N, 1.99; S: 4.56. Found: C, 49.30; H, 7.23; N, 1.95; S, 4.77.

2.5.8 [{2,6-(*i*-Pr$_2$PO)$_2$-3-(OMe)C$_6$H$_2$}Ni(NCMe)][OSO$_2$CF$_3$], 7

The procedure described above for the preparation of **2** was used for this synthesis using **7'** (201 mg, 0.395 mmol, 1.00 equiv). The desired product was obtained as a yellow solid that was evaporated from a yellow oil (188 mg, 81 %).

^{1}H NMR (400 MHz, $CDCl_3$): δ 1.25-1.37 (m, 24H, P(CHC(C***H$_3$***)$_2$)$_4$), 2.38 (s(br), 3H, NCC***H$_3$***), 2.61-2.43 (m, 4H, P(C***H***(CH$_3$)$_2$)$_4$), 3.72 (s, 3H, OC***H$_3$***), 6.35 (d, $^{3}J_{HH}$ = 9, 1H, C_{Ar}***H$_{meta}$***), 6.64 (d, $^{3}J_{HH}$ = 9, 1H, C_{Ar}***H$_{para}$***). ^{19}F NMR (282 MHz, $CDCl_3$) : δ -78.20 (s). ^{31}P{^{1}H} NMR (161 MHz, $CDCl_3$) : δ 195.7 (d, J_{PP} = 258, 1P), 191.39 (d, J_{PP} = 258, 1P). ^{13}C NMR (101 MHz, $CDCl_3$) : δ

3.53 (s, 1C, NC***C***H$_3$), 16.65 (s, 2C, P(CH(***C***H$_3$)$_2$), 16.78 (s, 2C, P(CH(***C***H$_3$)$_2$)) 17.46 (s, 2C, P(CH(***C***H$_3$)$_2$)), 17.52 (s, 2C, P(CH(***C***H$_3$)$_2$)), 28.57 (ABX, $^1J_{PC} + {}^3J_{PC}$ = 22, 2C, P(***C***H(CH$_3$)$_2$)$_2$), 28.37 (ABX, $^1J_{PC} + {}^3J_{PC}$ = 22, 2C, P(***C***H(CH$_3$)$_2$)$_2$), 56.98 (s, 1C, O***C***H$_3$), 105.03 (d, $^3J_{PC}$ = 13, 1C, ***C$_{Ar}$***H$_{meta}$), 115.11 (s, 1C, ***C$_{Ar}$***H$_{para}$), 123.82 (t, $^2J_{PC}$ = 20, Ni***C$_{ipso}$***), 140.98 (d, $^3J_{PC}$ = 15, 1C, ***C$_{Ar}$***OCH$_3$), 157.21 (dd, $^2J_{PC}$ = 13; $^4J_{PC}$ = 6, 1C, ***C$_{Ar}$***OP), 162.52 (dd, $^2J_{PC}$ = 11; $^4J_{PC}$ =7, 1C, ***C$_{Ar}$***OP). IR (solid state, cm^{-1}): 634 (SO), 1027 (SO$_3$), 1144 (CF$_3$), 1259 (SO$_3$), 1461 (C=C^{Ar}), 1570 (C=C^{Ar}), 2284 (C≡N). UV-vis ((CH$_2$Cl$_2$, [1x10^{-4}M]); λ_{max}, nm (ε, Lmol^{-1}cm^{-1}) : 279 (17577), 323 (11373), 384 (1881) . E-chem (NBu$_4$PF$_6$, 10^{-4}M in dry CH$_2$Cl$_2$, E_{ox} vs. FeCp$_2$ [$E_{1/2}$ vs. FeCp$_2$]): 938 mV [967 mV]. Anal. calcd. for C$_{22}$H$_{36}$F$_3$NNiO$_6$P$_2$S (620.23) : C, 42.60; H, 5.85; N, 2.26; S: 5.17. Found: C, 42.36; H 6.00; N, 2.11 ; S, 5.29.

2.5.9 [{2,6-(*i*-Pr$_2$PO)$_2$-3-(CO$_2$Me)C$_6$H$_2$}Ni(NCMe)][OSO$_2$CF$_3$], 8

The procedure described above for the preparation of **2** was used for this synthesis using **8'** (405 mg, 0.752 mmol, 1.00 equiv). The desired product was obtained as an orange solid that was in turn obtained by evaporation in air from an orange oil (360 mg, 89 %).

^{1}H NMR (500 MHz, CDCl$_3$): δ 1.31-1.41 (m, 24H, P(CHC(C***H$_3$***)$_2$)$_4$), 2.46 (s, 3H, NCC***H$_3$***), 2.59 (sept, $^3J_{HH}$ = 4, 4H, P(C***H***C(CH$_3$)$_2$)$_4$), 3.82 (s, 3H, C(O)OC***H$_3$***), 6.52 (d, $^3J_{HH}$ = 8, 1H, C$_{Ar}$***H$_{meta}$***), 7.72 (d, $^3J_{HH}$ = 8, C$_{Ar}$***H$_{para}$***). ^{31}P{^{1}H} NMR (202 MHz, CDCl$_3$) δ: 195.3 (s). ^{19}F{^{1}H} NMR (CDCl$_3$, 282 MHz): δ -77.80 (s). ^{13}C{^{1}H} NMR (125 MHz, CDCl$_3$): δ 4.26(s(br), 1C, NC***C***H$_3$), 8.90 (s, 1C, N***C***CH$_3$), 16.79 (s, 2C, P(CH(***C***H$_3$)$_2$)), 16.90 (s, 2C, P(CH(***C***H$_3$)$_2$)), 17.58 (vt $^vJ_{PC}$ = 2, 2C, P(CH(***C***H$_3$)$_2$)), 17.69 (vt, $^vJ_{PC}$ = 2, 2C, P(CH(***C***H$_3$)$_2$)), 28.59 (ABX, $^1J_{PC} + {}^3J_{PC}$ = 33, 2C, P(***C***H(CH$_3$)$_2$)$_2$), 28.67 (ABX, $^1J_{PC} + {}^3J_{PC}$ = 32, 2C, P(***C***H(CH$_3$)$_2$)$_2$), 51.96 (s, 1C, C(O)O***C***H$_3$), 106.79 (dd, $^3J_{PC}$= 7, $^5J_{PC}$ = 4; 1C, ***C$_{Ar}$***H$_{meta}$), 110.64 (dd, $^3J_{PC}$= 7, $^5J_{PC}$ = 5; 1C, ***C$_{Ar}$***H$_{para}$), 134.38 (s, 1C, ***C$_{Ar}$***C(O)OCH$_3$)), 165.12 (s, 1C, C$_{Ar}$***C***(O)OCH$_3$), 168.30 (vt, $^vJ_{PC}$ = 9, 1C, ***C$_{Ar}$*** (OP)), 171.91 (vt, $^vJ_{PC}$ = 8, 1C, ***C$_{Ar}$***OP)**.** IR (solid state, cm^{-1}): 637 (SO), 1032 (SO$_3$), 1149 (CF$_3$), 1272 (SO$_3$), 1383 (C=C^{Ar}), 1578 (C=C^{Ar}), 1712 (C=O), 2303 (C≡N). E-chem (NBu$_4$PF$_6$, 10^{-4}M in dry CH$_2$Cl$_2$, E_{ox} vs. FeCp$_2$): 1262 mV**.** UV-vis (CH$_2$Cl$_2$,[1x10^{-4}M] ; λ_{max}, nm (ε, Lmol^{-1}cm^{-1})): 249 (30114), 327 (12630), 346 (2461). Elemental analysis was not satisfactory for this complex, because it proved difficult to remove all traces of solvents.

2.5.10 [{2,6-(*t*Bu$_2$PO)$_2$C$_6$H$_3$}Ni(NCMe)][OSO$_2$CF$_3$], 9

The procedure described above for the preparation of **2** was used for this synthesis using **9'** (157 mg, 0.293 mmol, 1.00 equiv). The desired product was obtained as a yellow solid (178 mg, 94 %). Single crystals suitable for x-ray diffraction were obtained by slow evaporation in air from a dichloromethane solution layered with hexanes.

^{1}H NMR (500 MHz, $CDCl_3$): δ 1.44 (vt, $^vJ_{PH}$ = 5, 36H, P(C(C***H$_3$***)$_3$)$_4$) , 2.67 (s(br), 3H, NCC***H$_3$***), 6.47 (d, $^3J_{HH}$ = 10, 2H, (C$_{Ar}$***H$_{meta}$***)$_2$), 7.03 (t, $^3J_{HH}$ = 8, 1H, C$_{Ar}$***H$_{para}$***). ^{31}P{^{1}H} NMR (121 MHz, $CDCl_3$) δ : 197.8 (s)**.** ^{19}F{^{1}H} NMR (282 MHz, $CDCl_3$): δ -77.64(s). ^{13}C{^{1}H} NMR (125 MHz, $CDCl_3$): δ 4.51 (s(br), 1C, NC***C***H$_3$), 27.87 (s(br), 12C, P(C(***C***H$_3$)$_3$)$_4$), 40.02 (vt, $^vJ_{PC}$ = 8, 4C, P(***C***(CH$_3$)$_3$)$_4$), 106.21 (vt, $^vJ_{PC}$ = 6, 2C, (***C$_{Ar}$***H$_{meta}$)$_2$), 122.53 (t, $^2J_{PC}$ = 19, 1C, ***C$_{ipso}$***Ni), 131.10 (s, 1C, ***C$_{Ar}$***H$_{para}$), 135.89 (s, 1C, OSO$_2$***C***F$_3$), 169.70 (vt, $^vJ_{PC}$ = 8, 2C, (***C$_{Ar}$***OP)$_2$). IR (solid state, cm^{-1}): 635 (SO), 1027 (SO_3), 1144 (CF_3), 1263 (SO_3), 1477 (C=C^{Ar}), 1558 (C=C^{Ar}), 2293 (C≡N). E-chem (NBu_4PF_6, 10^{-4}M in dry CH_2Cl_2, E_{ox} vs. $FeCp_2$): 1298 mV. UV-vis ((CH_2Cl_2, [1x10^{-4}M]); λ_{max}, nm (ε, Lmol^{-1}cm^{-1})) : 258 (15464), 321 (9449), 338 (sh, 2378), 401 (305). Elemental analysis was not satisfactory for this complex, because it proved difficult to remove all traces of solvents.

2.5.11 [{2,6-(*t*Bu$_2$PO)$_2$-4-(CO$_2$Me)C$_6$H$_2$}Ni(NCMe)][OSO$_2$CF$_3$], 10

The procedure described above for the preparation of **2** was used for this synthesis using **10'** (270 mg, 0.455 mmol, 1.00 equiv). The desired product was obtained as a yellow solid (256 mg, 80 %). Single crystals suitable for x-ray diffraction were obtained by slow evaporation in air from a solution of $CDCl_3$ layered with hexanes.

^{1}H NMR (500 MHz, $CDCl_3$): δ 1.45 (vt, $^vJ_{PH}$ = 8, 36H, P(C(C***H$_3$***)$_3$)$_4$), 2.70 (s , 3H, NCC***H$_3$***), 3.87 (s, 3H, C$_{Ar}$COOC***H$_3$***)**,** 7.14 (s, 2H, C$_{Ar}$***H$_{meta}$***). ^{31}P{^{1}H} NMR (202 MHz, $CDCl_3$) δ : 199.3 (s)**.** ^{19}F{^{1}H} NMR (470 MHz, $CDCl_3$): δ -77.96(s). ^{13}C{^{1}H} NMR (125 MHz, $CDCl_3$): δ 4.66 (s, 1C, NC***C***H$_3$), 27.84 (s, 12C, P(C(***C***H$_3$)$_3$)$_4$), 40.28 (vt, $^vJ_{PC}$ = 8, 4C, P(***C***(CH$_3$)$_3$)$_4$), 52.47 (s, 1C, O***C***H$_3$), 107.14 (vt, $^vJ_{PC}$ = 6, 2C, (***C$_{Ar}$***H$_{meta}$)$_2$), 129.81 (t, $^2J_{PC}$ = 19, 1C, ***C$_{ipso}$***Ni), 133.28 (s, 1C, ***C$_{Ar}$***CO$_2$CH$_3$), 136.70 (s, 1C, OSO$_2$***C***F$_3$), 166.19 (s, 1C, C$_{Ar}$***C***O$_2$CH$_3$), 169.41 (vt, $^vJ_{PC}$ = 8, 2C, (***C$_{Ar}$***OP)$_2$). IR (solid state, cm^{-1}): 635 (SO), 1032 (SO_3), 1135 (CF_3), 1270 (SO_3), 1397 (C=C^{Ar}), 1552 (C=C^{Ar}),

1715 (C=O), 2315 (C≡N). E-chem (NBu_4PF_6, 10^{-4}M in dry CH_2Cl_2, E_{ox} vs. $FeCp_2$): 1457 mV. UV-vis ((CH_2Cl_2, [$1x10^{-4}$M]); λ_{max}, nm (ε, $Lmol^{-1}cm^{-1}$): 257 (19757), 335 (18544), 400 (718). Elemental analysis was not satisfactory for this complex, because it proved difficult to remove all traces of solvents.

2.6 Associated content

2.6.1 Supporting Information

The following materials are available free of charge via the Internet at http://pubs.acs.org: Tables of crystal data and collection/refinement parameters; a table of additional distances and angles for complexes **1-10** and **5'**; figures of molecular diagrams for complexes **2**, **3**, **5**, **5'** and **9**; ^{1}H, ^{31}P and ^{13}C NMR spectra of complexes **1-10**; a table with detailed IR frequencies assignments for complexes **1-10;** additional information for IR, electrochemical and ligand-exchange studies. Complete details of the X-ray analyses reported herein have been deposited at The Cambridge Crystallographic Data Center (CCDC 1044410 (**2**), 942873 (**3**), 942874 (**4**), 942876 (**5**), 942875 (**5'**), 942877 (**6**), 1044411 (**9**), 1044412 (**10**)). This data can be obtained free of charge via www.ccdc.cam.ac.uk/data_request/cif, or by e-mailing data_request@ccdc.cam.ac.uk, or by contacting The Cambridge Crystallographic Data Centre, 12 Union Road, Cambridge CD2 1EZ, UK; fax: +44 1223 336033. The Supporting Information is available free of charge on the ACS Publications website at DOI: 10.1021/acs.organomet.5b00272.

2.6.2 Acknowledgments

The authors are grateful to: NSERC of Canada for financial support of this work (Discovery and RTI grants to D.Z.); Université de Montréal (graduate fellowships to S.L.); Dr. Michel Simard and Ms. Francine Bélanger-Gariépy for their valuable assistance with crystallography and many interesting discussions; Ms. Elena Nadezhina for the elemental analyses; Dr. D. Rochefort for valuable advice regarding the electrochemical measurements; and the reviewers of our manuscript who recommended that we measure the open circuit (rest) potentials of our complexes and offered many valuable suggestions regarding the reporting of the NMR data. S.L. is also grateful to Centre

in Green Chemistry and Catalysis for a travel award, to J.-P. Cloutier for the loan of complexes used in the ligand exchange studies, and to all group members for many valuable discussions and practical advice.

Contribution de l’auteur

J’ai effectué toutes les manipulations, synthèses, études catalytiques et cinétiques dans cet article. De plus, j’ai rédigé le manuscrit et l’ai révisé avec l’aide de Pr. Zargarian.

Chapitre 3: On the Mechanism of Ni(II)-Promoted Michael-Type Hydroamination of Acrylonitrile and Its Substituted Derivatives

Article 2

Sébastien Lapointe and Davit Zargarian[†]

[†] Département de chimie, Université de Montréal, Montréal (Québec), Canada H3C 3J6

Reprinted (adapted) with permission from Lapointe S. and Zargarian D., *Dalton Trans*, 2016. Advance Article DOI: 10.1039/C6DT02105K

3.1 Abstract

Michael-type hydroamination of acrylonitrile and its substituted derivatives promoted by Ni(II) complexes is believed to proceed via an outer-sphere nucleophilic attack on the cationic adduct of the nitrile-coordinated substrate. As a test for the validity of this mechanistic postulate, we have sought to establish a correlation between the electrophilic character of the Ni(II) center and the degree to which it can activate the substrate toward nucleophilic attack by amines. This has been done by screening the catalytic activities of the cationic acetonitrile adducts [(R-POCOP)Ni($NCCH_3$)][OSO_2CF_3] bearing an electron-donating or electron-withdrawing substituent on the central aromatic ring of the POCOP ligand (R-POCOP= $\kappa^P, \kappa^C, \kappa^P$-2,6-(*i*-$Pr_2PO)_2$-4-R-$C_6H_2$; R= OMe (**3**), COOMe (**4**)). The catalytic activities for the addition of amines to crotonitrile, methacrylonitrile, and cinnamonitrile were found to depend on the precursor and the amine used, as well as on the reaction time. These studies were complemented by ligand exchange studies that established the relative binding order among the main components of a typical hydroamination mixture (RCN > amine > OSO_2CF_3), thus supporting the assertion that cationic nitrile adducts constitute the resting state in the catalytic manifold. We have also prepared and characterized the cationic acrylonitrile and cinnamonitrile adducts [(R-POCOP)Ni(NCCH=CHR')][OSO_2CF_3] (R'= H : R= COOMe (**7**) or OMe (**8**); R'= Ph: R= COOMe (**9**) or OMe (**10**)) as models of the postulated catalytic intermediates in the addition of amines to these substrates. To allow structural comparisons to the nitrile adducts, we have prepared and characterized the ammonia adducts [(R-POCOP)Ni(NH_3)][OSO_2CF_3] (R= H, **11**, and COOMe, **12**). The results of structural, spectroscopic, and reactivity studies carried out on these compounds and their implications for the mechanism of Michael-type hydroamination reactions promoted by the title system have been discussed

3.2 Introduction

Michael additions on acrylonitrile can proceed in an uncatalysed fashion with highly nucleophilic aliphatic amines,[61] but a catalyst is generally required when a wider range of amines is used. A catalyst is also required with all amines for the analogous amination of

acrylonitrile's substituted derivatives, including crotonitrile, methacrylonitrile, and cinnamonitrile. The most commonly used catalysts/promoters for these reactions are simple salts or complexes of early and late transition metals.[62] Although the mechanisms operating in these systems have not been established unequivocally, two different postulates have been proposed, an outer-sphere mechanism involving cationic adducts that serve to activate the *N*-coordinated nitrile substrate toward attack by the amine nucleophile (**Scheme 3.1**),[62g, 63] and an inner-sphere, insertion mechanism involving amine adducts and amido intermediates (**Scheme 3.2**).[64,]

Our group has shown that cationic Ni complexes featuring PCP- and POCOP-type pincer ligands are competent pre- catalysts for the Michael-type regioselective hydroamination of acrylonitrile and its substituted derivatives (**Equation 3.1**).[24a, 24b, 34, 35b]

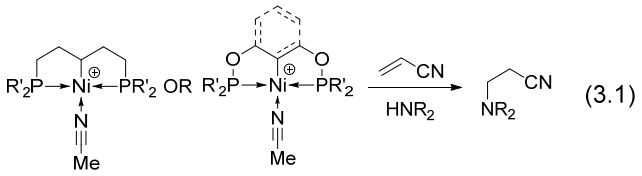

A number of studies have suggested that these reactions proceed by an outer-sphere mechanism involving an intermediate featuring the acrylonitrile substrate that, by virtue of being *N*-coordinated to a cationic Ni(II) center, is activated toward an attack by the amine nucleophile.[24a, 62a, 65] Evidence in support of this proposal includes the isolation and structural characterization in a PCP-Ni system of the two postulated cationic adducts, one bearing the acrylonitrile substrate and the other bearing the product of aniline addition to it (**Equation 3.2**).[24a]

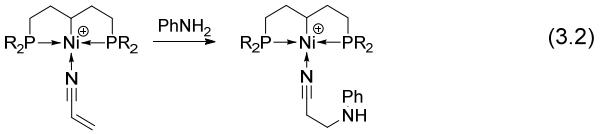

The outer-sphere mechanism invoked above would require that factors enhancing the electrophilicity of the Ni centre impart a favorable influence on catalytic activities, and a limited number of investigations have confirmed such a correlation. For instance, the more electrophilic POCOP-based systems display greater activities compared to their PCP counterparts.[24a] On the other hand, other variables such as the nature of POCOP

Scheme 3.1 An outer-sphere mechanism for hydroamination of acrylonitrile catalyzed by electrophilic metal complexes

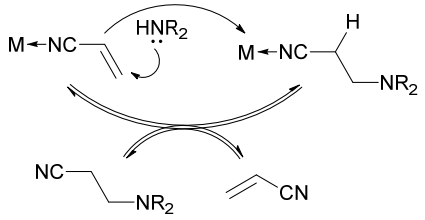

Scheme 3.2 An inner-sphere mechanism for hydroamination of acrylonitrile catalyzed by electrophilic metal complexes

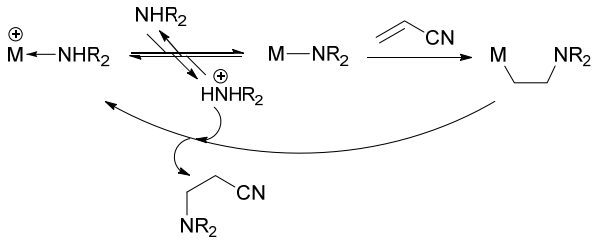

POCOP ligand backbone (aliphatic vs. aromatic) and *P*-substituents (*i*-Pr vs. Ph) do not appear to exert significant influence on catalytic reactivities. Thus, addition of aniline to acrylonitrile is fairly equally promoted by the aromatic- and aliphatic-backboned POCOP adducts $[(POCOP)Ni(NCMe)]^+$,[24b] whereas aromatic-backboned adducts featuring *i*-Pr_2P and Ph_2P moieties led to comparable catalytic activities.[35b]

Another potentially favorable factor for the (pincer)Ni(II)-promoted hydroamination of acrylonitrile and its substituted derivatives would be the presence of electron-withdrawing ring-substituents on the central aromatic ring of resorcinol-based POCOP ligands. To date, only one report has examined this issue and the results obtained were counter-intuitive: the cationic Ni adduct bearing a Cl-substituted POCOP ligand, $[(2,6\text{-}(i\text{-}Pr_2O)_2\text{-}3,5\text{-}Cl_2\text{-}C_6H)Ni(NCMe)]^+$, showed a *lower* catalytic activity for hydroamination of acrylonitrile relative to its unsubstituted analogue.[24a] It should be mentioned, however, that the weak catalytic performance observed in this case is likely a reflection of the limited thermal stability of this pre-catalyst and cannot disprove the anticipated impact of ring-substituents on catalytic activities.

Having developed practical synthetic routes to new POCOP-based cationic Ni(II) complexes featuring ring-substituents, and having established the relative stabilities and oxidation potentials of these complexes,[66] we set out to examine the catalytic activities of some of these species as a function of the ring substituents. The present report reports the catalytic activities of the cationic complexes [(4-R-POCOP)Ni(NCMe)][OSO_2CF_3] (R= OMe, **3**; CO_2Me, **4**) in the addition of various amines to methacrylonitrile, crotonitrile, and cinnamonitrile. The main objective of these catalytic tests was to examine whether or not the catalytic activities of **3** and **4** correlate with the electrophilicity of each species. We have also examined the spectra, solid state structures, and relative coordinating aptitudes of the different acrylonitrile, cinnamonitrile, and ammonia adducts [(4-R-POCOP)Ni-(NCCH=CHR')][OSO_2CF_3] (R= CO_2Me: R'= H (**7**), Ph (**9**); R= OMe: R'= H (**8**), Ph (**10**)) and [(4-R-POCOP)Ni(NH_3)][OSO_2CF_3] (R= H (**11**), CO_2Me (**12**)).

3.3 Results and discussion

3.3.1 Hydroamination tests

We began our studies by screening the catalytic reactivities of cationic acetonitrile adducts bearing an OMe or a CO_2Me substituent on the central aromatic ring of the pincer ligand. The catalytic tests were designed to establish whether the electronic impact of these ring substituents would have the anticipated influence on the hydroamination activities.

Initial results revealed that acrylonitrile is very reactive with a variety of Ni precursors, a fact that did not allow us to differentiate among the various precursors. Moreover, acrylonitrile does undergo uncatalysed Michael addition with some aliphatic amines (e.g., ca. 50% over 24 h at r.t. with morpholine),[24b] thus complicating our studies. In contrast, crotonitrile, methacrylonitrile, and cinnamonitrile are unreactive to amines in the absence of a suitable catalyst, proving to be much more challenging substrates for Ni-promoted Michael-type hydroamination reactions.[34] These substrates were, therefore, selected for our studies. Ten primary amine substrates were also selected to cover a wide range of nucleophilic and steric properties: seven aromatic (aniline; 2-X-aniline, X= F, Cl, Br, I; 4-NO_2-aniline; 2,5-dimethylaniline) and three aliphatic (cyclohexylamine, octylamine, and ethanolamine).

The acetonitrile adducts [(4-R-POCOP$^{i\text{-Pr}}$)Ni(NCMe)][OTf] (R= OMe (**3**), CO_2Me (**4**)) were synthesized and purified following previously reported procedures (**Scheme 3.3**)[66] and used as precursors for our catalytic tests, which were conducted (in triplicate) on THF solutions (total volume ~1 mL) containing one mmol each of the amine and nitrile substrates and NEt_3, plus the precursor Ni complex (0.01 mmol) and dodecane as internal standard (0.1 mmol). The reactions were performed by heating the samples at 50 °C for the designated time (2 or 20 h), and the final mixtures were analyzed by GC/MS; the conversions and yields were determined based on a calibration curve prepared using authentic samples of the anticipated products. The results of these tests are listed in **Table 1.1** and graphically plotted in **Figures A28** and **A29** (Annexe pour chapitre 3). (See also **Tables A3-A10** for more detailed results of all the catalytic runs.) These results lead us to the following general observations.

Scheme 3.3 Synthesis of cationic nitrile adducts **7-10** and previously reported complexes **1-6**.[24b, 66]

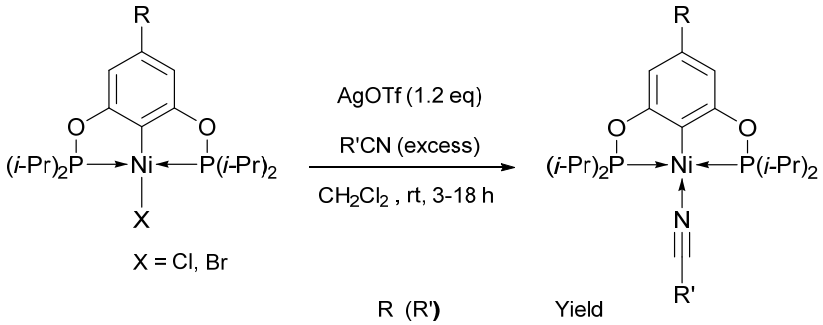

R (R')	Yield	
p-H (-CH_3)	80%	**1**
p-Me (-CH_3)	93%	**2**
p-OMe (-CH_3)	84%	**3**
p-CO_2Me (-CH_3)	81%	**4**
p-Br (-CH_3)	86%	**5**
m,m-tBu_2 (-CH_3)	87%	**6**
p-CO_2Me (-CH=CH_2)	80%	**7**
p-OMe (-CH=CH_2))	98%	**8**
p-CO_2Me (-CH=CH(C_6H_5))	63%	**9**
p-OMe (-CH=CH(C_6H_5))	70%	**10**

First, the predominant reactivity observed in nearly all cases consists of mono addition of one amine N-H bond across the double bond moiety of the nitrile substrates, but double N-H addition to give a tertiary amine was observed to a minor extent in the reactions of octylamine (see **Tables A5**, **A6**, **A9**, and **A10)**. Crotonitrile and methacrylonitrile showed varying activities

with all amines except 2-iodoaniline and 4-nitroaniline, whereas cinnamonitrile showed little or no activity with all amines except aniline (*vide infra*).

Second, reaction time appears to play an important role in the relative levels of catalytic activity for the two pre-catalysts examined. Thus, for the catalytic additions to crotonitrile and methacrylonitrile conducted over a short reaction time, precursor **4** proved to be more competent with nearly all aromatic amines aniline, 2-chloroaniline being the exception, whereas precursor **3** was more competent for the addition of aliphatic amines (**Table 1.1**). In contrast, precursor **3** is the best promoter for addition of nearly all amines when the catalytic reactions are allowed to proceed for 20 h (**Tables A3** vs **A4** and **A7** vs A**8**). A speculative explanation for these counter-intuitive observations involves the relative substitutional labilities of the two (R-POCOP)Ni systems: the stronger binding of the addition product to the Ni centre in the more electrophilic system **4** would hinder the product-substrate exchange equilibrium that we assume to be crucial for catalytic turn-overs; the impact of such a product inhibition would be more pronounced over longer reaction times. It should be emphasized, however, that this and similar conclusions remain to be tested against precise kinetic data that can identify the relative rates of the different steps in the catalytic manifold and the impact of various factors on these steps.[67]

Longer reaction times also appear to improve yields in some cases. For example, reaction of crotonitrile with aniline in the presence of catalyst **3** yields the mono addition product in ca. 29% over 2 h compared to ca. 48% over 20 h (See **Table A3** and **A4**). However, in other cases we noted that longer reaction times resulted in either no increase in yields or even a slight decrease. For instance, the reaction of crotonitrile with 2-bromoaniline in the presence of precursor **4** gave ca. 4% and 2% yields after 2 h and 20 h, respectively (See **Table A4** for reaction yields after 20h). Such apparent (and minor) degradations in yields are presumably due to secondary reactions of the products, but the precise reasons for these observations have not been examined.

A final observation relates to the relative reactivities of the nitrile substrates as a function of the substituents on the olefinic moiety: on the basis of the similar hydroamination yields obtained with crotonitrile and methacrylonitrile, it would appear that the electronic/steric impact

Table 3.1 Single and double addition products for hydroamination reaction of crotonitrile and methacrylonitrile promoted by precursors **3** and **4**.

Product	Nitrile	[Ni]	TON (yield, %)	TOF [h^{-1}]
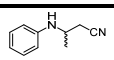 15a	Crotonitrile	**3**	28.6 ± 0.6	14.3 ± 0.3
		4	40 ± 1	20.0 ± 0.7
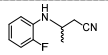 15b		**3**	4.9 ± 0.1	2.43 ± 0.03
		4	9 ± 2	4 ± 1
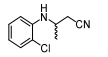 15c		**3**	2.6 ± 0.5	1.3 ± 0.3
		4	1.3 ± 0.2	0.7 ± 0.1
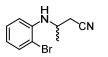 15d		**3**	2.0 ± 0.1	1.0 ± 0.1
		4	3.9 ± 0.4	2.0 ± 0.2
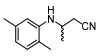 15f		**3**	1.1 ± 0.1	0.56 ± 0.04
		4	4.8 ± 0.3	2.4 ± 0.2
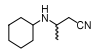 15h		**3**	36.4 ± 0.6	18.2 ± 0.3
		4	23.9 ± 0.6	11.9 ± 0.3
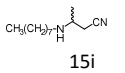 15i		**3**	56.1 ± 0.6	28.0 ± 0.3
		4	28.2 ± 0.8	14.1 ± 0.4
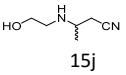 15j		**3**	18 ± 1	9.1 ± 0.7
		4	6.8 ± 0.1	3.4 ± 0.1
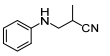 16a	Methacrylonitrile	**3**	21 ± 1	10.6 ± 0.7
		4	35 ± 1 38 ± 2 *	17.5 ± 0.7 19 ± 1 *
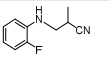 16b		**3**	5.2 ± 0.7	2.6 ± 0.4
		4	7.8 ± 0.4	3.9 ± 0.2
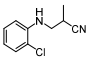 16c		**3**	3.2 ± 0.3	1.6 ± 0.2
		4	0	0
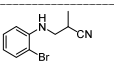 16d		**3**	2.4 ± 0.5	1.2 ± 0.2
		4	3.2 ± 0.5	1.6 ± 0.3
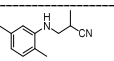 16f		**3**	7 ± 1	3.6 ± 0.5
		4	0.6 ± 0.1	0.30 ± 0.03
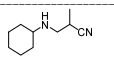 16h		**3**	39 ± 1	19.7 ± 0.6
		4	22.7 ± 0.6	11.3 ± 0.3
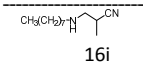 16i		**3**	34.6 ± 0.7	17.3 ± 0.3
		4	12 ± 1	6.1 ± 0.5
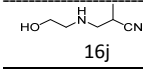 16j		**3**	14.6 ± 0.7	7.3 ± 0.4
		4	0	0

Reaction conditions: Amine (1 mmol), crotonitrile (14a) or methacrylonitrile (14b) (1 mmol), NEt_3 (1 mmol), **3** or **4** (1 mol%), dodecane (10 mol%, internal standard) and THF (500 µL), 50 °C, 2 h. GC/MS yields. Reactions were done in triplicate and the yields are the average of those three experiments. * In this experiment, 5 mmol of amine was used instead of 1 mmol.

of the Me group does not vary much as a function of its position (α vs. β relative to the CN moiety), whereas the presence of a Ph group (in cinnamonitrile) leads to a significant loss of reactivity. Indeed, hydroamination of cinnamonitrile occurred only with aniline and in the presence of precursor **4** (22 ± 1 % yield of 3-morpholino-3-phenylpropanenitrile, **Equation 3.3**), no reactivity being observed with other amines or in the presence of precursor **3**. It should be emphasized, however, that even this limited reactivity is significant for such a challenging substrate, and attests to the strong activating capacity of precursor **4**.

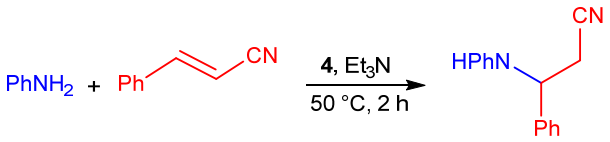

(3.3)

To sum up, the catalytic reactivities documented in **Table 1.1** and **Figures A28** and **A29** (Annexe pour chapitre 3) indicate that the activities of the precursors **3** and **4** are time- and amine-dependent, precursor **3** being more efficient for the addition of the more nucleophilic aliphatic amines at all time intervals, and precursor **4** being more efficient for the addition of the less nucleophilic anilines over 2 h. That the more electron-withdrawing CO_2Me substituent results in a greater activation of the more challenging substrates crotonitrile, methacrylonitrile, and particularly the quite inert cinnamonitrile toward nucleophilic attack by the less nucleophilic aniline is consistent with the anticipated substituent effect discussed above. On the other hand, it is not clear why the same effect is not observed for the reactions of the more nucleophilic aliphatic amines.

3.3.2 Cationic acrylonitrile and cinnamonitrile adducts

In the absence of an unambiguous correlation between substituent effects and catalytic Michael-type hydroamination activities, we set out to study the structures and substitutional labilities of the cationic adducts as models of reaction intermediates. Isolation of acrylonitrile adducts allowed us to study the substitutional lability of the nitrile substituent and establish whether amine adducts might be involved in the hydroamination catalytic cycle. In addition, the solid structure of one acrylonitrile adduct was studied by X-ray diffraction analysis. Unfortunately, the analogous studies could not be conducted on the corresponding crotonitrile

or methacrylonitrile adducts, because we did not succeed in isolating these derivatives. While it is tempting to conclude that this finding reflects the thermal instability of these adducts and might explain the limited reactivity of these substrates, this assertion is inconsistent with the successful preparation and isolation of cationic adducts with the least reactive substrate, cinnamonitrile. The solid state structures of the two cinnamonitrile adducts bearing the CO_2Me and OMe ring-substituents were investigated to gain insight into its inertness.

The acrylonitrile and cinnamonitrile adducts [(4-R-POCOP$^{i\text{-Pr}}$)Ni(NCH=C(H)R')][OTf] (R= CO_2Me: R'= H (**7**), Ph (**9**); R= OMe: R'= H (**8**), Ph (**10**)) were prepared following the same synthetic route used for accessing the analogous acetonitrile adducts **1-6**.[66] Treatment of the charge-neutral halo analogues (R-POCOP$^{i\text{-Pr}}$)NiX (X= Cl, Br)[25,11b] with AgOTf and R'C(H)=CHCN for 3 h at rt gave the target complexes **7-10** in 63-98% yields (See **Scheme 3.3**).

These complexes were then subjected to spectroscopic and X-ray diffraction studies, and the results were compared to data obtained for previously examined analogues in search of evidence demonstrating substrate activation upon RCN→Ni coordination. For example, comparison of IR data for **7-10** to the corresponding data for the previously reported acetonitrile complexes **1-6** should allow us to understand how the substituents present on the POCOP central ring and on the substrates can affect the electrophilicity of the nickel center and the substrate-Ni interaction. We have shown earlier[66] that the nature of the backbone substituent can have a significant impact on the nitrile stretching frequency, ν(C≡N), with frequencies of up to 2329 cm^{-1} for the CO_2Me substituted complex **4** and 2297 cm^{-1} for the OMe substituted complex **3**. In a similar manner, it would be interesting to know what is the effect of the nitrile substituent on the ν(C≡N) and how it compares to the closely related complexes reported previously.

Inspection of the IR data shown in **Table 3.2** leads to the following conclusions. First, we observe large and positive values of Δν(C≡N), implying a significant difference in the ν(C≡N) values for the free and nickel-bound nitrile substrates. Moreover, in all cases both ν(C≡N) and Δν(C≡N) values are greater in the adducts bearing the electron-withdrawing substituent. This observation is consistent with the reasoning that the enhanced electrophilicity of the nickel center in CO_2Me adducts **4**, **7**, and **9** increases the RCN→Ni electron donation, which in turn strengthens the C≡N bond; this follows from the anticipation that net σ-donation from the nitrile lone pair, which has partial anti-bonding character, should reinforce the C≡N

bond.[48b, 68] It should be noted, however, that while this trend is also observed in the cinnamonitrile analogues **9** and **10**, curiously the difference between the ν(C≡N) values in these complexes is very small: 2244 cm^{-1} vs 2241 cm^{-1}.

Table 3.2 IR ν(C≡N) data for complexes **1-4** and closely related systems

Complex	ν(C≡N) (cm^{-1})	Δν(C≡N) [nitrile] (cm^{-1})[c]
[(H-POCOP$^{i\text{-}Pr}$)Ni(NCMe)][OSO_2CF_3], **1** [a]	2297 (2292)[b]	+45 (+40)[b]
[(*p*-Me-POCOP$^{i\text{-}Pr}$)Ni(NCMe)][OSO_2CF_3], **2** [a]	2294	+42
[(*p*-OMe-POCOP$^{i\text{-}Pr}$)Ni(NCMe)][OSO_2CF_3], **3** [a]	2293	+41
[(*p*-CO_2Me-POCOP$^{i\text{-}Pr}$)Ni(NCMe)][OSO_2CF_3], **4** [a]	2329	+77
[(*p*-Br-POCOP$^{i\text{-}Pr}$)Ni(NCMe)][OSO_2CF_3], **5** [a]	2302	+50
[(*m,m-t*-Bu_2-POCOP$^{i\text{-}Pr}$)Ni(NCMe)][OSO_2CF_3], **6** [a]	2294	+42
[(*p*-CO_2Me-POCOP$^{i\text{-}Pr}$)Ni(NCCH=CH_2)][OSO_2CF_3], **7**	2291	+61
[(*p*-OMe-POCOP$^{i\text{-}Pr}$)Ni(NCCH=CH_2)][OSO_2CF_3], **8**	2251	+21
[(*p*-CO_2Me-POCOP$^{i\text{-}pr}$)Ni(NCCH=CHPh)][OSO_2CF_3], **9**	2244	+26
[(*p*-OMe-POCOP$^{i\text{-}Pr}$)Ni(NCCH=CHPh)][OSO_2CF_3], **10**	2241	+23
[(H-POCOP^{iPr})Ni(NCCH=CH_2)][OSO_2CF_3] [a]	2257	(+27) [b]
[(H-$POC_{sp3}OP^{iPr}$)Ni(NCCH=CH_2)][OSO_2CF_3] [a]	2252	(+22) [b]

a) Previously reported complexes.[24b] b) The ν(CN) values in parentheses were measured using KBr pellets to provide a comparison to the solid-state ATR measurements used in the discussion. c) Δν(CN) is relative to the free nitrile stretching frequency of the nitrile in brackets (Free acetonitrile: 2252 cm^{-1}; Free acrylonitrile: 2230 cm^{-1}; Free cinnamonitrile: 2218 cm^{-1})

Further comparison of the data for various adducts shows greater Δν(C≡N) values for acetonitrile relative to acrylonitrile and cinnamonitrile. For instance, the acetonitrile adducts show Δν(C≡N) values of +41 (**3**) and +77 (**4**), whereas the corresponding acrylonitrile and cinnamonitrile adducts show values of +21 (**8**), +61 (**7**), +23 (**10**), and +26 (**9**). While the precise reason for this discrepancy in the levels of activation of acetonitrile vs acrylonitrile and cinnamonitrile is not known at this stage,[69] this observation is reflected in the previously reported reactivity of acetonitrile adducts with amine nucleophiles (to form amidines).[34, 70]

3.3.3 Structural analyses of nitrile-bound complexes

The most pertinent structural parameters for the three cationic nitrile adducts complexes subjected to X-ray diffraction studies are listed in **Table 3.3**, and the front view of the molecular diagrams of adducts **7**, **8** and **10** are shown in **Figures 3.1** to **3.3**; the side views of the molecular

diagrams for these complexes are shown in **Figures A1-A3**, whereas details of the diffraction studies are given in **Tables A1** and **A2**

Table 3.3 Bond distances (Å) and angles (deg.) for complexes **1-6** and **7, 9** and **10**

Complex	Ni-C	Ni-N	N≡C	C=C [b]	Ni-P_1	Ni-P_2	P_1-Ni-P_2	C_1-Ni-N
1 [a]	1.881(2)	1.874(2)	1.140(3)		2.1683(7)	2.1704(7)	164.38(3)	175.8(1)
2 [a]	1.879(3)	1.875(2)	1.142(4)		2.1693(8)	2.1687(7)	163.52(3)	171.7(1)
3 [a]	1.884(2)	1.881(2)	1.135(3)		2.1784(5)	2.1747(5)	163.16(2)	176.84(7)
4 [a]	1.880(2)	1.879(2)	1.138(2)		2.1698(4)	2.1748(4)	164.45(1)	178.43(6)
5 [a]	1.879(3)	1.871(3)	1.145(4)		2.1685(9)	2.171(2)	164.44(4)	176.6(2)
6 [a]	1.890(2)	1.875(2)	1.140(2)		2.1785(5)	2.1640(4)	163.79(2)	170.35(6)
7	1.877(2)	1.873(2)	1.147(3)	1.319(3)	2.1798(5)	2.1777(5)	164.10(2)	176.62(8)
9	1.878(2)	1.867(2)	1.140(2)	1.333(3)	2.1801(4)	2.1758(5)	164.49(2)	177.14(7)
10	1.881(2)	1.864(2)	1.149(3)	1.316(4)	2.1709(6)	2.1740(6)	163.57(2)	178.59(9)

a) Previously reported complexes [24b, 66] b) Nitrile moiety alkene bond distances

The nickel center in structures **7**, **9**, and **10** adopts a square planar geometry displaying slight distortions from the ideal geometry, most of which are primarily due to the small bite angle of the POCOP ligands: P-Ni-P~163-164°. The displacement of the nickel atom out of the coordination plane (P_1-Ni-P_2-C_{ipso}) is very minor (<0.05(1) Å). We observe close to ideal C_{ipso}-Ni-N angles (ca. 177-179°) in all three complexes, with little or no lifting of the nitrile moiety out of the coordination plane. This contrasts with the parent acetonitrile complexes **2** and **6** where we have observed a significant deviation from the ideal square-planar geometry (C_{ipso}-Ni-N angles of ca. 170-172°).[66] The Ni-P (ca. 2.17 Å) distances in complexes **7**, **9** and **10** are very close to the corresponding distances found in the previously reported complexes **1-6**; however, there are statistically significant differences in Ni-N distances in these complexes (1.864(2)-1.879(2) Å). Finally, the N≡C distances between complexes 7 to 10 and 1 to 6 are, in a large majority, not statistically significantly different. Overall, the solid state data indicate that changing the nature of the Ni-bound nitrile ligand has a minor effect only on the Ni-N distances, but none on other distances and angles around the coordination plane.

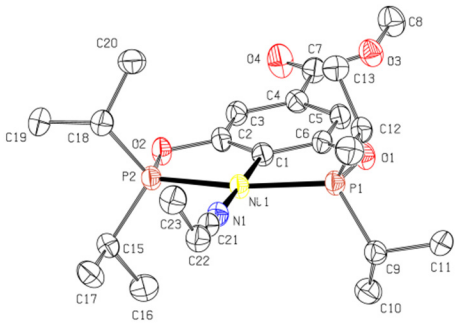

Figure 3.1 Front view of the molecular diagram for complex **7**. Thermal ellipsoids are shown at the 50% probability level. Hydrogens are omitted for clarity.

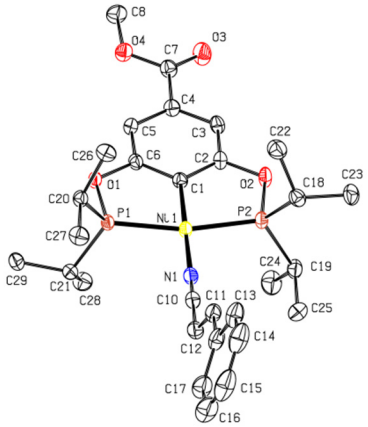

Figure 3.2 Front view of the molecular diagram for complex **9**. Thermal ellipsoids are shown at the 50% probability level. Hydrogens are omitted for clarity**.**

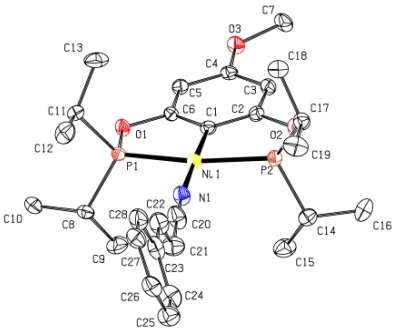

Figure 3.3 Front view of the molecular diagram for complex **10**. Thermal ellipsoids are shown at the 50% probability level. Hydrogens are omitted for clarity.

3.3.4 Formation of amine-bound complexes

The above proposed mechanistic schemes for metal-catalyzed hydroamination reactions under discussion invoked the intermediacy of cationic acrylonitrile adducts (outer-sphere mechanism, **Scheme 3.1**) or amine adducts (inner-sphere mechanism, **Scheme 3.2**), the latter converting to amido species that might undergo olefin insertion. The observation of thermally stable and isolable acrylonitrile and cinnamonitrile Ni adducts provides indirect support for the validity of the outer-sphere mechanism operating in our systems. In an effort to study the feasibility of the alternative inner-sphere mechanism in our (POCOP)Ni-based systems, we have examined the kinetic accessibility of cationic amine adducts to establish whether they can be viable intermediates in the catalytic cycle, and if so to isolate one or more examples of such adducts and study their structures and reactivities. NMR tube experiments were thus conducted to monitor the reaction of the charge-neutral triflate species, ($^{p\text{-OMe}}$POCOP)Ni(OTf) with excess amine; in the cases where amine adducts could be generated in-situ, they were treated with acrylonitrile to measure the relative binding forces of the two substrates. The results of these tests are summarized below.

In light of its prevalence in our hydroamination studies, aniline was the first amine tested. No color change was observed when 10 equiv of aniline was added to a 0.06 M C_6D_6 solution of the triflate complex ($^{p\text{-OMe}}$POCOP)Ni(OTf), but the ^{31}P NMR spectrum of the mixture showed two broad signals. The broad signal at ca. 186.5 ppm (See **Figure 3.4a**; $LW_{1/2}$ = 31 Hz) is attributed to ($^{p\text{-OMe}}$POCOP)Ni(OTf), while the other at ca. 189 ppm (See **Figure 3.4a**; $LW_{1/2}$ = 38 Hz) is believed to arise from the aniline adduct; based on their respective integration values, the major species is the triflate precursor (60:40). The analogous NMR test with the more nucleophilic cyclohexylamine showed a complete conversion of the triflate complex and emergence of a new major species showing a ^{31}P NMR signal at ca. 188.7 ppm (see **Figure 3.4b**; $LW_{1/2}$ = 5.4 Hz); a minor species is also present in this mixture (at ca. 190 ppm). Complete conversion of the triflate complex was also observed with piperidine (at ca. 188 ppm), but in this case we observed additional peaks in the upfield region of 50-70 ppm associated with decomposition products arising from hydrolysis or oxidation of the phosphinite moieties.

Finally, we were surprised to find that morpholine, whose nucleophilicity should be similar to that of piperidine and cyclohexylamine, reacted quite differently than its counterparts, displacing the triflate moiety only partially (~20%). The ^{31}P NMR spectrum of this mixture showed two new signals, the major one (accounting for ~18 % of the *P*-containing species) representing the morpholine adduct and the minor peak remaining unidentified. The above observations indicate that cyclohexylamine and piperidine act as stronger nucleophiles in displacing the triflate moiety, whereas the substitution reaction appears to be incomplete with aniline and morpholine.

While the relative binding aptitudes of amines and the triflate anion are interesting to note, a more important question in the context of the hydroamination mechanism is whether the amine substrates can compete with nitrile substrates for binding to the cationic Ni center. To answer this question, we reacted the in-situ generated amine adducts with acrylonitrile and monitored the ligand substitution reaction by ^{31}P NMR spectroscopy. Results of these tests showed that even a small amount of acrylonitrile (less than half the equiv of amines) led to an instantaneous and complete suppression of the signals for amine adducts and the sharp signal at ca. 195 ppm for the corresponding acrylonitrile adduct emerged in every case. This observation confirms the much greater binding aptitude of nitrile substrates and rules out scenarios involving the generation of amine adducts under the normal condition of the hydroamination catalysis wherein the amine and RCN substrates are normally present in a 1:1 ratio.

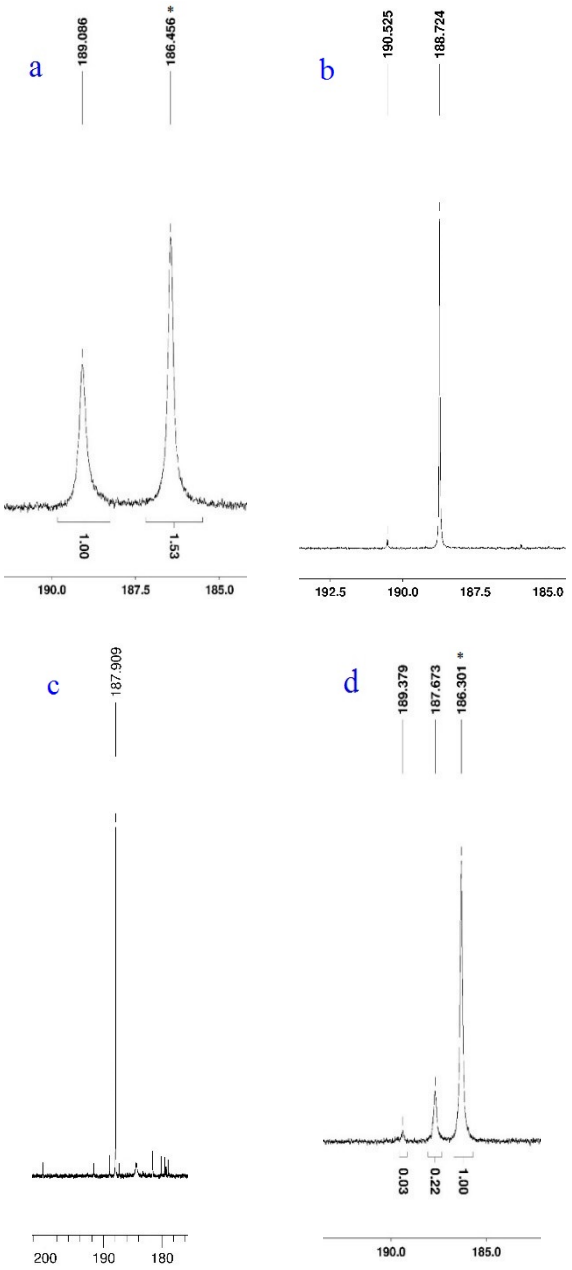

Figure 3.4 ^{31}P NMR (162 MHz, C_6D_6, rt) spectrums from the treatment of ($^{p\text{-OMe}}$POCOP)Ni-OTf (1-OTf) with 10 equiv of: aniline (a), cyclohexylamine (b), piperidine (c), and morpholine (d). Peaks marked with a star (*) symbol are due to the precursor complex.

3.3.5 Isolation of amine adducts

Although the above results discounted the possibility that amine adducts might form during the hydroamination catalysis in our system, we were nevertheless interested in isolating such species and examining their structures and reactivities. Unfortunately, none of the amine

adducts discussed above furnished isolable products, but an ammonia adduct was obtained serendipitously from the reaction of (R-POCOP$^{i\text{-Pr}}$)Ni(OTf) (R= H, CO_2Me) with tris(trimethylsilyl)amine ($N(SiMe_3)_3$); the same material was also isolated from the reaction of the triflate precursor with NH_4OH. These reactions and the complete characterization of the products [(R-POCOP$^{i\text{-Pr}}$)Ni(NH_3)][OTf] (R = H (**11**), CO_2Me (**12**)) are described below.

The reaction of (H-POCOP$^{i\text{-Pr}}$)Ni(OTf) with excess $N(SiMe_3)_3$ in relatively dry THF (~40 ppm H_2O) led to the disappearance of the ^{31}P NMR signal for the starting material and a new signal emerged at 189 ppm. X-ray diffraction studies conducted on a crystalline solid obtained from this sample revealed the formation of the ammonia adduct **11** (**Figure 3.5**); this species presumably arises from the hydrolysis of the N-Si bonds in the corresponding $N(SiMe_3)_3$ adduct. This hydrolysis scenario was supported by noting that adding one equiv of $N(SiMe_3)_3$ and only three equiv of water to the mixture of the triflate precursor gave the corresponding ammonia adduct with 71% yield over 2 h. We obtained the ammonia adducts **11** and **12** in 85% and 90% yields, respectively, by direct reaction of 1-10 equiv of NH_4OH with (R-POCOP$^{i\text{-Pr}}$)Ni-OTf (R = H, OMe). It should be added that a black oily residue was also formed in these reactions, pointing to possible decomposition of the complex.

Structural analyses of complexes **11** and **12** (See **Figure 3.6**) showed that they are globally quite similar to analogous cationic complexes **1-10** in terms of most bond distances and angles around the nickel atom (see **Table 3.3** and **43.**), the main exception being the Ni-N distances which are longer in the ammonia adducts (ca. 1.96 vs. 1.86-1.88 Å). Another important difference is the presence in complexes **11** and **12** of hydrogen bonding between a H atom in the NH_3 moiety and the O atom of the triflate moiety, with distances of 2.2(1) Å for **11** and 2.1(1) Å for **12**. The positions of the hydrogen atoms on the ammonia nitrogen atom were located using the electron density map and not refined using an ideal geometrical model.

The-above discussed direct pathway to the ammonia adduct is very interesting as it requires a very inexpensive and readily available nucleophile. Since it was shown previously that POCOP pincer complexes decompose in basic media,[40e] it is significant that the fragile P-O linkage of the POCOP ligands survives the basic aqueous conditions of the reaction with NH_4OH. The formation of this adduct also implies that ammonia is a much stronger ligand

compared to water, and the latter is in turn stronger than the triflate moiety as reported in a previous study.[35b]

Table 3.4 Bond distances (Å) and angles (deg.) for complexes **11** and **12**

	11	**12**
Ni-C	1.894(2)	1.890(2)
Ni-N	1.961(2)	1.962(2)
Ni-P1	2.1862(4)	2.1873(5)
Ni-P2	2.1850(4)	2.1807(5)
P1-Ni-P2	162.96(2)	163.37(2)
C1-Ni-N	177.01(6)	177.70(7)

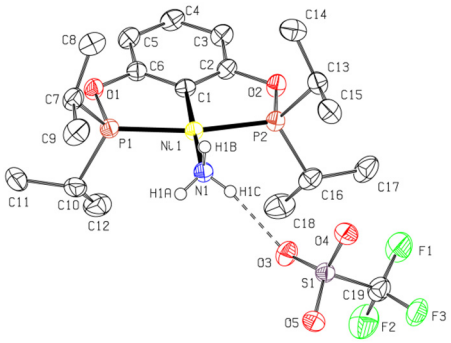

Figure 3.5 Molecular diagram for complex **11.**

Thermal ellipsoids are shown at the 50% probability level. Hydrogens are omitted for clarity

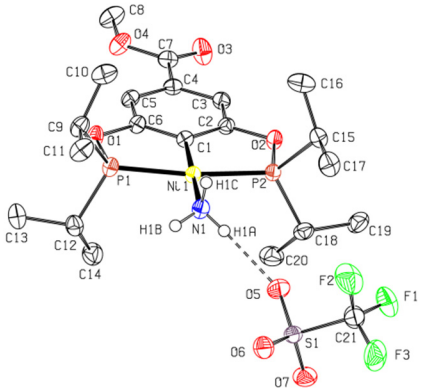

Figure 3.6 Molecular diagram for complex **6**. Thermal ellipsoids are shown at the 50% probability level. Hydrogens are omitted for clarity

As a final test for the feasibility of the inner-sphere mechanism, we treated the ammonia adducts with NaH in an effort to form the postulated charge-neutral Ni-amido derivatives via deprotonation; these reactions failed to generate the target Ni-NH_2 species, leading instead to the decomposition of the starting materials, presumably because of secondary reactions at the relatively fragile P-O linkage.[40e] Finally, addition of excess acetonitrile to the ammonia adducts **11** and **12** at r.t. resulted in significant broadening of the original ^{31}P NMR signal of the ammonia adduct, giving $LW_{1/2}$ of 127 Hz with 10 equiv of MeCN and 187 Hz with 50 equiv. These observations imply that ammonia is a highly competitive nucleophile for binding to the Ni center.

3.4 Conclusion

This study has generated a number of findings in support of the outer-sphere reaction mechanism postulated for the Ni(II)-promoted Michael-type hydroamination of acrylonitrile and its substituted derivatives. For instance, ligand binding studies showed that the cationic, nitrile-coordinated adducts of the substrates are the dominant species under the conditions of the catalytic reactions (1:1 mixture of amines and nitrile substrates); this observation is consistent with the idea that the key role of the Ni(II) center in the catalytic cycle is to activate the substrate toward nucleophilic attack by amines.[71] Indeed, cationic adducts of crotonitrile and methacrylonitrile could be isolated and characterized spectroscopically. The catalytic tests undertaken also showed that addition of aniline to crotonitrile and methacrylonitrile over a short time period (2 h) proceed with higher yields in the presence of pre-catalyst **4**, the more electrophilic of the two cationic acetonitrile adducts tested. Moreover, this same pre-catalyst was the only one that could promote the addition of aniline to cinnamonitrile, the least reactive Michael acceptor examined.

On the other hand, some of the observations from our catalytic tests appear to be inconsistent with the main elements of the outer-sphere proposal. For instance, for the addition of the more nucleophilic aliphatic amines onto crotonitrile and methacrylonitrile, the greater catalytic activities were observed with complex **3**, the *less* electrophilic of the two pre-catalysts investigated, regardless of the time period over which the catalytic reactions were monitored.

This finding does not correlate well with a mechanism in which activation of the nitrile-coordinated substrate plays an important role in determining reactivities.[72] Moreover, allowing a longer reaction time resulted in a reversal of catalytic activities for the addition of aniline: complex **3** led to higher yields when the reactions were allowed to run over 20 h.

Finally, the structural analyses of the substrate adduct **7**, **9**, and **10** revealed no concrete structural evidence for the anticipated activation of the nitrile-coordinated acrylonitrile or cinnamonitrile substrate. These observations suggest that even if the outer-sphere postulate fairly represents the "true" mechanism of action in this system, there are many kinetic subtleties that must be understood in order to rationalize all observations. We have speculated that one such subtlety is that the stronger nitrile-Ni binding anticipated with the more electrophilic precursor **4** can result in a stronger binding of the addition product; such a product inhibition factor would, in turn, hinder the product-substrate exchange equilibrium that is crucial for turnover in the envisaged catalytic cycle.

The somewhat ambiguous nature of the above results prompted us to isolate and study amine adducts that are postulated to be involved in the alternative, inner-sphere mechanism for the title reactions. Although ligand exchange studies showed that certain amines have sufficiently strong binding capacities to generate observable amine adducts, we were unable to isolate thermally stable adducts of the amines that are active in hydroamination reactions with the nitrile substrates in question. However, two new cationic ammonia adducts were isolated, which allowed us to study the structures of these rare complexes. Finally, preliminary ligand exchange studies showed that ammonia-Ni interaction is sufficiently robust so as not result in displacement of the NH_3 moiety by large excess of acetonitrile.

Future studies will aim to examine more closely the kinetics of the Michael-type hydroamination of acrylonitrile with the objective of establishing the relative importance of the various steps in the postulated reaction mechanism, including coordination-activation of the nitrile substrate, nucleophilic attack by amines, H^+-transfer, as well as product inhibition. Of utmost importance will be to identify unequivocally which, if any, of these steps is the rate-determining event in the catalytic process

3.5 Experimental section

3.5.1 General procedures

Unless otherwise indicated, all manipulations were carried out under a nitrogen atmosphere using standard Schlenk and glovebox techniques. The solvents were dried by passage over activated alumina contained in MBRAUN-SPS systems and analyzed by a Coulorimetric Karl Fischer titrator to acceptable water content. Triethylamine was dried by distillation over CaH_2. The following reagents and NMR solvents were purchased from Sigma-Aldrich and used without further purification: acrylonitrile, methacrylonitrile, crotonitrile, cinnamonitrile, silver trifluoromethanesulfonate, C_6D_6 and $CDCl_3$.

NMR spectra were recorded using Bruker AVII400 and AV500 spectrometers. Chemical shift values are reported in ppm (δ) and referenced internally to the residual solvent signals (^1H and ^{13}C: 7.26 and 77.16 ppm for $CDCl_3$; 7.16 and 128.06 ppm for C_6D_6) or externally (^{31}P, H_3PO_4 in D_2O, δ = 0). Coupling constants are reported in Hz. Due to either insufficiently concentrated samples or an insufficient number of scans collected, we were unable to ^{13}C signals for some quaternary carbons. In the case of the ^{13}C signal for the triflate moiety, a similar observation has been reported previosuly in closely related complexes.[24b] The IR spectra were recorded on a Bruker Alpha-P FTIR (4000-400 cm^{-1}). The elemental analyses were performed by the Laboratoire d'Analyse Élémentaire, Département de Chimie, Université de Montréal. Synthesis and characterization of complexes **1**-**6** as well as the triflate complex have been reported elsewhere.[24b, 66] Synthesis of the neutral bromo or chloro precursors were done following reported procedures.[24b, 25]

Ligand exchange reactions with the charge-neutral triflate complex and different amines and acrylonitrile were probed as follows. To an NMR tube containing a 0.086 M solution of the charge-neutral triflate complex (prepared following a procedure published elsewhere[35b]) was added 10 equiv of the target amine. The ^{31}P NMR spectrum was recorded following a vigorous shaking of the sample tube to ensure complete mixing. To the same solution was added 3.0 equiv of acrylonitrile and another ^{31}P NMR spectrum was recorded after more vigorous shaking.

Catalytic tests were performed following this general procedure. In a sealable vial was placed the amine and nitrile substrates (1 mmol each), NEt_3 (1 mmol), the internal standard (dodecane, 0.1 mmol), and 0.5 mL of a 0.02 M solution of the Ni precursor (**3** or **4**) in THF, and the resulting mixture was heated at 50 °C for the designated time. A small aliquot of the final mixture was diluted with acetone (~100x) and analyzed by GC/MS. The conversion and yield were determined based on a calibration curve prepared using authentic samples of the anticipated products.

3.5.2 [(2,6-(*i*-$Pr_2OP)_2$4-$(CO_2CH_3)C_6H_2$)Ni(NCCHCH$_2$)][OSO_2CF_3] (7).

To a Schlenk flask containing the charge-neutral chloro complex (2,6-(*i*$Pr_2OP)_2$-4-$(CO_2Me)C_6H_2$)NiCl [25] (114 mg, 0.230 mmol, 1.00 equiv) in dichloromethane (15 mL) was added silver triflate (71 mg, 0.28 mmol, 1.2 equiv) and acrylonitrile (5 mL) at rt. The solution was then agitated for 3 h and filtered to remove the insoluble silver salts. Evaporation of the filtrate gave the desired product as a yellow solid (125 mg, 80%). Single crystals suitable for diffraction studies were obtained from slow evaporation of a concentrated THF solution of the complex.

^{1}H NMR (400 MHz, $CDCl_3$) δ 1.35 (q, J_{HH} = 7, 12H, P(CHC(C***H*****$_3$**)$_2$)$_2$), 1.42 (q, J_{HH} = 7, 12H, P(CHC(C***H*****$_3$**)$_2$)$_2$), 2.57 (sept, J_{HH} = 6, 4H, P(C***H***C$(CH_3)_2)_4$), 3.86 (s, 3H, CO_2C***H*****$_3$**), 6.15 (dd, J_{HH} = 12; 18, 1H, NCC***H***=CH_2), 6.33 (d, J_{HH} = 12, 1H, NCCH=C***H***H), 6.42 (d, J_{HH} = 18, 1H, NCCH=CH***H***). ^{13}C{^{1}H} NMR (101 MHz, $CDCl_3$) δ 16.86 (s, 4C, P(CH(***C***$H_3)_2)_2$), 17.60 (t, J_{PC} = 3, 4C, P(CH(***C***$H_3)_2)_2$), 28.68 (t, J_{PC} = 11, 4C, P(***C***H$(CH_3)_2)_4$), 52.4 (s, 1C, C_{Ar}-CO_2***C***H_3), 107.10 (t, J_{PC} = 6, 2C, ***C$_{Ar}$***H), 107.33 (s, 1C, Ni-***C$_{ipso}$***), 133.18 (s, 1C, ***C$_{Ar}$***CO_2CH_3), 141.38 (s, 1C, NCCH=***C***H_2), 166.27 (s, 1C, C_{Ar}***C***O_2CH_3), 168.94 (t, J_{PC} = 9, 2C, (***C$_{Ar}$***-OP)$_2$). ^{31}P{^{1}H} NMR (162 MHz, C_6D_6) δ 192.2 (s). ^{19}F {^{1}H} NMR (376 MHz, $CDCl_3$) δ -77.97 (s). Elemental analysis was not satisfactory for this complex, because it proved difficult to remove all traces of solvents.

3.5.3 [(2,6-(*i*-$Pr_2OP)_2$4-$(OCH_3)C_6H_2$)Ni(NCCHCH$_2$)][OSO_2CF_3] (8).

The procedure described above for the preparation of 7 was used for this synthesis, using (2,6-(*i*$Pr_2OP)_2$-4-$(OMe)C_6H_2$)NiCl[25] (199 mg, 0.430 mmol, 1.00 equiv) as starting material. The desired product was obtained as a yellow solid (271 mg, 98%).

^{1}H NMR (500 MHz, C_6D_6) δ 1.15 (q, J_{HH} = 8, 12H, P(CHC(C***H***$_3$)$_2$)$_2$), 1.36 (q, J_{HH} = 9, 12H, P(CHC(C***H***$_3$)$_2$)$_2$), 2.41 (sept, J_{HH} = 8, 4H, P(C***H***C(CH$_3$)$_2$)$_4$), 3.18 (s, 3H, OC***H***$_3$), 5.61 (s(br), 1H, NCCH=C***H***H), 5.70 (s(br), 1H, NCC***H***=CH$_2$), 6.00 (d(br), J_{HH} = 23, 1H, NCCH=CH***H***). 6.19 (s, 2H, (C$_{Ar}$***H***)$_2$). ^{13}C{^{1}H} NMR (125 MHz, C_6D_6) δ 16.71 (s, 4C, P(CH(***C***H$_3$)$_2$)$_2$), 17.58 (t, J_{PC} = 3, 4C, P(CH(***C***H$_3$)$_2$)$_2$), 28.58 (t, J_{PC} = 11, 4C, P(***C***H(CH$_3$)$_2$)$_4$), 55.11 (s, 1C, C$_{Ar}$O***C***H$_3$), 93.50 (vt, $^{v}J_{PC}$ = 8, 2C, (***C$_{Ar}$***H$_{meta}$)$_2$), 107.28 (s, 1C, Ni-***C$_{ipso}$***), 140.61 (s, 1C, NCCH=***C***H$_2$), 163.79 (s, 1C, ***C$_{Ar}$***OCH$_3$), 170.00 (t, J_{PC} = 9, 2C, (***C$_{Ar}$***-OP)$_2$). ^{31}P{^{1}H} NMR (162 MHz, C_6D_6) δ 194.9 (s). ^{19}F{^{1}H} NMR (376 MHz, C_6D_6) δ -77.48 (s). Elemental analysis was not satisfactory for this complex, because it proved difficult to remove all traces of solvents

3.5.4 [(2,6-(*i*-Pr$_2$OP)$_2$4-(CO$_2$CH$_3$)C$_6$H$_2$)Ni(NCCH=CHPh)][OSO$_2$CF$_3$] (9).

To a Schlenk flask containing the charge-neutral chloro complex (2,6-(*i*Pr$_2$OP)$_2$-4-(CO$_2$Me)C$_6$H$_2$)NiCl[25] (268 mg, 0.540 mmol, 1.00 equiv) in dichloromethane (15 mL) was added silver triflate (167 mg, 0.650 mmol, 1.20 equiv) and cinnamonitrile (682 µL, 5.43 mmol, 10.0 equiv) at rt. The solution was then agitated overnight and filtered to remove the insoluble silver salts. Single crystals suitable for x-ray diffraction were obtained by slow evaporation in air of the dichloromethane solution. The crystals obtained were washed with cold hexanes and crushed, giving a yellow-orange powder (252 mg, 63%).

^{1}H NMR (400 MHz, C_6D_6) δ 1.08 (q, J_{HH} = 8, 12H, P(CHC(C***H***$_3$)$_2$)$_2$), 1.33 (q, J_{HH} = 8, 12H, P(CHC(C***H***$_3$)$_2$)$_2$), 2.36 (sept, J_{HH} = 8, 4H, P(C***H***C(CH$_3$)$_2$)$_4$), 3.43 (s, 3H, CO$_2$C***H***$_3$), 6.65-7.04 (m(br), 7H, NCC***H***=C***H***(C$_6$***H$_5$***)), 7.38 (s, 2H, (C$_{Ar}$***H***)$_2$). ^{13}C NMR (101 MHz, $CDCl_3$) δ 16.87 (s, 4C, P(CH(***C***H$_3$)$_2$)$_2$), 17.69 (t, J_{PC} = 3, 4C, P(CH(***C***H$_3$)$_2$)$_2$), 28.80 (t, J_{PC} = 12, 4C, P(***C***H(CH$_3$)$_2$)$_4$), 52.45 (s, 1C, C$_{Ar}$CO$_2$***C***H$_3$), 96.09 (s, 1C, NC***C***H=CH(C$_6$H$_5$)), 107.24 (s, 2C, ***C$_{Ar}$***H$_{meta}$) 127.62 (s, 2C, NCCH=CH(***C$_{ortho}$***C$_4$H$_5$)), 129.23 (s, 2C, NCCH=CH(***C$_{meta}$***C$_4$H$_5$)), 131.51 (s, 1C, NCCH=CH(***C$_{para}$***C$_5$H$_5$)), 133.51 (s, 1C, NCCH=CH(***C$_{ipso}$***C$_5$H$_5$)), 151.41 (s, 1C, NC***C***H=CH(C$_6$H$_5$)), 166.27 (s, 1C, C$_{Ar}$***C***O$_2$CH$_3$), 168.94 (t, J_{PC} = 9, 2C, (***C$_{Ar}$***-OP)$_2$). ^{31}P{^{1}H} NMR (162 MHz, $CDCl_3$) δ 194.27 (s). ^{19}F{^{1}H} NMR (376 MHz, $CDCl_3$) δ -77.98 (s). Elemental analysis was not satisfactory for this complex, because it proved difficult to remove all traces of solvents

3.5.5 [(2,6-(*i*-Pr$_2$OP)$_2$4-(OCH$_3$)C$_6$H$_2$)Ni(NCCH=CHPh)][OSO$_2$CF$_3$] (10).

The same procedure described above for the preparation of **9** was used for this synthesis, using **(2,6-(*i*Pr$_2$OP)$_2$-4-(OMe)C$_6$H$_2$)NiBr** [11b] (500 mg, 0.980 mmol, 1.00 equiv) and furnished a yellow-orange powder (486 mg, 70 %).

^{1}H NMR (400 MHz, C$_6$D$_6$) δ 1.18 (q, J_{HH} = 8, 12H, P(CHC(C***H***$_3$)$_2$)$_2$), 1.38 (q, J_{HH} = 8, 12H, P(CHC(C***H***$_3$)$_2$)$_2$), 2.46 (sept, J_{HH} = 8, 4H, P(C***H***C(CH$_3$)$_2$)$_4$), 3.18 (s, 3H, **OC*H*$_3$)**, 6.02 (s, 2H, C$_{Ar}$***H*$_{meta}$**), 6.35 (s(br), 1H, NCC***H***=CH(C$_6$H$_5$)), 7.05 (s(br), 3H, NCCH=C***H***(C$_6$(***H*$_{ortho}$**)$_2$H$_3$)), 7.53 (m(br), 3H, NCCH=CH(C$_6$H$_2$(***H*$_{meta}$**)$_2$***H*$_{para}$**)). ^{13}C NMR (101 MHz, CDCl$_3$) δ 16.87 (s, 4C, P(CH(***C***H$_3$)$_2$)$_2$), 17.66 (s, 4C, P(CH(***C***H$_3$)$_2$)$_2$), 28.64 (t, J_{PC} = 12, 4C, P(***C***H(CH$_3$)$_2$)$_4$), 55.68 (s, 1C, C$_{Ar}$O***C***H$_3$), 93.24 (t, J_{PC} = 7, 1C, ***C*$_{Ar}$**H$_{meta}$), 95.360 (s, 1C, NC***C***H=CH(C$_6$H$_5$)), 113.05 (t, J_{PC} = 21, 1C, N***C***CH=CH(C$_6$H$_5$)) 128.15 (s, 2C, NCCH=CH(***C*$_{ortho}$**C$_4$H$_5$)), 129.22 (s, 2C, NCCH=CH(***C*$_{meta}$**C$_4$H$_5$)), 131.94 (s, 1C, NCCH=CH(***C*$_{para}$**C$_5$H$_5$)), 133.27 (s, 1C, NCCH=CH(***C*$_{ipso}$**C$_5$H$_5$)), 163.55 (s, 1C, ***C*$_{Ar}$**OCH$_3$), 169.28(t, J_{PC} = 9, 2C, (***C*$_{Ar}$**-OP)$_2$). ^{31}P{^{1}H} NMR (202 MHz, CDCl$_3$) δ 194.37 (s). ^{19}F{^{1}H} NMR (470 MHz, CDCl$_3$) δ -78.13 (s). Anal. calcd. for C$_{38}$H$_{47}$F$_3$N$_2$NiO$_6$P$_2$S (837.5): C, 54.50; H, 5.66; N, 3.34; S: 3.83. Found: C, 55.04; H, 5.81; N, 3.50; S, 3.37.

3.5.6 [(2,6-(*i*Pr$_2$OP)$_2$C$_6$H$_3$)Ni(NH$_3$)][OSO$_2$CF$_3$] (11).

Procedure 1. To a Schlenk flask containing the charge-neutral triflate complex (2,6-(*i*Pr$_2$OP)$_2$C$_6$H$_3$)Ni(OSO$_2$CF$_3$) (1-OTf) (975 mg, 1.78 mmol, 1.00 equiv) was added tris(trimethylsillyl)amine (415 mg, 1.78 mmol, 1.00 equiv) and water (96 µL, 5.3 mmol, 3.0 equiv) at rt. The solution was then agitated for 2 h and the resulting insoluble, black oily residue was removed. Evaporation of the solution gave the desired product as a yellow solid (715 mg, 71 %). Single crystals suitable for x-ray diffraction were obtained by a slow evaporation in air of an acetone solution.

Procedure 2. To a Schlenk flask containing the charge-neutral bromo complex (2,6-(*i*Pr$_2$OP)$_2$C$_6$H$_3$)NiBr (240 mg, 0.500 mmol, 1.00 equiv) in THF (15 mL) was added NH$_4$OH (38.9 µL, 1.00 mmol, 2.00 equiv) and AgOTf (154 mg, 0.600 mmol, 1.20 equiv) at rt. The solution was then agitated for 2 h, filtered to remove the AgBr salts, and the organic phase

separated. Evaporation of the solution gave the desired product as a yellow solid (254 mg, 90 %).

^{1}H NMR (400 MHz, C_6D_6): δ 1.10 (q, J_{HH} = 7, 12H, P(CHC(C***H*****3**)2)2), 1.32 (q, J_{HH} = 8, 12H, P(CHC(C***H*****3**)2)2), 2.34 (sept, J_{HH} = 7, 4H, P(C***H***C(CH3)2)4), 2.96 (s(br), 3H, N***H*****3**), 6.46 (d, J_{HH} = 8, 2H, C_{Ar}-***H*****meta**), 6.80 (t, J_{HH} = 8, 1H, C_{Ar}-***H*****para**). ^{13}C{^{1}H} NMR (101 MHz, $CDCl_3$) δ 16.80 (s, 4C, P(CH(***C***H3)2)2), 17.77 (t, J_{PC} = 3, 4C, P(CH(***C***H3)2)2), 28.21 (t, J_{PC} = 11, 4C, P(***C***H(CH3)2)4), 105.73 (t, J_{PC} = 6, 2C, (***C*****Ar**-Hmeta)2), 130.25 (s, 1C, ***C*****Ar**-Hpara), 168.90 (t, J_{PC} = 9, 2C, (***C*****Ar**-OP)2). ^{31}P{^{1}H} NMR (162 MHz, C_6D_6) δ 189.42 (s). ^{19}F {^{1}H} NMR (376 MHz, C_6D_6) δ -77.97 (s). Anal. calcd. for $C_{19}H_{34}F_3NNiO_5P_2S$ (566.18): C, 40.31; H, 6.05; N, 2.47; S: 5.66. Found: C, 40.95; H, 6.11; N, 2.18; S, 5.13.

3.5.7 [(2,6-(*i*Pr$_2$OP)$_2$-4-(CO$_2$CH$_3$)C$_6$H$_2$)Ni(NH$_3$)][OSO$_2$CF$_3$] (12).

The procedure 2 described above for the preparation of 11 was used for this synthesis using (2,6-(*i*Pr$_2$OP)$_2$-4-(CO$_2$Me)C$_6$H$_2$)NiBr [11b] (215 mg, 0.400 mmol, 1.00 equiv). The desired product was obtained as a yellow solid (211 mg, 85 %). Crystals suitable for x-ray diffraction were obtained by slow evaporation from a concentrated acetone solution.

^{1}H NMR (500 MHz, C_6D_6): δ 1.06 (q, J_{HH} = 7, 12H, P(CHC(C***H*****3**)2)2), 1.28 (q, J_{HH} = 8, 12H, P(CHC(C***H*****3**)2)2), 2.31 (sept, J_{HH} = 7, 4H, P(C***H***C(CH3)2)4), 3.00 (s(br), 3H, N***H*****3**), 3.43 (s, 3H, OC***H*****3**) 7.42 (s, 2H, C_{Ar}-***H*****meta**). ^{13}C{^{1}H} NMR (126 MHz, $CDCl_3$) δ 16.46 (s, 4C, P(CH(***C***H3)2)2), 17.62 (s, 4C, P(CH(***C***H3)2)2), 28.40 (t, J_{PC} = 11, 4C, P(***C***H(CH3)2)4), 51.72 (s, 1C, O***C***H3) 107.05 (t, J_{PC} = 6, 2C, ***C*****Ar**-Hmeta), 131.41 (s, 1C, ***C*****ipso**-Ni), 133.29 (s, 1C, ***C*****Ar**CO2CH3) 166.13 (s, 1C, CArCO2CH3), 168.90 (t, J_{PC} = 9, 2C, ***C*****Ar**-OP). ^{31}P{^{1}H} NMR (202 MHz, C_6D_6) δ 190.94 (s). ^{19}F {^{1}H} NMR (376 MHz, C_6D_6) δ -78.03 (s). Anal. calcd. for $C_{21}H_{36}F_3N_1Ni_1O_7P_2S_1$ (624.22): C, 40.41; H, 5.81; N, 2.24; S: 5.14. Found: C, 40.26; H, 5.87; N, 2.16; S, 4.92.

3.6 Acknowledgments

The authors are grateful to: NSERC of Canada for financial support of this work (Discovery and RTI grants to D.Z.); Dr. Michel Simard and Ms. Francine Bélanger-Gariépy for

their valuable assistance with crystallography and many interesting discussions; Ms. Elena Nadezhina for the elemental analyses; Mr. Jean-Philippe Cloutier for the DFT calculations that helped shed some light on the IR results; and reviewers of our manuscript for many valid and insightful suggestions. S.L. is also grateful to Centre in Green Chemistry and Catalysis for a travel award and to all group members for many valuable discussions and practical advice.

Contribution de l’auteur

J’ai effectué toutes les manipulations, synthèses, études catalytiques et cinétiques dans ce chapitre libre. De plus, j’ai rédigé le chapitre libre et l’ai révisé avec l’aide de Pr. Zargarian.

Chapitre 4: Application of Cationic Acetonitrile Nickel Pincer Complexes as Catalysts in Michael-type hydroamination and hydroalkoxylation of nitriles

Sébastien Lapointe and Davit Zargarian[†]

[†] Département de chimie, Université de Montréal, Montréal (Québec), Canada H3C 3J6

Chapitre en rédaction libre

4.1 Abstract

This report presents the results of a catalyst screening and mechanistic study on the aza-Michael addition reaction of acrylonitrile and its substituted derivatives (also known as hydroamination when an amine is used, and hydroalkoxylation when an alcohol is used) catalyzed by a family of cationic POCOP-type pincer nickel complexes featuring different substitution patterns on the central aromatic ring. Whereas the impact of POCOP-substituents on the catalytic activities of the precatalysts is not clear-cut, our results show that the type of amine, alcohol, and nitrile substituent used has significant influence on the outcome of the catalytic reactions. Thus, the addition of aniline to acrylonitrile proceeds with mostly quantitative yields in only 2 h at 50 °C with all catalysts screened (turnover numbers, TON, of 100 or 200 with 1 mol% or less of catalyst). The catalysis is quite rapid at 50 °C (TON ~83 in 5 min), but much slower reactions are observed at r.t. (TON~ 20 in 4 h). Lower catalytic activities were also noted with anilines bearing a halide at the *ortho* position of the Ph ring: Yields = 71 % for F, ~64 % for Cl and Br, and 36 % for I. The corresponding activity with 2,5-Me_2-aniline was 80 %. These results underline the greater importance of steric versus electronic factors for this reaction. Aliphatic amines showing activities for addition to acrylonitrile include benzylamine (100 %), cyclohexylamine (64 %), octylamine (61 %), *N*-ethylaniline (54 %), ethanol amine (21 %), and *i*-Pr_2NH (3 %). It should be noted that significant amounts of double-addition products $RN(CH_2CH_2CN)_2$ are also generated from the addition to acrylonitrile by octylamine (yield = 34 %) as well as aniline and its substituted derivatives $ArNH_2$ (Yield =3-16 %). Ethanol amine also generates a double-addition product (yield = 10 %), but in this case the side-product arises from the reaction of the OH moiety in the mono-addition product. In comparison to acrylonitrile, all other nitrile substrates proved less reactive. Thus, addition various amines to crotonitrile and methacrylonitrile proceeded with the following yields: aniline (21 % and 28 %), cyclohexylamine (39 % and 36 %), octylamine (34 % and 56 %), and ethanol amine (14 % and 18 %). Very small amounts of double-addition side-products are observed with crotonitrile and methacrylonitrile, but are still present. The least reactivity was observed with cinnamonitrile: among the amines tested, morpholine was the only one that showed some reactivity (22 % yield). Finally, addition of phenol and its substituted derivatives to acrylonitrile

proceeded with much lower yields compared to amines: PhOH (16 %), 3,4,5-Me_3-PhOH (20 %), 3-OMe-PhOH (14 %), and 3-CF_3-PhOH (12 %). Addition of these alcohols to crotonitrile gave even lower activities (2-6 % yield), while methacrylonitrile and cinnamonitrile were completely inert.

A number of kinetic studies and ligand exchange tests have provided interesting insights on the mechanism of this aza-Michael addition (hydroamination) in our system. Monitoring the addition of aniline to acrylonitrile by ^{1}H NMR under pseudo-first order conditions showed results consistent with a second order reaction, but there are some indications that more complex behavior takes place at different stages of the catalysis, in particular after ca. 90% of the nitrile substrate has been consumed. Product inhibition is also believed to play a role in the kinetics as inferred from the competitive binding of the nitrile moiety in the addition product. These and other observations have allowed us to propose a slightly modified mechanism for this hydroamination of acrylonitrile catalyzed by $[(R\text{-POCOP})Ni(NCR)]^+$.

4.2 Introduction

Amines have been one of the most important classes of compounds since the beginning of chemistry, and they have been used in diverse applications ranging from solvents to additives and dyes, and they are very much present in pharmaceuticals and biologically active compounds. Many types of reactions involving amines have been developed in the past, but many of them needed complex amines which were not always easy to prepare and could be quite hazardous to handle. However, in this paper we will investigate an atom-economical and green method of preparing amine derivatives by a Michael addition reaction of amines (or as a more general concept, hydroamination) on nitriles.

Michael addition is the general concept of 1,4-additions to C=X multiple bonds. In this chapter, we focus on amine additions. Michael additions can happen in two different pathways : intermolecular or intramolecular. Many different types of compounds can, and have been, prepared using the intramolecular pathway, mostly to form different types of heterocycles by the addition of an aminoalkene substrate. Intramolecular hydroaminations have been studied very intensively, with the first example reported by Marks[73] in 1989 using rare-earth metal

catalysts. Also, many of the catalysts used are early-transition metal catalysts, as they have a greater propensity towards the addition of the amine on the metal center, which is an important step in this intramolecular mechanism. Late-transition metal catalysts, lanthanides and simple salts have also been widely used as catalysts.[61, 62d-f, 62i, 74] Hydroamination reactions can also be catalyzed by a variety of Lewis acids[75] and, in some cases, even Brønsted acids.[76]

Intermolecular hydroamination usually requires more forcing conditions and has a narrower range of compatible substrates. They usually involve either nonactivated olefins or activated alkenes that can coordinate through binding of the olefin moiety onto the active site. These types of addition reactions are usually not possible without the use of a metal, and usually have high activation barriers. In the case of some activated alkenes, the use of a metal is not necessary for the reaction to occur, but these usually require more demanding conditions to proceed; moreover, these reactions work with a very limited range of substrates. Nonactivated olefins are often used with late transition metals and usually require expensive and noble metals to activate the double bond. A very recent review[77] covers many aspects of late-transition metal catalyzed hydroamination reactions. However, there also are quite a few examples of early transition metal systems that react with non-activated olefins, such as with Ti or Zr. [78]

Nevertheless, the last few years have witnessed an increasing interest for the study of Michael addition reactions thanks to the emergence of pincer complexes featuring stable backbones and a labile coordination site around the metal center. Many different types of catalysts and metals have been developed that allow efficient activation of the olefinic double bond, thus facillitating the subsequent nucleophilic attack by the amine. Interestingly, a few systems have shown that ammonium salts can be used as the nucleophile in the Michael addition of acrylonitrile promoted by a $PC_{sp3}P$ palladium complex; the mechanism of these reactions has been intensively studied by Trogler [62a, 79] and others.[80]

Cationic pincer complexes promote the intermolecular hydroamination of activated (functionalized) alkenes, because the greater electrophilicity of the metal center in these compounds favors their binding through the functional group (e.g., the nitrile moiety of acrylonitrile) and further activates the double bond towards nucleophilic attack by an amine. Our group has previously studied the cationic complex **1** ([(2,6-(*i*-$Pr_2OP)_2C_6H_3$)$Ni(NCCH_3)$][OSO_2CF_3])[24b] and its BPh_4[24a] analogue in the intermolecular

hydroamination of acrylonitrile with different amines. The neutral trifluoromethanesulfonate (triflate) derivatives [(POCOP^{R})Ni(OTf)] (OTf= OSO_2CF_3; R = *i*Pr, Ph] have also been used as pre-catalysts with different primary amines and in the presence of additives.[35b] However, these pre-catalysts proved less versatile than their cationic counterparts because they were prone to hydrolysis, the facile displacement of the OTf moiety by residual water leading to less active aquo adducts (when R = *i*Pr) or triggering a decomposition to a catalytically inert octahedral tetra(aqua) complex (when R = Ph).[35b]

The electrophilic nature of the nickel center in the cationic compounds facilitates the hydroamination reaction, but this reactivity appears to be limited to acrylonitrile only, substituted derivatives such as methacrylonitrile or crotonitrile giving very poor yields or no reaction at all.[24b] This limitation prompted us to study the impact of placing electron-withdrawing substituents on the aromatic backbone of the POCOP ligands in anticipation of enhancing the activating capacity of our cationic complexes and magnifying the δ^+ character of the alkene moiety of coordinated substrates, thus facilitating nucleophilic attack on less reactive substrates. This report describes the catalytic activities of the complexes **1-6** [66] with the general formula [(R-POCOP$^{R'}$)Ni(NCMe)][OSO_2CF_3], where R is a ring substituent and R' is a *P*-substituent (R' = *i*Pr : R = H (**1**), *p*-Me(**2**), *p*-OMe(**3**), *p*-CO_2Me(**4**), *p*-Br(**5**), *m,m*-*t*Bu_2(**6**)), in the hydroamination and hydroalkoxylation reactions on acrylonitrile and its substituted derivatives, as well as some attempts at a better understanding of the mechanism underlying these reactions.

4.3 Results and Discussion

4.3.1 Hydroamination studies

In this report, different aromatic and aliphatic amines were screened for their activities in the hydroamination reaction with the nitrile (RCN) substrates shown in **Scheme 4.1**. The effect of different electron-withdrawing or donating groups on both the amine moiety and on the aromatic backbone of catalysts **1-6** have been examined. We have also investigated different substitutents on the nitrile moiety. As will be explained below, good results were achieved with some aromatic amines with acrylonitrile. Compared to other catalytic systems,[34] we found that

methacrylonitrile and crotonitrile were quite active. High yields of the expected products were also obtained in most cases with acrylonitrile, in particular when aromatic primary amines were used. On the other hand, the reactivity of cinnamonitrile was not achieved except with morpholine, and even then only low yields was observed. Plots of the hydroamination of acrylonitrile (14c), crotonitrile (14a) and methacrylonitrile (14b) with catalysts **1-6** over 2 h are given in **Figures 4.1-3**; plots for the remaining yield (TON) and TOF (TON/time, h^{-1}) over 2 and 20 h are given in Figures **A4.1-25**. These plots attest to the absence of a strong correlation between catalytic activities and the choice of substituents on either the POCOP moiety or the amine.

Scheme 4.1 Hydroamination of nitriles catalyzed by complexes **1-6**

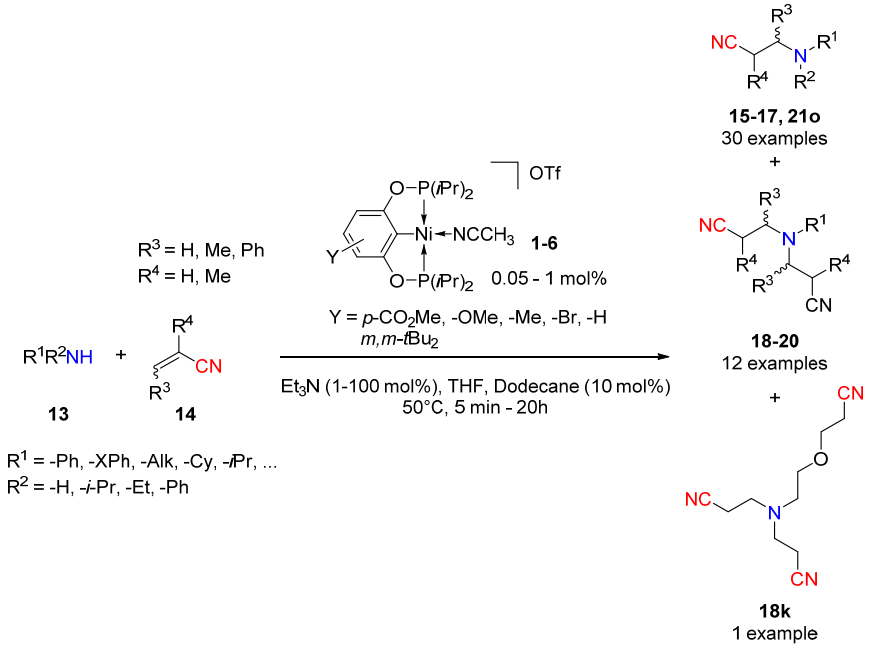

4.3.2 Reactions with acrylonitrile

Previous studies on hydroamination of acrylonitrile catalyzed by late-transition metal systems[24b, 34] usually report higher TON with aliphatic amines rather than aromatic ones under similar conditions, an outcome that is expected and can be rationalized based on the higher nucleophilicity of aliphatic amines. Therefore, we were surprised to observe that addition of aniline to acrylonitrile catalyzed by our complexes gave better yields than addition of any

aliphatic amine. Thus, with all cationic catalysts tested, aniline gave quantitative yields after 2 h at 50 °C (see General procedures for catalytic runs in "Annexe pour Chapitre 4" for the experimental conditions). In contrast, addition of a more nucleophilic aliphatic amine such as cyclohexylamine gave only between 50 % to 64 % yield under the same conditions. It is also important to note that control experiments (using no catalyst) led to no reaction for up to 20h under standard conditions for all amines except for cyclohexylamine (**13h**) and octylamine (**13i**), as well as benzylamine (**13m**) and n-ethylaniline (**13n**) ; where the products **15h**, **15i**, **15m** and **15n** were obtained in 16 %, 5 %, 30 % and 30 % yields, respectively (see **Scheme 4.2**). After 20 h and in the absence of catalyst, we obtain more of the expected product **15h** and **15i** in 26 % yield and 45 % yield, respectively (See **Table A4.13** in "*Annexe pour Chapitre 4*"). The factors responsible for the lower activity observed with aliphatic amines has been investigated in detail and will be described later.

As is depicted in **Scheme 4.2**, addition of most amines to acrylonitrile gave modest yields. Analysis of the results with differently substituted aromatic amines gives us an idea of the impact of these substituents on reaction yields. A mechanism wherein the rate limiting step is a nucleophilic attack by the amine on a coordinated nitrile would require that weakly nucleophilic amines should be ineffective or completely inactive in the hydroamination reaction. Thus, we see that the reactions using *p*-nitroaniline in the presence of complexes **1-6** and a variety of nitriles did not produce any of the expected products, which is consistent with the above-postulated mechanism. 2-Haloanilines also seem to give lower reaction yields, but consideration of the yields observed 2-fluoroaniline (ca. 71%), 2-chloroaniline (ca. 64%), 2-bromoaniline (ca. 65%), and 2-iodoaniline (ca. 36 %) suggests that steric factors might be at work. The importance of steric effects but also electronic effects can be seen with the analogous reaction with *o,m*-dimethylaniline (**13f**), which gives higher yield (ca. 80 %), but less than that of aniline (quantitative). We thus believe that a complex combination of both steric and electronic factors might explain this behavior. The *o*-Me group increases the steric hindrance in the complex as well as the nucleophilicity of the amine, and the *m*-Me group renders the amine more nucleophile, which explains its greater reactivity compared to the less nucleophilic halo-substituted anilines even if the steric hindrance could suggest otherwise.

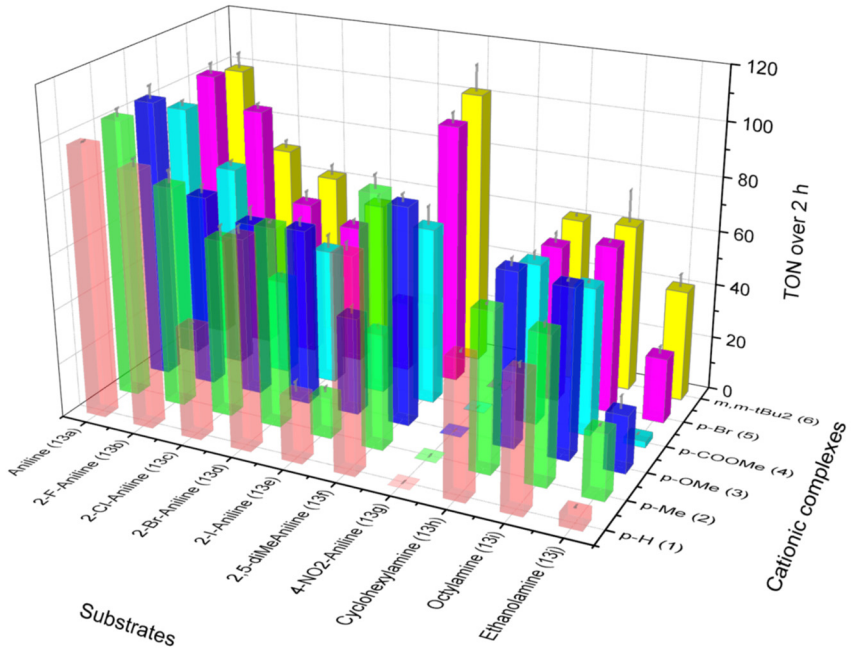

Figure 4.1 Plot of the yield (TON) for the hydroamination of acrylonitrile (14c) catalyzed by **1-6** for the mono-addition product over 2 h.

Scheme 4.2 Substrate scope for the hydroamination of acrylonitrile with complex **3** [a]

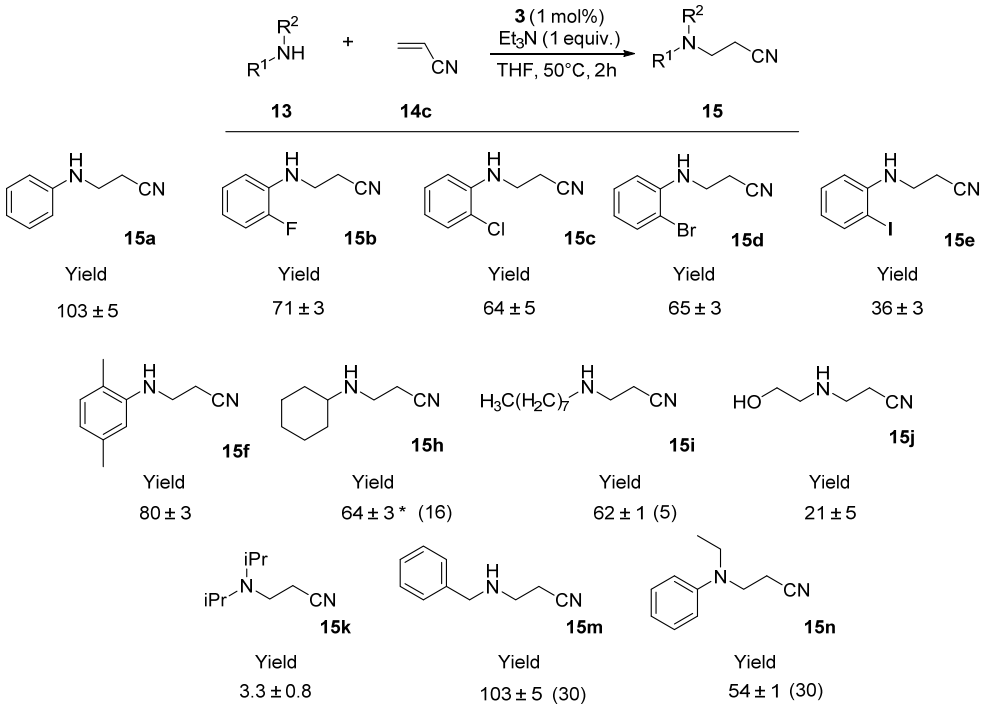

a) Reaction conditions: Amine (1 mmol), nitrile (1 mmol), NEt_3 (1 mmol), **3** (1 mol%), dodecane (10 mol%, internal standard) and THF (500 µL), 50 °C, 2 h. GC/MS yields. Values in parentheses represent the yield of the expected product obtained in the absence of catalyst under the same conditions *The amount of double-addition product is quite important in this reaction (~ 34 %)

Another impact of using a strongly nucleophilic amine is further reactivity of the mono-addition product to give tertiary amines as side-products. For instance, reaction of cyclohexylamine with acrylonitrile catalyzed by **2** leads to bis-addition products $CyN(CH_2CH_2CN)_2$ to a much greater extent (34 % yield) than does aniline (ca. 3 % yield). To investigate this hypothesis, we have done some competition reaction between the mono-addition product of aniline and cyclohexylamine with acrylonitrile, which is discussed later in **Section 4.4**.

Using the typical reaction conditions, we have tested different primary and secondary amines to further probe the flexibility of our catalytic system (**Scheme 4.2**). We have tested some secondary amines such as diisopropylamine (**13k**), diphenylamine (**13l**) and n-ethylaniline

(**13n**) as well as benzylamine as a primary amine (**13m**). From these amines, only diisopropylamine, benzylamine and n-ethylaniline gave the expected mono-addition product over 2 h in the standard conditions, with ca. 3 % yield (**15k**), 100 % yield (**15m**) and 54 % yield (**15n**), respectively. Increasing the reaction time to 20 h either gives the same yield of mono-addition product for benzylamine (quantitative) or slighty increases the yield for n-ethylaniline (71 % yield).We are confident, however, that other types of amines that display similar electronic and steric proprieties could also be used in our system

4.3.3 Reactions with nitriles other than acrylonitrile

Our previous studies[24b, 34] have shown that addition of a number of amines to crotonitrile or methacrylonitrile is much more sluggish relative to acrylonitrile. It is interesting to note that in one of those studies,[34] for the reaction of aniline with crotonitrile, we could only attain around 9 % yield over 24 h at 60 °C for the mono-addition product. More interesting is that they could not observe any reaction with methacrylonitrile in our system. On the other hand, our system gives much better yields for both the crotonitrile and methacrylonitrile reaction with aniline, with an average of 32 % and 33 % yields for all catalysts. Considering the greater range of compounds that could be made from the use of nitrile substrates bearing substituted on the double-bond compared to acrylonitrile, it is important to develop a catalyst that can facilitate the formation of hydroamination products under the right conditions.

Another surprising observation in our studies on the hydroamination of crotonitrile and methacrylonitrile is that, contrary to the results with acrylonitrile, most aromatic amines are less reactive than their aliphatic counterparts. For instance, aniline (**13a**) gives average yields of 26% compared to 47% with octylamine (**13k**) and 31% with cyclohexylamine (**13h**) (see **Figures A4.2-3**). It is also interesting to note that while the uncatalyzed reaction of cyclohexylamine and octylamine with acrylonitrile furnishes a small quantity of addition products (16 % and 5 % yields in 2 h, respectively), none of the amines screened give addition product after either 2 h or 20 h with crotonitrile (14a), methacrylonitrile (14b) or cinnamonitrile (14d).

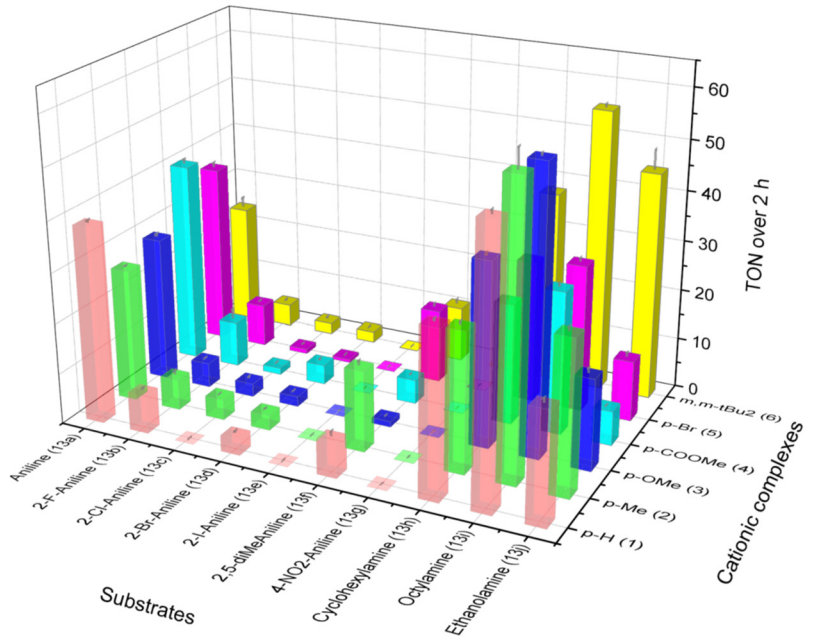

Figure 4.2 Plot of the yield (TON) for the hydroamination of crotonitrile (14a) catalyzed by **1-6** for the mono-addition product over 2 h.

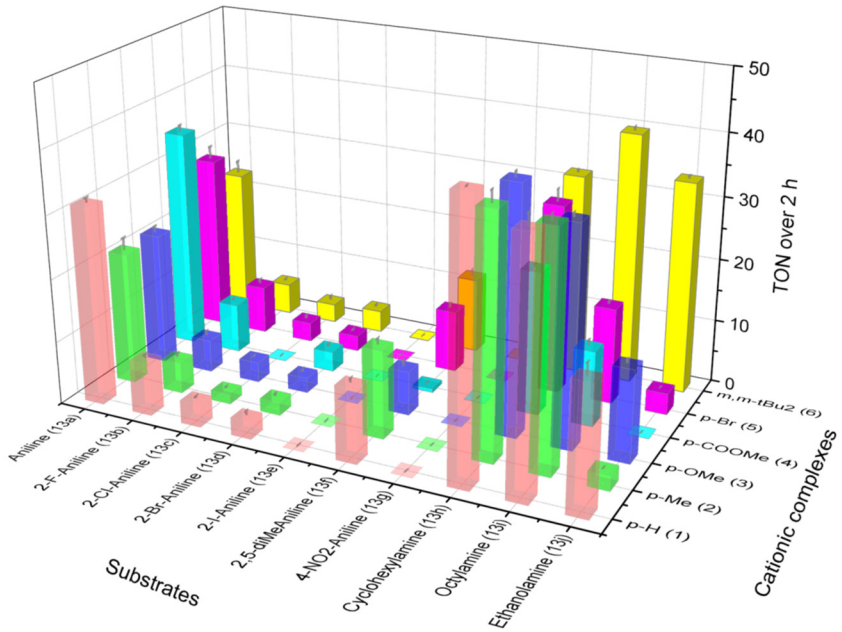

Figure 4.3 Plot of the yield (TON) for the hydroamination of methacrylonitrile (14b) catalyzed by **1-6** for the mono-addition product over 2 h.

Scheme 4.3 Substrate scope for the hydroamination of crotonitrile and methacrylonitrile with complex **3**[a].

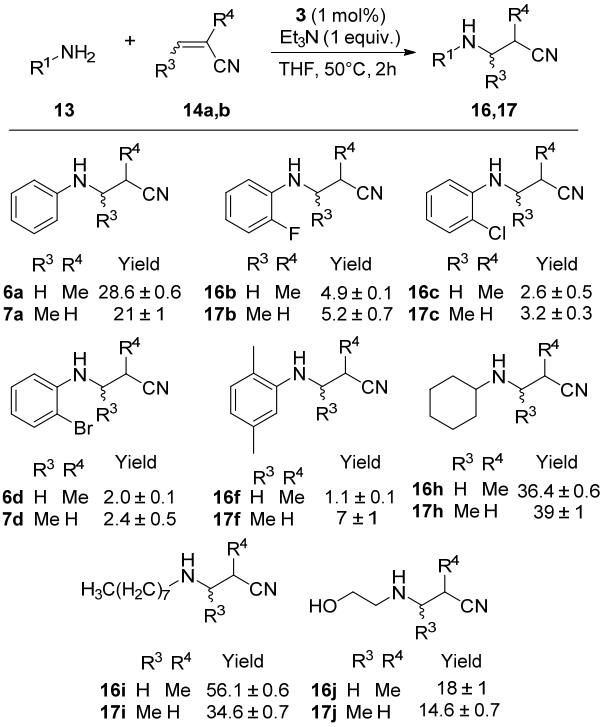

a) Reaction conditions: Amine (1 mmol), nitrile (1 mmol), NEt_3 (1 mmol), **3** (1 mol%), dodecane (10 mol%, internal standard) and THF (500 µL), 50 °C, 2 h. GC/MS yields.

We also tried hydroamination in the presence of cinnamonitrile, a more sterically hindered nitrile, but it only reacted in the presence of the very nucleophilic morpholine and only in poor yields (22 %). Interestingly, a previous study in our group[34] has reported the formation of an amidine when morpholine reacts with cinnamonitrile in the presence of **1**, and also in poor yields (36%) over 24 h. However, in the presence of our substituted cationic POCOP catalysts, the MS fragmentation pattern of the reaction suggested that the nature of the product obtained under similar conditions is the expected product **21o** and not the previously reported amidine. No reaction was observed in the absence of catalyst when cinnamonitrile is used.

4.3.4 Reaction conditions and optimization for the hydroamination of acrylonitrile

In order to determine the scope of our catalytic system, we have probed different reaction conditions. For the sake of conducting systematic and reliable screening tests, we have used two time intervals, 2 h and 20 h, and all the analyses were done in triplicate. In general, running the reaction for the longer interval of 20 h increased the yields only slightly. For the typical reaction of acrylonitrile with aniline catalyzed by **4**, we have also investigated the lower limits of reaction time (down to 5 min) and catalyst loading (down to 0.05 mol%); the results are shown in **Table A4.1** in "*Annexe pour Chapitre 4*". We observed that quantitative yields were obtained over 2 h or 20 h even when the catalyst loading was lowered from 1% to to 0.5%. Lowering the catalyst loading further by a factor of 20 (0.05 mol%) still yielded some expected product; 13% yield and 95% yield over 2 h and 20 h, respectively. For the reaction of aniline with acrylonitrile (1 mol% catalyst loading), lowering the reaction time from 20 h down to 5 mins still gave good yield (84%) of the expected product, **15a**.

Table 4.1 Optimization of the reaction conditions for the hydroamination of acrylonitrile catalyzed by **4**.

Substrate	Product	Catalyst loading [mol%]	Time	TON	TOF [a] [h^{-1}]
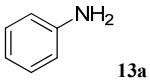 **13a**	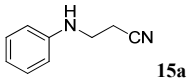 **15a**	1	2 h	95 ± 2	47,5 ± 0,8
			5 mins	84 ± 2	1013 ± 26
			15 mins	100 ± 2	400 ± 7
			30 mins	108 ± 13	215 ± 25
			1 h	115 ± 4	115 ± 4
		0,5	2 h	199,3 ± 0,5	99,7 ± 0,2
			(20h)	(207 ± 4)	(10,4 ± 0,2)
		0,05	2 h	13 ± 2	6,5 ± 0,9
			(20h)	(95 ± 6)	(4,8 ± 0,3)

a) TON and TOF are the average of three experiments under the same conditions.

As pointed out in a previous study for aza-Michael additions of nitriles by a Zr complex,[81] added bases are not essential for the reaction to occur but addition of base to the reaction mixture serves to improve the yield. From a practical point of view, using stoichiometric amounts of base should be avoided, and thus we tested the impact of using little base, down to 1 mol%. For the typical reaction of aniline with acrylonitrile using **4** as the

catalyst, using 1 mol% Et_3N gave 35 % yield, which is lower than the 95 % yield obtained under the same conditions but with 100 mol% of Et_3N. We have also studied the impact of temperature on the reaction, which has shown that for the addition of aniline to acrylonitrile (14c) and crotonitrile (14a) catalyzed by **6** we obtain 20 % and 10 % yields, respectively, in 4 h at room temperature compared to 100 % and 24 % yields, respectively, in 2 h at 50 °C.

4.3.5 Double and triple addition products

Upon closer analysis of the reaction mixture after each experiment, we have found a significant amount of double addition products (**18-20**), and in one case, even triple addition product (**18k**) (See **Scheme 4.4** and **4.5**). The double-addition products are present with all three nitriles studied and can account, in some cases, for a significant amount of the side products and in some cases even the major product obtained. This is a very interesting result, as some of those tri-substituted amine products are used as dyes, more precisely as disperse azo dyes for textile dying, and many patents and publications exist on those compounds.[82]

Scheme 4.4 Double and triple addition products for hydroamination of acrylonitrile by complex **3**[a].

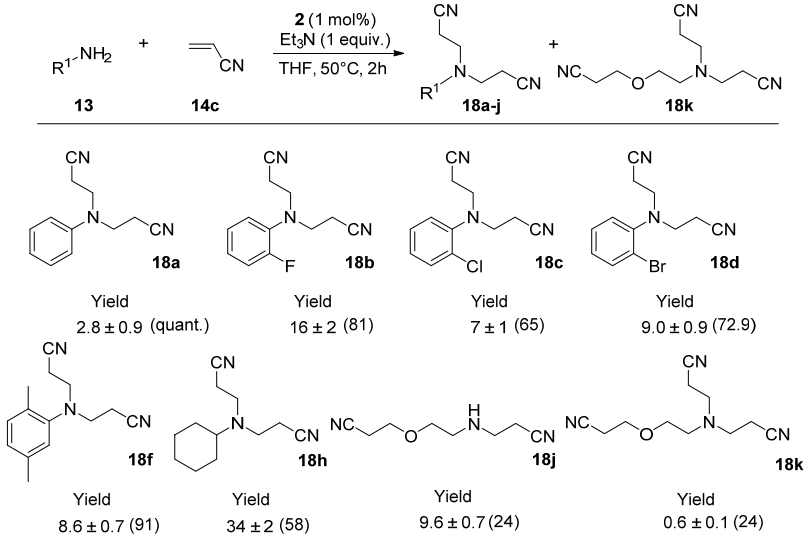

a) Reaction conditions: Amine (1 mmol), nitrile (1 mmol), NEt_3 (1 mmol), **2** (1 mol%), dodecane (10 mol%, internal standard) and THF (500 µL), 50 °C, 2 h. GC/MS yields. Values in parentheses are the yield for the mono-addition products (**15**) under the same reaction conditions.

Scheme 4.5 Double and triple addition vs single addition products for hydroamination of crotonitrile and methacrylonitrile by complex **3**[a].

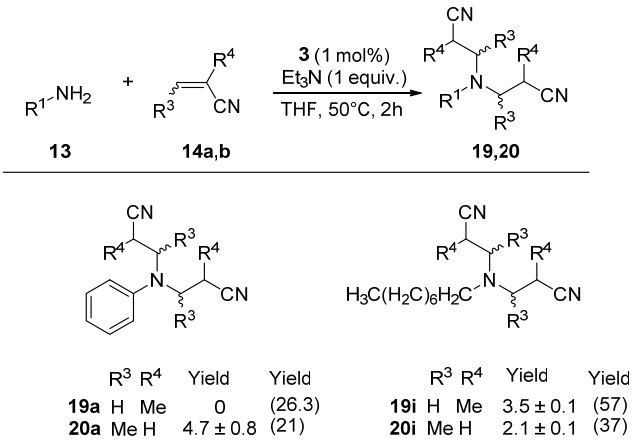

	R3	R4	Yield	Yield
19a	H	Me	0	(26.3)
20a	Me	H	4.7 ± 0.8	(21)

	R3	R4	Yield	Yield
19i	H	Me	3.5 ± 0.1	(57)
20i	Me	H	2.1 ± 0.1	(37)

a) Reaction conditions: Amine (1 mmol), nitrile (1 mmol), NEt_3 (1 mmol), **3** (1 mol%), dodecane (10 mol%, internal standard) and THF (500 μL), 50 °C, 2 h. GC/MS yields. Values in parentheses are the yield for the mono-addition products (**16**) under the same reaction conditions.

4.3.6 Hydroalkoxylation studies

To expand the application of our cationic system in catalysis, we have also done some tests to know how alcohols fare in the addition to nitriles. Some studies on hydroalkoxylation of nitriles were done previously in our group[34, 35b]. To asses both the electronic and steric factors, we have used both electron-withdrawing (*m*-CF_3, *m*-OMe) groups on the phenol moiety, as well as a sterically hindered and electron-donating alcohol (*m,p,m*-Me_3-phenol) and we compare their activities to an aliphatic alcohol (3-Cl-1-propanol) and to the unsubstituted aromatic alcohol (phenol) for the addition on acrylonitrile. We also studied their reactivity with a more hindered nitrile (crotonitrile). To test these substrates, we used catalyst **2** and followed the general procedure for catalytic runs in "*Annexe pour Chapitre 4*".

We first observe that hydroalkoxylation with our cationic system gives much lower yields than most hydroamination reactions involving similar substrates (see **Scheme 4.6**). Reacting the cationic complex **2** in the presence of base, the alcohol and a nitrile gave similar

results for aromatic alcohols, and no reaction in the presence of an aliphatic alcohol, over 2 h. In the case of acrylonitrile, *m,m,p*-triMePhOH (**22b**) gave the best yields, with 20 %, followed by PhOH (**22a**) (ca. 16 %), *m*-OMePhOH (**22c**) (ca. 15 %) and *m*-CF_3PhOH (**22d**) (ca. 12 %). When crotonitrile was used, the yields unsurprisingly dropped much lower based on the substrate: **22c** (ca. 6 %), **22d** (ca. 3 %), **22a** (ca. 3 %) and **22b** (ca. 2 %). No reaction was observed for the aliphatic amine 3-Cl-1-propanol, as well as in the absence of catalysts for any of the substrates. Also, a previous study in our group showed that a base, Et_3N, is necessary for the reaction to occur.[35b] It is interesting to note that the yield obtained for this reaction seems to follow the electronic nature of the substrates: the more electron-donating substrate **22b** gives better yields than the less donating **22a** and the electron-withdrawing substrates **22c** and **22d**. However, as **22b** exhibits steric hindrance on both *ortho* position of the aromatic ring, we can't conclude based solely on the electronic nature of the substrates.

Scheme 4.6 Substrate scope for the hydroalkoxylation reaction by **2**[a]

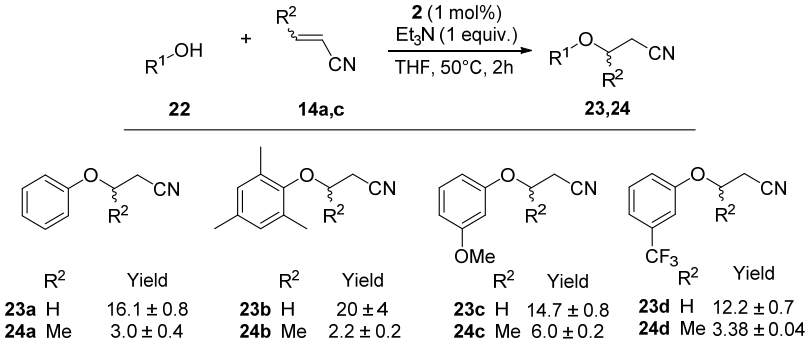

a) Reaction conditions: Alcohol (1 mmol), nitrile (1 mmol), NEt_3 (1 mmol), **2** (1 mol%), dodecane (10 mol%, internal standard) and THF (500 µL), 50 °C, 2 h. GC/MS yields.

4.3.7 Comparison of catalytic reactivities of Ni complexes with literature precedents

One of the earliest reports of the catalytic addition of aniline to acrylonitrile comes from the group of Trogler,[62a, 79] where they obtained TONs of 40-50 in the presence of a palladium complex and under slightly different conditions. More recent reports on the hydroamination of

acrylonitrile include complexes of nickel,[83] copper,[64b, 84] and even stannane [85] (anti-Markovnikov product).

Interestingly, high TONs in the range of up to 10^3 were be obtained with a nickel pincer complex reported previously in our group.[24b] Although we were not able to obtain such high yields with our system, we are still able to achieve moderate TONs of up to 200 (quantitative yield) for the addition of aniline to acrylonitrile, using only 0.5 mol% catalyst, all while staying at the relatively low temperature of 50 °C over only 2 h.

Studies by Togni[62c, 65] report the addition some amines (morpholine, piperidine, aniline and some substituted anilines) to crotonitrile and methacrylonitrile with different nickel complexes, with some reporting up to 70 % and 35 % yield for the addition of aniline to crotonitrile and methacrylonitrile, respectively, whereas we obtain, for addition to crotonitrile and methacrylonitrile, up to 40 % and 38 % over 2 h. By increasing the reaction time to 20h, we obtained up to ca. the57 % for both crotonitrile and methacrylonitrile addition product, which comes closer to the reported values for different systems.

Another study[86] has reported that addition of aniline catalyzed by the dicationic nickel compound [Ni(*Pigiphos*)(THF)][$(ClO_4)_2$] (Pigiphos = (*R*)-(*S*)-Pigiphos = bis{(*R*)-1-[(*S*)-2-(diphenylphosphino)ferrocenyl]ethyl}cyclohexylphosphine) affords yields of 26% (crotonitrile) and 17 % (methacrylonitrile) using 5 mol% catalyst loadings, compared to average yields of 32 % (crotonitrile) and 33 % (methacrylonitrile) with only 1 mol% catalyst in our system. They also require longer reaction times (24 h) although with lower temperatures (r.t.), and the reactions are done in the presence of OPIC.BF_4, an ionic liquid (OPIC.BF_4 = 1-octylpicolinium tetrafluoroborate), and can be done in pure ionic liquid or in the presence of a 2:1 ionic liquid: hexanes mixture.

It should be noted here that this is by no means an exhaustive comparison of catalytic systems and that there exist many more systems that are more active than ours. We also have limited ourselves to a few nickel-containing catalytic systems for ease of comparison.

4.4 Mechanistic investigations

Some of the observations in this report hint at different mechanistic features for our system as compared to previously studied systems. One of the main differences is the observation of much more double and even triple addition products in our system, whereas very little or no double addition product has been observed in other systems. Another difference is that in our case more nucleophilic amines seem to be less reactive than substantially less nucleophilic ones, at least for the hydroamination of acrylonitrile.

We first started by trying to analyze the overall reaction order of the hydroamination reaction, under pseudo first-order conditions. By analyzing the concentration of acrylonitrile left in the system over 4 h and plotting ln{[Acrylonitrile]/[Acrylonitrile]$_0$} vs time we obtained results that seem to show that the overall order of the reaction might be 2 since all those are fitted nicely with exponential decay functions (See **Figures A26-29** in "Annexe pour Chapitre 4"). However, plotting 1/[Acrylonitrile] – 1/[Acrylonitrile]$_0$ vs. time complicates the primary conclusion that the overall order is 2 because we obtain a plateau after what seem to be a somewhat linear fit (See **Figures A30-34**), which is a sign of catalyst degradation, and could make the exponential decay that we observed in **Figures A26-29** a more complicated combination of a first order reaction with a plateau.

Moreover, as alluded to earlier, our system seems to act slightly differently compared to very closely related systems in terms of double and even triple addition products.[24a] Therefore, this could complicate the determination of the overall reaction order, as there could be now a possible product inhibition.

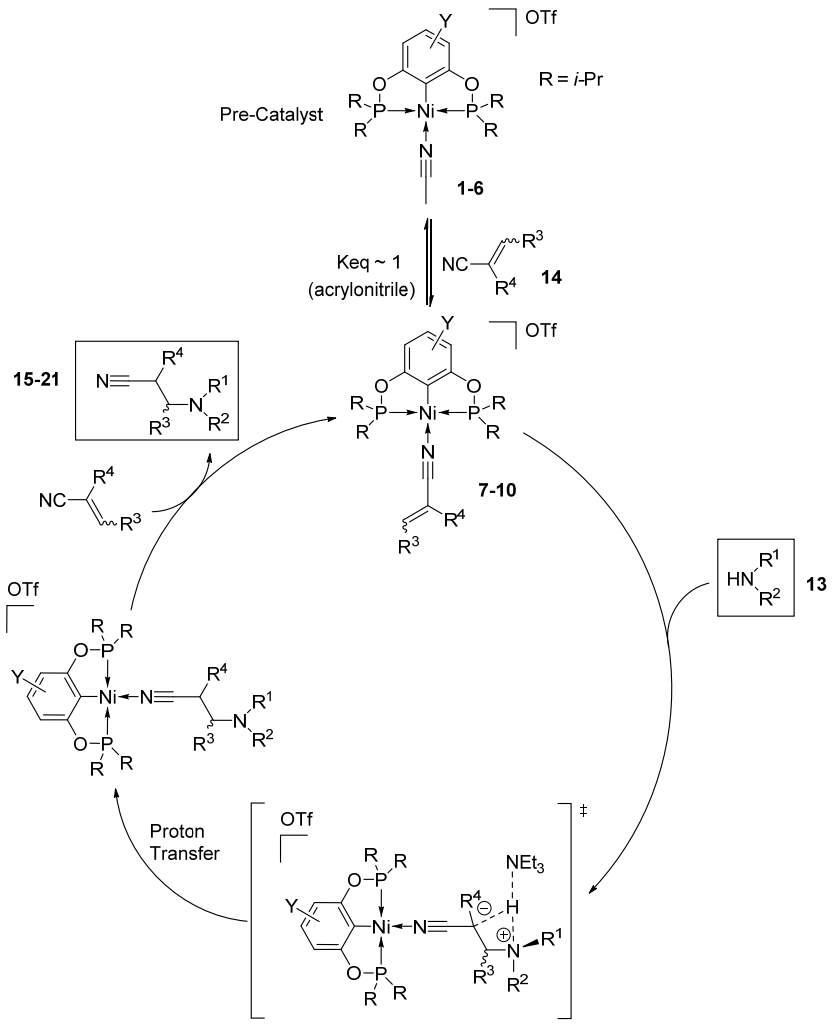

Figure 4.6 Proposed mechanism based on literature precedents[24a]

To study this product inhibition phenomenon, we have done a competition reaction between cationic complexes **3** or **4** and either the mono-addition product of the hydroamination of acrylonitrile with aniline (**15a**, 3-anilinopropionitrile) or with cyclohexylamine (**15h**, (3-cyclohexylamino)propanenitrile). To a ~ 0.04 M solution of **3** or **4** in C_6D_6 is added 0.1 to 10 equivalents of **15a** or **15h** with vigorous shaking, and a ^{31}P NMR spectra is taken after each addition as well as without added product. Upon addition, the chemical shift gradually shifts from the acetonitrile-bound complex towards the chemical shift for the complex with either **15a** or **15h** coordinated, [(R-POCOP)Ni(NCCH$_2$CH$_2$NHR')][OTf] (R = OMe, CO$_2$Me; R' = Cy, Ph). Upon addition of 0.1 equivalents of the addition product, we observe a rather broad signal, hinting at a persistent equilibrium between two species. The signal then sharpens to a $LW_{1/2}$ of

~ 6 Hz when using **15a** and to ~40 Hz for **15h**. **Figure 4.7** shows the lower field shift of the signal, as well as the decrease in $LW_{1/2}$ as the concentration of **15a** increases, until there is almost no more change in the linewidth or the chemical shift, at around 2 equivalents of **15a** added. Stacked spectra for the reaction of **15a** and **4**, as well as for the reaction of **15h** and **4** are presented in the **Figures A4.40** and **A4.44**. We can safely assume that the nature of the nitrile (either acetonitrile or acrylonitrile) bound to the starting cationic complex (**3** or **4**) does not affect the results obtained as it was shown previously in our group that K_{eq} of the exchange between acetonitrile and acrylonitrile in a similar system is unity.[39a] Using acetonitrile adducts in this product inhibition study might also be favorable as it prevents the formation of double-addition products resulting from the attack of either **15a** or **15h** on the acrylonitrile double bond.

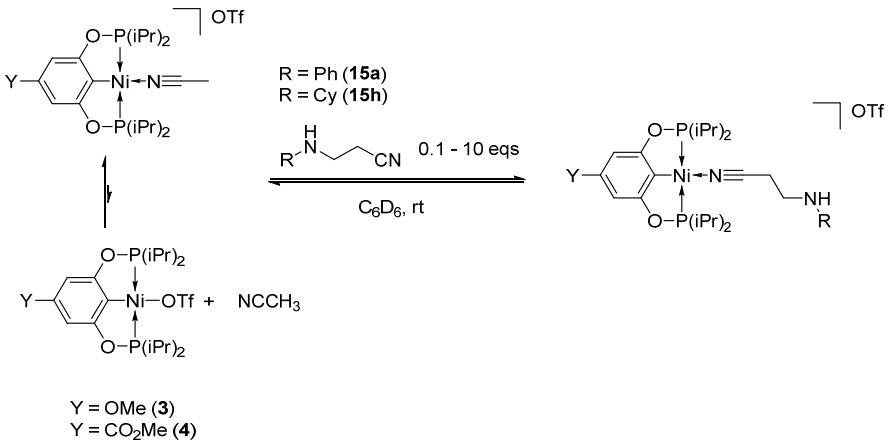

Scheme 4.7 Exchange reaction between cationic catalysts **3** and **4** and **15a** or **15h**.

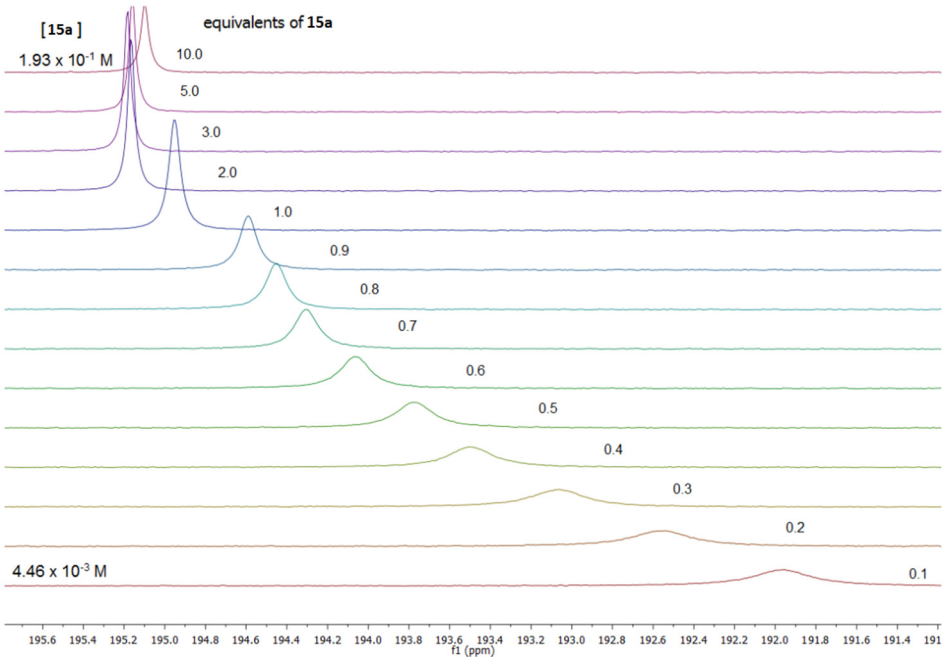

Figure 4.7 Stacked ^{31}P NMR spectra showing the change in both chemical shift and $LW_{1/2}$ with the addition of **15a** in the presence of **3**.

See caption of Figure A4.37 for experimental conditions.

As a first step towards a better comprehension of the exchange mechanism in our system, we aimed to determine the rates of exchange of **15a** and **15h** with catalysts **3** and **4** using a lineshape analysis of the reaction depicted in **Scheme 4.7**. To do that, we applied the **Equation 4.1** that was adapted in part from Loewenstein *et al.*[87] and the inverse relation between τ and the rate of the exchange reaction, V_{ex}. This formula is applicable for fast exchange regimes, where P_i, δ_i,$w_{1/2}$, and $w_{0,1/2}$ are, respectively, the mole fraction of **15a** or **15h**, the chemical shift of the observed signal in Hz, the linewidth at half-height of the observed signal and the linewidth at half-height of the starting complex without exchange.

$$\boldsymbol{V_{ex}} = \frac{\mathbf{1}}{\boldsymbol{\tau}} = \frac{\sum_{i=1}^{n} \boldsymbol{P_i \delta_i^2}}{\boldsymbol{\pi\left(w_{\frac{1}{2}} - w_{\frac{1}{2}}^{0}\right)}} \qquad (4.1)$$

First, we plotted the logarithm exchange rate (V_{ex}) vs. [**15a**] catalyzed by **3** (See **Figure A4.34**). We observed a different behavior when the amount of **15a** added was under 1 equivalent

([**15a**] < 0.04 M) compared to the behavior at higher concentrations of **15a**. We obtained both an exponential regime under 1 equivalent of **15a** and a linear regime at higher concentrations (See **Figure A4.34**) Moreover, plotting the logarithm of the exchange rate vs. the logarithm of the concentration of **15a** gave two linear slopes (See **Figure A4.35**), corresponding to two observed rate constants (K_{obs}) of 1.2 x 10^{8} s^{-1} and 7.9 x 10^{11} s^{-1} (See **Table A4.16**) for concentrations of **15a** below 2.12 x 10^{-2} M and over 2.51 x 10^{-2} M, respectively. We also observed a change in the rate of exchange and K_{obs} with the concentration of **15a** when catalyst **4** was used in the same reaction. However, the behavior is more complicated as we obtained three linear regimes under the same conditions (see **Figure A4.37**) instead of an exponential and a linear regime with catalyst **3**. We also obtained observed rate constants of 1 x 10^{8} s^{-1}, 3.2 x 10^{10} s^{-1} and 1 x 10^{9} s^{-1} (see **Table A4.17**) for concentrations under 1.56 x 10^{-2} M, between 1.93 x 10^{-2} M and 3.31 x 10^{-2} M, and over 3.63 x 10^{-2} M, respectively.

Surprisingly, using a different amine, **15h**, and catalyst **4** still gave more than one observed rate constant but in this case it is lower at higher concentration of added **15h**. We obtained an observed rate constant of 3.09 x 10^{8} s^{-1} when there's 1 equivalent or less of **15h** added ([**15h**] < 3.25 x 10^{-2} M) and an observed rate constant of 8.51 x 10^{6} s^{-1} at higher concentrations. Although this seems to point out that the cyclohexylamine-containing nitrile (**15h**) would exchange more slowly than the phenyl-containing nitrile (**15a**) in the presence of catalyst **4** at higher concentrations of **15h**, it is important to point out that this exchange is much faster (many exchanges per seconds) than the overall reaction rate (a few reactions per hours) which might not be a significant contributor to the overall reaction, along with other factors that we did not take into account.

We also need to point out that there seems to be an equilibrium between the triflate moiety and the acetonitrile ligand of the cationic complex (which is fast, but shifted to the acetonitrile-bound complex). This is seen when taking an NMR spectrum of the cationic adduct in C_6D_6 by a larger than average ^{31}P NMR signal in the absence of any additive. It can also be shown by the enlargement of the ^{31}P NMR signal of the cationic adduct when a large excess of AgOTf is added to reaction mixture, although no new signal is observed in the expected region of the OTf-bound complex (ca. 185 ppm). Thus, the exchange might not happen only from the bound acetonitrile to the bound **15a** or **15h**, but also with the weakly bound OTf moiety, making

it harder to determine the exact kinetics of the exchange. Thus, the measured kinetics is most likely the sum of the rates for the exchange of the acetonitrile by the OTf moiety and by **15a** or **15h**. However, since we believe that the exchange of the acetonitrile moiety with the OTf moiety is of a smaller magnitude than the exchange with either **15a** or **15h**, we can safely assume that the kinetics measured by the experiments are largely representative of the kinetics of the latter exchange.

We also tested if the amine would compete with the addition product for the active site. If the rate-determining step of the mechanism does involve the competition between the addition product and the amine for the nucleophilic attack on the bound nitrile, we should see some effect of adding an excess of amine to the reaction mixture. Addition of an excess of amine should, in fact, reduce the amount of double addition products and consequently increase the yield of the mono-addition products. We conducted tests on two systems; the first containing aniline (**13a**), **4** (1 mol%), and crotonitrile (14a), gives the mono-addition product (**16a**) in moderate yields under normal conditions (40 %). The second test was performed on a less reactive system, where ethanolamine (**13j**) reacts with acrylonitrile (14c) and **4**. In this system, the mono-addition product is obtained in very low yields under normal conditions (2.3 %) and the double addition product is obtained in slightly better yields (8 %). When an excess of amine (5 equivalents) was used, the first system gave the same yields, with the mono-addition product in 38 % and no double addition products formed, whereas the second system gave around twice the yield for both the mono- and double-addition products with 6.9 % and 17 %, respectively. These results indicate that changing the concentration of amine does not seem to influence significantly the yield of the mono-addition product and even increases the amount of double-product obtained, which disfavors a mechanism where the rate-determining step involves the competition between the mono and double-addition product.

Although our system seems to show some unusual behaviours, further studies will be necessary to completely uncover the full extent of the mechanism for our system as it seems to be more complex than what was proposed in previous works.[81]

4.5 Conclusions

This study has led to some interesting results for the application of cationic POCOP nickel complexes as catalysts for the hydroamination and hydroalkoxylation of activated nitriles. This study has shown that our catalytic system can achieve mostly quantitative yields of the addition products of aniline and acrylonitrile in only 2 h at 50 °C and is active towards a large selection of aromatic or aliphatic amines. For the standard reaction of aniline and acrylonitrile at 50 °C, we retained complete catalytic activity by lowering the amount of catalyst by half (0.5 mol%) and even some reactivity (~ 13 % yield) by lowering by a factor of 20 (0.05 mol%). Our catalytic system is quite fast, as in only 5 minutes we obtained **15a** in ~83 % yield but higher yields can also be achieved in 20 h. Our system is also active at r.t., although with quite drastic decreases in yields, from quantitative yields in 2 h at 50 °C to 20 % yield at r.t. in 4 h for the reaction of aniline and acrylonitrile. It is important to note that no reactions occurred in the absence of catalyst for any amines with either crotonitrile or methacrylonitrile, and only a few amines reacted in the absence of any catalysts wth acrylonitrile under standard conditions: cyclohexylamine (**15h**, 15 % yield), octylamine (**15i**, 5 % yield), benzylamine (**15m**, 30 % yield) and n-ethylaniline (**15n**, 30% yield). Another interesting fact is that our system seems to be active even towards the addition product, as many amines and nitriles show double and in one case even triple addition products. These double additions can range from minor to even the major product in a very few cases. This is intresting as only few catalytic systems promote the double functionalization of nitriles, leading to potentially interesting compounds.[24a] Testing our catalytic system in the presence of substituted alcohols for the hydroalkoxylation of acrylonitrile and crotonitrile yielded average results in the range of 12 % to 20 % yield for acrylonitrile and 2 % to 6 % yield for crotonitrile. They were unfortunately lower than what was obtained with the unsubstituted complex **1** reported previously in our group.[35b]

However, the most interesting results we have been able to obtain with our system is the ability to add both aliphatic and aromatic amines in good yields onto sterically encumbered nitriles such as crotonitrile, methacrylonitrile and even cinnamonitrile. Whereas a previous study in our group[34] shows that the unsubstituted cationic POCOP complex **1** adds aniline to crotonitrile in only 9 % yield with no reaction towards methacrylonitrile in 24 h, our system can

achieve an average of 32 % yield for crotonitrile and 33 % yield for methacrylonitrile in only 2 h. Addition of certain amines to encumbered nitriles is also shown in other systems by Togni,[62c, 65, 86, 88] where they report 70 % and 35% yields for the addition of aniline to crotonitrile and methacrylonitrile, respectively. Surprisingly, in our system, using more encumbered nitriles seems to favor the addition of aliphatic amines rather than aromatic amines, with average yields of 26 % for aniline compared to 47 % with octylamine and 31 % for cyclohexylamine. We have also previously reported[34] the reaction of cinnamonitrile and morpholine to form the product of amidination in 36 % in 24 h in the presence of the unsubstituted cationic POCOP complex **1**. However, our system enabled us to obtain exclusively the markovnikov addition product (3-morpholino-3-phenylpropionitrile) in 22 % yield (as confirmed by the MS fragmentation pattern).

We were also able to gain some insights on the mechanism of hydroamination in our system, as it appears to be slightly different than previously proposed mechanisms. Analysing the hydroamination of acrylonitrile under pseudo-first order conditions by ^{1}H NMR seem to point to a complex overall reaction order, most likely a second order, but some apparent catalyst decomposition or other deviation from linearity makes it difficult to conclude on the overall reaction order. Another interesting feature of our system is that there's a non-negligible amount of double-addition products formed in many reactions. This bring a new light and possibly added value on the mostly well known of aza-Michael addition of nitrile to amines (or hydroamination of nitriles), as those double-addition products (mostly of substituted anilines) are important components of azo disperse dyes.[82a, 82b, 89]

Although there is a potential exchange between the nitrile and the triflate moiety in the cationic complex which might affect the determination of the rate, we were able to show that there is a significant amount of product inhibition in our catalytic system, with some complex behaviour such as multiple rates of exchange of nitriles **15a** or **15h** with catalysts **3** or **4** depending on the concentration of **15a** or **15h**. At this point we cannot uncover the full extent of the mechanism, which appears to contain many side-reactions and equilibria, and further studies will be needed to fully understand it.

Chapitre 5 : Conclusions et perspectives

Les complexes cationiques POCOP de nickel sont des catalyseurs qui présentent une stabilité importante et une grande versatilité autant au niveau électronique que stérique. Le ligand de type POCOP permet d'obtenir des complexes cationiques de nickel dont le centre métallique est significativement plus électrophile que les complexes cationiques comportant des ligands de type PCP ou NCN. L'électrophilie accrue des complexes POCOP de nickel cationique rend ces derniers des candidats idéaux pour des réactions nécessitant l'activation d'une oléfine par coordination au centre métallique, tel que la réaction d'hydroamination. Le caractère δ^+ accru de la double liaison lorsque l'oléfine est coordonée au nickel permet une vitesse d'attaque accrue par des nucléophiles tels que des amines, des alcohols, ou des thiols. Il est possible de moduler le caractère électrophile du centre métallique en modifiant le squellette aromatique du ligand POCOP, augmentant ainsi la versatilité des complexes cationiques de type POCOP de nickel.

Le chapitre 2 a permis de mieux comprendre l'effet de substituants à caractère plus ou moins électrophile sur le cycle aromatique du ligand. L'ajout d'un groupement électro-attracteur tel que le groupement CO_2Me sur le cycle aromatique, combiné à l'ajout d'un groupement *tert*-butyle sur les groupements phosphines permet d'atteindre le plus haut potentiel d'oxydation jamais obtenu pour un complexe POCOP cationique de nickel, sois 1457 mV. Le degré d'électrophilie du centre métallique peut aussi être déterminé indirectement par l'analyse de la fréquence d'étirement du lien nitrile du ligand acétonitrile lié au nickel. Plusieurs autres groupements ayant un caractère donneur plus ou moins important (OMe, Me, H, Br, *t*-Bu) ont été préparés et leur propriétés électroniques et stériques ont été analysés. Bien que la plupart des analyses effectuées (IR, RMN, UV-VIS, Voltampérométrie cyclique) permettent de dresser un portait semblable des tendances plus ou moins donneur des substituants, la corrélation entre les différentes techniques d'analyse (notamment entre IR et la voltampérométrie cyclique) n'est pas toujours parfaite, surtout entre les séries comportant des groupements différents sur les phosphines (*i*-Pr vs *t*-Bu).

Dans le but de mieux comprendre la stabilité des complexes cationiques vis-à-vis d'additifs ou de complexes neutres dans un milieu réactionnel, la réaction entre un

complexe bromé (R-POCOP)NiBr et cationique [(R-POCOP)Ni(NCMe)][OTf] (R = H, OMe, CO_2Me) a permis d'obtenir que le ligand acétonitrile peu être facilement déplacé par le ligand bromure, et ce plus le caractère électrophile du centre métallique est important. De plus, l'analyse a permis de découvrir que le ligand acétonitrile peut être déplacé, jusqu'à un certain point, par le contre-ion triflate (OTf). De plus, une réaction intéressante a été observée lors de l'ajout de ferrocène à une solution relativement concentrée de certains complexes cationiques suffisamment électrophiles. La solution change immédiatement de couleur de jaune à vert très foncé, indicateur de la formation de l'espèce cationique $[FeCp_2][OTf]$ dans le milieu. De plus, des cristaux du cation ferrocénium triflate ont été isolés, ce qui suggère que le complexe cationique, en présence de ferrocène ($FeCp_2$) est réduit en une espèce Ni(I) de formule possible (R-POCOP)Ni(NCMe).

Le troisième chapitre a permis l'étude de la stabilité et de la structure de complexes cationiques comportant un ligand amine en plus de la préparation de nouveaux complexes cationiques comportant des ligands nitriles. En effet, en présence d'un excès de certaines amine tel que morpholine, cyclohexylamine, aniline ou encore pipéridine, en présence du complexe ($^{p\text{-OMe}}$POCOP)Ni(OTf), on observe la formation du complexe dont l'amine est coordonée au centre métallique, soit complètement pour la pipéridine et la cyclohexylamine, ou encore partiellement pour l'aniline et la morpholine. Ceci pourrait suggérer que le cycle catalytique pour notre système soit différent de celui proposé dans la littérature, puisqu'il y aurait inhibition de la formation du produit d'hydroamination. Toutefois, en présence d'une faible quantité d'acrylonitrile, les signaux en RMN ^{31}P disparaissent tous et le signal de l'adduit acrylonitrile apparait, et ce pour chacune des amines étudiées.

Toutefois, ce n'est pas toutes les amines qui sont autant labile. En effet, le complexe $[(R\text{-POCOP})Ni(NH_3)][OTf]$ est obtenu avec de bons rendements à partir du complexe neutre triflate, soit par addition de $N(SiMe_3)_3$ et l'hydrolyse subséquente des liens N-Si en présence d'eau, soit directement par réaction avec NH_4OH. De plus, en présence de 10 ou même 50 équivalents d'acétonitrile, il n'y a qu'un équilibre et non pas une conversion complète entre les deux espèces, ce qui suggère qu'en présence de NH_4OH en tant

qu'amine, la réaction d'hydroamination ne devrais avoir lieu que très lentement ou pas du tout.

Un des résultats intéressant de notre étude provient de l'activité de nos complexes envers l'addition de différentes amines sur des nitriles substitués. Selon une étude publiée précedemment par notre groupe,[34] l'addition d'aniline sur le crotonitrile et le methacrylonitrile à l'aide de **1** ne permet d'obtenir que 9 % de rendement du produit d'addition, et aucune réactivité n'est observée avec le méthacrylonitrile. Notre système catalytique, quant à lui, a permis d'obtenir en moyenne des réactivités beaucoup plus importantes pour la réaction entre l'aniline et le crotonitrile (32 % de rendement) ou le méthacrylonitrile (33 % de rendement). Toutefois, d'autres études sur des systèmes différents permettent d'obtenir de plus importants rendements, jusqu'à 70 %.[62c, 65] De plus, il a été aussi possible d'obtenir le produit d'addition Markovnikov exclusivement entre le cinnamonitrile et la morpholine, bien qu'avec un faible rendement (22 %). Ce qui est intéressant de ce résultat est qu'une publication antérieure de notre groupe[34] a étudié cette réaction dans des conditions très similaires et ont obtenu la formation du produit d'amidination et non pas d'addition sur la double liaison (avec un rendement similaire de 36 %). Ainsi, notre système catalytique permet l'obtention de manière exclusive le produit d'addition Markovnikov sur le double lien d'un nitrile encombré.

Probablement le résultat le plus intéressant de cette étude, et qui différencie notre système de ceux précédemment étudiés, est que nous obtenons, dans plusieurs cas, un produit secondaire provenant de l'addition du produit de la réaction sur une deuxième molécule de nitrile, produisant ainsi un produit contenant deux fonctions nitriles. Ces produits ont une application importante en tant que colorant azo en industrie.[82a, 82b, 89]

Bien que nous obtenions des rendements bons pour l'hydroamination de nitriles, nous ne pouvons pas extraire une tendance quant à l'effet de la nature du substituant du catalyseur sur la réactivité. Toutefois, en comparaison au système ne possédant pas de substituants sur le cycle aromatique, notre système permet d'obtenir une réactivité accrue au niveau de l'addition d'amines sur des nitriles substitués. De plus, dans certains cas, il a été possible d'obtenir une quantité significative de composé de double addition et même de triple addition, ce qui pourrais augmenter la valeur de ce type de réactions.

Enfin, le chapitre 4 étudie l'application de plusieurs composés cationiques (comparativement à seulement deux dans le chapitre 3) en tant que catalyseur dans la réaction d'hydroamination et d'hydroalkoxylation de différents nitriles avec des amines variées. Ce chapitre a permis de déterminer l'efficacité des complexes cationiques POCOP de nickel dans les réactions d'hydroamination ; notamment la réaction avec l'aniline et l'acrylonitrile, qui offrent une conversion complète en seulement 2 h à 50 °C. La rapidité du catalyseur dans la réaction d'hydroamination de l'acrylonitrile est démontrée par la formation du produit d'hydroamination a 83 % en seulement 5 minutes. Il est aussi possible de diminuer le pourcentage de catalyseur utilisé jusqu'à 0.5 % sans affecter le rendement de la réaction de façon substantielle. Il est possible de diminuer davantage la quantité de catalyseur utilisée jusqu'à 0.05 % et obtenir le produit d'hydroamination mais avec un faible TON (13) Toutefois, notre système n'est pas aussi actif que certains publiés précédemment quant à l'addition d'aniline sur l'acrylonitrile, avec un TON maximum de 200 tandis qu'un système très similaire publié précédemment dans notre groupe est actif jusqu'à 1000 TON.[24b]

En outre, ce chapitre a tenté d'explorer la nature du mécanisme de la réaction d'hydroamination de notre système catalytique. Nous avons tenté de déterminer en premier lieu l'ordre de la réaction d'hydroamination globale pour certain catalyseur par RMN ^{1}H, sans pouvoir conclure avec certitude sur l'ordre final entre autres à cause d'une apparente dégradation du catalyseur, bien que celui-ci semble être de second ordre. Bien qu'il y ait un échange possible entre le contre-ion triflate et le complexe cationique qui pourrais rendre plus difficile la détermination de la constante de vitesse de la réaction, nous avons démontrés qu'il y a un degré important de « product inhibition » dans notre système catalytique. Ce « product inhibition » semble adopter un comportement complexe tel qu'une dépendence envers les concentrations de **15a** ou **15h** sur les vitesses d'échange des nitriles **15a** ou **15h** avec les catalyseurs **3** ou **4**.

Enfin, des études subséquentes seront nécessaires pour une compréhension complète du mécanisme de réaction entre les complexes cationiques POCOP de nickel et les différents substrats et produit d'addition dans le milieu réactionnel. Par exemple, l'utilisation d'amines primaire simple telles que l'isopropylamine, ou encore des alcohols

aliphatiques tels que l'alcool benzylique n'ont pas été étudiés. Un aspect qui serait fort intéressant d'étudier est la nature du solvant dans les réactions d'hydroamination ou d'hydroalkoxylation, et le rôle de celui-ci dans notre système catalytique. Il serait peut-être même possible d'augmenter grandement les rendements de certaines réactions, soit en utilisant le nitrile comme solvant (conditions « neat »), ou encore en changeant la nature du solvant utilisé (comme par exemple le dichlorométhane). Un aspect qui mérite davantage d'attention au niveau du chapitre 3 est la réactivité et l'utilisation des complexes amines et surtout du complexe ammoniac. L'étude des propriétés de l'adduit ammoniac pourrais converger vers une application où l'utilisation de conditions spécifique permettrait de libérer sélectivement de l'ammoniac dans un milieu où l'utilisation de sources d'ammoniac naturelle n'est pas possible.

Notes et Références

(1) Gildner, P. G.; Colacot, T. J. *Organometallics* **2015**.

(2) (a) Li, M.; Wang, C.; Ge, H. *Org. Lett.* **2011,** *13,* 2062; (b) Bilodeau, F.; Brochu, M.-C.; Guimond, N.; Thesen, K. H.; Forgione, P. *J. Org. Chem.* **2010,** *75,* 1550.

(3) Mazuela, J.; Verendel, J. J.; Coll, M.; Schäffner, B.; Börner, A.; Andersson, P. G.; Pàmies, O.; Diéguez, M. *J. Am. Chem. Soc* **2009,** *131,* 12344.

(4) Wang, D.; Astruc, D. *Chemical Reviews* **2015,** *115,* 6621.

(5) Maluenda, I.; Navarro, O. *Molecules* **2015,** *20,* 7528.

(6) Chinchilla, R.; N?jera, C. *Chem. Soc. Rev.* **2011,** *40,* 5084.

(7) Kobayashi, H.; Fukuoka, A., Chapter 2 - Current Catalytic Processes for Biomass Conversion. In *New and Future Developments in Catalysis*, Suib, S. L., Ed. Elsevier: Amsterdam, 2013; pp 29.

(8) Unit, E. C. C. EDGAR - Emission Database for Global Atmospheric Research. http://edgar.jrc.ec.europa.eu/.

(9) Moulton, C. J.; Shaw, B. L. *J. Chem. Soc., Dalton Trans.* **1976**.

(10) (a) van Koten, G.; Jastrzebski, J. T. B. H.; Noltes, J. G.; Spek, A. L.; Schoone, J. C. *J. Organomet. Chem.* **1978,** *148,* 233; (b) van Koten, G.; Timmer, K.; Noltes, J. G.; Spek, A. L. *J. Chem. Soc., Chem. Commun.* **1978,** 250.

(11) (a) Karlen, T.; Dani, P.; Grove, D. M.; Steenwinkel, P.; van Koten, G. *Organometallics* **1996,** *15,* 5687; (b) Vabre, B.; Spasyuk, D. M.; Zargarian, D. *Organometallics* **2012,** *31,* 8561.

(12) (a) Fan, L.; Ozerov, O. V. *Chem. Commun.* **2005,** 4450; (b) Haenel, M. W.; Oevers, S.; Angermund, K.; Kaska, W. C.; Fan, H. J.; Hall, M. B. *Angew. Chem., Int. Ed.* **2001,** *40,* 3596; (c) Groux, L. F.; Belanger-Gariepy, F.; Zargarian, D. *Can. J. Chem.* **2005,** *83,* 634; (d) Ohff, M.; Ohff, A.; van, d. B. M. E.; Milstein, D. *J. Am. Chem. Soc.* **1997,** *119,* 11687; (e) Ingleson, M. J.; Fullmer, B. C.; Buschhorn, D. T.; Fan, H.; Pink, M.; Huffman, J. C.; Caulton, K. G. *Inorg. Chem.* **2008,** *47,* 407; (f) Dani, P.; Karlen, T.; Gossage, R. A.; Gladiali, S.; Van, K. G. *Angew. Chem., Int. Ed.* **2000,** *39,* 743; (g) Okamoto, K.; Kanbara, T.; Yamamoto, T.; Wada, A. *Organometallics* **2006,** *25,* 4026; (h) Liu, A.; Zhang, X.; Chen, W. *Organometallics* **2009,** *28,* 4868; (i) Vabre, B.; Canac, Y.; Duhayon, C.; Chauvin, R.; Zargarian, D. *Chem. Commun.* **2012,** *48,* 10446; (j) Hao, J.; Vabre, B.; Mougang-Soume, B.; Zargarian, D. *Chem. - Eur. J.* **2014,** *20,* 12544.

(13) Gorla, F.; Togni, A.; Venanzi, L. M.; Albinati, A.; Lianza, F. *Organometallics* **1994,** *13,* 1607.

(14) Nishiyama, H.; Shiomi, T.; Tsuchiya, Y.; Matsuda, I. *J. Am. Chem. Soc* **2005,** *127,* 6972.

(15) (a) Takenaka, K.; Minakawa, M.; Uozumi, Y. *J. Am. Chem. Soc* **2005,** *127,* 12273; (b) Uozumi, Y.; Tanaka, H.; Shibatomi, K. *Org. Lett.* **2004,** *6,* 281.

(16) Peris, E.; Mata, J.; Loch, J. A.; Crabtree, R. H. *Chem. Commun.* **2001,** 201.

(17) (a) Motoyama, Y.; Okano, M.; Narusawa, H.; Makihara, N.; Aoki, K.; Nishiyama, H. *Organometallics* **2001,** *20,* 1580; (b) Motoyama, Y.; Narusawa, H.; Nishiyama, H. *Chem. Commun.* **1999,** 131.

(18) Baratta, W.; Chelucci, G.; Gladiali, S.; Siega, K.; Toniutti, M.; Zanette, M.; Zangrando, E.; Rigo, P. *Angew. Chem. Int. Ed.* **2005,** *44,* 6214.

(19) Rimml, H.; Venanzi, L. M. *J. Organomet. Chem.* **1983,** *259,* C6.

(20) Gossage, R. A.; Jastrzebski, J. T. B. H.; van, K. G. *Angew. Chem., Int. Ed.* **2005,** *44,* 1448.

(21) (a) Castonguay, A.; Sui-Seng, C.; Zargarian, D.; Beauchamp, A. L. *Organometallics* **2006,** *25,* 602; (b) Jude, H.; Bauer, J. A. K.; Connick, W. B. *Inorg. Chem.* **2002,** *41,* 2275; (c) Bibal, C.; Mazières, S.; Gornitzka, H.; Couret, C. *Polyhedron* **2002,** *21,* 2827; (d) Contel, M.; Stol, M.; Casado, M. A.; Van, K. G. P. M.; Ellis, D. D.; Spek, A. L.; Van, K. G. *Organometallics* **2002,** *21,* 4556.

(22) Morales-Morales, D.; Grause, C.; Kasaoka, K.; Redón, R. o.; Cramer, R. E.; Jensen, C. M. *Inorg. Chim. Acta* **2000,** *300-302,* 958.

(23) Bedford, R. B.; Draper, S. M.; Noelle Scully, P.; Welch, S. L. *New Journal of Chemistry* **2000,** *24,* 745.
(24) (a) Castonguay, A.; Spasyuk, D. M.; Madern, N.; Beauchamp, A. L.; Zargarian, D. *Organometallics* **2009,** *28,* 2134; (b) Pandarus, V.; Zargarian, D. *Organometallics* **2007,** *26,* 4321; (c) Pandarus, V.; Zargarian, D. *Chem. Commun.* **2007,** 978.
(25) Vabre, B.; Lindeperg, F.; Zargarian, D. *Green Chem.* **2013,** *15,* 3188.
(26) Kimura, T.; Uozumi, Y. *Organometallics* **2006,** *25,* 4883.
(27) (a) Huber, T. A.; Belanger-Gariepy, F.; Zargarian, D. *Organometallics* **1995,** *14,* 4997; (b) Bayrakdarian, M.; Davis, M. J.; Reber, C.; Zargarian, D. *Can. J. Chem.* **1996,** *74,* 2194; (c) Casty, G. L.; Lugmair, C. G.; Radu, N. S.; Tilley, T. D.; Walzer, J. F.; Zargarian, D. *Organometallics* **1997,** *16,* 8; (d) Huber, T. A.; Bayrakdarian, M.; Dion, S.; Dubuc, I.; Belanger-Gariepy, F.; Zargarian, D. *Organometallics* **1997,** *16,* 5811; (e) Vollmerhaus, R.; Belanger-Gariepy, F.; Zargarian, D. *Organometallics* **1997,** *16,* 4762; (f) Fontaine, F.-G.; Kadkhodazadeh, T.; Zargarian, D. *Chem. Commun.* **1998,** 1253; (g) Dubois, M.-A.; Zargarian, D. In *The influence of indenyl substituents on the catalytic reactivities of new indenyl nickel complexes*, American Chemical Society: 1999; pp INOR; (h) Dubuc, I.; Dubois, M.-A.; Belanger-Gariepy, F.; Zargarian, D. *Organometallics* **1999,** *18,* 30.
(28) Gomez-Benitez, V.; Baldovino-Pantaleon, O.; Herrera-Alvarez, C.; Toscano, R. A.; Morales-Morales, D. *Tetrahedron Lett.* **2006,** *47,* 5059.
(29) (a) Kleij, A. W.; Gossage, R. A.; Gebbink, R. J. M. K.; Brinkmann, N.; Reijerse, E. J.; Kragl, U.; Lutz, M.; Spek, A. L.; van, K. G. *J. Am. Chem. Soc.* **2000,** *122,* 12112; (b) van de Kuil, L. A.; Grove, D. M.; Gossage, R. A.; Zwikker, J. W.; Jenneskens, L. W.; Drenth, W.; van Koten, G. *Organometallics* **1997,** *16,* 4985.
(30) Vabre, B.; Lambert, M. L.; Petit, A.; Ess, D. H.; Zargarian, D. *Organometallics* **2012,** *31,* 6041.
(31) Spasyuk, D. M.; Zargarian, D.; van, d. E. A. *Organometallics* **2009,** *28,* 6531.
(32) Vabre, B.; Canac, Y.; Duhayon, C.; Chauvin, R.; Zargarian, D. *Chem. Commun. (Cambridge, U. K.)* **2012,** *48,* 10446.
(33) Spasyuk, D. M.; Zargarian, D.; van der Est, A. *Organometallics* **2009,** *28,* 6531.
(34) Lefèvre, X.; Durieux, G.; Lesturgez, S.; Zargarian, D. *J. Mol. Catal. A: Chem.* **2011,** *335,* 1.
(35) (a) Lefèvre, X.; Durieux, G.; Lesturgez, S.; Zargarian, D. *Journal of Molecular Catalysis A: Chemical* **2011,** *335,* 1; (b) Salah, A. B.; Offenstein, C.; Zargarian, D. *Organometallics* **2011,** *30,* 5352.
(36) Moulton, C. J.; Shaw, B. L. *J. Chem. Soc., Dalton Trans.* **1976,** 1020.
(37) Van Koten, G. *Pure Appl. Chem.* **1989,** *61,* 1681.
(38) (a) van Koten, G. *J. Organomet. Chem.* **2013,** *730,* 156; (b) van Koten, G., The Monoanionic ECE-Pincer Ligand: A Versatile Privileged Ligand Platform—General Considerations. In *Top Organometal Chem*, van Koten, G.; Milstein, D., Eds. Springer Berlin Heidelberg: Berlin, Heidelberg, 2013; Vol. 40, pp 1; (c) Morales-Morales, D.; Jensen, C. G. M., *The Chemistry of Pincer Compounds*. Elsevier Science: 2011; (d) Poverenov, E.; Milstein, D., Noninnocent Behavior of PCP and PCN Pincer Ligands of Late Metal Complexes. In *Top Organometal Chem*, van Koten, G.; Milstein, D., Eds. Springer Berlin Heidelberg: 2013; Vol. 40, pp 21; (e) Roddick, D., Tuning of PCP Pincer Ligand Electronic and Steric Properties. In *Top Organometal Chem*, van Koten, G.; Milstein, D., Eds. Springer Berlin Heidelberg: 2013; Vol. 40, pp 49.
(39) (a) Castonguay, A.; Sui-Seng, C.; Zargarian, D.; Beauchamp, A. L. *Organometallics* **2006,** *25,* 602; (b) Kennedy, A. R.; Cross, R. J.; Muir, K. W. *Inorg. Chim. Acta* **1995,** *231,* 195; (c) Huck, W. T. S.; Snellink-Ruël, B.; van Veggel, F. C. J. M.; Reinhoudt, D. N. *Organometallics* **1997,** *16,* 4287; (d) Kozhanov, K. A.; Bubnov, M. P.; Cherkasov, V. K.; Fukin, G. K.; Abakumov, G. A. *Chem. Commun.* **2003,** 2610; (e) Kozhanov, K. A.; Bubnov, M. P.; Cherkasov, V. K.;

Vavilina, N. N.; Efremova, L. Y.; Artyushin, O. I.; Odinets, I. L.; Abakumov, G. A. *Dalton Trans.* **2008,** 2849; (f) Cámpora, J.; Palma, P.; del Río, D.; Álvarez, E. *Organometallics* **2004,** *23,* 1652; (g) Cámpora, J.; Palma, P.; del Río, D.; Conejo, M. M.; Álvarez, E. *Organometallics* **2004,** *23,* 5653; (h) Castonguay, A.; Beauchamp, A. L.; Zargarian, D. *Organometallics* **2008,** *27,* 5723; (i) Boro, B. J.; Duesler, E. N.; Goldberg, K. I.; Kemp, R. A. *Inorg. Chem.* **2009,** *48,* 5081; (j) Schmeier, T. J.; Hazari, N.; Incarvito, C. D.; Raskatov, J. A. *Chem. Commun.* **2011,** *47,* 1824; (k) Levina, V. A.; Rossin, A.; Belkova, N. V.; Chierotti, M. R.; Epstein, L. M.; Filippov, O. A.; Gobetto, R.; Gonsalvi, L.; Lledós, A.; Shubina, E. S.; Zanobini, F.; Peruzzini, M. *Angew. Chem. Int. Ed.* **2011,** *50,* 1367; (l) van der Boom, M. E.; Liou, S.-Y.; Shimon, L. J. W.; Ben-David, Y.; Milstein, D. *Inorg. Chim. Acta* **2004,** *357,* 4015; (m) Castonguay, A.; Beauchamp, A. L.; Zargarian, D. *Inorg. Chem.* **2009,** *48,* 3177.

(40) (a) Gómez-Benítez, V.; Baldovino-Pantaleón, O.; Herrera-Álvarez, C.; Toscano, R. A.; Morales-Morales, D. *Tetrahedron Lett.* **2006,** *47,* 5059; (b) Vabre, B.; Petiot, P.; Declercq, R.; Zargarian, D. *Organometallics* **2014,** *33,* 5173; (c) Estudiante-Negrete, F.; Hernández-Ortega, S.; Morales-Morales, D. *Inorg. Chim. Acta* **2012,** *387,* 58; (d) Chakraborty, S.; Krause, J. A.; Guan, H. *Organometallics* **2009,** *28,* 582; (e) Zhang, J.; Medley, C. M.; Krause, J. A.; Guan, H. *Organometallics* **2010,** *29,* 6393; (f) Chakraborty, S.; Patel, Y. J.; Krause, J. A.; Guan, H. *Polyhedron* **2012,** *32,* 30.

(41) (a) Hao, J.; Mougang-Soume, B.; Vabre, B.; Zargarian, D. *Angew. Chem., Int. Ed.* **2014,** *53,* 3218; (b) Pandarus, V.; Castonguay, A.; Zargarian, D. *Dalton Trans.* **2008,** 4756.

(42) (a) Spasyuk, D. M.; Zargarian, D. *Inorg. Chem.* **2010,** *49,* 6203; (b) Zhang, B.-S.; Wang, W.; Shao, D.-D.; Hao, X.-Q.; Gong, J.-F.; Song, M.-P. *Organometallics* **2010,** *29,* 2579; (c) Niu, J.-L.; Chen, Q.-T.; Hao, X.-Q.; Zhao, Q.-X.; Gong, J.-F.; Song, M.-P. *Organometallics* **2010,** *29,* 2148; (d) Spasyuk, D. M.; Gorelsky, S. I.; van, d. E. A.; Zargarian, D. *Inorg. Chem.* **2011,** *50,* 2661; (e) Yang, M.-J.; Liu, Y.-J.; Gong, J.-F.; Song, M.-P. *Organometallics* **2011,** *30,* 3793; (f) Sanford, J.; Dent, C.; Masuda, J. D.; Xia, A. *Polyhedron* **2011,** *30,* 1091.

(43) (a) Fan, L.; Foxman, B. M.; Ozerov, O. V. *Organometallics* **2004,** *23,* 326; (b) Ozerov, O. V.; Guo, C.; Fan, L.; Foxman, B. M. *Organometallics* **2004,** *23,* 5573; (c) Liang, L.-C.; Chien, P.-S.; Huang, Y.-L. *J. Am. Chem. Soc* **2006,** *128,* 15562; (d) Liang, L.-C.; Chien, P.-S.; Lin, J.-M.; Huang, M.-H.; Huang, Y.-L.; Liao, J.-H. *Organometallics* **2006,** *25,* 1399; (e) Adhikari, D.; Huffman, J. C.; Mindiola, D. J. *Chem. Commun.* **2007,** 4489; (f) Adhikari, D.; Pink, M.; Mindiola, D. J. *Organometallics* **2009,** *28,* 2072; (g) Fryzuk, M. D.; Montgomery, C. D. *Coord. Chem. Rev.* **1989,** *95,* 1; (h) Fryzuk, M. D.; MacNeil, P. A. *J. Am. Chem. Soc* **1981,** *103,* 3592.

(44) (a) Vechorkin, O.; Proust, V.; Hu, X. *J. Am. Chem. Soc* **2009,** *131,* 9756; (b) Madhira, V. N.; Ren, P.; Vechorkin, O.; Hu, X.; Vicic, D. A. *Dalton Trans.* **2012,** *41*; (c) Breitenfeld, J.; Scopelliti, R.; Hu, X. *Organometallics* **2012,** *31,* 2128.

(45) (a) Zargarian, D.; Castonguay, A.; Spasyuk, D., ECE-Type Pincer Complexes of Nickel. In *Top Organometal Chem*, van Koten, G.; Milstein, D., Eds. Springer Berlin Heidelberg: 2013; Vol. 40, pp 131; (b) Wang, Z.-X.; Liu, N. *Eur. J. Inorg. Chem.* **2012,** *2012,* 901.

(46) (a) Chakraborty, S.; Zhang, J.; Krause, J. A.; Guan, H. *J. Am. Chem. Soc* **2010,** *132,* 8872; (b) Knapen, J. W. J.; van der Made, A. W.; de Wilde, J. C.; van Leeuwen, P. W. N. M.; Wijkens, P.; Grove, D. M.; van Koten, G. *Nature* **1994,** *372,* 659.

(47) Salah, A. B.; Zargarian, D. *Dalton Trans.* **2011,** *40,* 8977.

(48) (a) Choi, J.; MacArthur, A. H. R.; Brookhart, M.; Goldman, A. S. *Chem. Rev.* **2011,** *111,* 1761; (b) Zhu, K.; Achord, P. D.; Zhang, X.; Krogh-Jespersen, K.; Goldman, A. S. *J. Am. Chem. Soc* **2004,** *126,* 13044; (c) Krogh-Jespersen, K.; Czerw, M.; Zhu, K.; Singh, B.; Kanzelberger, M.; Darji, N.; Achord, P. D.; Renkema, K. B.; Goldman, A. S. *J. Am. Chem. Soc* **2002,** *124,* 10797; (d) Göttker-Schnetmann, I.; White, P.; Brookhart, M. *J. Am. Chem. Soc* **2004,** *126,* 1804; (e) Roddick, D. M. *Top. Organomet. Chem.* **2013,** *40,* 49.

(49) Pratt, D. A.; Pesavento, R. P.; van der Donk, W. A. *Org. Lett.* **2005,** *7,* 2735.

(50) *Based on two CCDC surveys, both conducted on November 4th 2014, of all structurally characterized nickel compounds containing a covalently bonded triflate anion, and of all complexes bearing at least one Ni-N≡CR moieties*.

(51) *It has been shown that the presence of t-Bu substituents ortho to the phosphinite moieties in (POCOP)NiBr generates significantly shorter P-Ni bond distances. See: ref. 15a*.

(52) (a) Chakraborty, S.; Patel, Y. J.; Krause, J. A.; Guan, H. *Angew. Chem., Int. Ed.* **2013,** *52,* 7523; (b) Lefevre, X.; Spasyuk, D. M.; Zargarian, D. *Journal of Organometallic Chemistry* **2011,** *696,* 864.

(53) Liang, S.; Wang, H.; Deb, T.; Petersen, J. L.; Yee, G. T.; Jensen, M. P. *Inorg. Chem.* **2012,** *51,* 12707.

(54) Rozenel, S. S.; Kerr, J. B.; Arnold, J. *Dalton Trans.* **2011,** *40,* 10397.

(55) *The relative ν(C≡N) values observed in these adducts is also reflected in the greater electrophilicity of the double bond moiety in the acrylonitrile adduct of 1 in regard to its aliphatic counterpart (See Table 2).*

(56) *It should be noted that this comparison was based on ν(C≡N) values measured under identical experimental conditions, i.e., using KBr disks for the comparison between [(H-POCOP^{Ph})Ni(NCMe)][OSO$_2$CF$_3$] and **1**, and using solid samples in ATR-IR to compare **1** to **9**)*.

(57) *Note : both of these signals are fairly broad, $LW_{1/2}$ being ~ 118 Hz for the new signal at ca.193-194 ppm and 115 Hz for the cationic adduct 8 signal at ca. 195 ppm.*

(58) Grove, D. M.; Van Koten, G.; Ubbels, H. J. C.; Zoet, R.; Spek, A. L. *Organometallics* **1984,** *3,* 1003.

(59) *To better understand the curious formation of the triflate derivatives (NCN)Ni(OTf) and (PC$_{sp3}$P$^{i\text{-}Pr}$)Ni(OTf) in non-negligible amounts, we set out to establish if they arise from the corresponding acetonitrile adducts bearing triflate counter-anions. The following experiment was conducted for this purpose: to a 0.04 or 0.08 mM C$_6$D$_6$ solution of complex **1** was added 1-10 equivalents of silver triflate, the sample was agitated periodically, and the ^{31}P NMR spectra were recorded after 24 h. The original signal broadened slightly but there was no trace of the triflate derivative (singlet at 185 ppm) or any other new species. This lead us to believe that there might indeed be an equilibrium where the triflate moiety would exchange with the acetonitrile ligand, albeit it being shifted much more to the acetonitrile adduct.*

(60) Foti, M. C.; Daquino, C.; Mackie, I. D.; DiLabio, G. A.; Ingold, K. U. *J. Org. Chem.* **2008,** *73,* 9270.

(61) Xu, L.-W.; Li, L.; Xia, C.-G. *Helv. Chim. Acta* **2004,** *87,* 1522.

(62) (a) Seligson, A. L.; Trogler, W. C. *Organometallics* **1993,** *12,* 744; (b) Kawatsura, M.; Hartwig, J. F. *Organometallics* **2001,** *20,* 1960; (c) Fadini, L.; Togni, A. *Chem. Commun.* **2003,** 30; (d) Ranu, B. C.; Banerjee, S. *Org. Lett.* **2005,** *7,* 3049; (e) Reddy, K. R.; Kumar, N. S. *Synlett* **2006,** 2246; (f) Rosenfeld, D. C.; Shekhar, S.; Takemiya, A.; Utsunomiya, M.; Hartwig, J. F. *Org. Lett.* **2006,** *8,* 4179; (g) Phua, P. H.; Mathew, S. P.; White, A. J. P.; de Vries, J. G.; Blackmond, D. G.; Hii, K. K. *Chemistry – A European Journal* **2007,** *13,* 4602; (h) Corberán, R.; Marrot, S.; Dellus, N.; Merceron-Saffon, N.; Kato, T.; Peris, E.; Baceiredo, A. *Organometallics* **2009,** *28,* 326; (i) Azizi, N.; Baghi, R.; Ghafuri, H.; Bolourtchian, M.; Hashemi, M. *Synlett* **2010,** 379; (j) Kim, S.; Kang, S.; Kim, G.; Lee, Y. *J Org Chem* **2016,** *81,* 4048.

(63) (a) Michael, F. E.; Cochran, B. M. *J. Am. Chem. Soc.* **2006,** *128,* 4246; (b) Cochran, B. M.; Michael, F. E. *J. Am. Chem. Soc.* **2008,** *130,* 2786.

(64) (a) Munro-Leighton, C.; Blue, E. D.; Gunnoe, T. B. *J. Am. Chem. Soc* **2006,** *128,* 1446; (b) Munro-Leighton, C.; Delp, S. A.; Blue, E. D.; Gunnoe, T. B. *Organometallics* **2007,** *26,* 1483; (c) Taylor, J. G.; Adrio, L. A.; Hii, K. K. *Dalton Trans.* **2010,** *39,* 1171.

(65) Fadini, L.; Togni, A. *Tetrahedron: Asymmetry* **2008,** *19,* 2555.

(66) Lapointe, S.; Vabre, B.; Zargarian, D. *Organometallics* **2015,** *34,* 3520.

(67) The authors wish to thank a reviewer of the manuscript for asking that we include this clarification here for the readers' benefit.
(68) Chaquin, P.; Canac, Y.; Lepetit, C.; Zargarian, D.; Chauvin, R. *Int. J. Quantum Chem* **2016,** n/a.
(69) Simple DFT calculations carried out on acetonitrile, acrylonitrile, and cinnamonitrile and have shown extensive mixing of the C=C bending mode CN stretching oscillator in acrylonitrile and cinnamonitrile, whereas no significant mixing was observed in acetonitrile. This might offer a partial explanation for why ν(CN) values of these two nitriles are impacted differently upon coordination to the cationic Ni(II) centre. We thank a reviewer of our manuscript for suggesting that we probe this possibility.
(70) Vabre, B.; Canac, Y.; Lepetit, C.; Duhayon, C.; Chauvin, R.; Zargarian, D. *Chemistry – A European Journal* **2015,** *21,* 17403.
(71) It should be recognized here that the absence of detectable quantities of the postulated amine adducts does not rule out the possibility that these species can form in small quantities and might indeed act as intermediates in the alternative inner-sphere mechanistic scenario. We thank a reviewer of our manuscript for suggesting that this point be stated clearly.
(72) Our working hypothesis has been, and remains, that the attack of the amine on the olefin is rate-limiting. However, a reviewer of our manuscript has pointed out correctly that our observations to date do not substantiate this hypothesis; therefore, the rate-limiting step in this process should be considered unknown.
(73) Gagne, M. R.; Marks, T. J. *J. Am. Chem. Soc* **1989,** *111,* 4108.
(74) (a) Wang, Z. J.; Benitez, D.; Tkatchouk, E.; Goddard III, W. A.; Toste, F. D. *J. Am. Chem. Soc* **2010,** *132,* 13064; (b) Field, L. D.; Messerle, B. A.; Vuong, K. Q.; Turner, P. *Organometallics* **2005,** *24,* 4241; (c) Kim, S.; Kang, S.; Kim, G.; Lee, Y. *J. Org. Chem.* **2016**; (d) Wang, J.; Xu, F.; Cai, T.; Shen, Q. *Org. Lett.* **2008,** *10,* 445.
(75) Cheng, X.; Xia, Y.; Wei, H.; Xu, B.; Zhang, C.; Li, Y.; Qian, G.; Zhang, X.; Li, K.; Li, W. *Eur. J. Org. Chem.* **2008,** *2008,* 1929.
(76) Xu, X.; Zhang, X.; Wang, Z.; Kong, M. *RSC Advances* **2015,** *5,* 40950.
(77) Huang, L.; Arndt, M.; Gooßen, K.; Heydt, H.; Gooßen, L. J. *Chemical Reviews* **2015,** *115,* 2596.
(78) (a) Ryken, S. A.; Schafer, L. L. *Acc Chem Res* **2015,** *48,* 2576; (b) Lui, E. K. J.; Schafer, L. L. *Advanced Synthesis & Catalysis* **2016,** *358,* 713.
(79) Seligson, A. L.; Trogler, W. C. *Organometallics* **1993,** *12,* 738.
(80) (a) van, d. B. M. E.; Milstein, D. *Chem. Rev. (Washington, DC, U. S.)* **2003,** *103,* 1759; (b) Kraatz, H.-B.; Milstein, D. *J. Organomet. Chem.* **1995,** *488,* 223.
(81) El-Zoghbi, I.; Kebdani, M.; Whitehorne, T. J. J.; Schaper, F. *Organometallics* **2013,** *32,* 6986.
(82) (a) Sartori, M. F. Azo dyes for polyester fiber. US2782187, 1957; (b) Feng, G.; Sun, Y.; Chen, M.; Jian, W. Preparation of azo disperse dyes. CN104059377A, 2014; (c) Mishra, S. K.; Mishra, S. K. *J. Teach. Res. Chem.* **2000,** *7,* 14.
(83) Reyes-Sanchez, A.; Garcia-Ventura, I.; Garcia, J. J. *Dalton Trans.* **2014,** *43,* 1762.
(84) Zhu, S.; Niljianskul, N.; Buchwald, S. L. *J. Am. Chem. Soc* **2013,** *135,* 15746.
(85) Zhang, S.; Wei, Y.; Yin, S.; Au, C.-t. *Catal. Commun.* **2011,** *12,* 712.
(86) Fadini, L.; Togni, A. *Helv. Chim. Acta* **2007,** *90,* 411.
(87) Loewenstein, A.; Connor, T. M. *Berichte der Bunsengesellschaft für physikalische Chemie* **1963,** *67,* 280.
(88) Gischig, S.; Togni, A. *European Journal of Inorganic Chemistry* **2005,** *2005,* 4745.
(89) (a) Hutchings, M. G. Azo dyestuffs. GB2011454A, 1979; (b) Li, B. Grinding coupling method for preparing disperse dyes. CN103450699A, 2013; (c) Tang, B.; Qiu, J.; Ju, B.; Zhang,

S. Method for preparing weakly alkaline arylamine diazonium salt and method for preparing tertiary amine-type weakly alkaline arylamine azo dye from the same. CN104926685A, 2015.

(90) SAINT *Integration Software for Single Crystal Data*, Release 6.06; Bruker AXS Inc.: Madison, WI, 1999.

(91) Sheldrick, G. M. *SADABS, Bruker Area Detector Absorption Corrections*, 1999; Bruker AXS Inc.: Madison, WI, 1999.

(92) XPREP *X-ray Data Preparation and Reciprocal Space Exploration Program*, Release 5.10; Bruker AXS Inc.: Madison, WI, 1997.

(93) SHELXTL *The Complete Software Package for Single Crystal Structure Determination*, Release 5.10; Bruker AXS Inc.: Madison, WI, 1997.

(94) (a) Sheldrick, G. M. *SHELXS97, Program for the Solution of Crystal Structures*, Univ. of Gottingen: Germany, 1997; (b) Sheldrick, G. M. *SHELXL97, Program for the Refinement of Crystal Structures*, Univ. of Gottingen: Germany, 1997.

(95) Hansch, C.; Leo, A.; Taft, R. W. *Chem. Rev.* **1991,** *91,* 165.

(96) Sheldrick, G. *Acta Crystallographica Section A* **2008,** *64,* 112.

(97) Sheldrick, G. *Acta Crystallographica Section A* **2015,** *71,* 3.

(98) Dolomanov, O. V.; Bourhis, L. J.; Gildea, R. J.; Howard, J. A. K.; Puschmann, H. *J. Appl. Crystallogr.* **2009,** *42,* 339.

(99) Lapointe, S.; Zargarian, D. *Dalton Trans.* **2016**.

A1 - Annexe pour chapitre 2

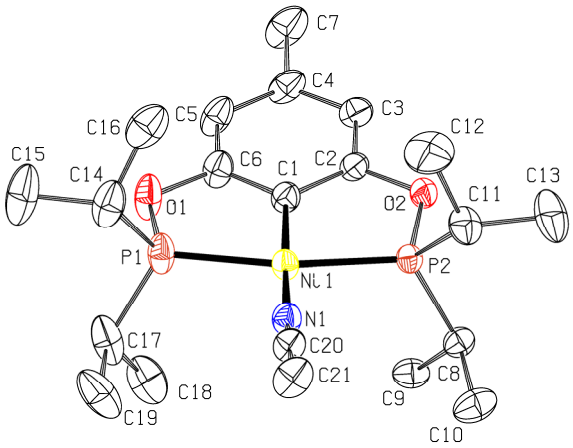

Figure A2.1 Molecular diagram for complex **2.**

Thermal ellipsoids are shown at the 50% probability level. Hydrogens are omitted for clarity.

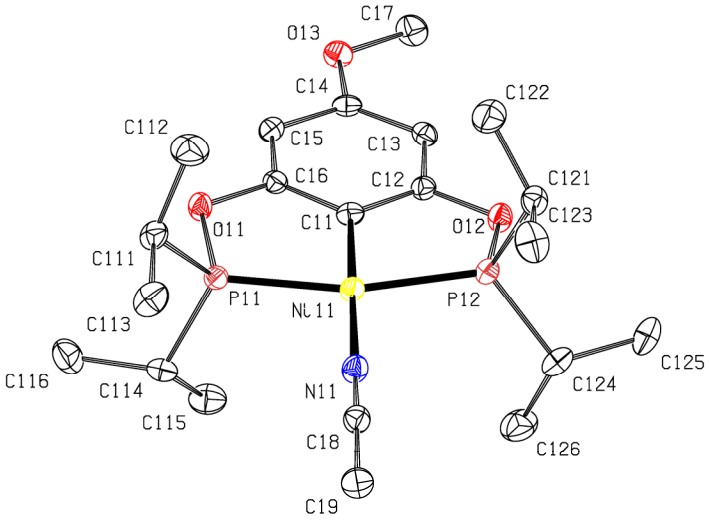

Figure A2.2 Molecular diagram for complex **3.**

Thermal ellipsoids are shown at the 50% probability level. Hydrogens are omitted for clarity.

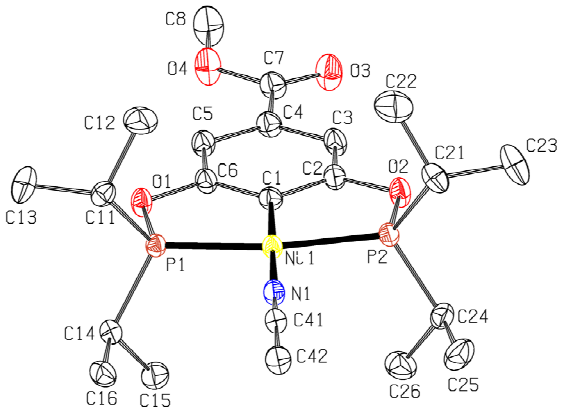

Figure A2.3 Molecular diagram for complex **4.**

Thermal ellipsoids are shown at the 50% probability level. Hydrogens are omitted for clarity.

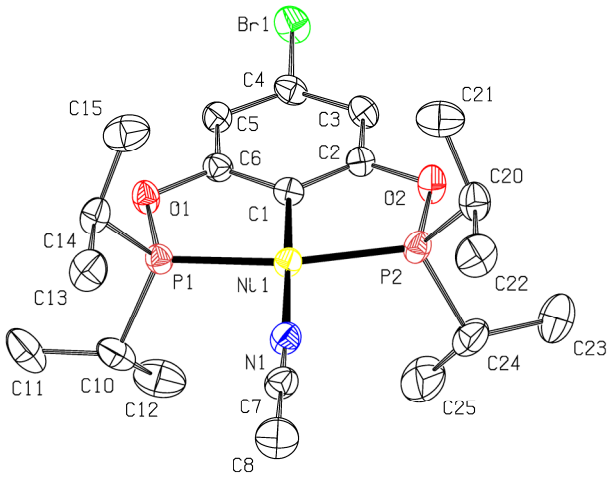

Figure A2.4 Molecular diagram for complex **5.**

Thermal ellipsoids are shown at the 50% probability level. Hydrogens are omitted for clarity.

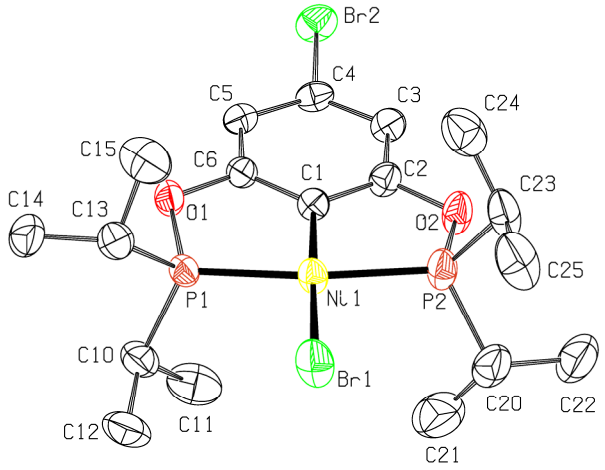

Figure A2.5 Molecular diagram for complex **5'.**

Thermal ellipsoids are shown at the 50% probability level. Hydrogens are omitted for clarity.

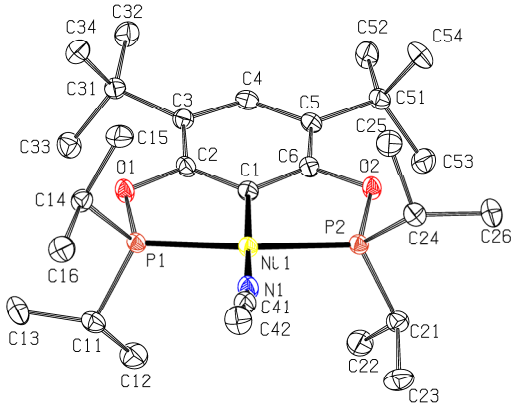

Figure A2.6 Molecular diagram for complex **6.**

Thermal ellipsoids are shown at the 50% probability level. Hydrogens are omitted for clarity.

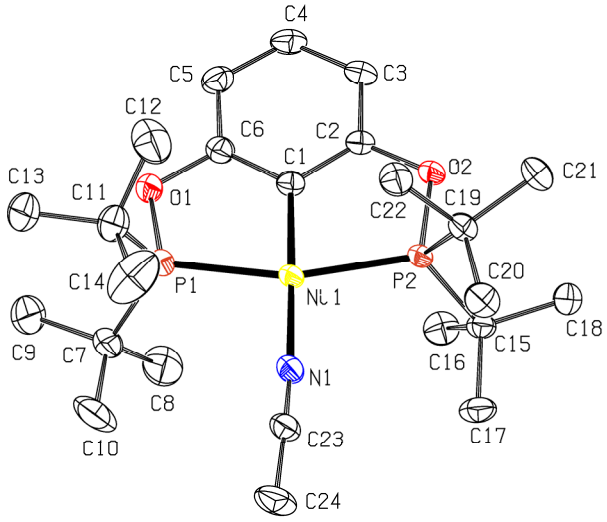

Figure A2.7 Molecular diagram for complex **9.**

Thermal ellipsoids are shown at the 50% probability level. Hydrogens are omitted for clarity.

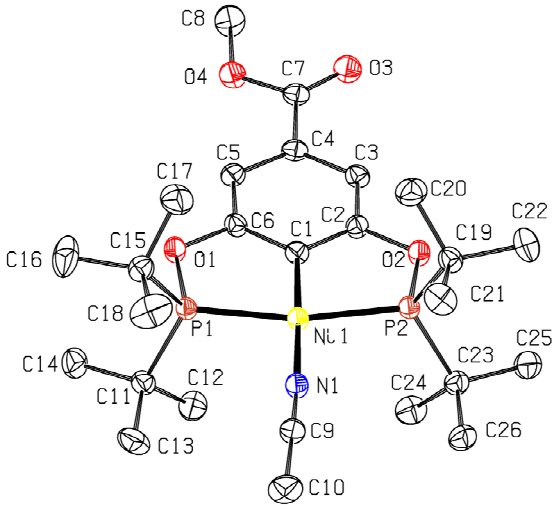

Figure A2.8 Molecular diagram for complex **10.**

Thermal ellipsoids are shown at the 50% probability level. Hydrogens are omitted for clarity.

Table A2.1 Crystal Data, Collection, and Refinement Parameters for complexes **2** to **5**

	[(*p*-MePOCOP$^{i\text{-}Pr}$)Ni(NCCH$_3$)][OTf] (**2**)	[(*p*-OMePOCOP$^{i\text{-}Pr}$)Ni(NCCH$_3$)][OTf] (**3**)	[(*p*-CO$_2$MePOCOP$^{i\text{-}Pr}$)Ni(NCCH$_3$)][OTf] (**4**)	[(*p*-BrPOCOP$^{i\text{-}Pr}$)Ni(NCCH$_3$)][OTf] (**5**)
Chemical formula	$C_{21}H_{36}NNiO_2P_2,CF_3O_3S$	$C_{21}H_{36}NNiO_3P_2,CF_3O_3S$	$C_{22}H_{36}NNiO_4P_2,CF_3O_3S$	$C_{20}H_{33}BrNNiO_2P_2,CF_3O_3S$
Crystal colour	yellow	yellow	yellow	yellow
Fw; *F*(000)	604.23; 3792	620.23; 1296	648.24; 2704	669.10; 2736
T (K)	100	100(2)	100	150
wavelength (Å)	1.54178	1.54178	1.54178	1.54178
space group	P21/c	P2(1)	Pbca	P212121
a (Å)	17.2664(5)	7.8233(6)	8.7522(3)	12.5191(5)
b (Å)	29.5903(8)	30.142(2)	20.3175(6)	15.3796(7)
c (Å)	18.8491(5)	12.1730(9)	33.7301(10)	30.0110(13)
α (deg)	90	90.00	90	90
β (deg)	115.471(1)	91.384(3)	90	90
γ (deg)	90	90.00	90	90
Z	12	4	8	8
V (Å^3)	8694.3(4)	2869.6(4)	5998.0(3)	5778.3(4)
ρ_{calcd} (g·cm^{-3})	1.385	1.436	1.436	1.538
μ (mm^{-1})	3.130	3.204	3.118	4.761
θ range (deg); completeness	2.835 − 70.068; 1.000	2.93 − 71.08; 0.999	2.62 − 71.15; 0.999	2.94 − 69.76; 0.998
collected reflections; R_σ	170890; 0.0261	112735; 0.0183	237936; 0.0091	231975; 0.0156
unique reflections; R_{int}	170890; 0.0557	112735; 0.0335	237936; 0.038	231975; 0.049
R1[a]; wR2[b] [I > 2σ(I)]	0.0526; 0.1399	0.0253; 0.0677	0.0315; 0.0895	0.0351; 0.0976
R1; wR2 [all data]	0.0577; 0.1457	0.0255; 0.0678	0.0326; 0.0906	0.0352; 0.0978
GOF	1.027	1.062	1.049	1.064
largest diff peak and hole	2.499 and -0.954	0.382 and -0.291	0.504 and -0.274	1.358 and -1.181
Flack (X) parameter	N/D	0.085(8)	N/D	0.011(14)

a) $R_1=\Sigma(||F_o|-|F_c||)/\Sigma|F_o|$ b) $wR_2=\{\Sigma[w(F_o^2-F_c^2)^2]/\Sigma[w(F_o^2)^2]\}^{½}$

Table A2.2 Crystal Data, Collection, and Refinement Parameters for complexes **6, 9, 10** and **5'**

	[(*m,m-t*-Bu_2POCOP^{i-Pr})Ni($NCCH_3$)][OTf] (**6**)	[(*p*-OMePOCOP^{t-Bu})Ni($NCCH_3$)][OTf] (**9**)	[(*p*-CO_2MePOCOP^{t-Bu})Ni($NCCH_3$)][OTf] (**10**)	(*p*-BrPOCOP^{i-Pr})NiBr (**5'**)
chemical formula	$C_{28}H_{50}NNiO_2P_2,CF_3O_3S$	$C_{24}H_{42}NNiO_2P_2,CF_3O_3S$	$C_{26}H_{44}NNiO_4P_2,CF_3O_3S$	$C_{18}H_{30}Br_2NiO_2P_2$
crystal colour	yellow	yellow	yellow	yellow
Fw; F(000)	702.41; 744	646.30; 680	704.34; 1480	558.89; 2256
T (K)	100	100	100	150
wavelength (Å)	1.54178	1.54178	1.54178	1.54178
space group	P-1	P-1	P21/n	C2/c
a (Å)	12.2437(3)	7.8959(2)	7.9471(2)	32.477(2)
b (Å)	12.5695(3)	11.9279(3)	12.5511(4)	7.9125(6)
c (Å)	13.8799(4)	16.3259(4)	33.5307(10)	19.2364(14)
α (deg)	63.3389(15)	88.4540(10)	90	90
β (deg)	65.9230(15)	87.7560(10)	92.9800(10)	111.212(3)
γ (deg)	75.9872(15)	87.0870(10)	90	90
Z	2	2	4	8
V (Å3)	1738.30(8)	1533.95(7)	3339.99(17)	4608.4(6)
ρcalcd (g·cm-3)	1.342	1.399	1.401	1.611
μ (mm-1)	2.683	2.993	2.843	6.660
θ range (deg); completeness	3.80 − 70.46; 0.953	2.709 − 69.595; 0.994	2.639 − 69.643; 1.000	2.92 − 69.74; 0.997
collected reflections; Rσ	42991; 0.0157	51249; 0.0232	86369; 0.0199	122201; 0.0149
unique reflections; Rint	42991; 0.027	51249; 0.0432	86369; 0.0480	122201; 0.050
R1a; wR2b [I > 2σ(I)]	0.0313; 0.1077	0.0380; 0.1034	0.0312; 0.0868	0.0339; 0.0870
R1; wR2 [all data]	0.0353; 0.1150	0.0397; 0.1052	0.0318; 0.0873	0.0344; 0.0874
GOF	1.014	1.026	1.056	1.071
largest diff peak and hole	0.584 and -0.344	0.735 and -0.513	0.398 and -0.403	1.652 and -0.775
Flack (X) parameter	N/D	N/D	N/D	N/D

a) $R_1=\Sigma(||F_o|-|F_c||)/\Sigma|F_o|$ b) $wR_2=\{\Sigma[w(F_o^2-F_c^2)^2]/\Sigma[w(F_o^2)^2]\}^{½}$

Table A2.3 Additional bond distances (Å) in complexes **1-10**

Complex	C_{Ar}-O_1	C_{Ar}-O_2	O_1-P_1	O_2-P_2	Ni-O (OTf)
1[a]	1.390(3)	1.401(3)	1.6520(16)	1.6491(16)	4.274
2	1.392(3)	1.391(3)	1.647(2)	1.6455(18)	5.405
3	1.391(2)	1.387(2)	1.6512(12)	1.6556(13)	4.512
4	1.3922(17)	1.3862(17)	1.6499(10)	1.6480(11)	4.912
5	1.381(4)	1.382(4)	1.655(2)	1.648(2)	3.894
6	1.4050(18)	1.3981(18	1.6413(11)	1.6397(11)	4.626
9	1.388(2)	1.386(2)	1.6479(13)	1.6538(12)	4.167
10	1.3811(18)	1.3891(18)	1.6458(10)	1.6519(10)	3.934

a) Previously reported complex [24b, 24c]

Table A2.3 (contd.) - Additional bond angles (deg) in complexes **1-10**

Complex	C_{Ar}-O_1-P_1	C_{Ar}-O_2-P_2	Ni-P_1-O_1	Ni-P_2-O_2
1[a]	111.47(14)	111.95(14)	106.16(6)	106.04(6)
2	111.56(17)	111.87(15)	106.37(7)	105.95(7)
3	111.54(10)	110.98(11)	106.18(5)	105.93(5)
4	111.82(9)	112.26(9)	106.18(4)	105.63(4)
5	111.90(19)	112.25(19)	105.86(8)	105.70(9)
6	111.99(9)	113.54(10)	106.13(4)	104.92(4)
9	112.12(11)	112.80(11)	105.42(5)	105.01(5)
10	112.75(9)	112.28(9)	105.17(4)	105.42(4)

a) Previously reported complex [24b, 24c]

Details of the diffraction studies

Crystals of compound **2** were obtained by slow diffusion of hexanes into a $CDCl_3$ solution of the complex at ambient temperature. Crystals of compound **3** were obtained by slow diffusion of hexanes into an acetone solution of the complex. Crystals of compound **4** were obtained by a slow diffusion of hexanes into an acetonitrile solution of the complex. Crystals of compound **5** and **6** were obtained from a slow diffusion of hexane in a dichloromethane solution of the complex. The crystallographic data for complexes **3, 4** and **6** were collected on a Bruker APEX II equipped with an Incoatec I\muS microsource and a Quazar MX monochromator. The crystallographic data for compounds **2, 5, 5', 9** and **10**, were collected on a Bruker Microstar generator (Microsource) equipped with a Helios optics, a Kappa Nonius goniometer, and a Platinum135 detector. Cell refinement and data reduction were done using SAINT.[90] An empirical absorption correction, based on the multiple measurements of equivalent reflections, was applied using the program SADABS.[91] The space group was confirmed by XPREP routine [92] in the program SHELXTL.[93] The structures were solved by direct methods and refined by full-matrix least-squares and difference Fourier techniques with SHELX-97.[94] All non-hydrogen atoms were refined with anisotropic displacement parameters. Hydrogen atoms were set in calculated positions and refined as riding atoms with a common thermal parameter. Complex **2** showed disorder on the triflate moieties and on some isopropyl moieties. All atoms were refined anisotropically, with restraints on thermal anisotropic parameters (EADP), mostly of the triflate moiety. Disordered positions of the isopropyl moieties and of the acetonitrile moiety were optimized using mild constraints (SADI) and restraint (EADP, acetonitrile moiety).

2.7.3 IR analysis

Table A2.4 Detailed IR frequencies assignments for complexes **1-10**

Complex	ν(C≡N) /cm^{-1}	ν(C=O) /cm^{-1}	ν(SO_3) /cm^{-1}	ν(SO_3) /cm^{-1}	ν(SO) /cm^{-1}	ν(CF_3) /cm^{-1}	ν(C_{Ar}=C_{Ar}) /cm^{-1}	ν(C_{Ar}=C_{Ar}) /cm^{-1}
1	2297		1032	1267	636	1142	1442	1566
2	2294		1030	1262	636	1141	1464	1555
3	2293		1030	1266	636	1140	1462	1561
4	2329	1716	1029	1259	635	1140	1456	1550
5	2302		1032	1264	637	1142	1466	1554
6	2294		1028	1251	636	1143	1459	1552
7	2284		1027	1259	634	1144	1461	1570
8	2303	1712	1032	1272	637	1149	1462	1561
9	2293		1027	1263	635	1144	1441	1558
10	2315	1715	1032	1270	635	1135	1451	1552

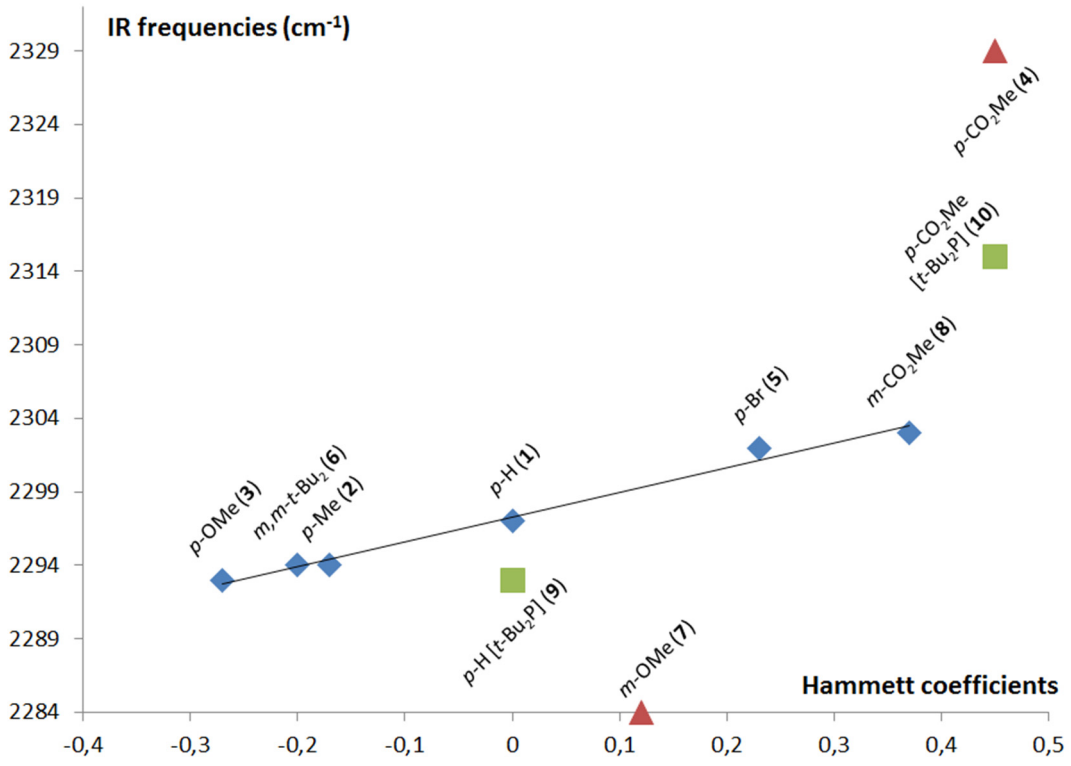

Figure A2.9 Relationship between ν(C≡N) values for complexes **1-10** and their corresponding σ_m and σ_p Hammett coefficients.[95]

A linear regression value of R2 = 0.9862 is obtained for the equation y = 16.801x + 2297.3 when the outlier points (red triangles) and t-Bu2P containing complexes 9 and 10 (green squares) are excluded from the equation.

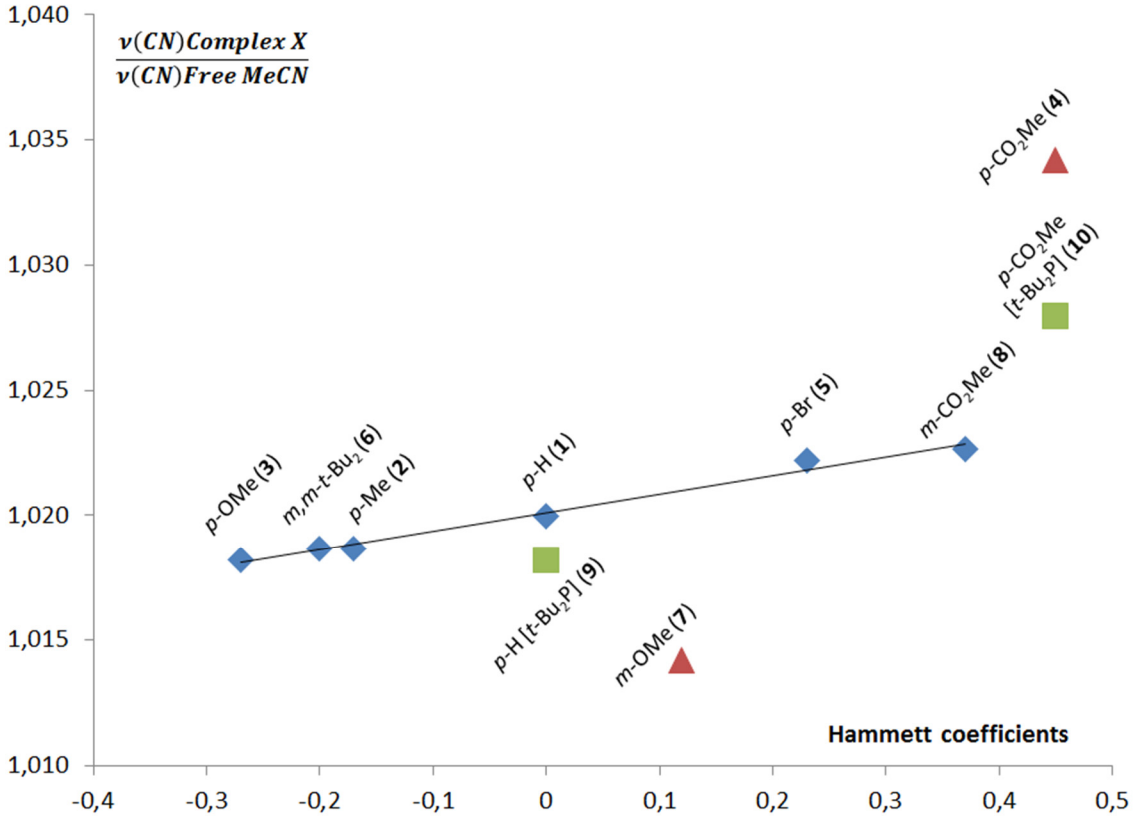

Figure A2.10 Relationship between ν(C≡N) values for complexes **1-10** normalized towards the ν(C≡N) of the free MeCN and their corresponding σ_m and σ_p Hammett coefficients.[95]

A linear regression value of R2 = 0.9862 is obtained for the equation y = 0.0075x + 1.0201 when the outlier points (red triangles) and *t*-Bu$_2$P containing complexes **9** and **10** (green squares) are excluded from the equation.

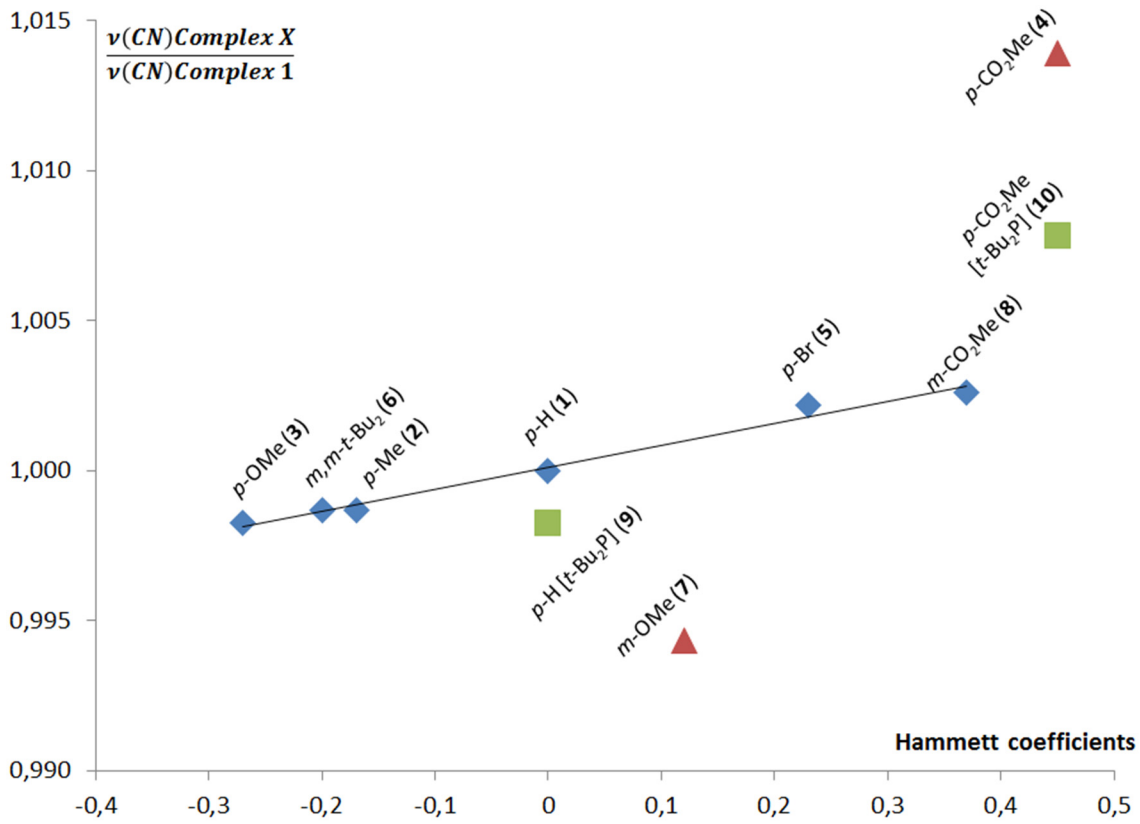

Figure A2.11 Relationship between ν(C≡N) values for complexes **1-10** normalized towards the ν(C≡N) of the unsubstituted complex **1** and their corresponding σ_m and σ_p Hammett coefficients.[95]

A linear regression value of $R_2 = 0.9862$ is obtained for the equation $y = 0.0073x + 1.0001$ when the outlier points (red triangles) and t-Bu_2P containing complexes **9** and **10** (green squares) are excluded from the equation.

2.7.4 NMR analysis

Table A2.5 NMR chemical shifts (ppm) of **1-10** and **1'-10'**

R	Complex	^{31}P shift [b]	^{1}H shift of NCC$\underline{H_3}$[b]	^{13}C shift of NC$\underline{C}$H$_3$[b]
H	1[a]	192.9	2.38	3.63
p-Me	2	193.4	2.42	3.91
p-OMe	3	191.6	2.39	3.98
p-CO_2Me	4	196.4	2.52	4.18
p-Br	5	195.7	2.37	3.84
m,*m*-t-Bu$_2$	6	192.9	2.38	4.22
m-OMe	7	191.4 (d), 195.7 (d)[c]	2.38	3.53
m-CO_2Me	8	195.3	2.46	4.26
H [P(t-Bu$_2$)]	9	197.8	2.67	4.51
p-CO_2Me [P(t-Bu$_2$)]	10	199.3	2.70	4.66
H	1'[a]	191.5		
p-Me	2'[a]	189.1		
p-OMe	3'[a]	190.6		
p-CO_2Me	4'[a]	190.6		
p-Br	5'	190.8		
m,*m*-t-Bu$_2$	6'[a]	185.2		
m-OMe	7'[a]	187.5(d), 192.2(d)[d]		
m-CO_2Me	8'[a]	190.4(d), 192.1(d)[e]		
H [P(t-Bu$_2$)]	9'[a]	191.0		
p-CO_2Me [P(t-Bu$_2$)]	10'[a]	191.8		

a) Previously reported complexes.[24b,11b] b) NMR spectra were recorded in in $CDCl_3$ (complexes **2-10**) or C_6D_6 (**1** and **1'-10'**). c) AB signal, $J_{PP} \approx 258$ Hz. d) AB signal, $J_{PP} \approx 318$ Hz. e) AB signal, $J_{PP} \approx 323$ Hz.

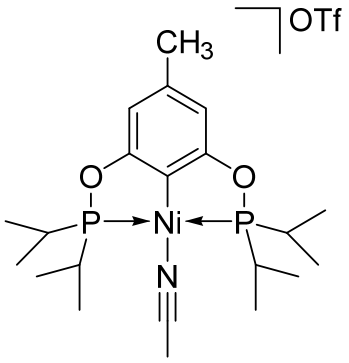

Figure A2.12 Representation of complex [{2,6-(*i*-Pr$_2$PO)$_2$-4-(Me)C$_6$H$_2$}Ni(NCMe)][OSO$_2$CF$_3$] (**2**)

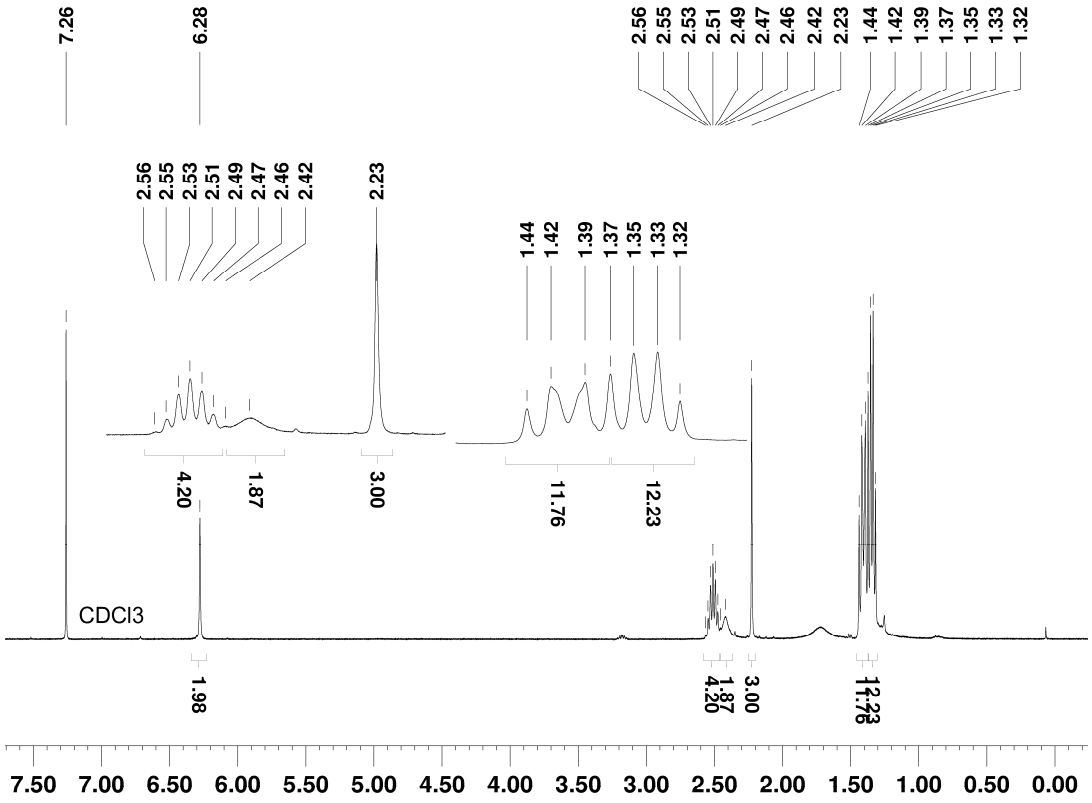

Figure A2.13 ^{1}H NMR (400 MHz) spectra of complex **2** in CDCl$_3$

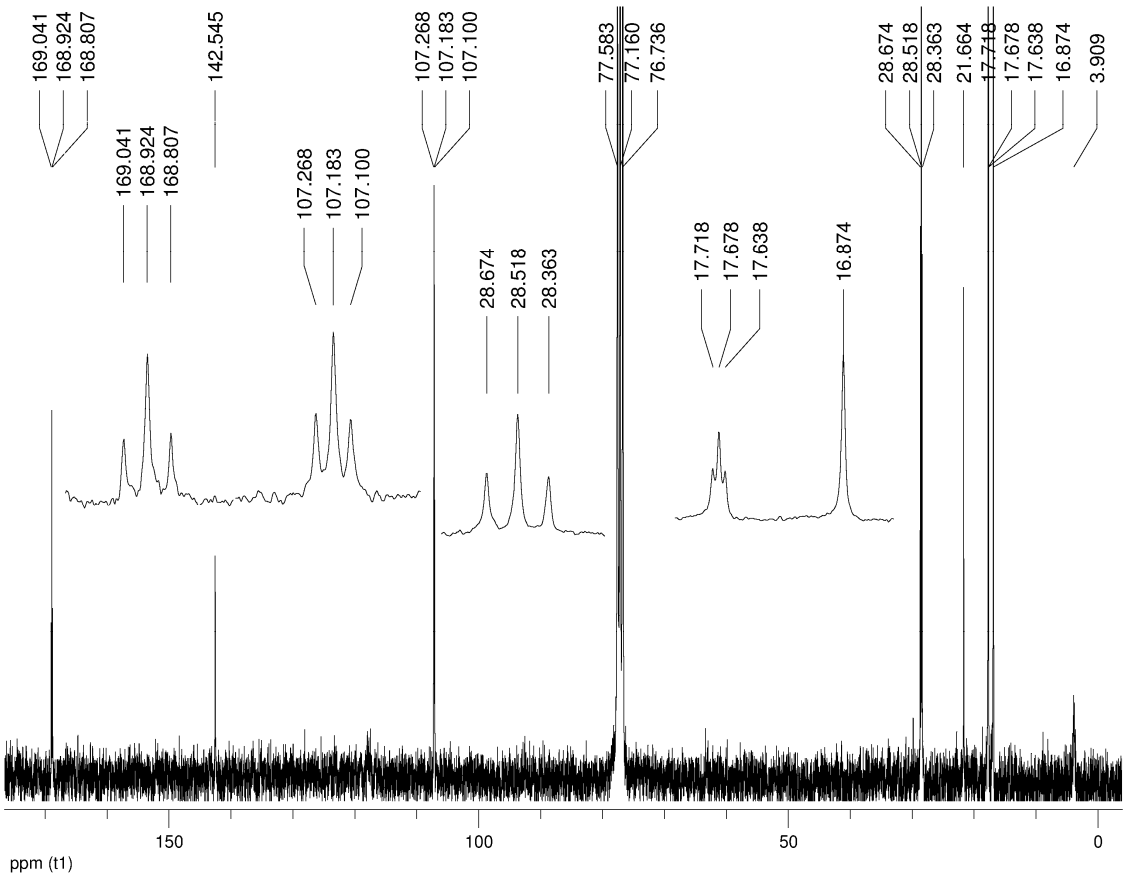

Figure A2.14 ^{13}C NMR (75 MHz) spectra of complex **2** in $CDCl_3$.

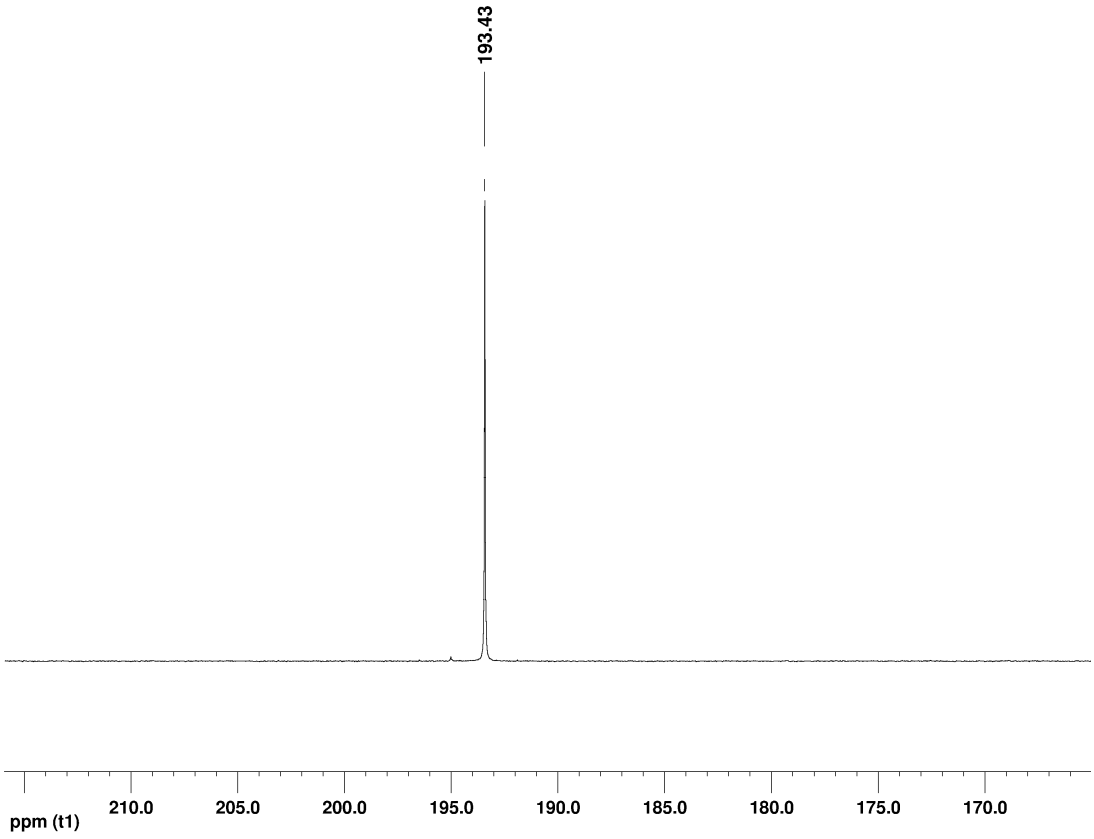

Figure A2.15 ^{31}P NMR (202 MHz) spectra of complex **2** in $CDCl_3$

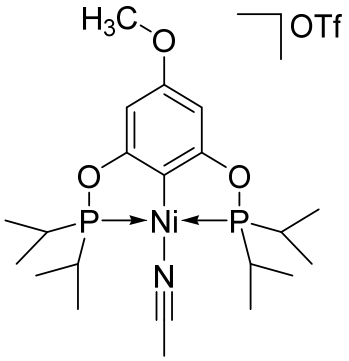

Figure A2.16 Representation of complex [{2,6-(*i*-Pr$_2$PO)$_2$-4-(OMe)C$_6$H$_2$}Ni(NCMe)][OSO$_2$CF-$_3$] (**3**)

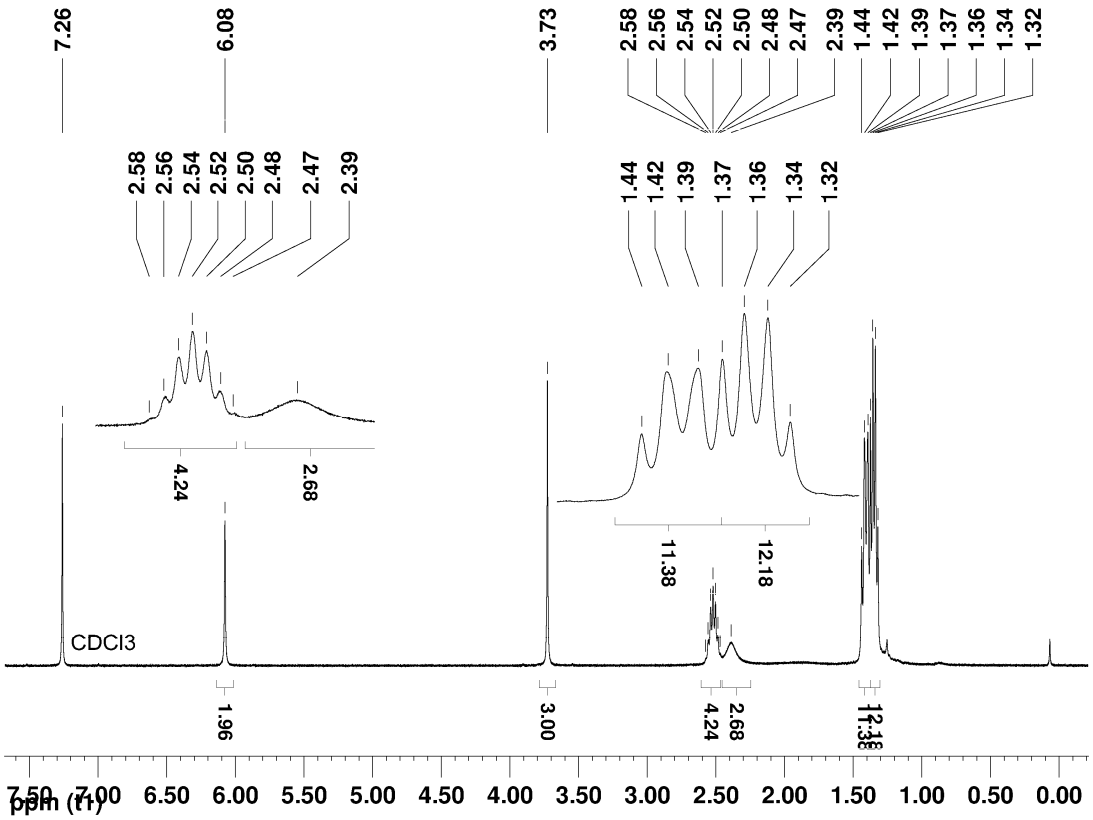

Figure A2.17 ^{1}H NMR (400 MHz) spectra of complex **3** in $CDCl_3$

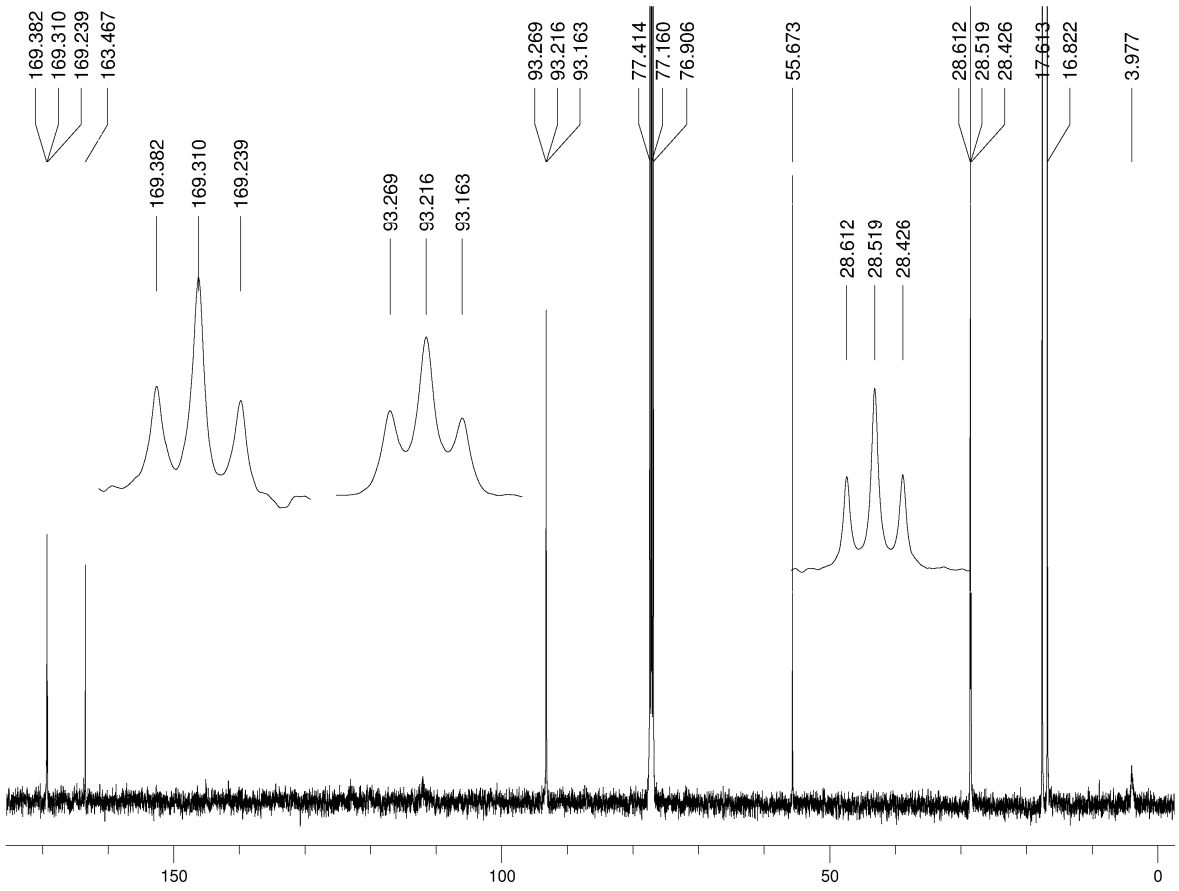

Figure A2.18 ^{13}C NMR (125 MHz) spectra of complex **3** in $CDCl_3$

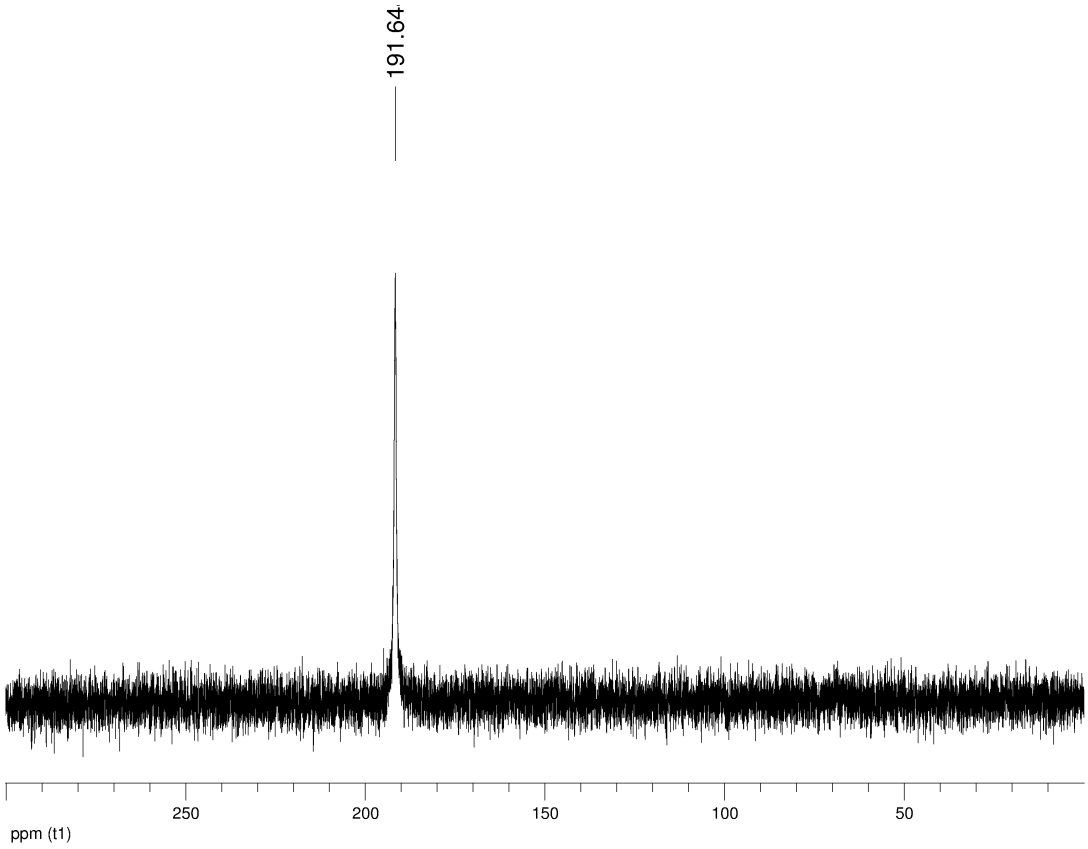

Figure A2.19 ^{31}P NMR (121 MHz) spectra of complex **3** in $CDCl_3$

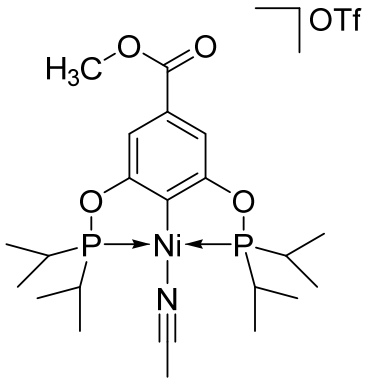

Figure A2.20 Representation of complex [{2,6-(*i*-$Pr_2PO)_2$-4-(CO-$_2$Me)C_6H_2}Ni(NCMe)][OSO_2CF_3] (**4**)

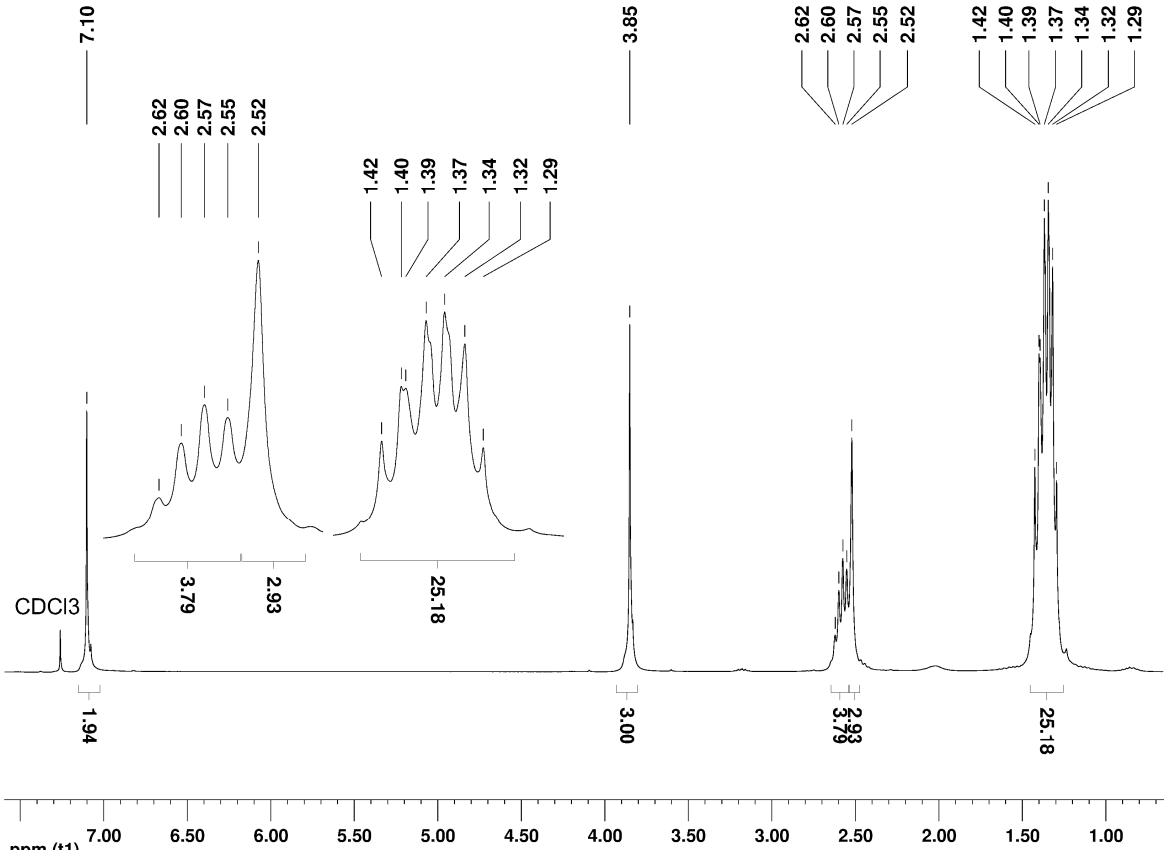

Figure A2.21 ^{1}H NMR (300 MHz) spectra of complex **4** in $CDCl_3$

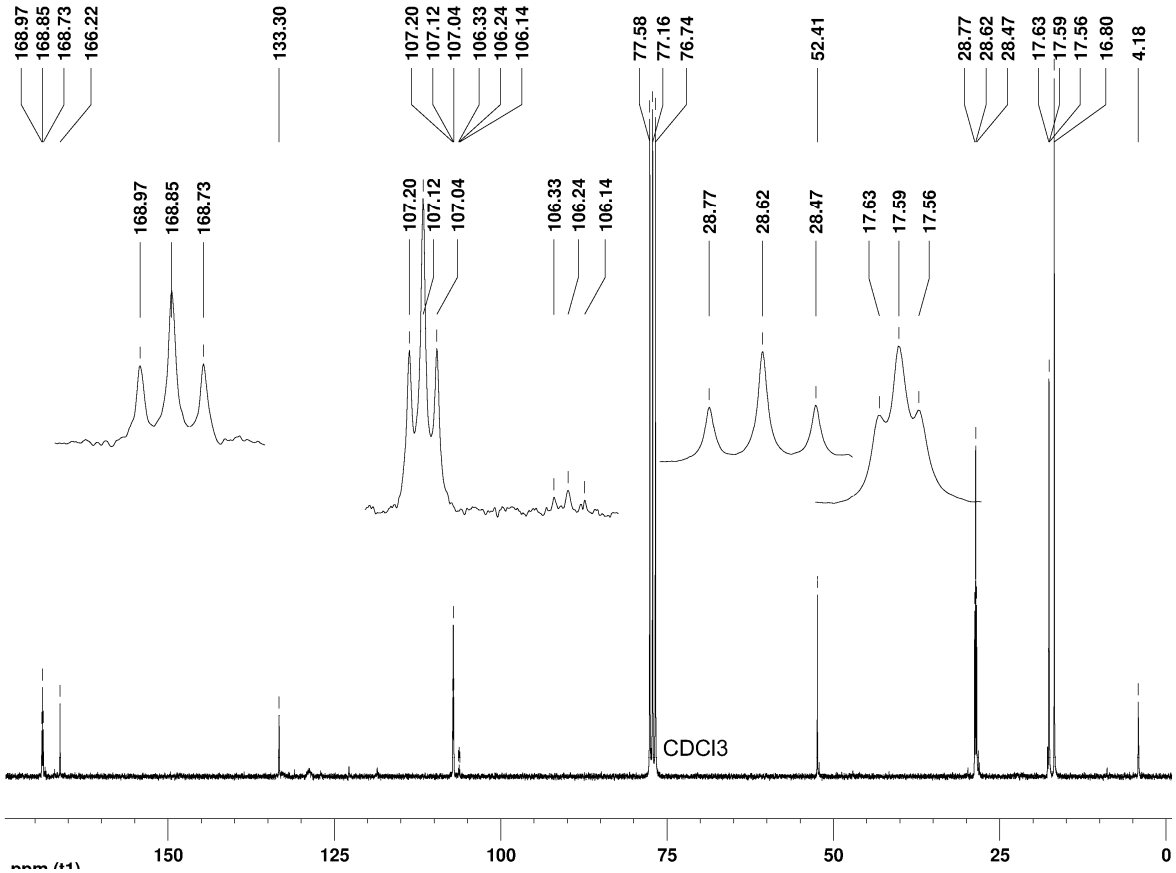

Figure A2.22 ^{13}C NMR (75 MHz) spectra of complex **4** in $CDCl_3$

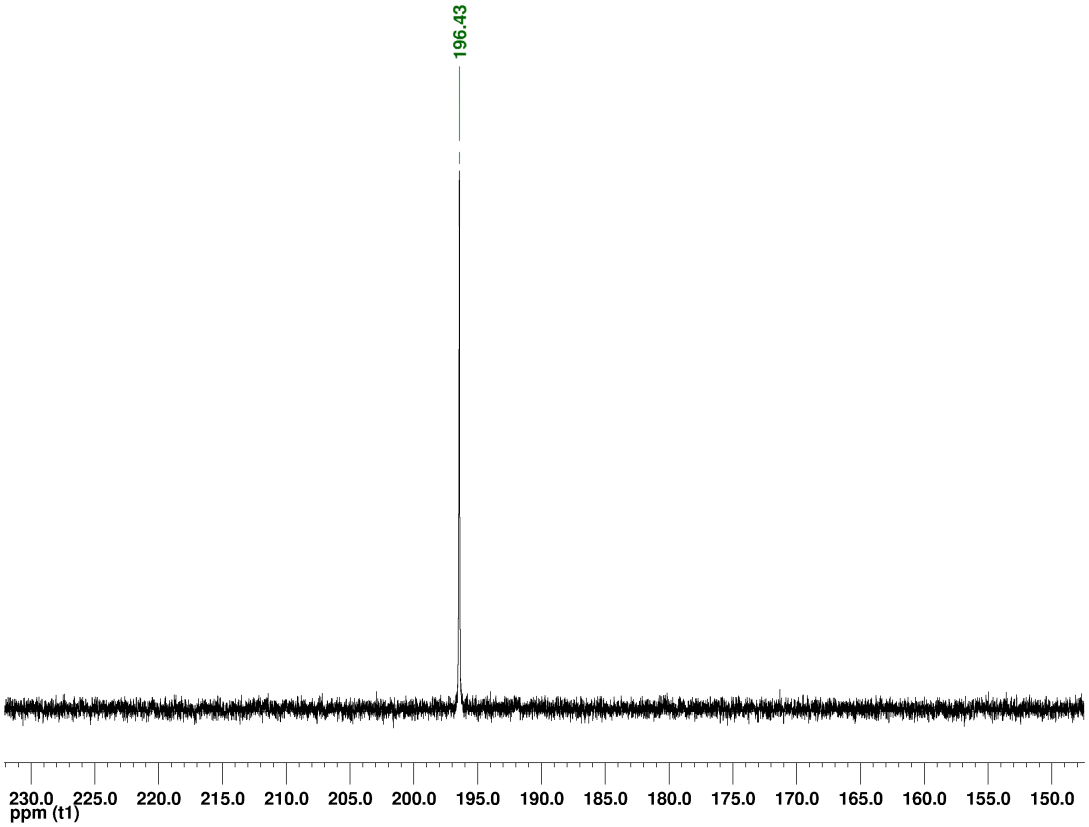

Figure A2.23 ^{31}P NMR (161 MHz) spectra of complex **4** in $CDCl_3$

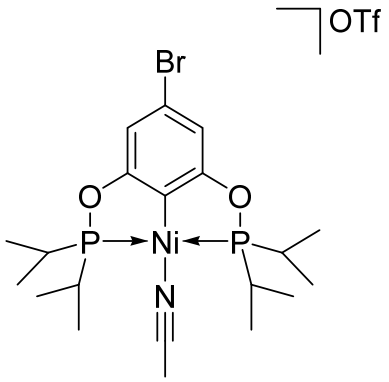

Figure A2.24 Representation of complex [{2,6-(*i*-$Pr_2PO)_2$-4-(Br)C_6H_2}Ni(NCMe)][OSO_2CF_3] (**5**)

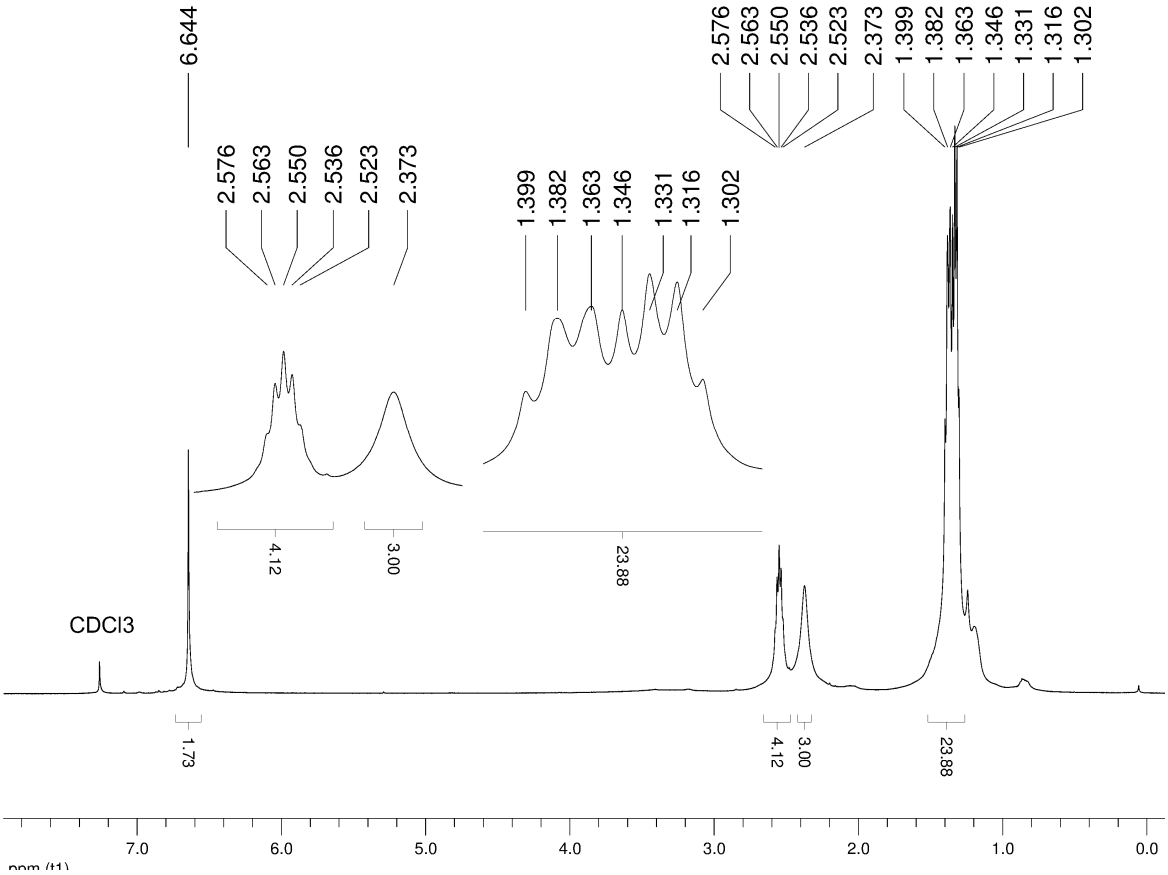

Figure A2.25 ^{1}H NMR (500 MHz) spectra of complex **5** in $CDCl_3$

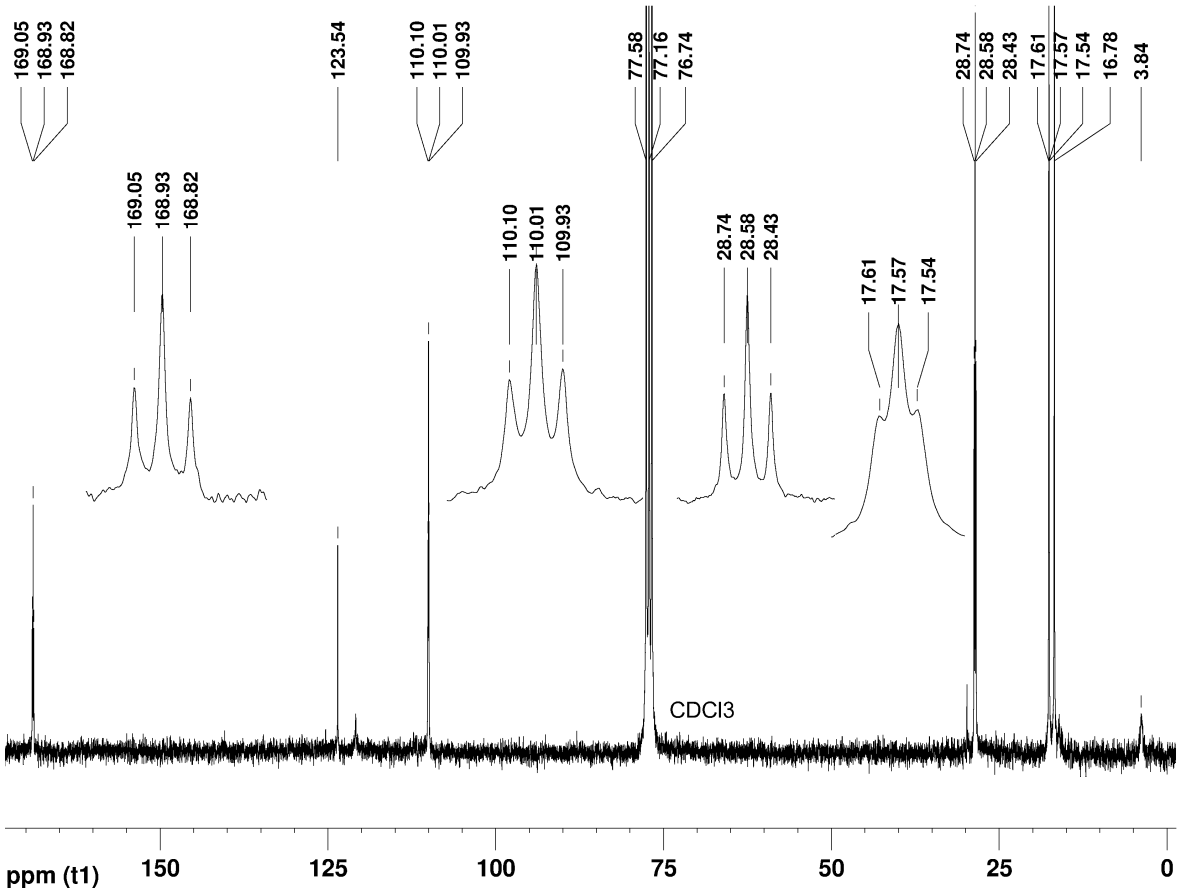

Figure A2.26 ^{13}C NMR (75 MHz) spectra of complex **5** in $CDCl_3$

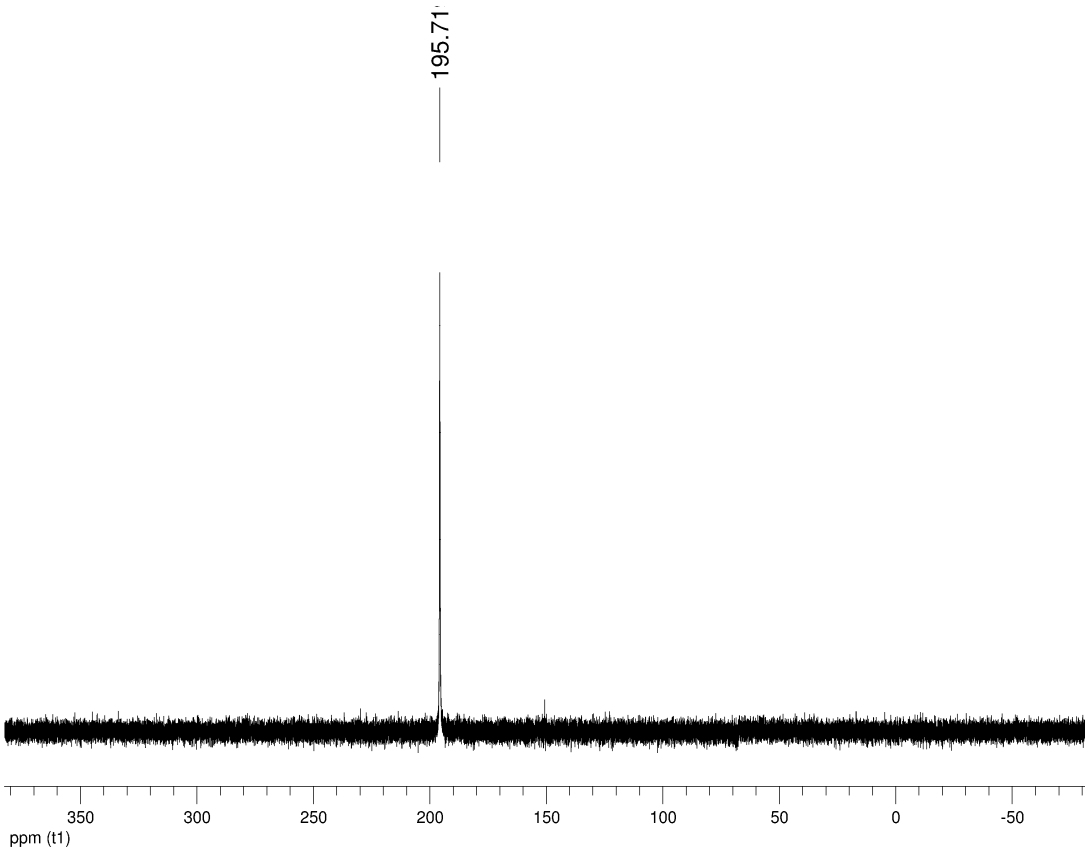

Figure A2.27 ^{31}P NMR (161 MHz) spectra of complex **5** in $CDCl_3$

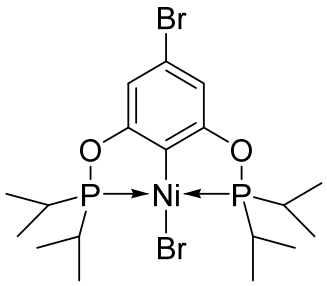

Figure A2.28 Representation of complex {2,6-(*i*-Pr$_2$PO)$_2$-4-(Br)C$_6$H$_2$}NiBr (**5'**)

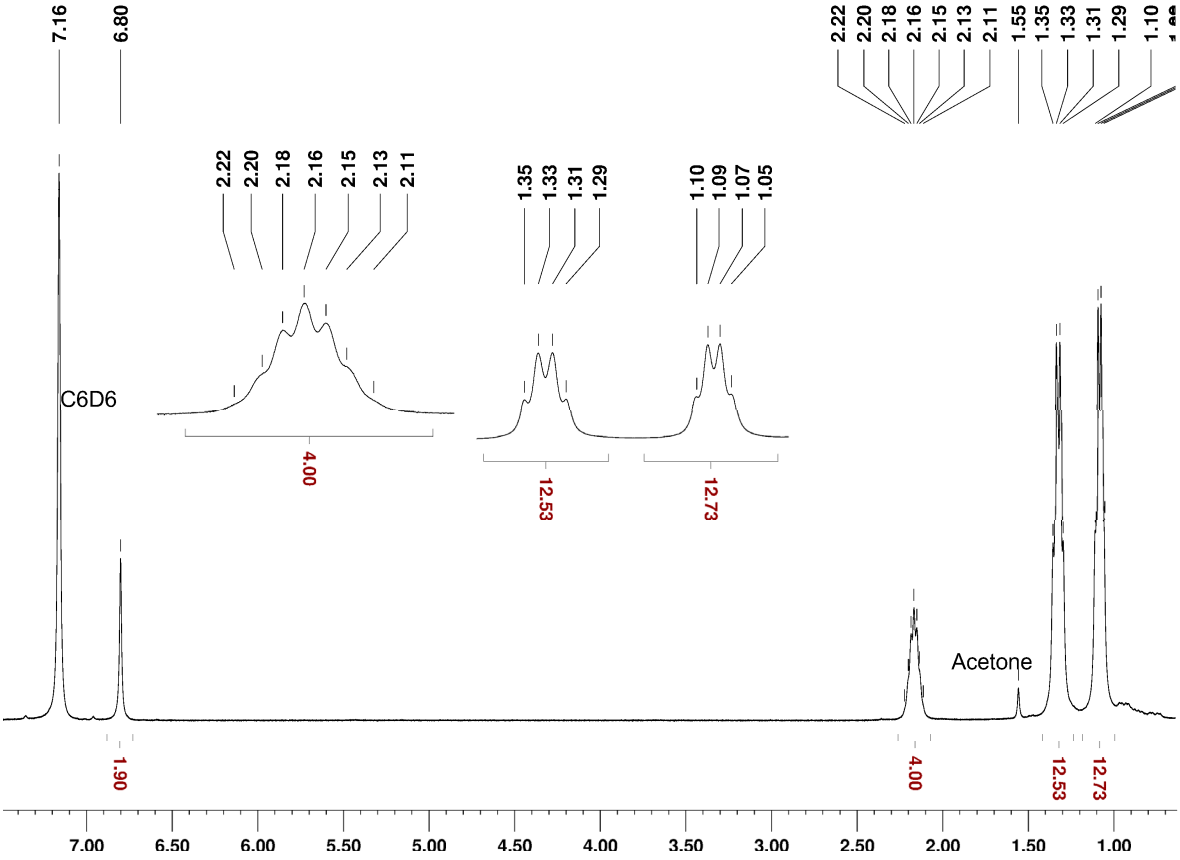

Figure A2.29 ^{1}H NMR (400 MHz) spectra of complex **5'** in C$_6$D$_6$

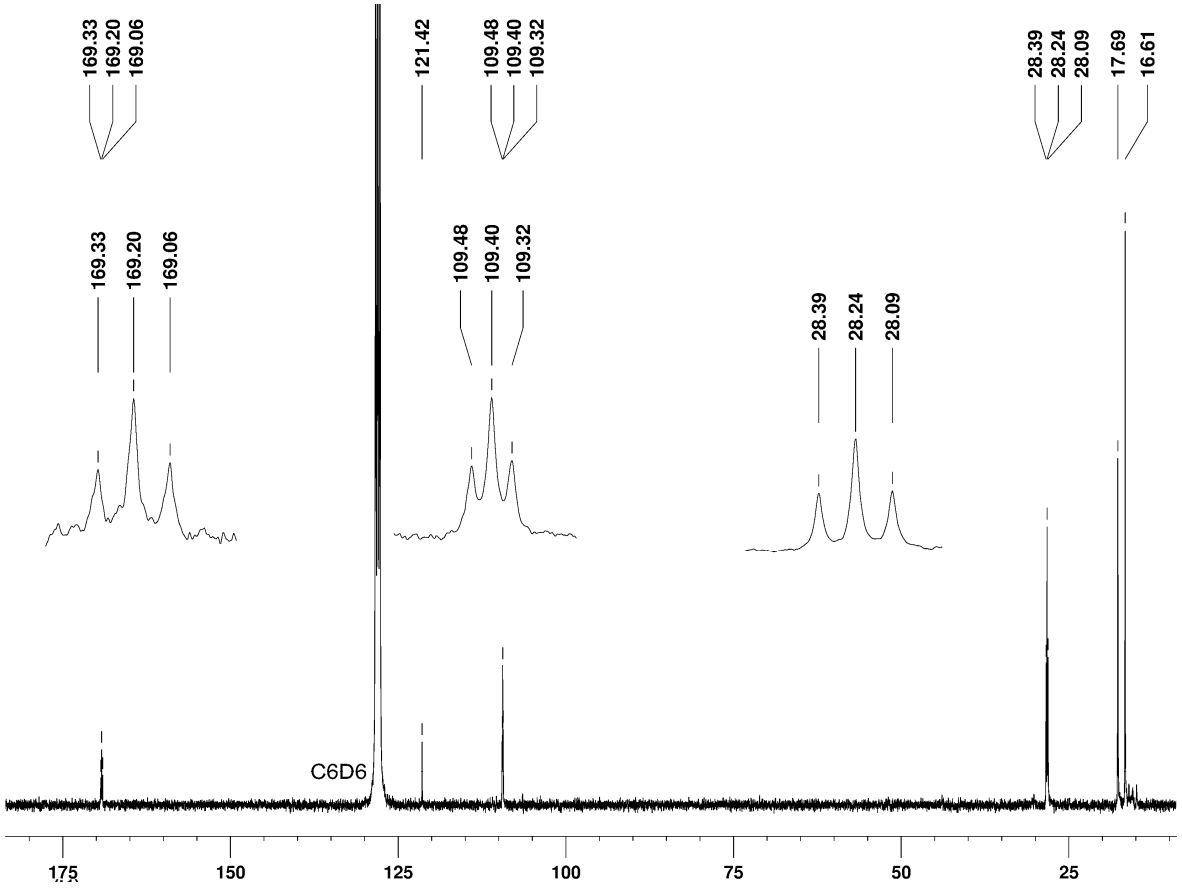

Figure A2.30 ^{13}C NMR (75 MHz) spectra of complex **5'** in C_6D_6

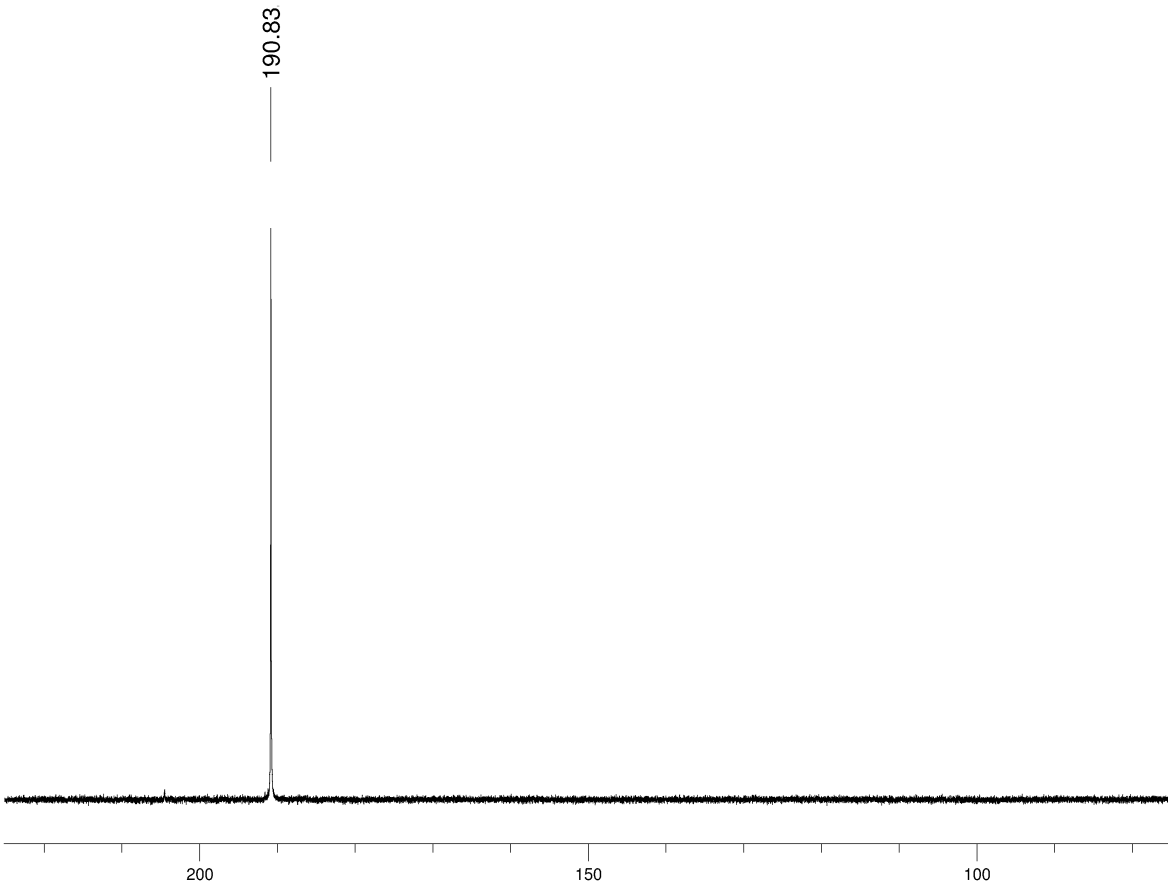

Figure A2.31 ^{31}P NMR (161 MHz) spectra of complex **5'** in C_6D_6

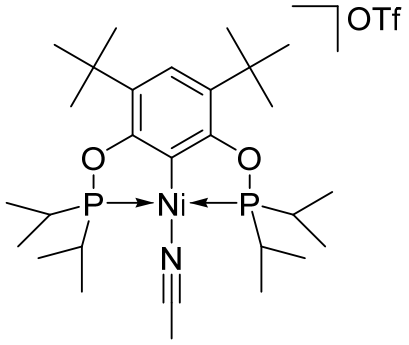

Figure A2.32 Representation of complex [{2,6-(*i*-Pr$_2$PO)$_2$-3,5-(*t*-Bu)$_2$C$_6$H}Ni(NCMe)][OSO$_2$CF$_3$] (**6**)

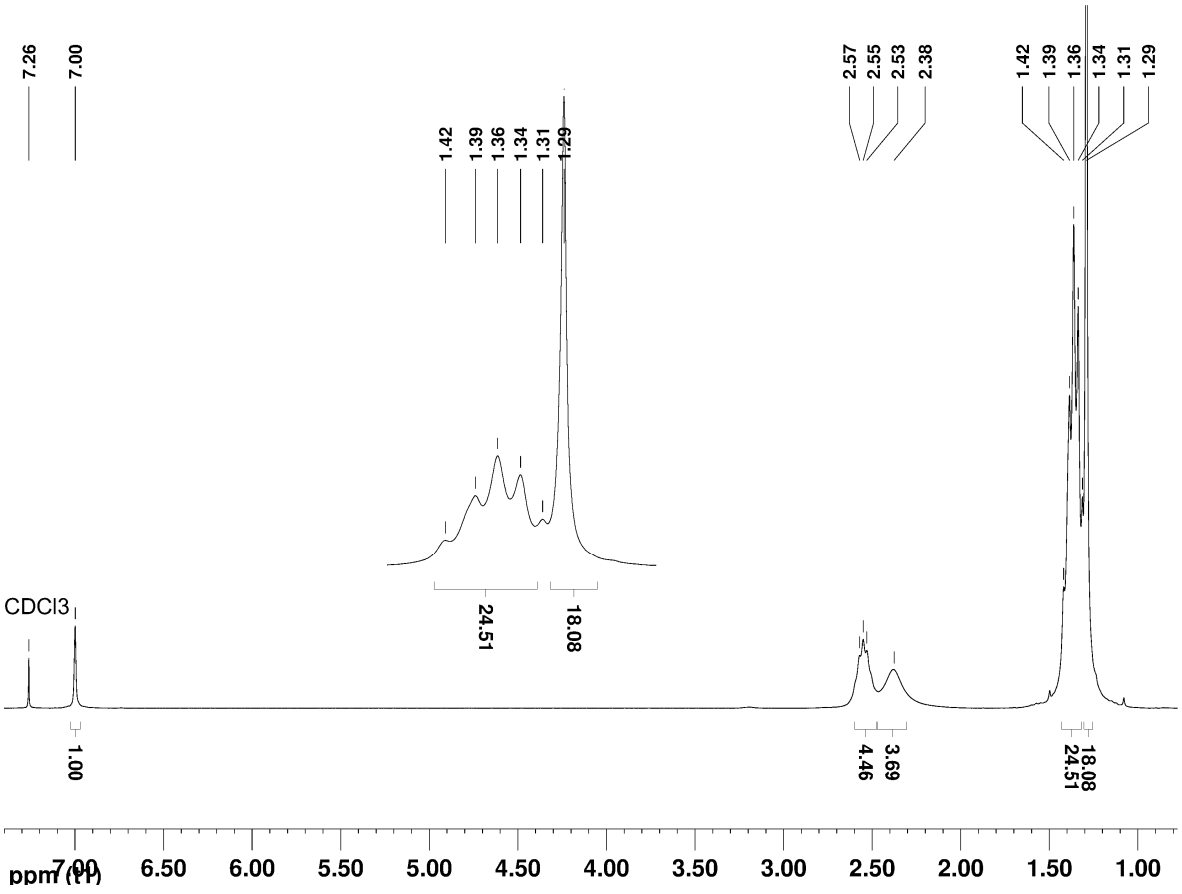

Figure A2.33 ^{1}H NMR (300 MHz) spectra of complex **6** in CDCl$_3$

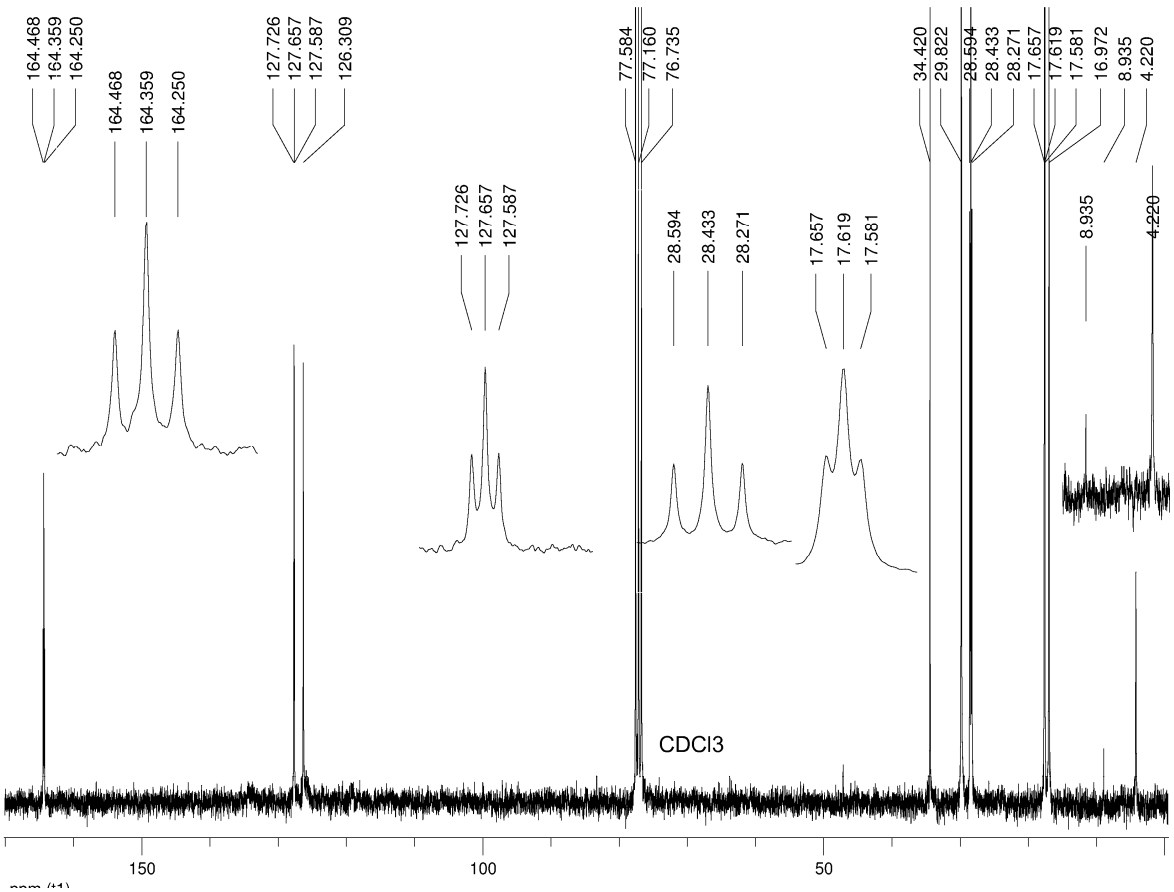

Figure A2.34 ^{13}C NMR (75 MHz) spectra of complex **6** in $CDCl_3$

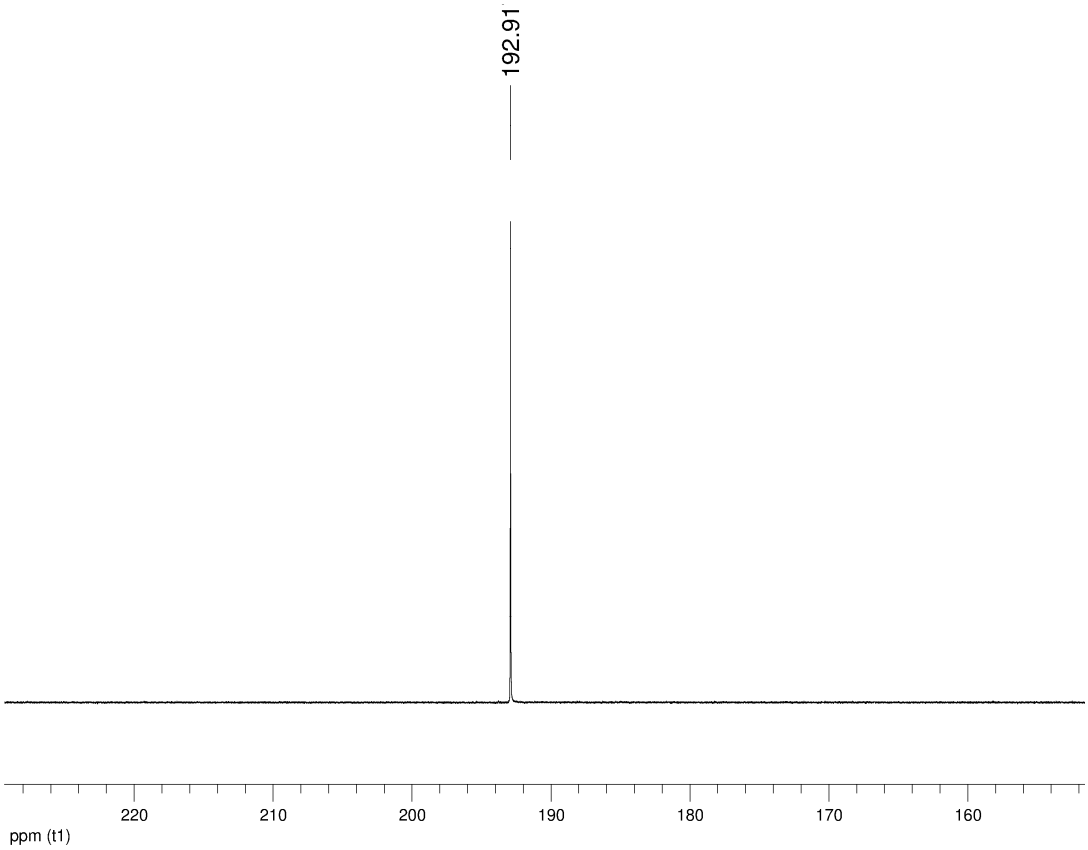

Figure A2.35 ^{31}P NMR (161 MHz) spectra of complex **6** in $CDCl_3$

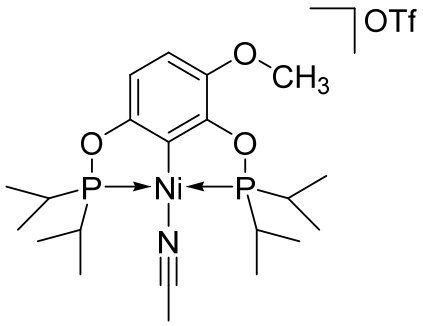

Figure A2.36 Representation of complex [{2,6-(*i*-Pr$_2$PO)$_2$-3-(OMe)C$_6$H$_2$}Ni(NCMe)][OSO$_2$CF$_3$] (**7**)

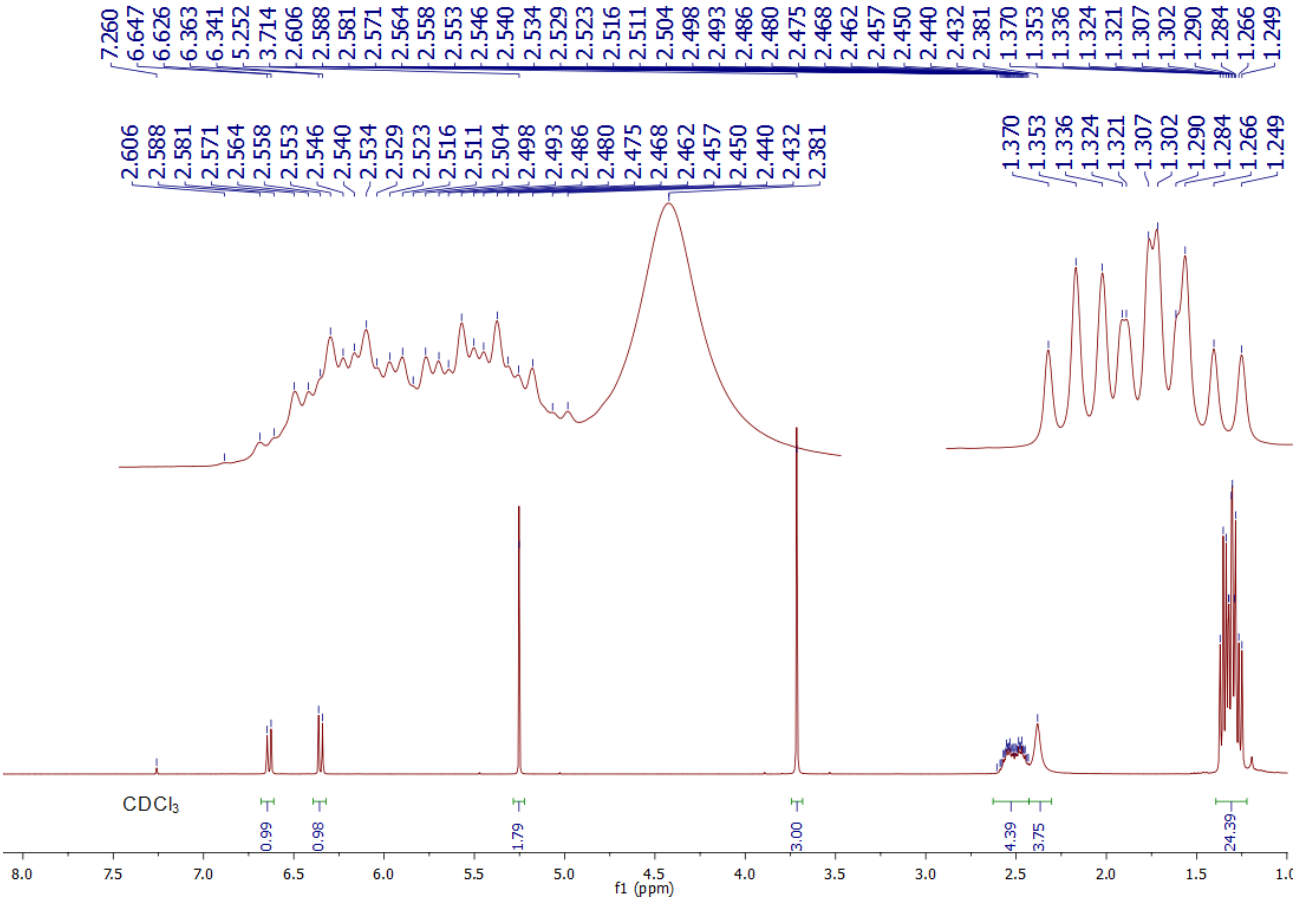

Figure A2.37 ^{1}H NMR (400 MHz) spectra of complex **7** in CDCl$_3$

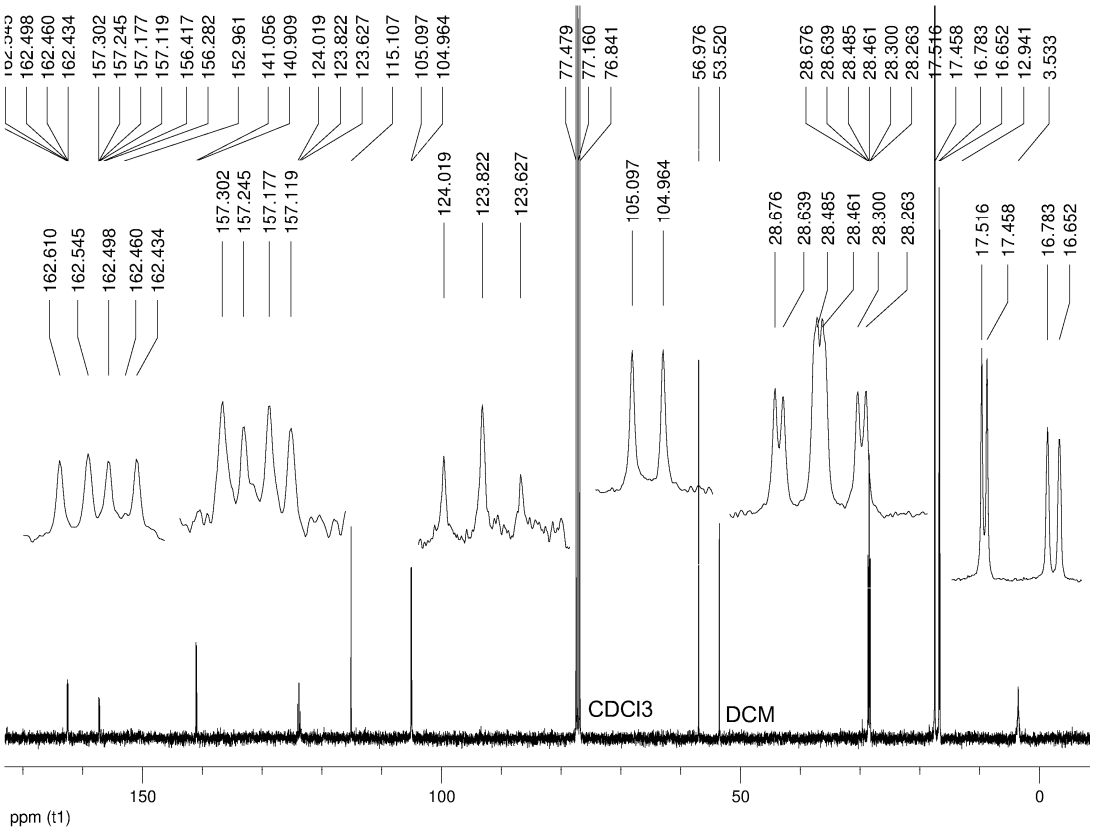

Figure A2.38 ^{13}C NMR (101 MHz) spectra of complex **7** in $CDCl_3$

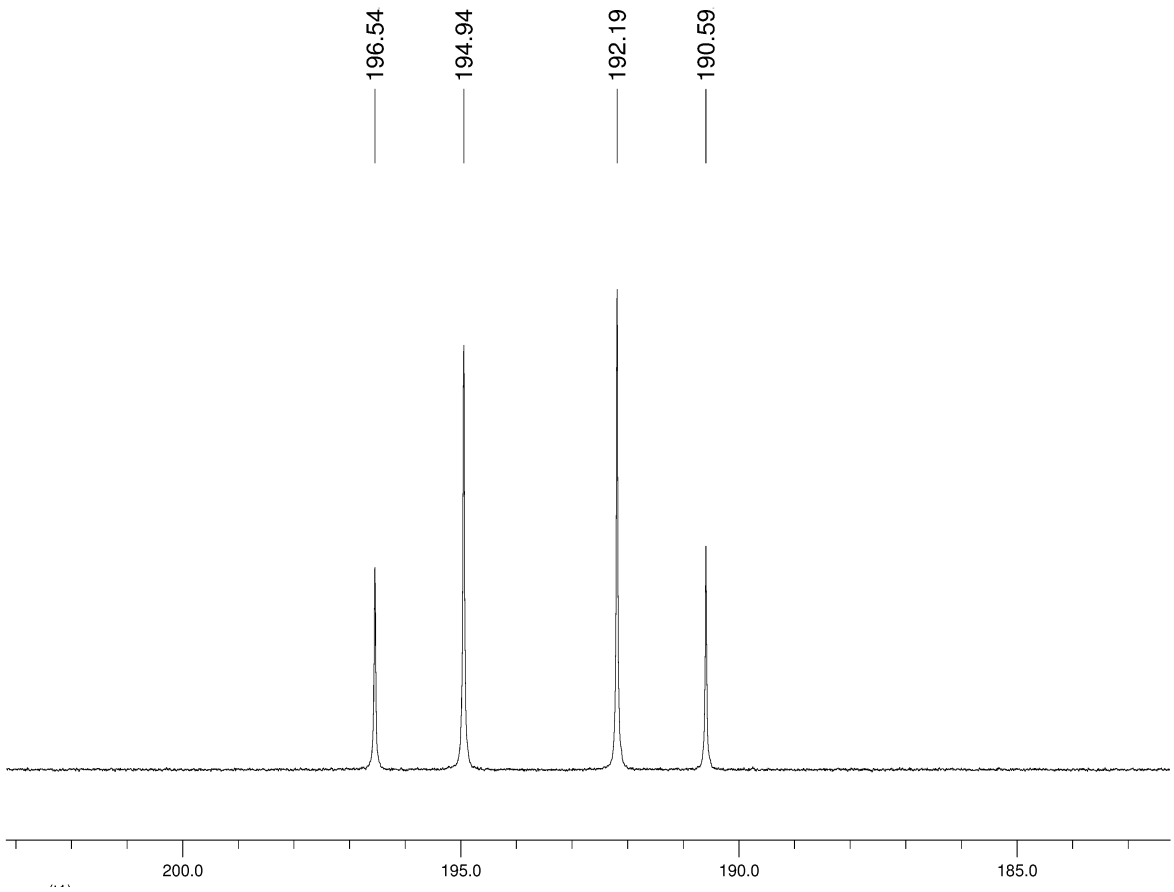

Figure A2.39 ^{31}P NMR (161 MHz) spectra of complex **7** in $CDCl_3$

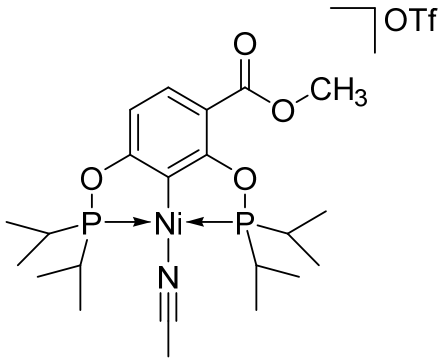

Figure A2.40 Representation of complex [{2,6-(*i*-$Pr_2PO)_2$-3-$(CO_2Me)C_6H_2$}Ni(NCMe)][OSO_2CF_3] (**8**)

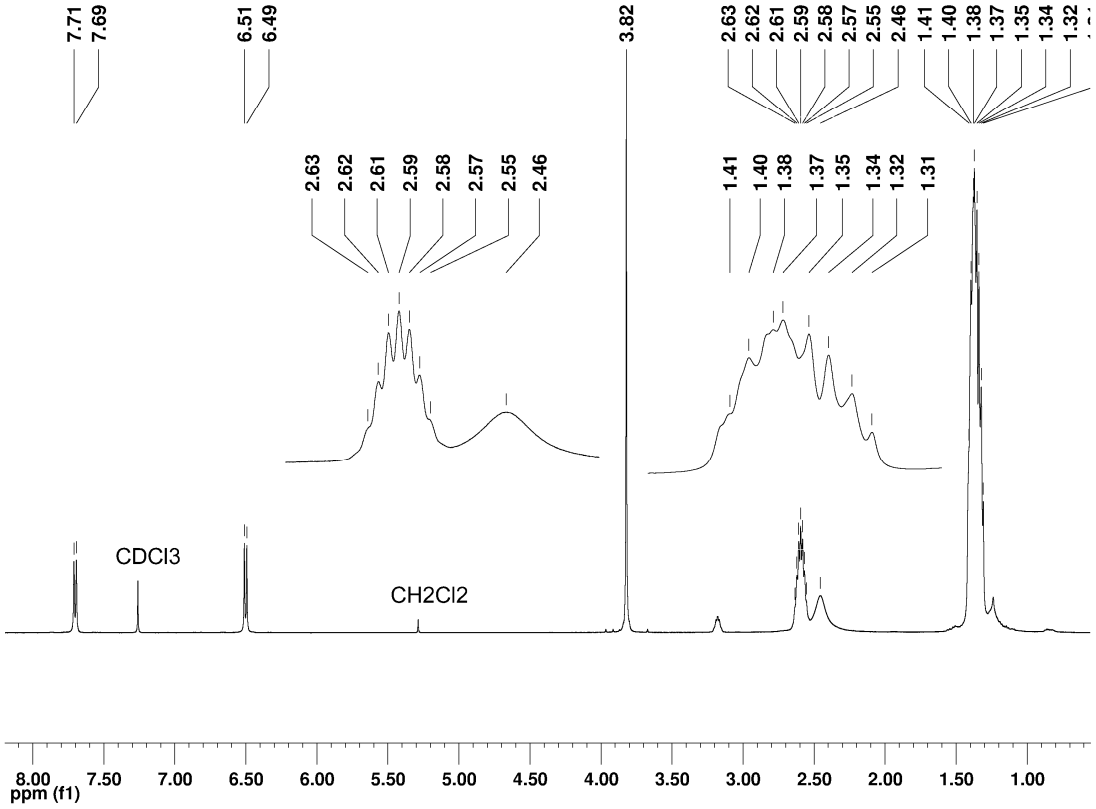

Figure A2.41 ^{1}H NMR (500 MHz) spectra of complex **8** in $CDCl_3$

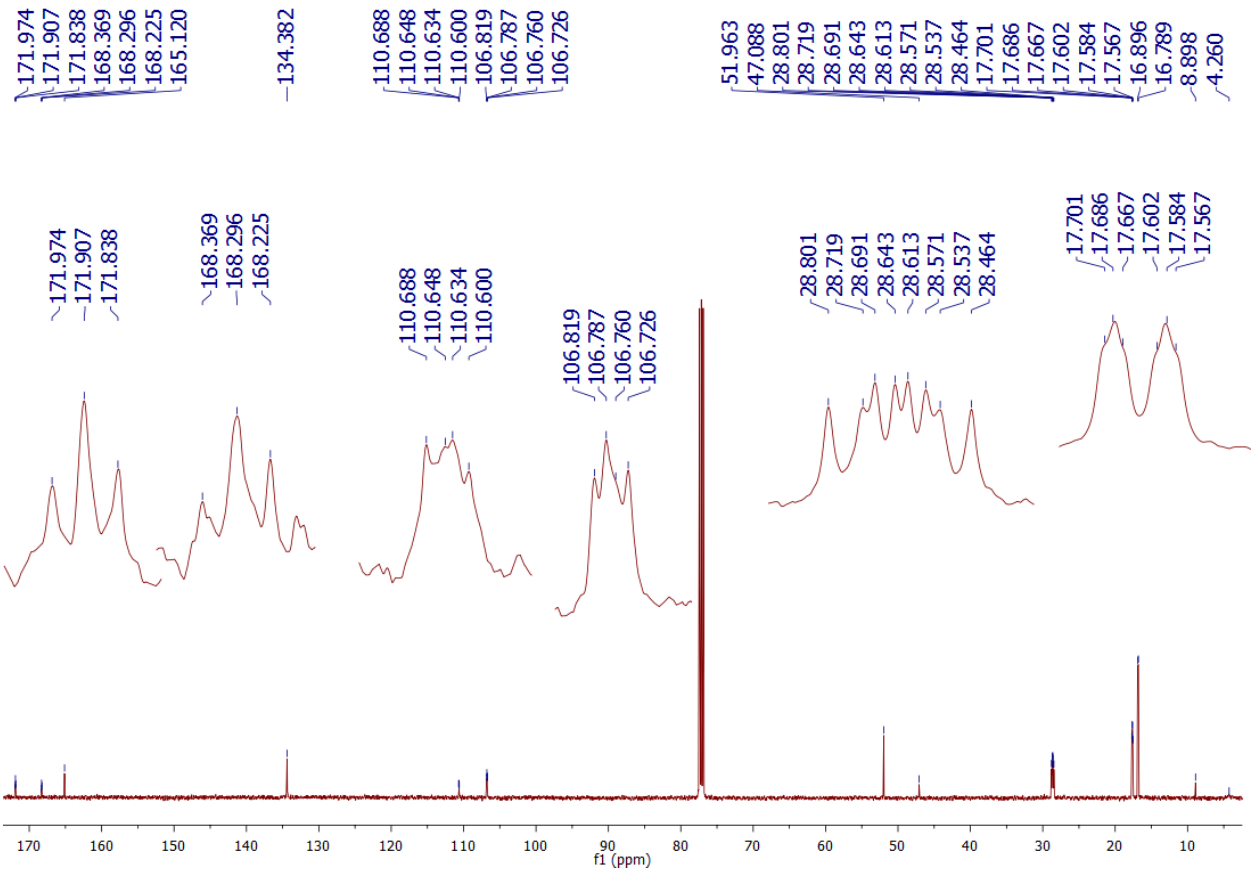

Figure A2.42 ^{13}C NMR (125 MHz) spectra of complex **8** in $CDCl_3$

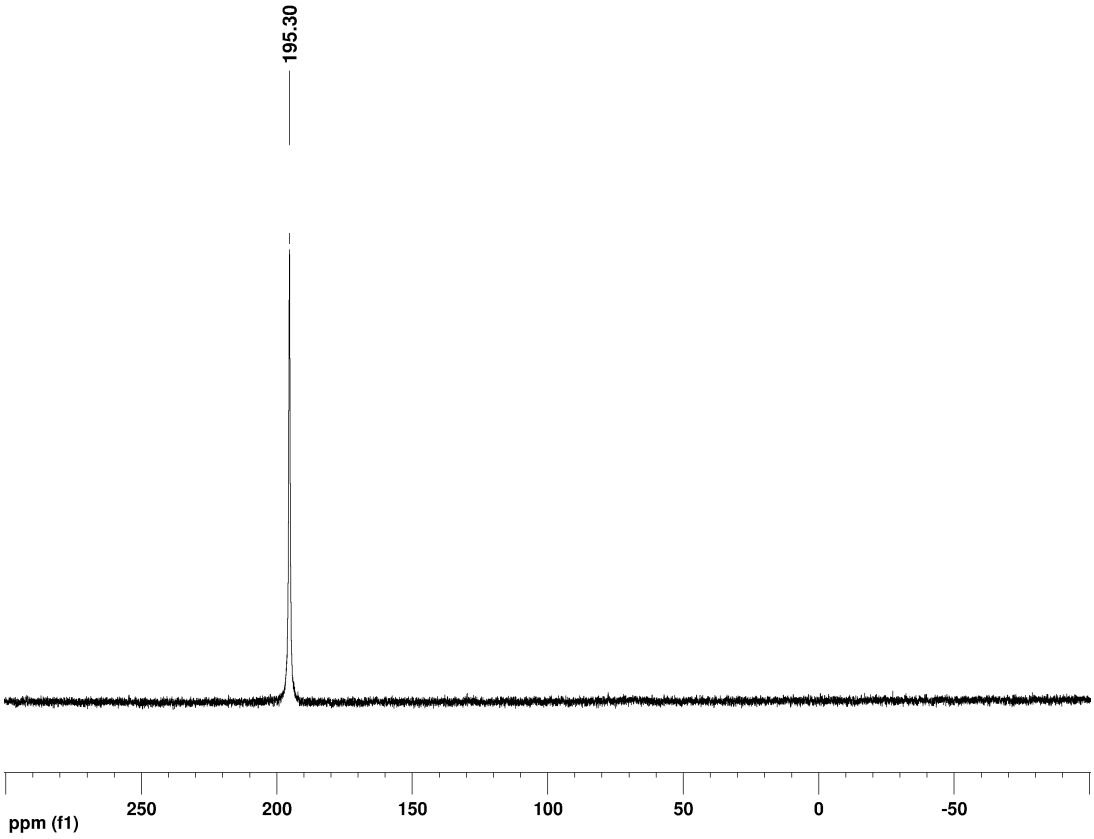

Figure A2.43 ^{31}P NMR (202 MHz) spectra of complex **8** in $CDCl_3$

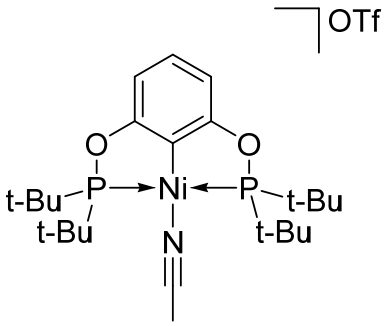

Figure A2.44 Representation of complex [{2,6-(*t*-Bu$_2$PO)$_2$C$_6$H$_3$}Ni(NCMe)][OSO$_2$CF$_3$] (**9**)

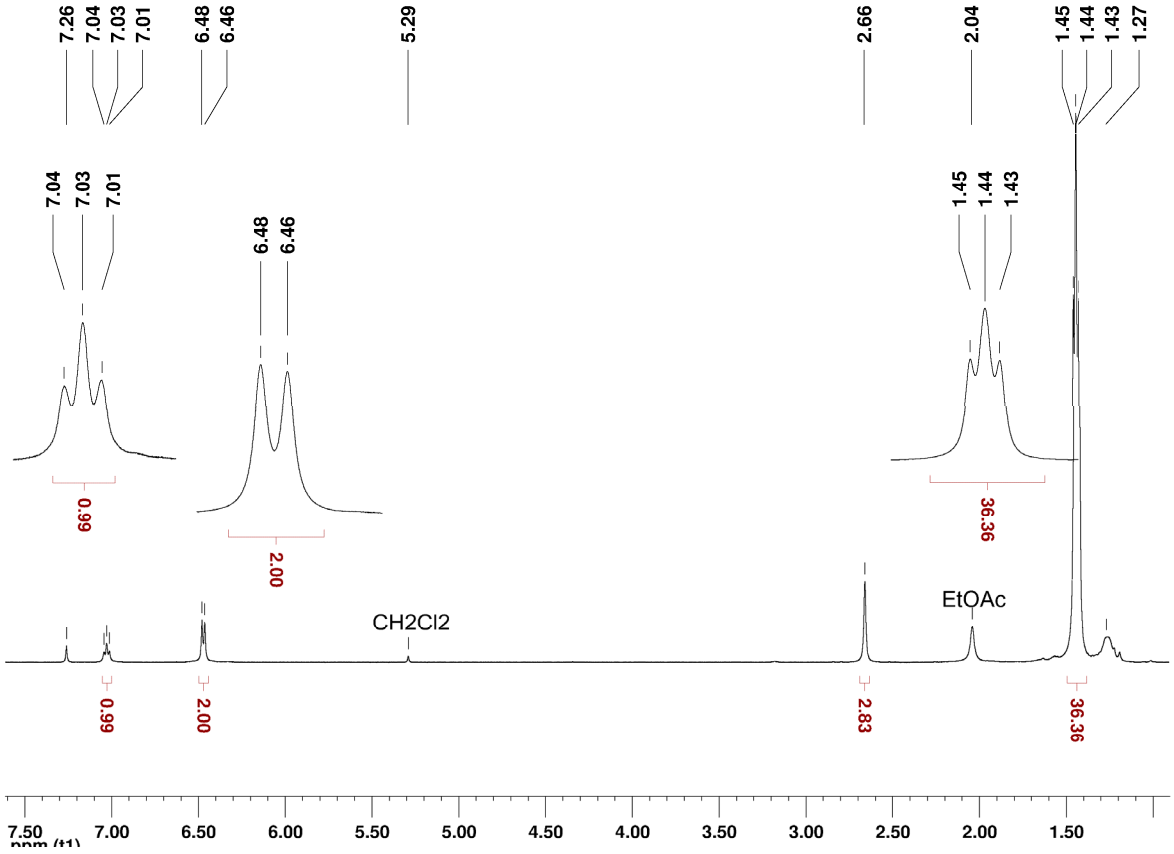

Figure A2.45 ^{1}H NMR (500 MHz) spectra of complex **9** in CDCl$_3$

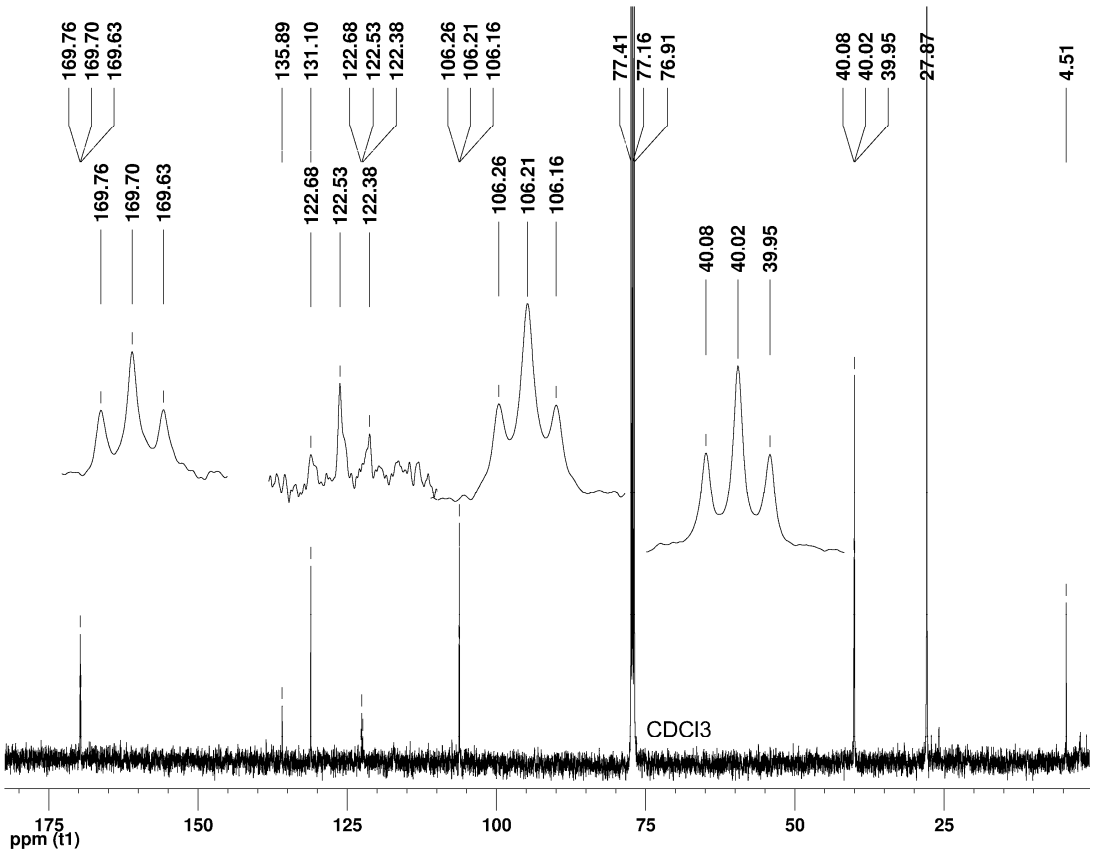

Figure A2.46 ^{13}C NMR (125 MHz) spectra of complex **9** in $CDCl_3$

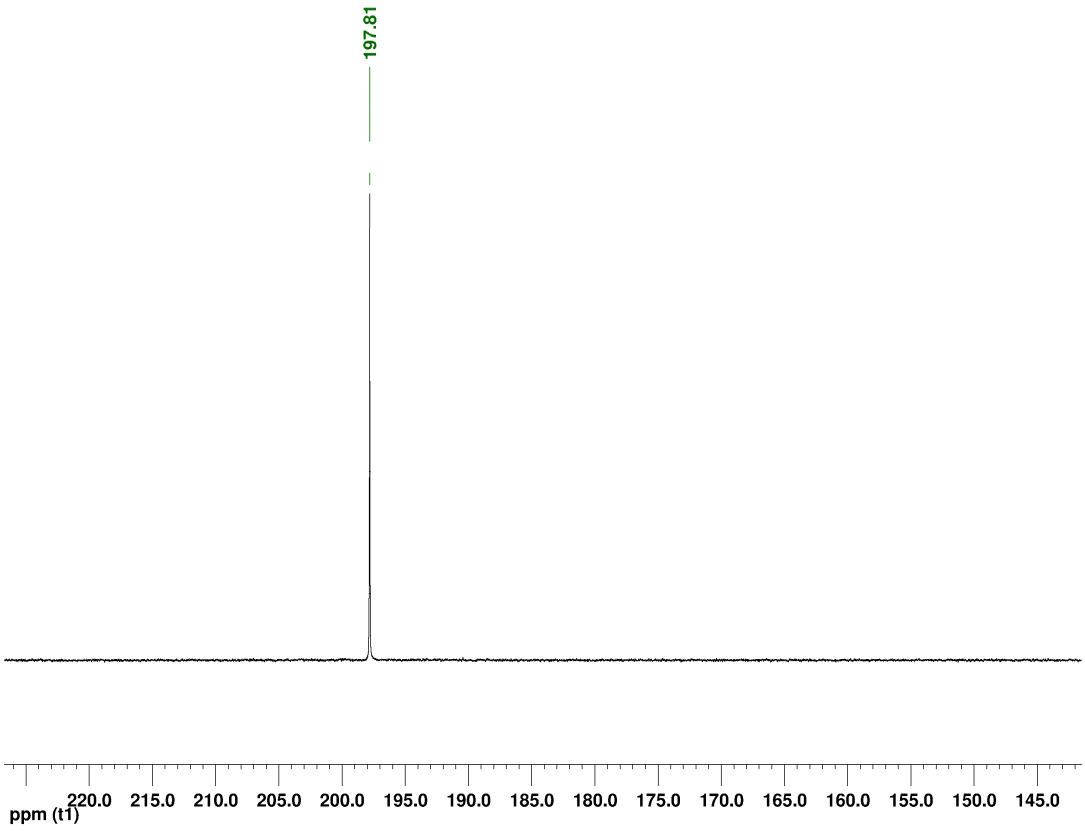

Figure A2.47 ^{31}P NMR (121 MHz) spectra of complex **9** in $CDCl_3$

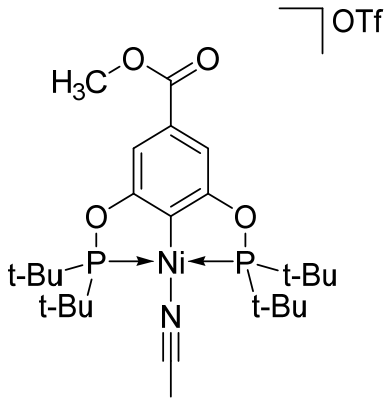

Fig. A2.48 Representation of complex [{2,6-(*t*-Bu$_2$PO)$_2$-4-(CO$_2$Me)C$_6$H$_2$}Ni(NCMe)][OSO$_2$CF-$_3$] (**10**)

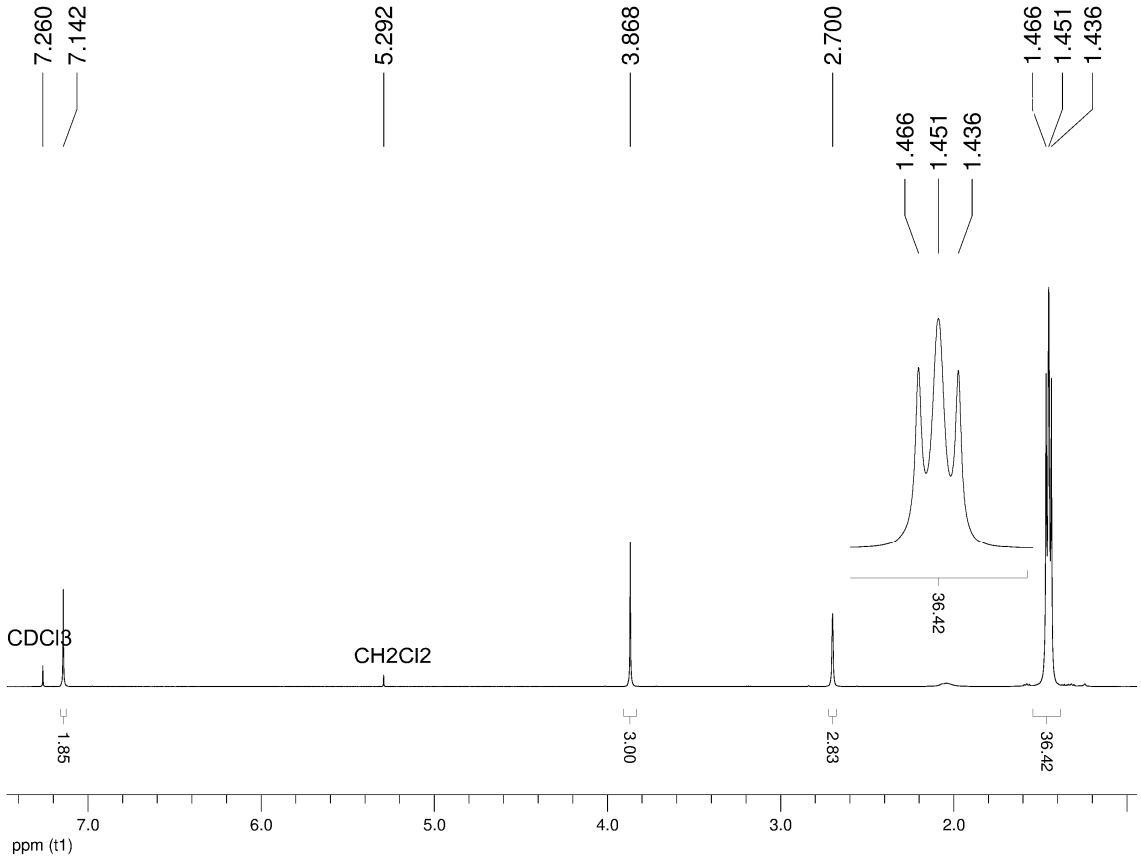

Figure A2.49 ^{1}H NMR (500 MHz) spectra of complex **10** in CDCl$_3$

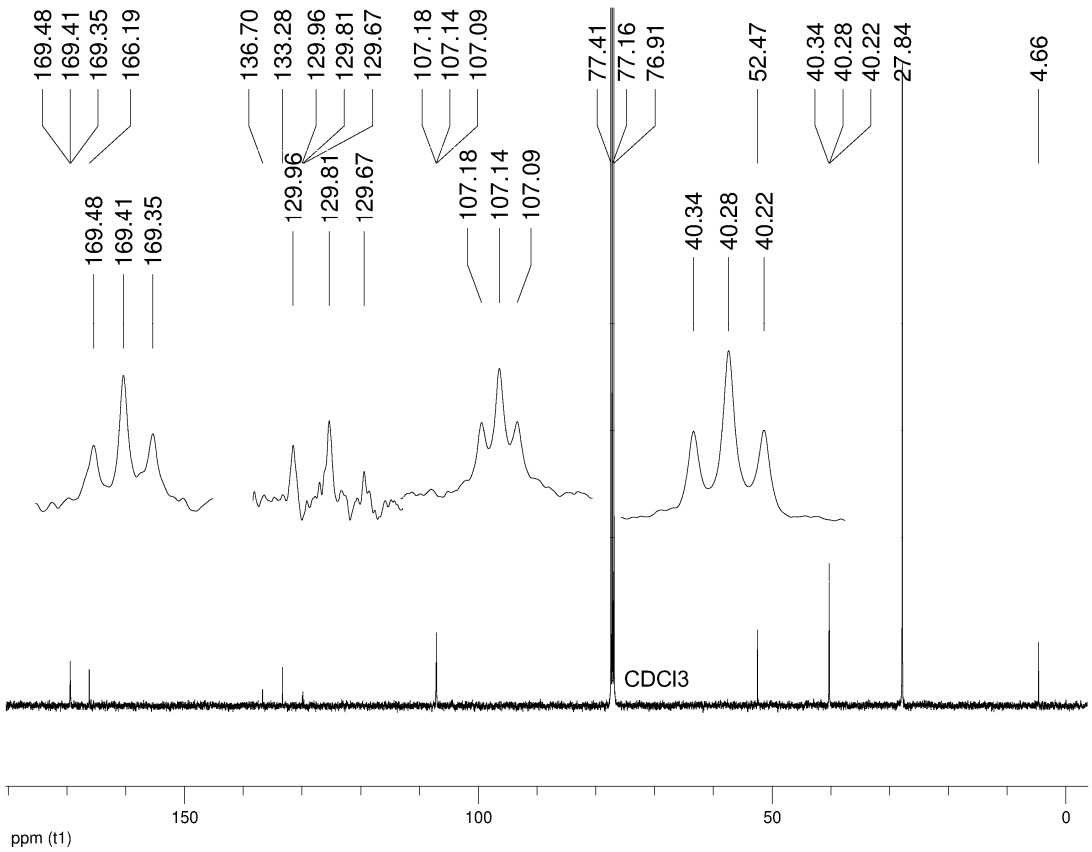

Figure A2.50 ^{13}C NMR (125 MHz) spectra of complex **10** in $CDCl_3$

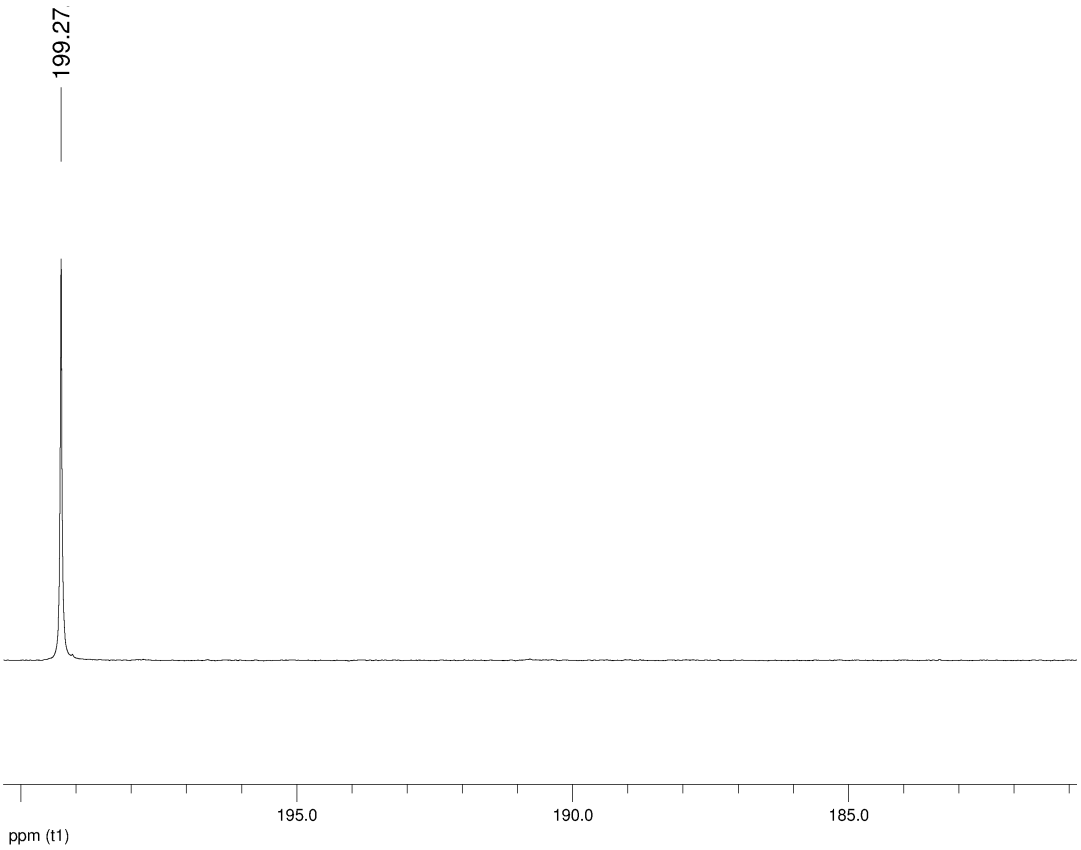

Figure A2.51 ^{31}P NMR (202 MHz) spectra of complex **10** in $CDCl_3$

UV-Vis analysis

Table A2.6 UV-Vis data for complexes **1-10** and **1'-10'**

Complex	λ_{max} / nm (ε / M^{-1} cm^{-1})		
1[a]	379 (1375)	325 (8520)	302 (3560)
2	382 (938)	327 (4425)	300 (2302)
3	382 (912)	329 (4214)	299 (1858)
4	390 (1677)	341 (5111)	329 (4791)
5	386 (1221)	328 (6245)	303 (3547)
6	386 (912)	327 (2691)	299 (2432)
7	384 (1881)	323 (11373)	279 (17577)
8	346 (2461)	327 (12630)	249 (30114)
9	401 (305)	338 (sh, 2378) 321(9449)	258 (15464)
10	400 (718)	335 (18544)	257 (19757)
1'[a]	391 (1643)	338 (8772)	304 (2735)
2'[a]	390 (1653)	338 (9817)	304 (2735)
3'[a]	389 (1995)	337 (11473)	321(sh, 5430)
4'[a]	390 (4754)	360 (12693)	325(sh, 4629)
5'	391 (2070)	341 (13600)	306 (2900)
6'[a]	388 (837)	338 (4240)	307 (2030)
7'[a]	389 (158)	337 (900)	
8'[a]	397 (157)	341 (817)	
9'[a]	407 (198)	334 (916)	
10'[a]	413 (228)	360 (1040)	

a) Previously reported complexes.[24b,11b] CH_2Cl_2 solutions (10^{-4} M) were used for the analysis.

Cyclic Voltammetry analysis

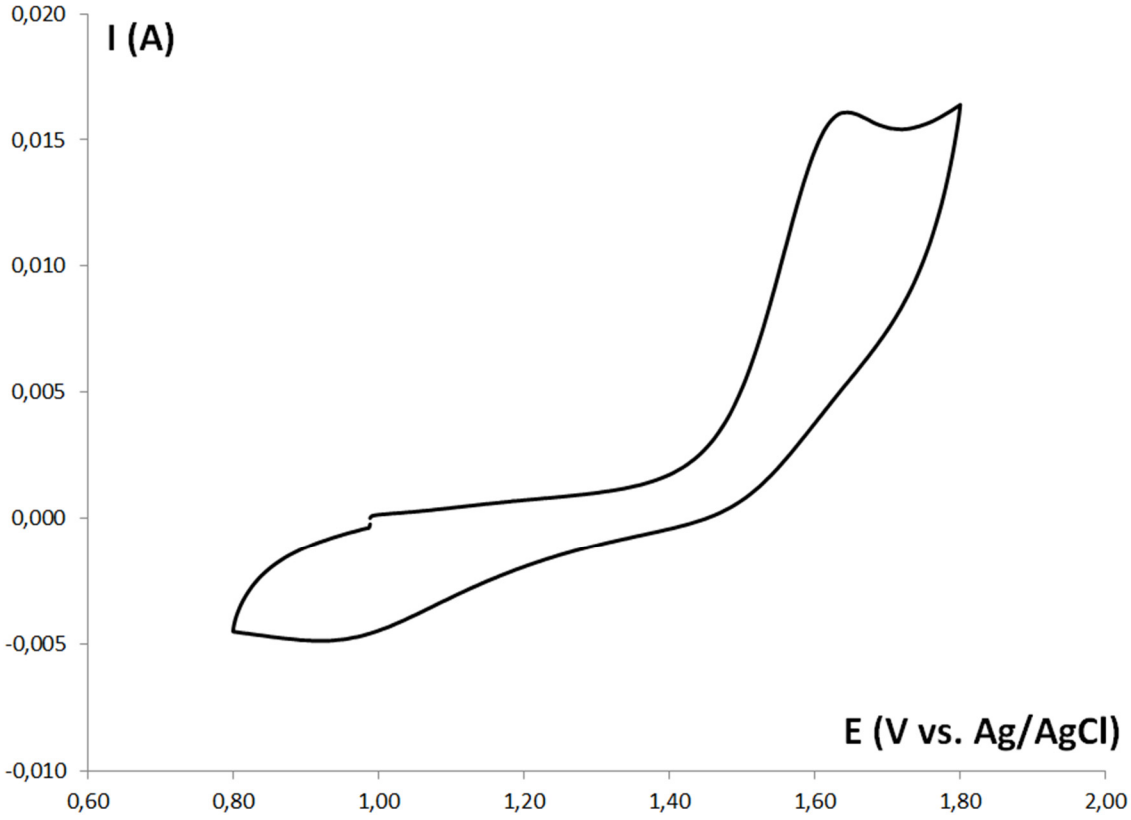

Figure A2.52 Cyclic Voltammogram of complex **2.**

See caption of **Figure 2.5** for measurement details

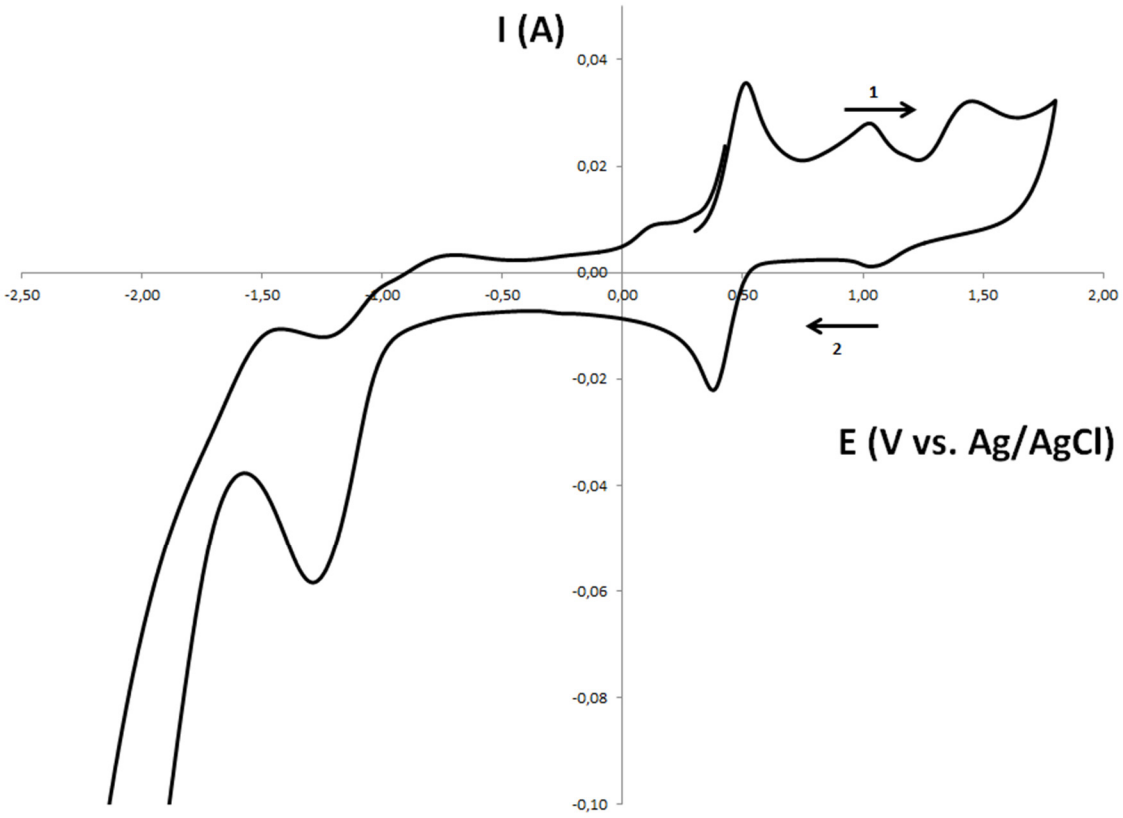

FigureA2.53 Cyclic Voltammogram of complex **2** with addition of 1 equiv. of $FeCp_2$**.**

See caption of **Figure 2.5** for measurement details

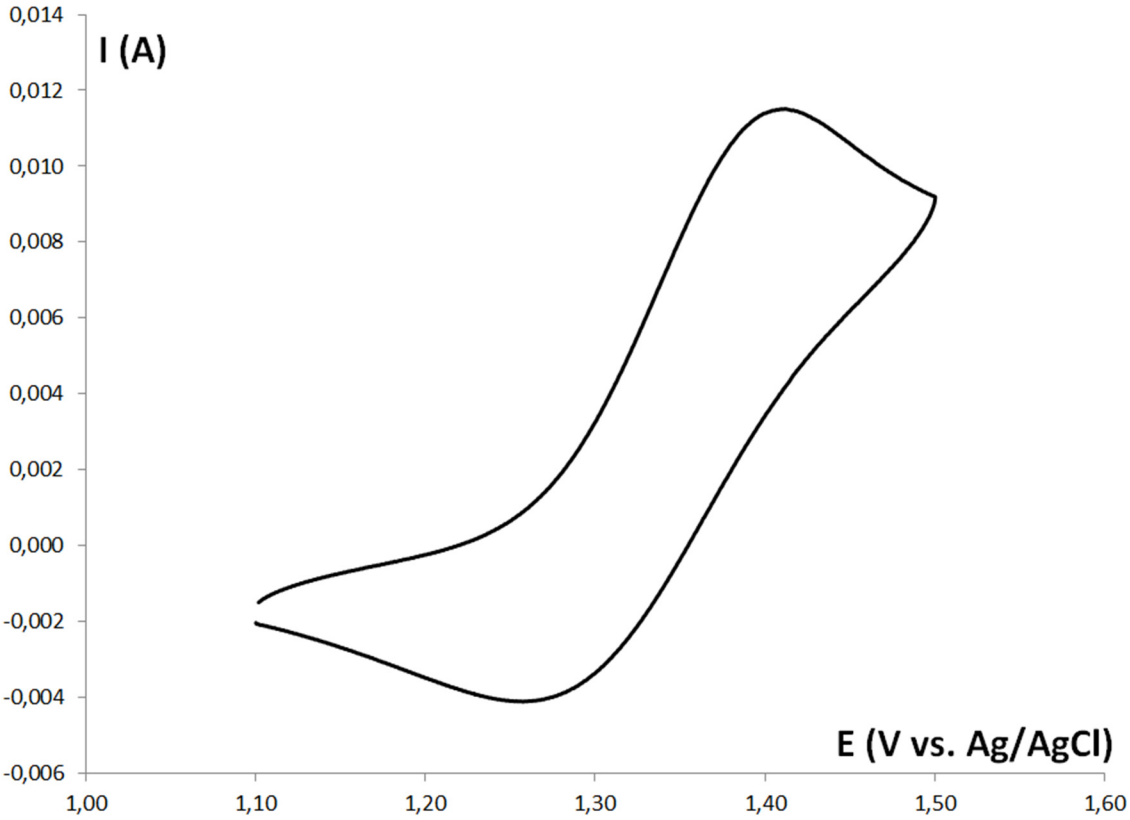

Figure A2.54 Cyclic Voltammogram of complex **3.**

See caption of **Figure 2.5** for measurement details

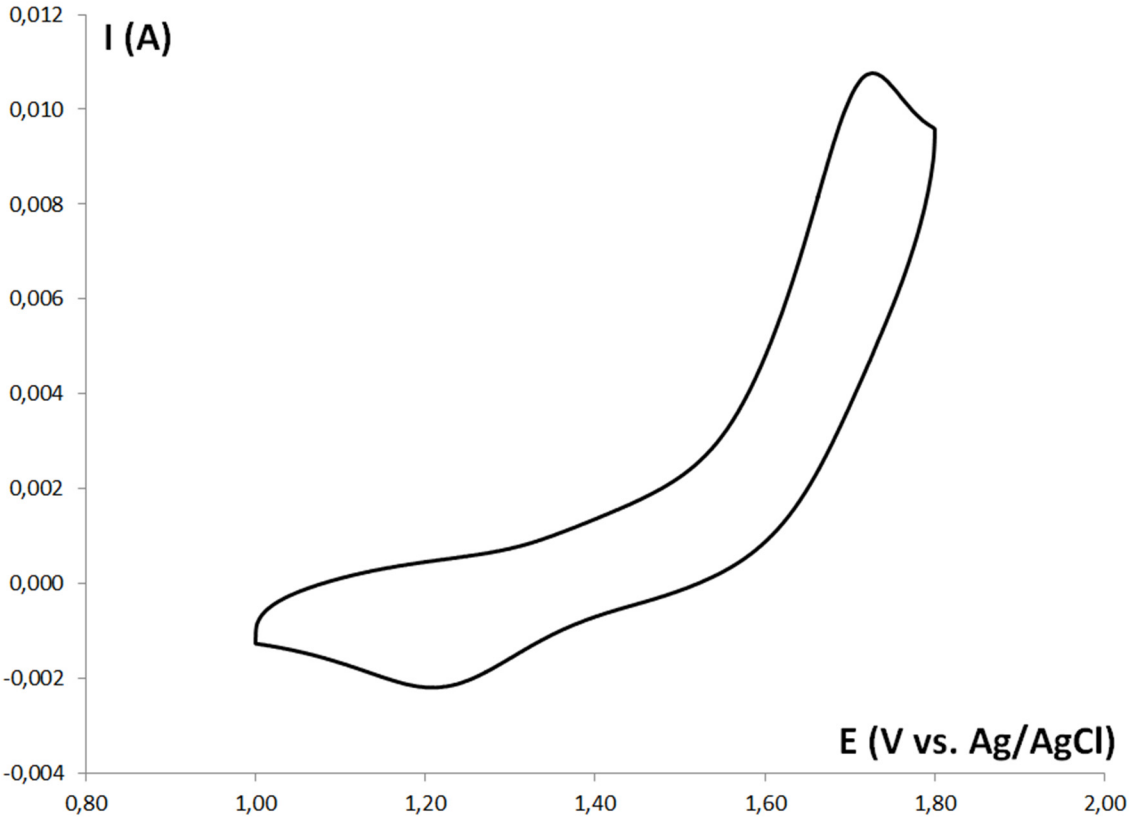

Figure A2.55 Cyclic Voltammogram of complex **4.**

See caption of **Figure 2.5** for measurement details

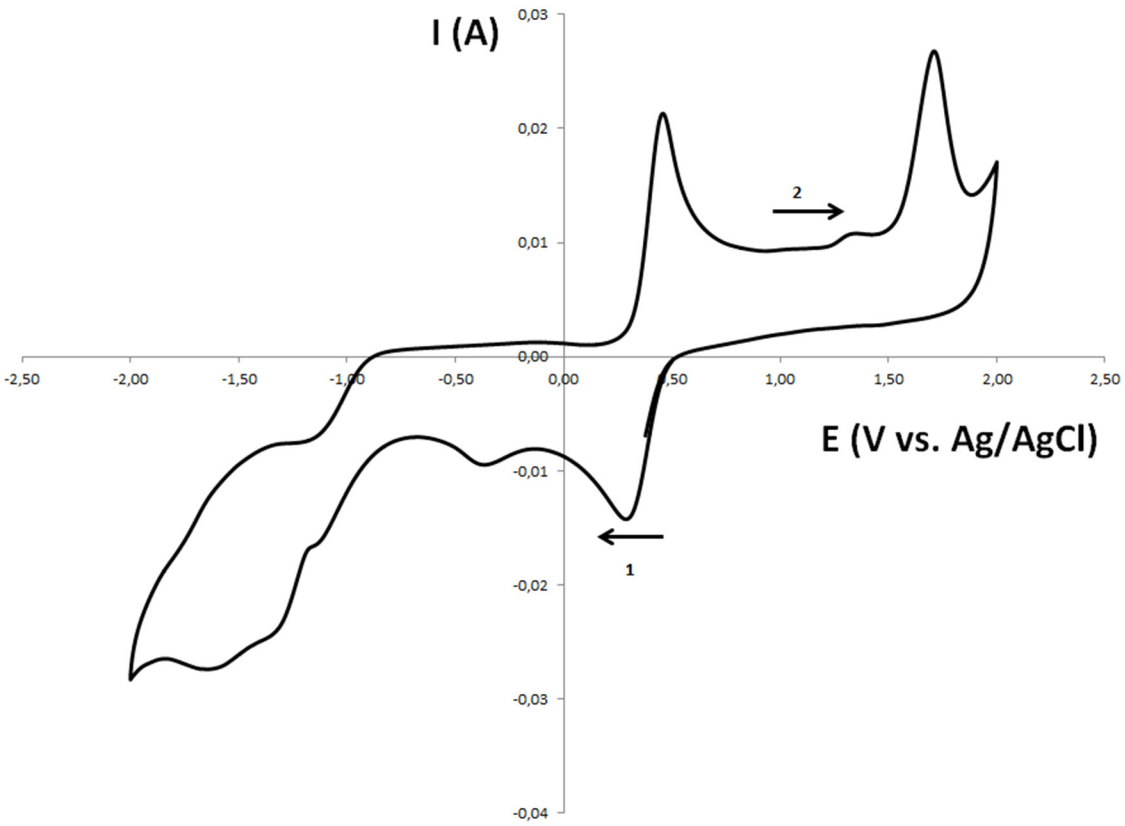

Figure A2.56 Cyclic Voltammogram of complex **4** with addition of 1 equiv. of $FeCp_2$.

See caption of **Figure 2.5** for measurement details

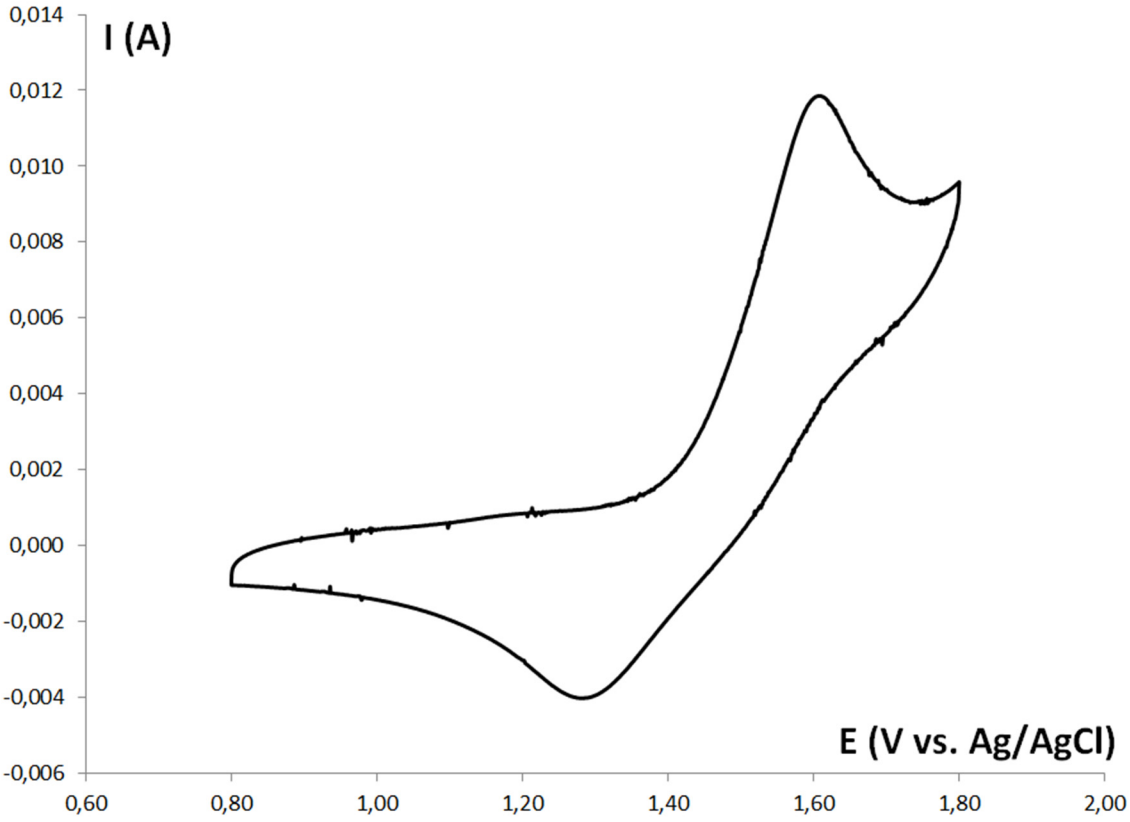

Figure A2.57 Cyclic Voltammogram of complex **5.**

See caption of **Figure 2.5** for measurement details

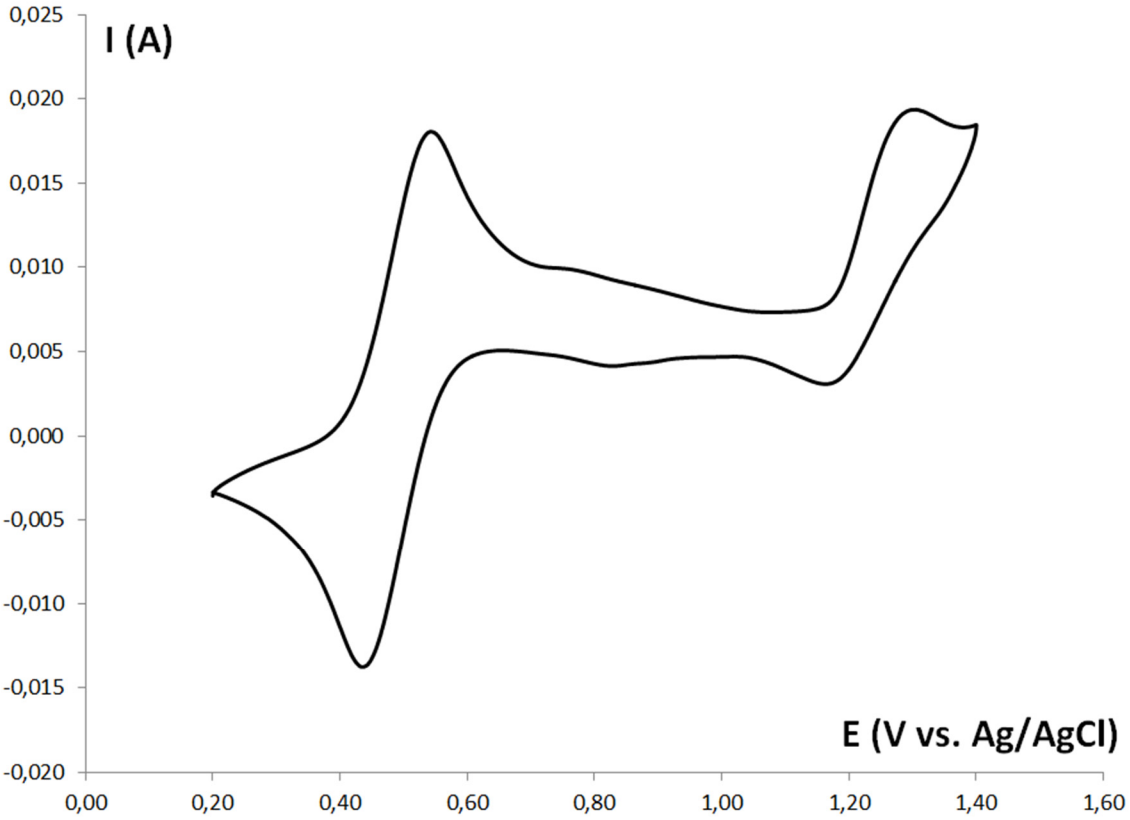

Figure A2.58 Cyclic Voltammogram of complex **5'** with added $FeCp_2$.

See caption of **Figure 2.5** for measurement details

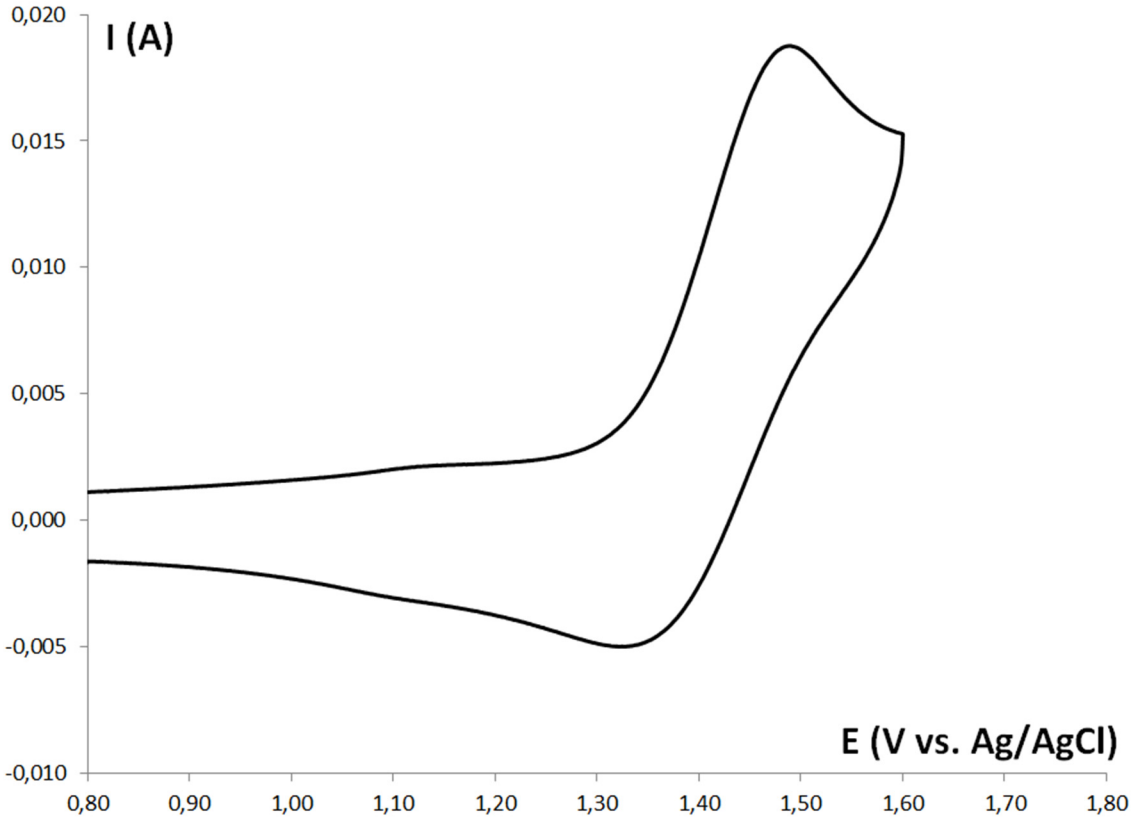

Figure A2.59 Cyclic Voltammogram of complex **6.**

See caption of **Figure 2.5** for measurement details

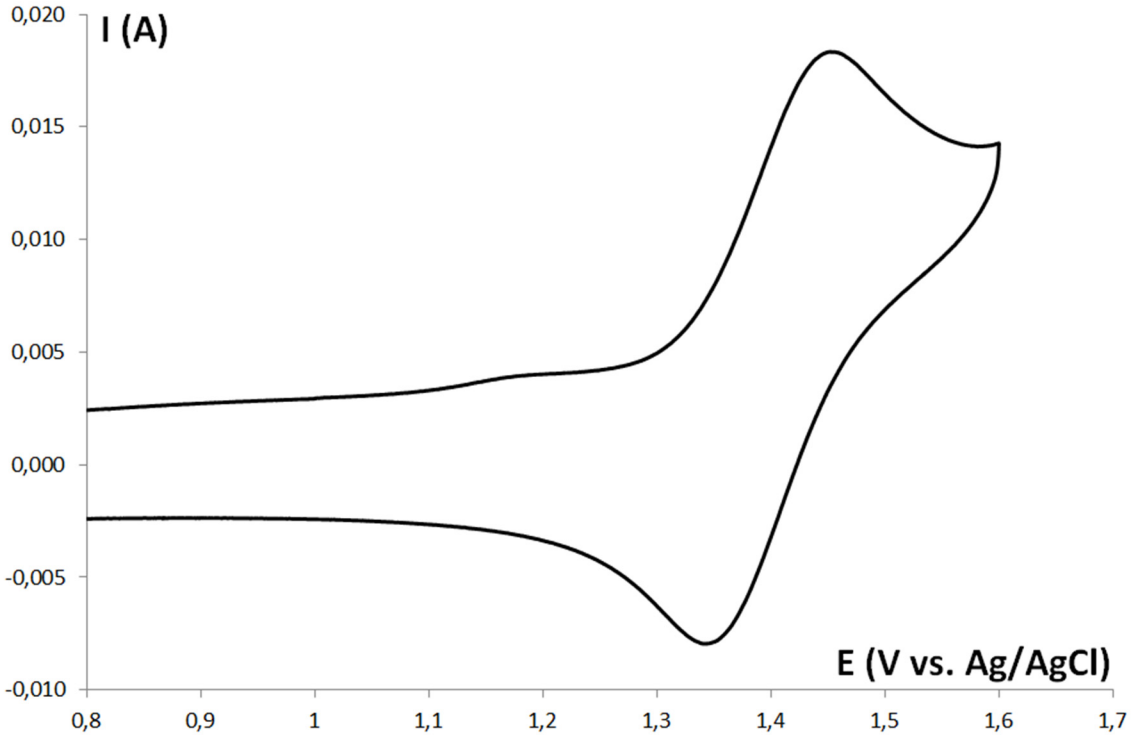

Figure A2.60 Cyclic Voltammogram of complex **7.**

See caption of **Figure 2.5** for measurement details

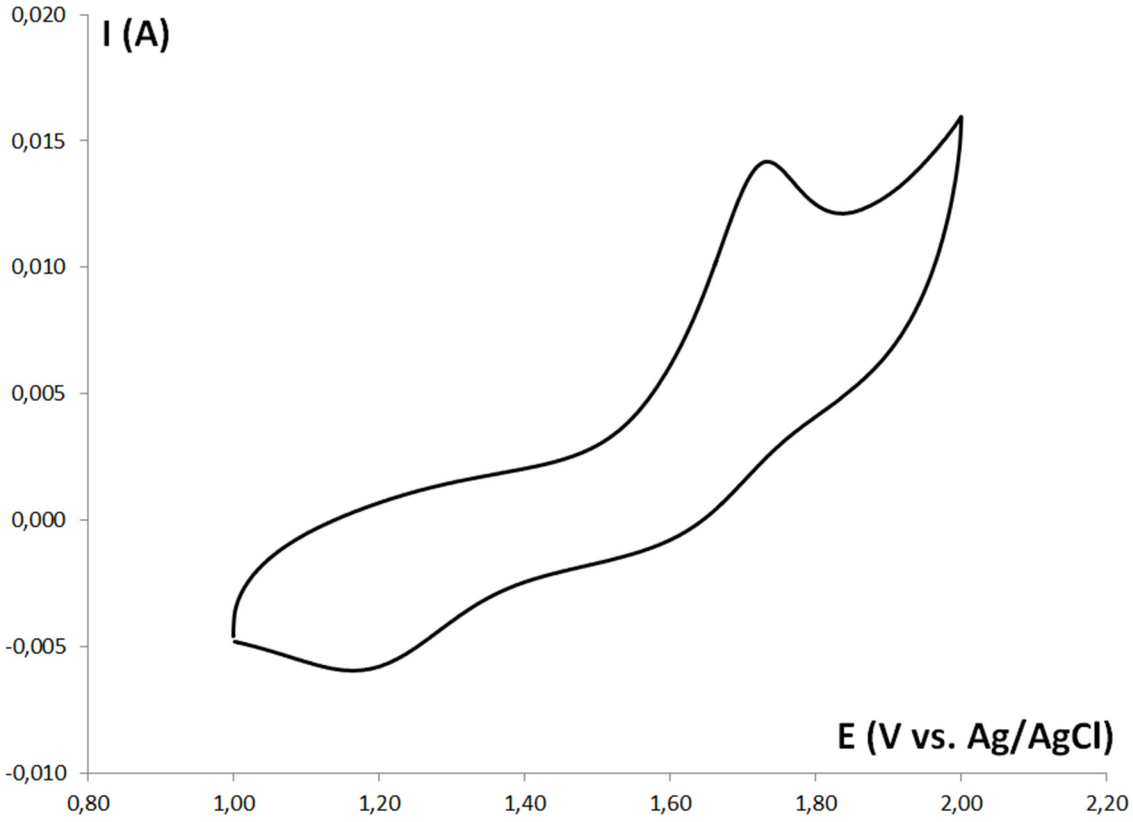

Figure A2.61 Cyclic Voltammogram of complex **8.**

See caption of **Figure 2.5** for measurement details

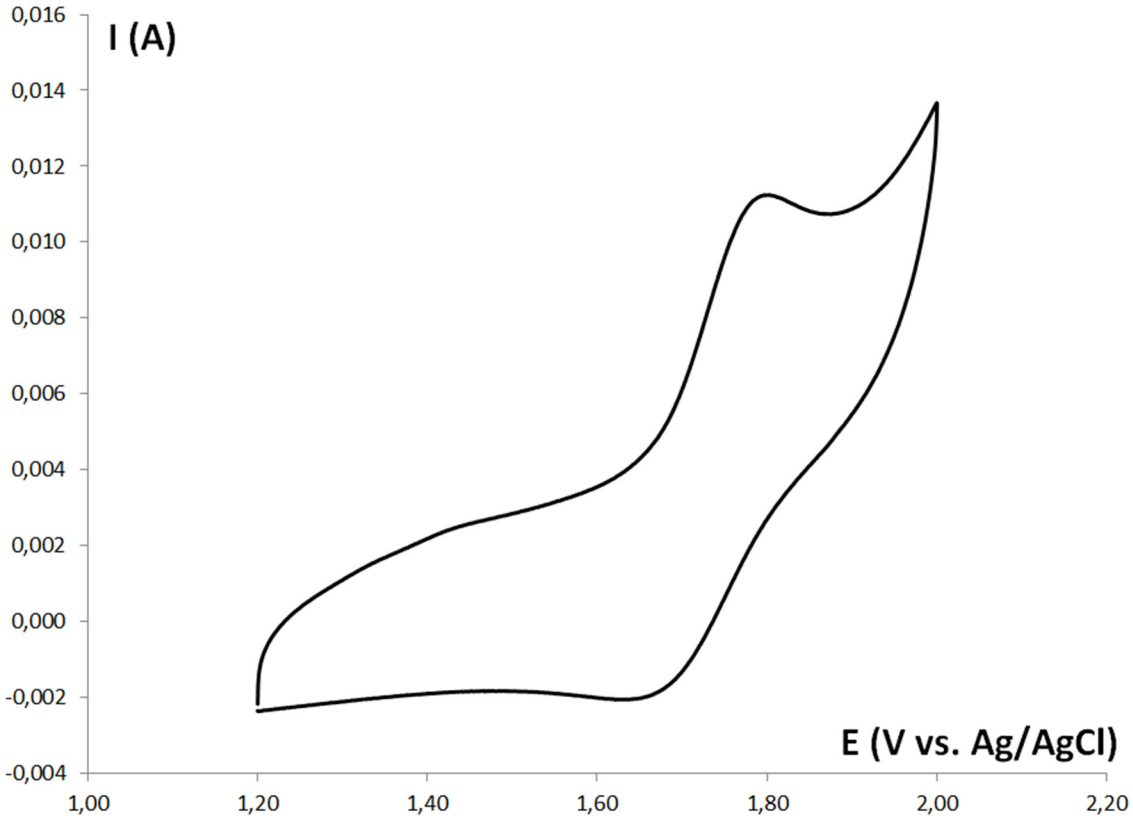

Figure A2.62 Cyclic Voltammogram of complex **9.**

See caption of **Figure 2.5** for measurement details

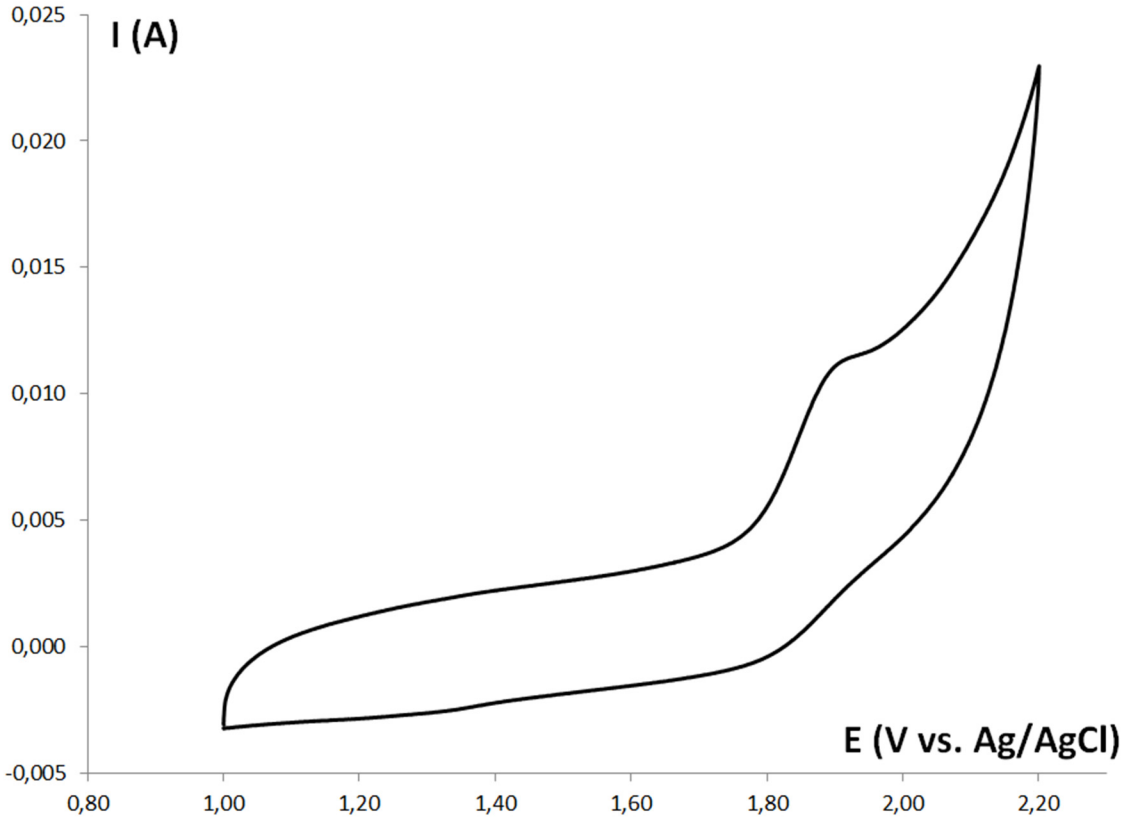

Figure A2.63 Cyclic Voltammogram of complex **10.**

See caption of **Figure 2.5** for measurement details

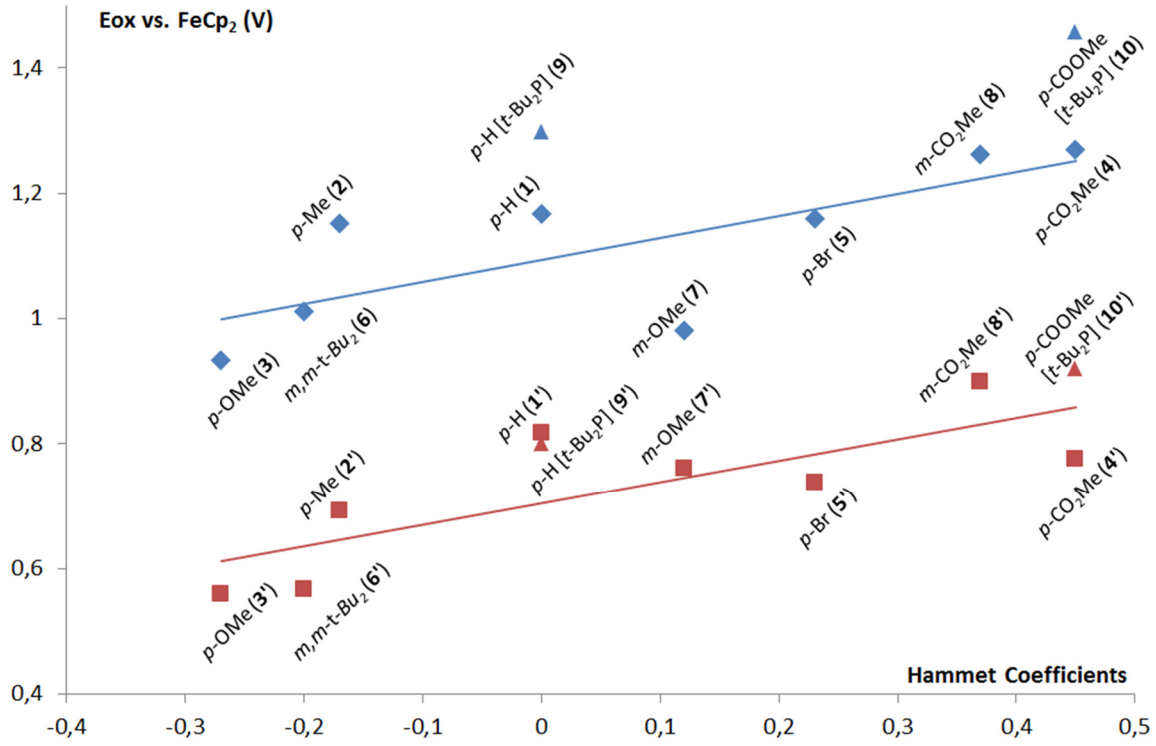

Figure A2.64 Relationship between E_{ox} values for cationic **1-10** (blue diamonds and triangles) and neutral bromo complexes **1'-10'** (red squares and triangles) vs. their corresponding σ_m and σ_p Hammett coefficients.[95]

Linear regression were performed on cationic complexes ($y = 0.3514x + 1.0935$, $R^2 = 0.5607$) and neutral bromide complexes ($y = 0.3431x + 0.7083$, $R^2 = 0.627$). Complexes **9**, **10**, **9'** and **10'** were not used for the determination of the linear regression as they have different *P*-substituents.

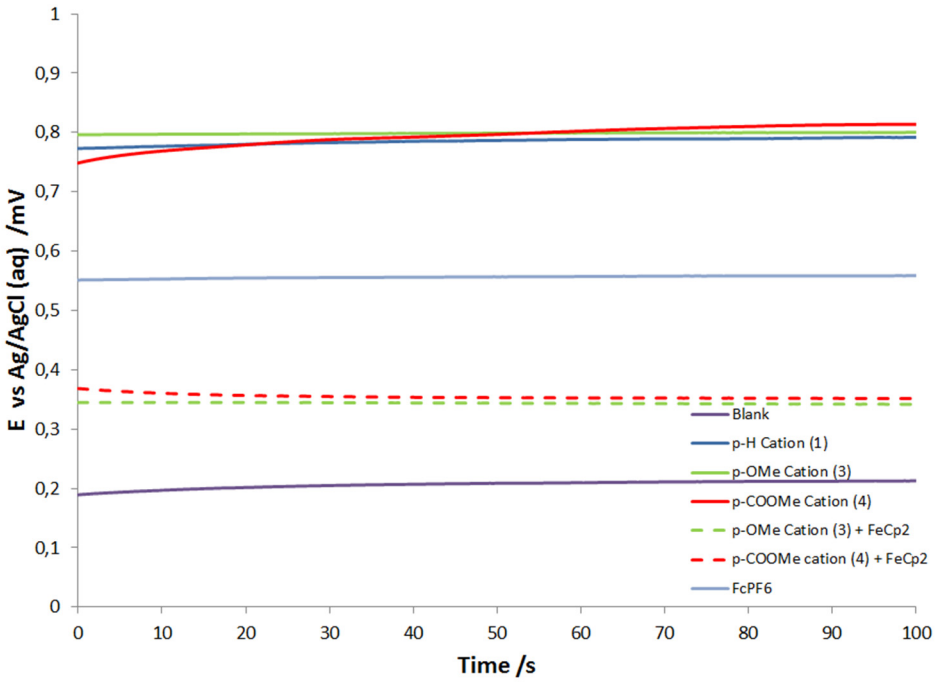

FigureA2.65 Open Circuit Potentials for complexes **1, 3** and **4** and (for **3** and **4**) with added $FeCp_2$ (1 equiv).

The measurements were carried out at 298 K using dry CH_2Cl_2 solutions containing equimolar quantities of the given complex and $[Bu_4N][PF_6]$ as electrolyte (10^{-4} M). The samples were purged for 2 min by bubbling a stream of N_2 prior to beginning the measurements, and a N_2 atmosphere was maintained over the samples throughout the measurements. The potentials were measured at an interval of 0.25 seconds for 100 seconds. The solutions turned dark green/black after addition of the $FeCp_2$.

Table A2.7 Rest Potentials of Complexes **1, 3** and **4.**

Complex	E (mV) vs Ag/AgCl(aq)	E (mV) vs Blank [a]
1	788	579
3	799	591
4	801	593
3 + $FeCp_2$	353	145
4 + $FeCp_2$	343	134
$[FeCp_2][PF_6]^{a-}$	557	349
Blank[b]	209	0

a) Values were measured in the experimental conditions. b) The blank is a 0.1 M solution of the electrolyte, $[NBu_4][PF_6]$, in dry CH_2Cl_2.

Ligand-Exchange analysis

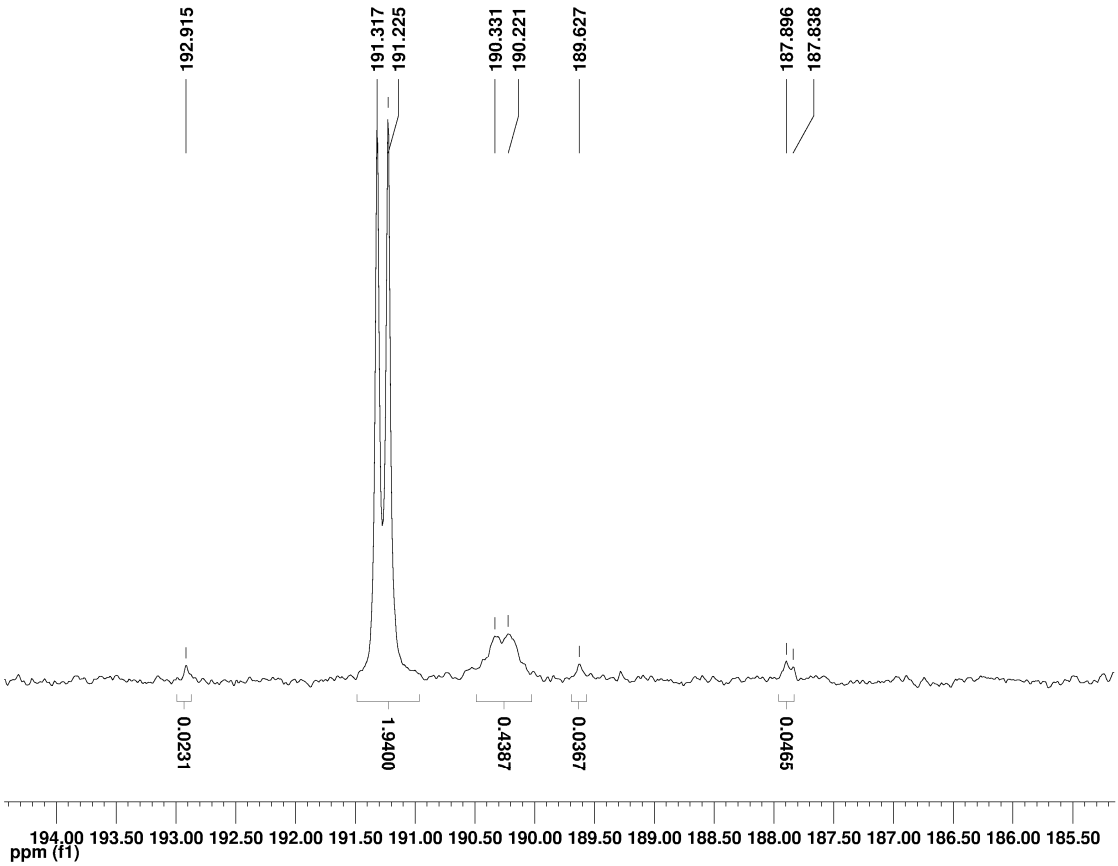

Figure A2.66 ^{31}P NMR spectra (202 MHz) of the reaction of (^{Me}NCN)NiBr and complex **8** in C_6D_6

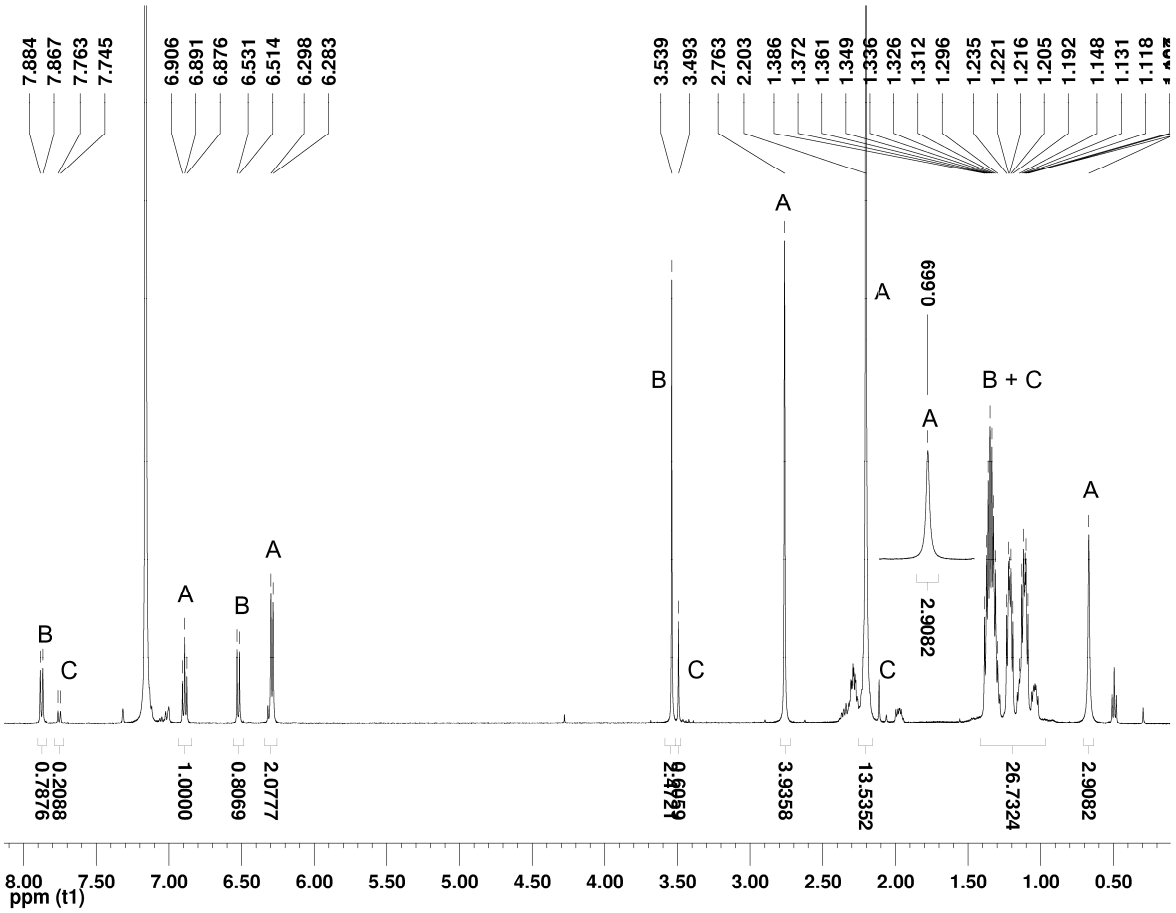

Figure A2.67 ^{1}H NMR spectra (500 MHz) of the reaction of (^{Me}NCN)NiBr and complex **8** in C_6D_6.

"A" corresponds to the signals for the cationic complex [(NCN)Ni(NCMe)][OSO_2CF_3], "B" corresponds to the signals for the complex (*m*-CO_2Me-POCOP)Ni-Br and "C "corresponds to the signals of the complex (*m*-CO_2Me-POCOP)Ni-OTf.

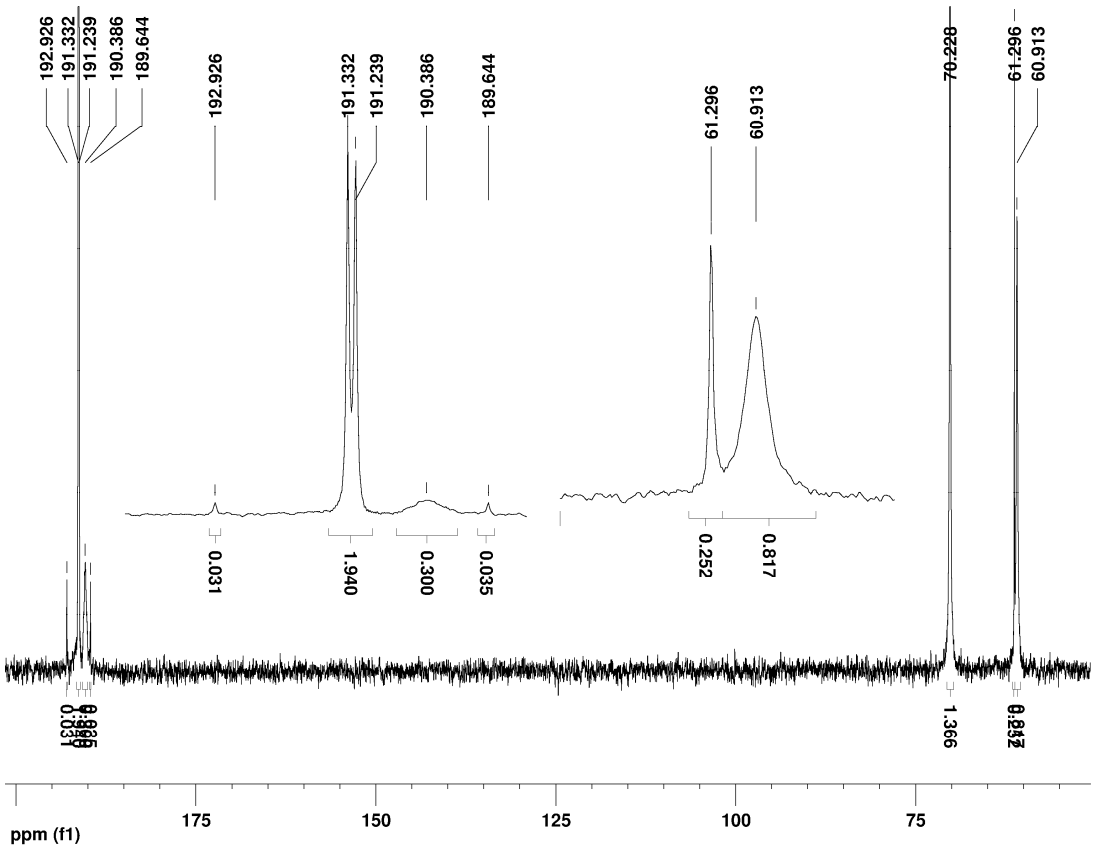

Figure A2.68 ^{31}P NMR spectra of the reaction of (PCP$^{i\text{-Pr}}$)NiBr and complex **8** in C_6D_6

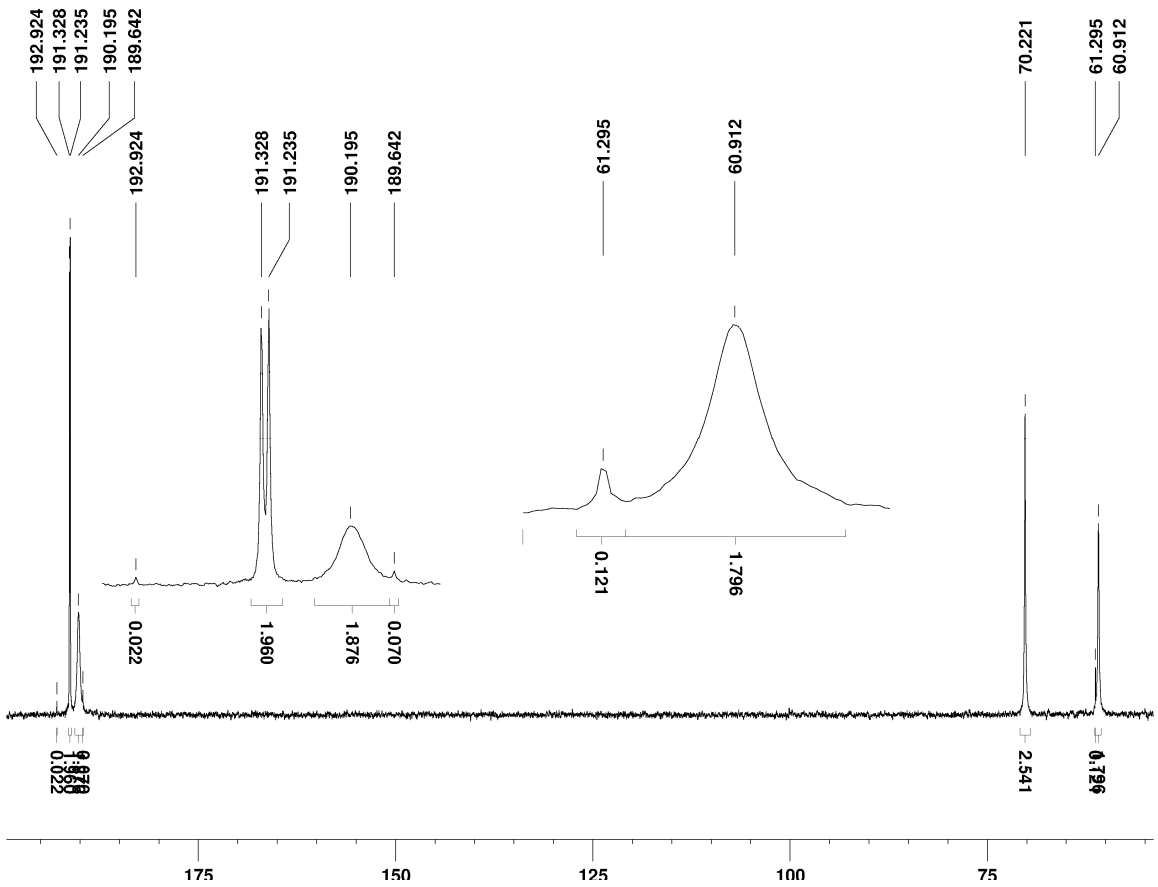

Figure A2.69 ^{31}P NMR spectra of the reaction of (PCP$^{i\text{-Pr}}$)NiBr and complex **8** in C_6D_6 after addition of 0.5 equivalents of AgOTf to the reaction mixture**.**

A2 Annexe du chapitre 3

Table A3.1 Crystal Data, Collection, and Refinement Parameters for complexes **7 , 9** and **10**

	7	**9**	**10**
chemical formula	$C_{23}H_{36}NNiO_4P_2,CF_3O_3S$	$C_{29}H_{40}NNiO_4P_2,CF_3O_3S$	$C_{28}H_{40}NNiO_3P_2,C_9H_7N,CF_3O_3S$
crystal colour	yellow	yellow	yellow
***Fw*; *F*(000)**	660.25; 688	736.34; 1536	838.00; 1753
***T* (K)**	100	100	100
wavelength (Å)	1.34139	1.54178	1.34139
space group	P -1	P 1 21/n 1	P 1 21/n 1
***a* (Å)**	8.1449(4)	7.88780(8)	9.2880(6)
***b* (Å)**	10.6295(5)	10.89270(11)	35.220(2)
c (Å)	18.1924(8)	40.6954(4)	12.8458(8)
α (deg)	78.203(2)	90	90
β (deg)	77.454(2)	91.8910(5)	102.689(4)
γ (deg)	89.556(2)	90	90
Z	2	4	4
***V* (Å^3)**	1503.84(12)	3494.62(6)	4099.5(5)
ρ_{calcd} (g·cm^{-3})	1.458	1.400	1.358
μ (mm^{-1})	5.020	2.748	3.755
θ range (deg); completeness	2.213 − 60.849; 1.000	2.172 − 71.668; 0.999	2.183 − 60.730; 0.999
collected reflections; R_σ	45548; 0.0342	92637; 0.0099	61357; 0.0307
unique reflections; R_{int}	45548; 0.0550	92637; 0.0250	61357; 0.0463
R1[a]; wR2[b] [I > 2σ(I)]	0.0370; 0.0946	0.0316; 0.0821	0.0477; 0.1155
R1; wR2 [all data]	0.0481; 0.1008	0.0320; 0.0824	0.0518; 0.1178
GOF	1.044	1.124	1.108
largest diff peak and hole	0.646 and -0.375	0.387 and -0.272	1.524 and -0.427

a) $R_1=\Sigma(||F_o|-|F_c||)/\Sigma|F_o|$ b) $wR_2=\{\Sigma[w(F_o^2-F_c^2)^2]/\Sigma[w(F_o^2)^2]\}^{½}$

Table A3.2 Crystal Data, Collection, and Refinement Parameters for complexes **11** and **12**

	11	**12**
chemical formula	$C_{18}H_{34}NNiO_2P_2,CF_3O_3S$	$C_{20}H_{36}NNiO_4P_2,CF_3O_3S$
crystal colour	yellow	colourless
***Fw*; *F*(000)**	566.18; 592	624.22; 652
***T* (K)**	100	100
wavelength (Å)	1.34139	1.34139
space group	P -1	P -1
***a* (Å)**	7.5940(3)	7.5293(3)
***b* (Å)**	12.8525(5)	11.2755(5)
***c* (Å)**	14.7380(5)	17.2859(7)
α (deg)	76.845(2)	84.276(2)
β (deg)	76.375(2)	88.649(2)
γ (deg)	73.105(2)	87.103(2)
Z	2	2
***V* (Å^3)**	1317.91(9)	1458.08(11)
ρ_{calcd} (g·cm^{-3})	1.427	1.422
μ (mm^{-1})	5.625	5.154
θ range (deg); completeness	2.724 − 60.788; 1.000	2.235 − 60.764; 0.998
collected reflections; R_σ	38553; 0.0318	42662; 0.0316
unique reflections; R_{int}	38553; 0.0486	42662; 0.0505
R1[a]; wR2[b] [I > 2σ(I)]	0.0298; 0.0776	0.0327; 0.0885
R1; wR2 [all data]	0.0337; 0.0798	0.0361; 0.0903
GOF	1.067	1.078
largest diff peak and hole	0.543 and -0.294	0.609 and -0.234

a) $R_1=\Sigma(||F_o|-|F_c||)/\Sigma|F_o|$ b) $wR_2=\{\Sigma[w(F_o^2-F_c^2)^2]/\Sigma[w(F_o^2)^2]\}^{1/2}$

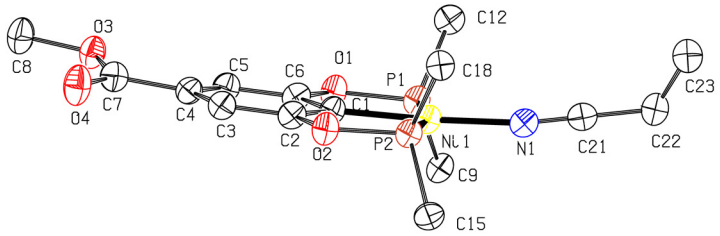

Figure A3.1 Side view of the molecular diagram for complex **7.**

Thermal ellipsoids are shown at the 50% probability level. *P*-substituents and hydrogens are omitted for clarity.

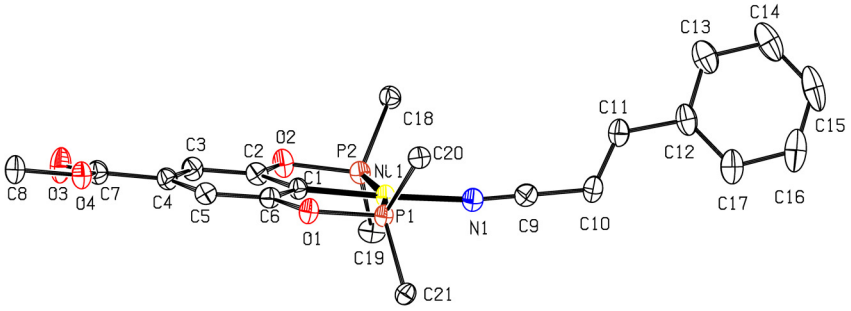

Figure A3.2 Side view of the molecular diagram for complex **9.**

Thermal ellipsoids are shown at the 50% probability level. *P*-substituents and hydrogens are omitted for clarity

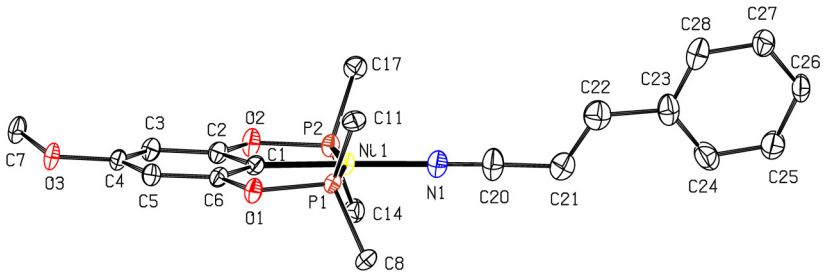

Figure A3.3 Side view of the molecular diagram for complex **10.**

Thermal ellipsoids are shown at the 50% probability level. *P*-substituents and hydrogens are omitted for clarity

Details of the diffraction studies

Crystals of compound **7** were obtained by slow evaporation of a concentrated THF solution at r.t. Crystals of compound **9** and **10** were obtained by slow evaporation of a concentrated dichloromethane solution at r.t. Crystals of compound **11** and **12** were obtained by slow evaporation of a concentrated acetone solution at r.t. The crystallographic data for all complexes were collected on a Bruker Venture Metaljet equipped with a Metal Jet source, an Helios MX Mirror Optics monochromator and a Bruker Photon 100 CMOS Detector. Cell refinement and data reduction were done using the ShelXL routine version July 2014.[96] An empirical absorption correction, based on the multiple measurements of equivalent reflections, was applied. The space group was confirmed by ShelXT [97] routine in the program OLEX2.[98] The structures were solved by direct methods (ShelXT) and refined by full-matrix least-squares and difference Fourier techniques with OLEX2.[98] All non-hydrogen atoms were refined with anisotropic displacement parameters. Hydrogen atoms were set in calculated positions and refined as riding atoms with a common thermal parameter

NMR Analysis

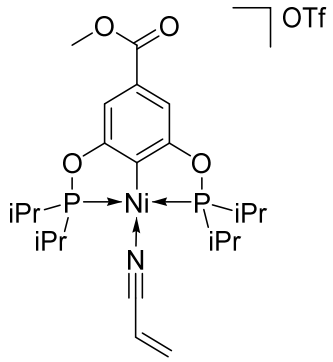

Figure A3.4 Representation of complex [{2,6-(*i*Pr$_2$PO)$_2$-4-(CO$_2$Me)C$_6$H$_2$}Ni(NCCH=CH$_2$)][OSO$_2$CF$_3$] (**7**).

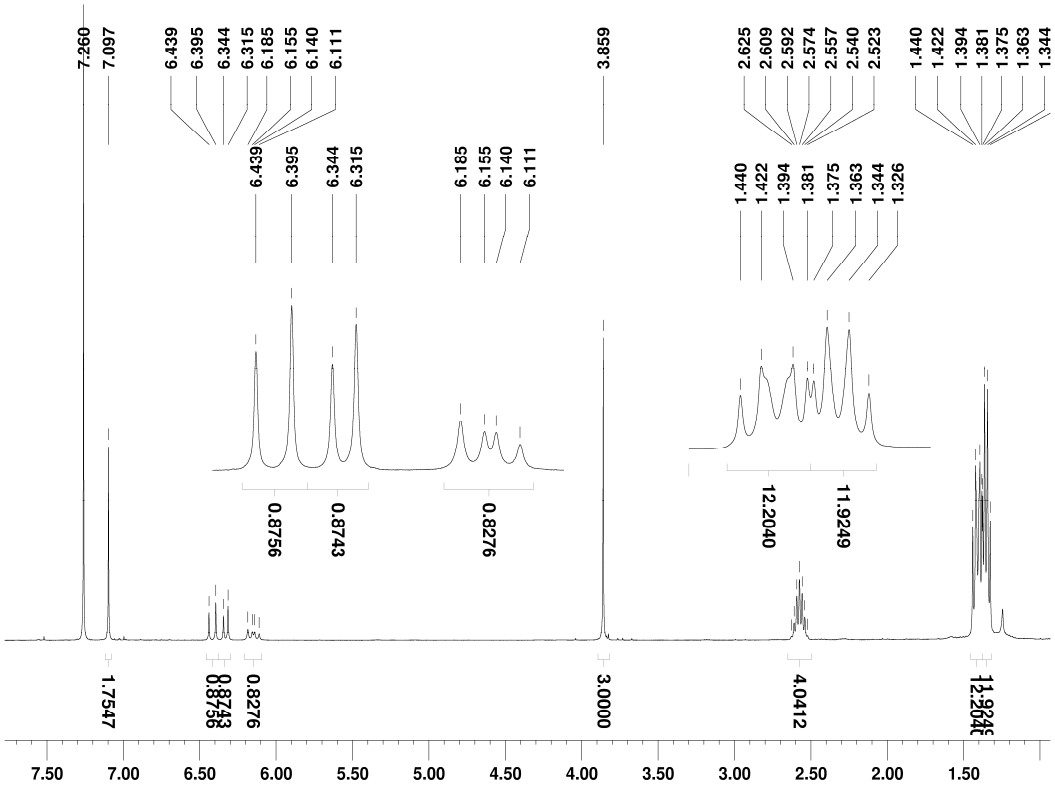

Figure A3.5 ^{1}H NMR spectra (400 MHz) of complex **7** in CDCl$_3$.

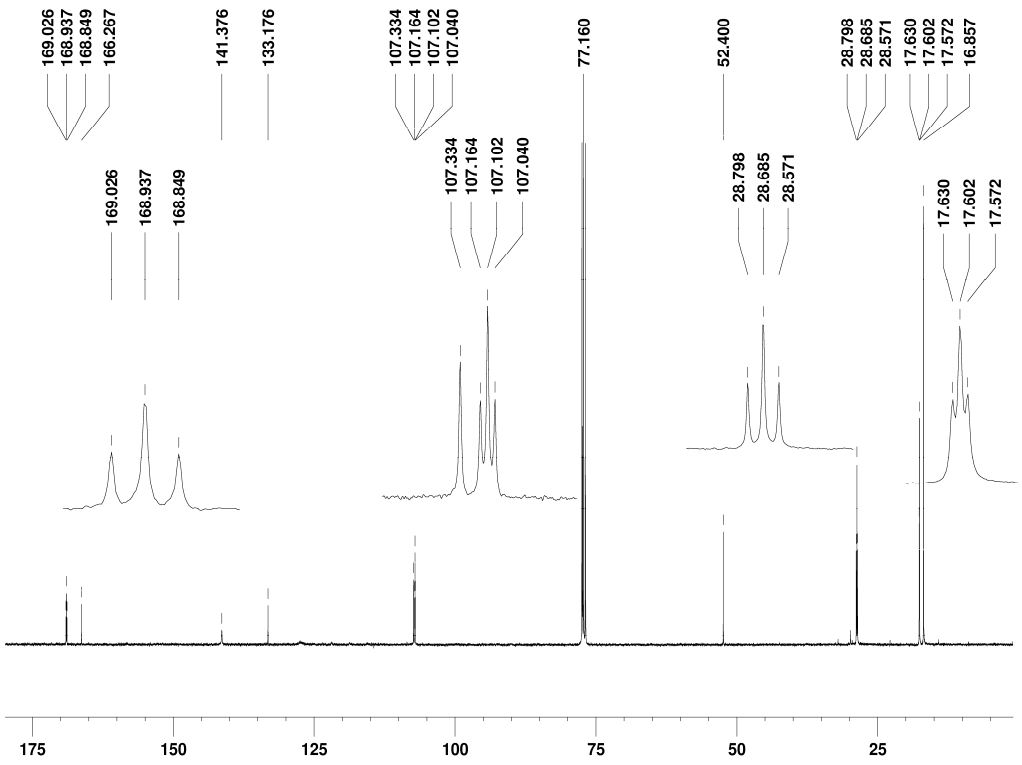

Figure A3.6 $^{13}C\{^{1}H\}$ NMR spectra (101 MHz) of complex **7** in $CDCl_3$.

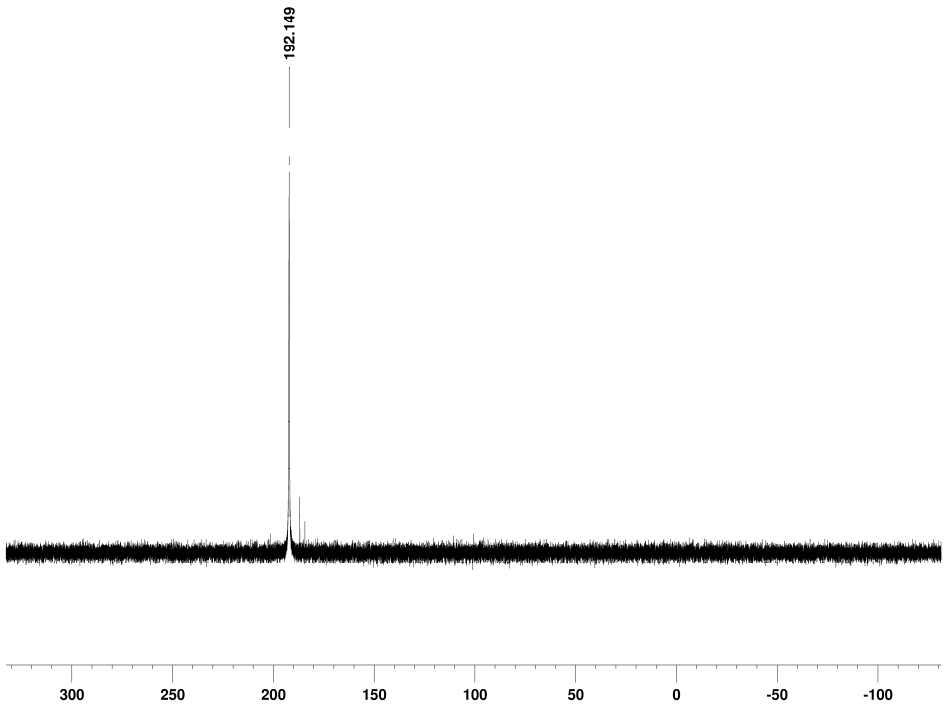

FigureA3.7 $^{31}P\{^{1}H\}$ NMR spectra (162 MHz) of complex **7** in $CDCl_3$.

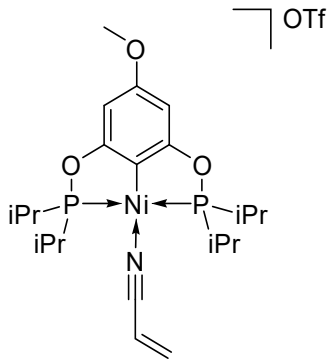

Figure A3.8 Representation of complex [{2,6-(*i*Pr$_2$PO)$_2$-4-(OMe)C$_6$H$_2$}Ni(NCCH=CH$_2$)][OSO$_2$CF$_3$] (**8**).

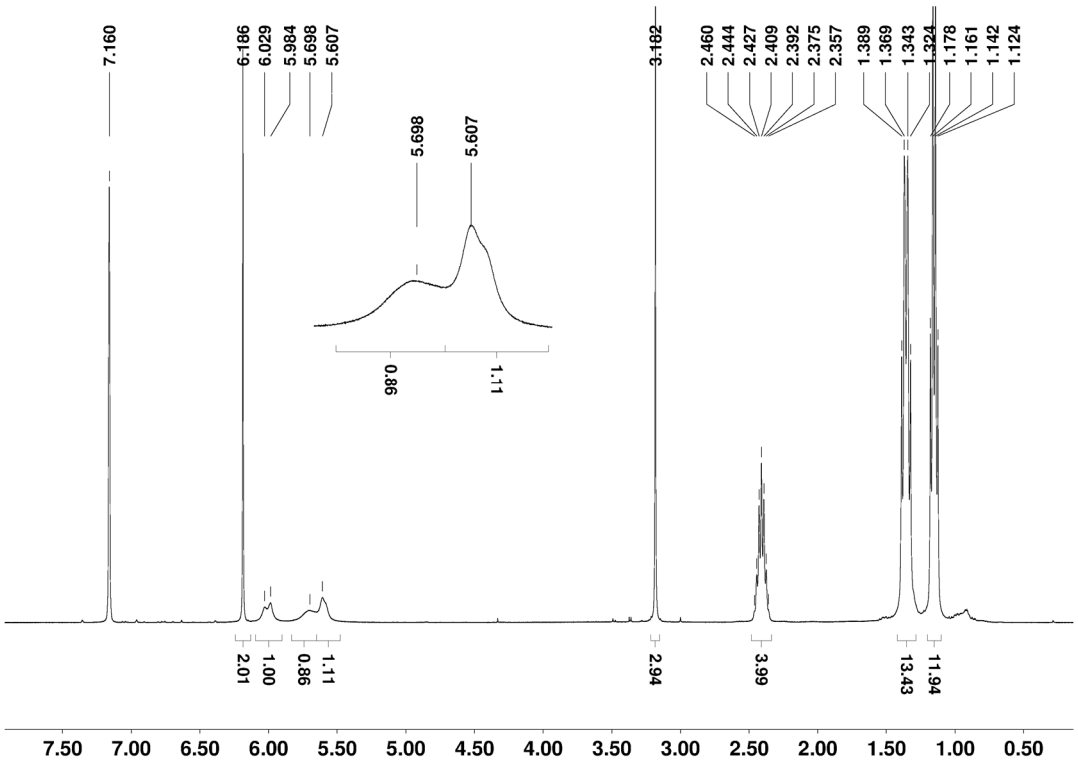

Figure A3.9 ^{1}H NMR spectra (500 MHz) of complex **8** in C$_6$D$_6$.

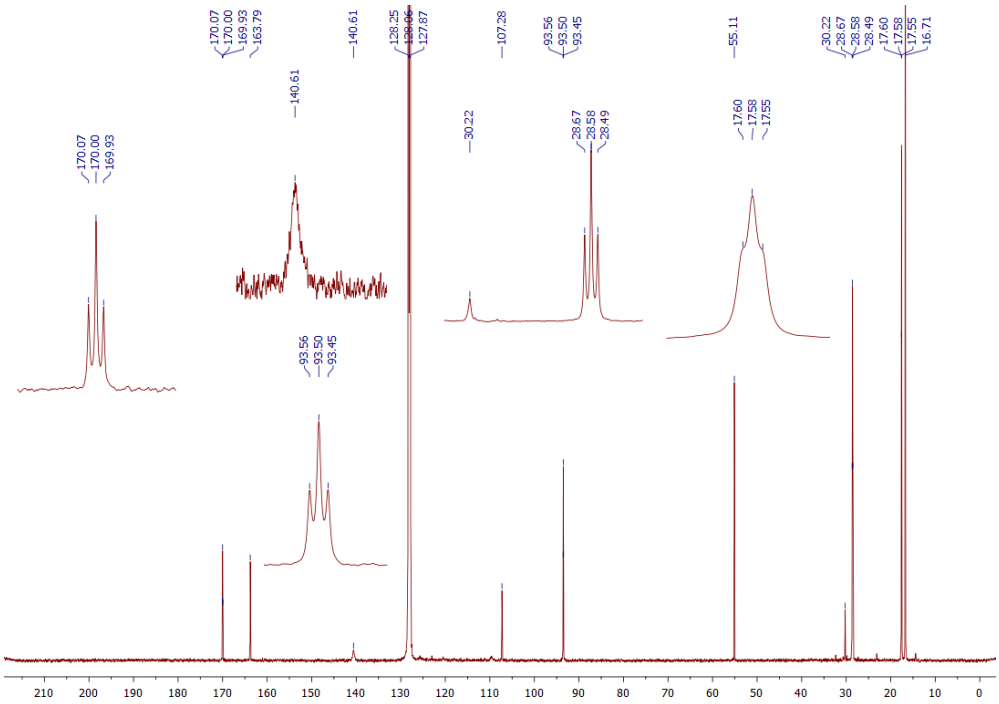

Figure A3.10 $^{13}C\{^{1}H\}$ NMR spectra (125 MHz) of complex **8** in C_6D_6.

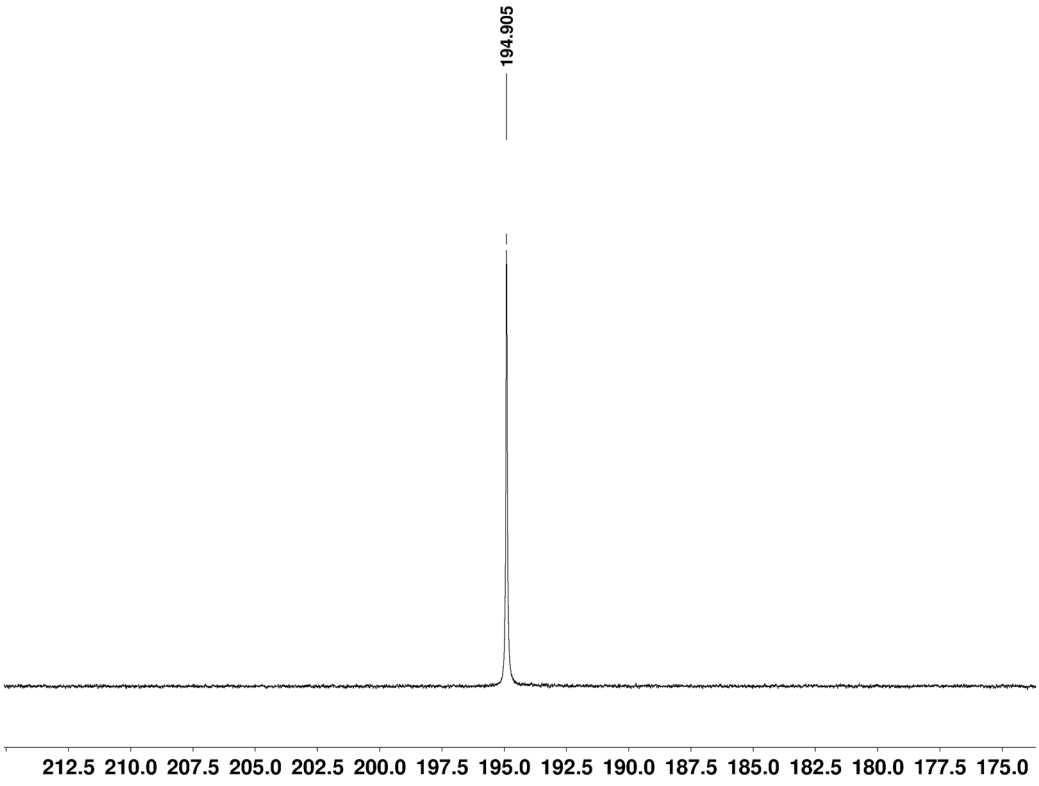

Figure A3.11 $^{31}P\{^{1}H\}$ NMR spectra (162 MHz) of complex **8** in C_6D_6.

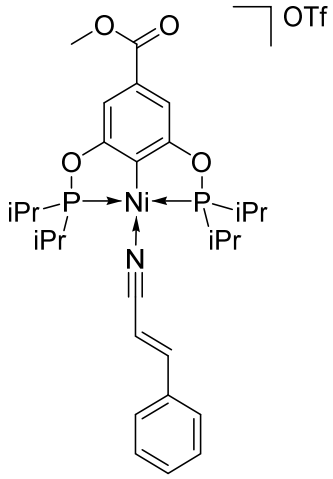

Figure A3.12 Representation of complex [{2,6-(*i*Pr$_2$PO)$_2$-4-(CO$_2$Me)C$_6$H$_2$}Ni(NCCH=CHPh)][OSO$_2$CF$_3$] (**9**).

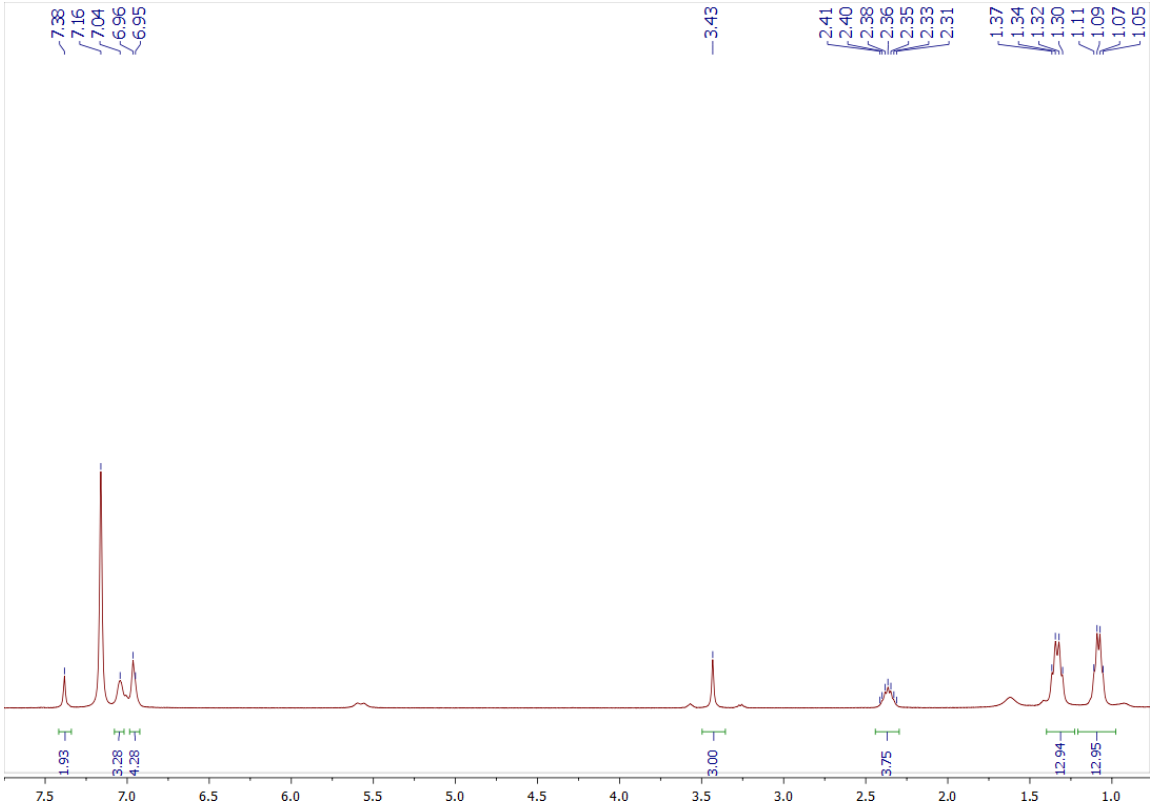

Figure A3.13 ^{1}H NMR spectra (400 MHz) of complex **9** in C$_6$D$_6$.

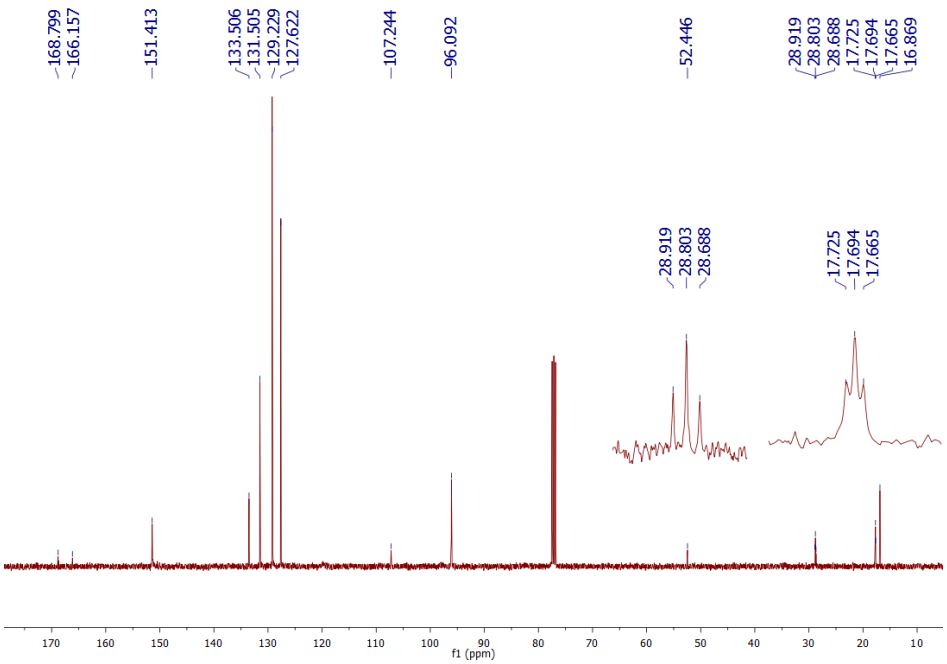

Figure A3.14 $^{13}C\{^{1}H\}$ NMR spectra (MHz) of complex **9** in $CDCl_3$.

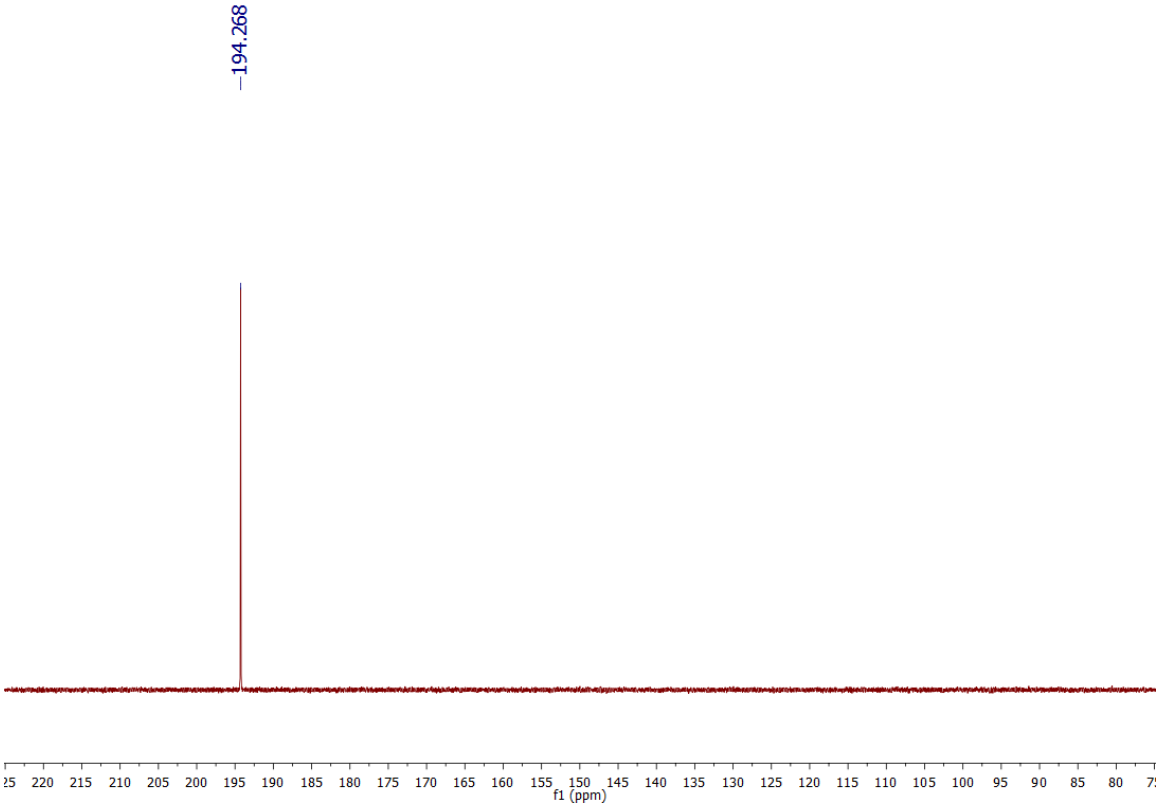

Figure A3.15 $^{31}P\{^{1}H\}$ NMR spectra (MHz) of complex **9** in $CDCl_3$.

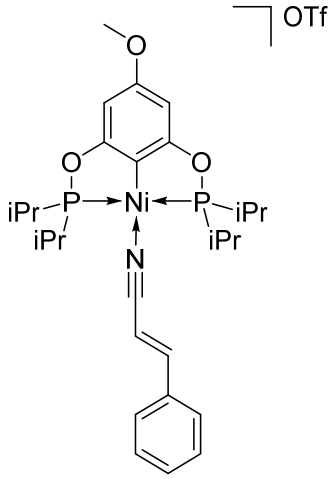

Figure A3.16 Representation of complex [{2,6-(*i*Pr$_2$PO)$_2$-4-(OMe)C$_6$H$_2$}Ni(NCCH=CHPh)][OSO$_2$CF$_3$]. (NCCH=CHPh) (**10**).

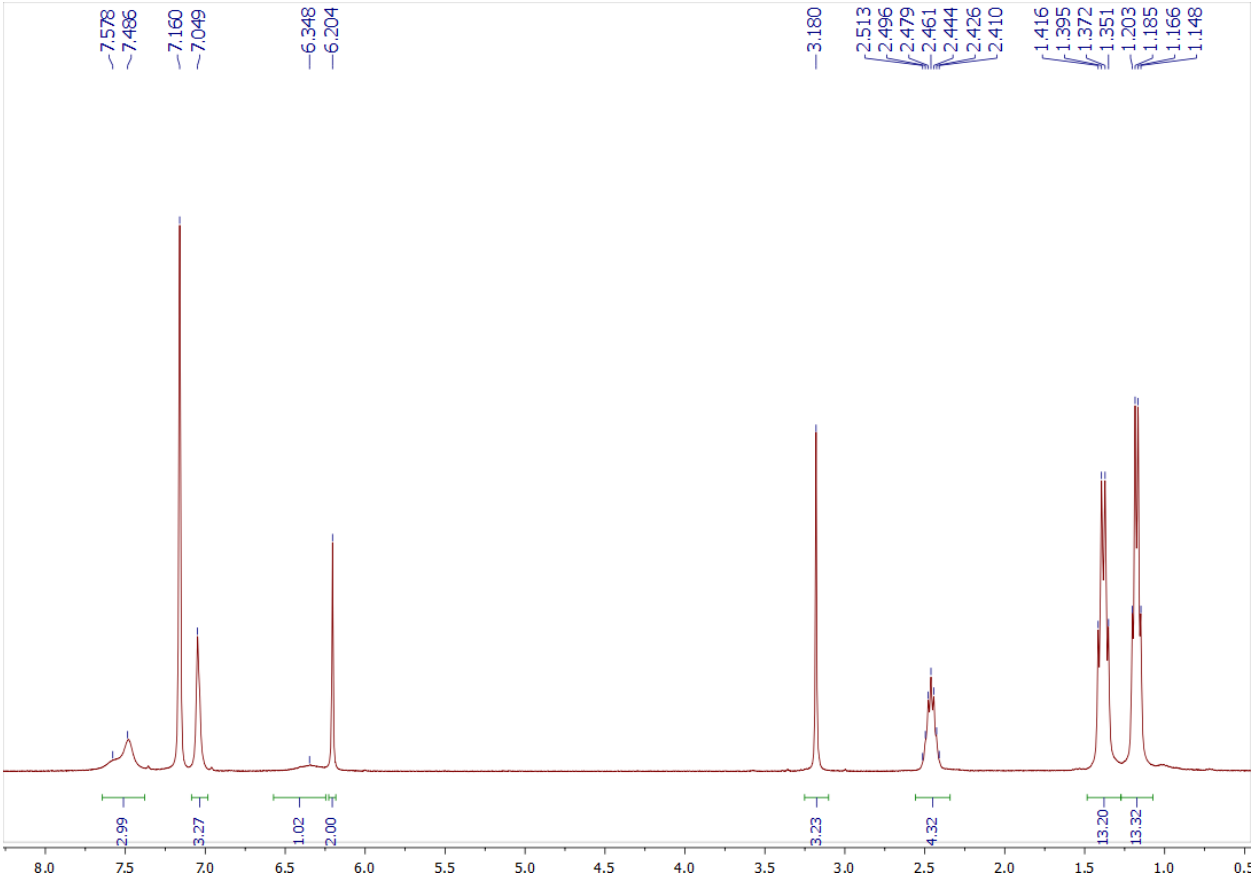

Figure A3.17 ^{1}H NMR spectra (400 MHz) of complex **10** in C$_6$D$_6$.

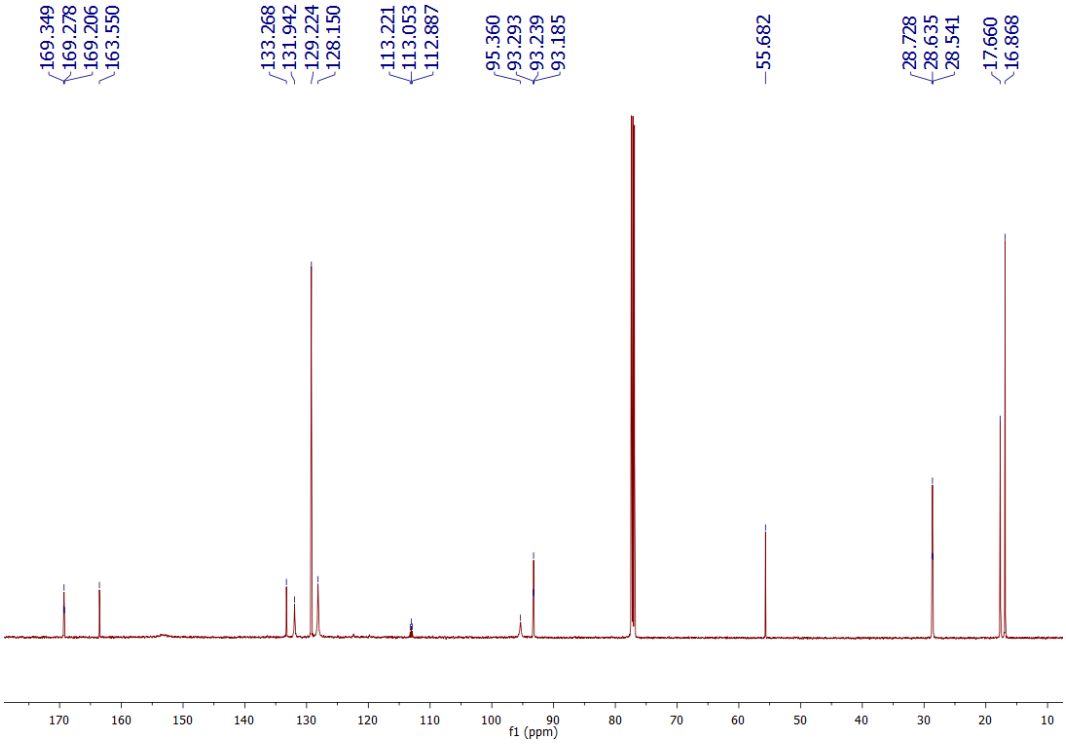

FigureA3.18 $^{13}C\{^{1}H\}$ NMR spectra (101 MHz) of complex **10** in $CDCl_3$.

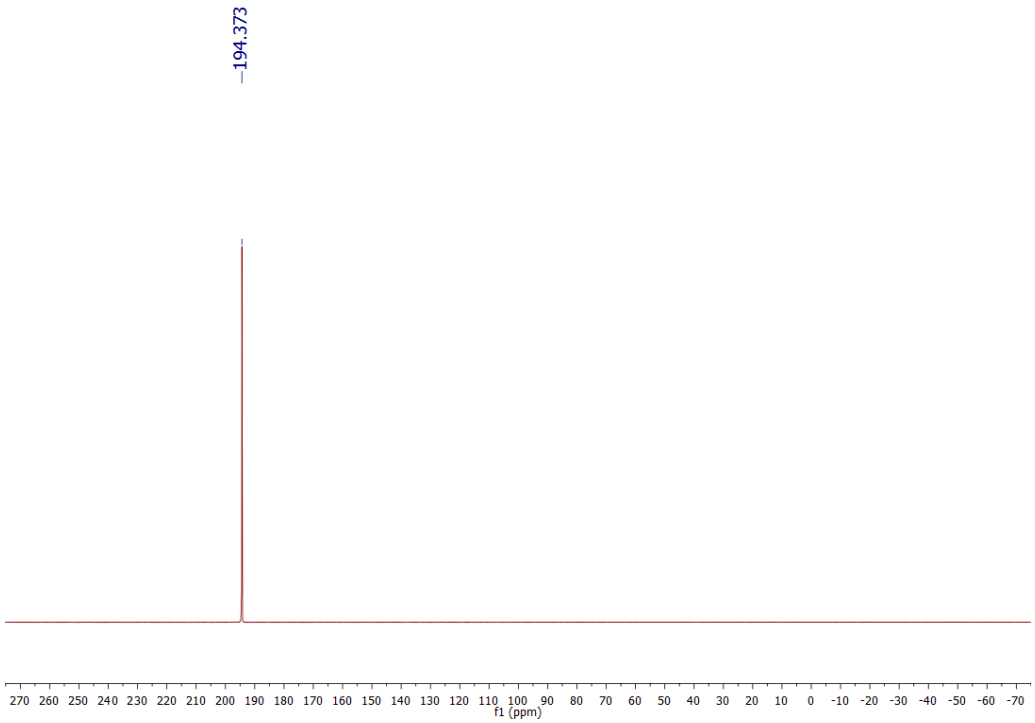

Figure A3.19 $^{31}P\{^{1}H\}$ NMR spectra (162 MHz) of complex **10** in $CDCl_3$.

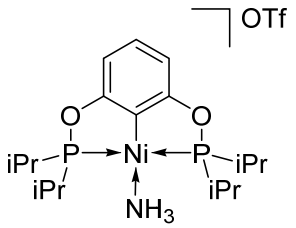

Figure A3.20 Representation of complex [{2,6-(*i*Pr$_2$PO)$_2$C$_6$H$_3$}Ni(NH$_3$)][OSO$_2$CF$_3$] (**11**).

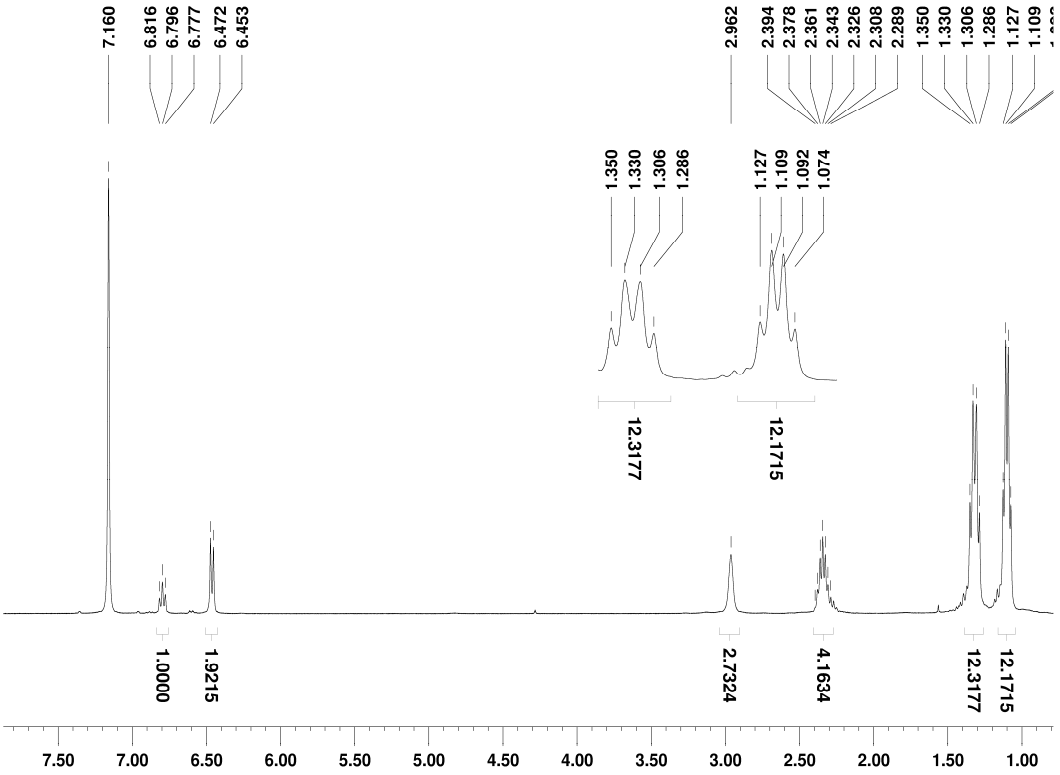

Figure A3.21 ^{1}H NMR spectra (400 MHz) of complex **11** in C$_6$D$_6$.

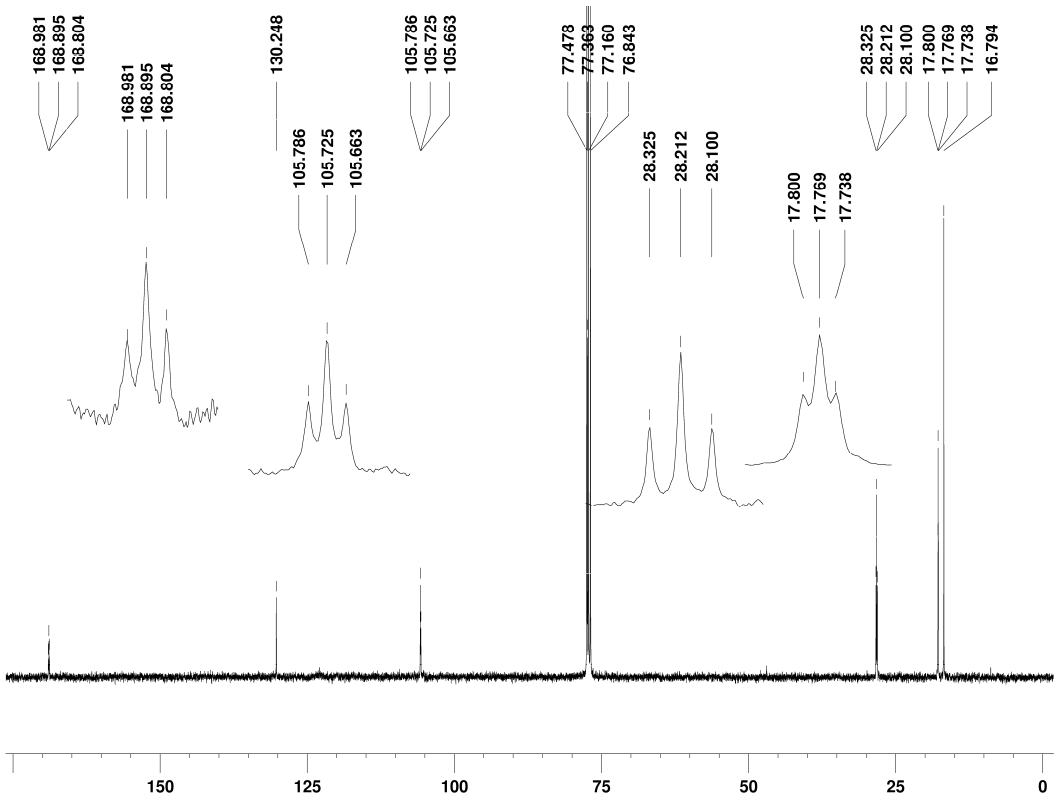

Figure A3.22 $^{13}C\{1H\}$ NMR spectra (101 MHz) of complex **11** in $CDCl_3$.

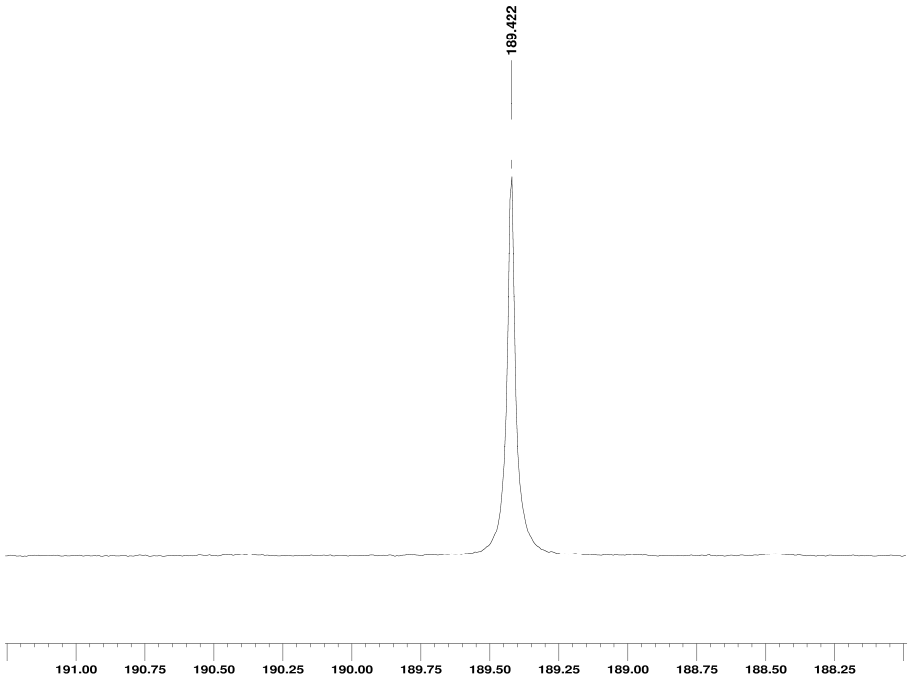

Figure A3.23 $^{31}P\{^{1}H\}$ NMR spectra (162 MHz) of complex 11 in C_6D_6.

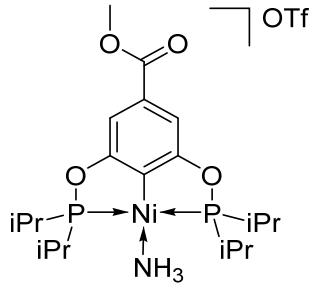

Figure A3.24 Representation of complex [{2,6-(*i*Pr$_2$PO)$_2$-4-(CO$_2$Me)C$_6$H$_2$}Ni(NH$_3$)][OSO$_2$CF$_3$] (**12**).

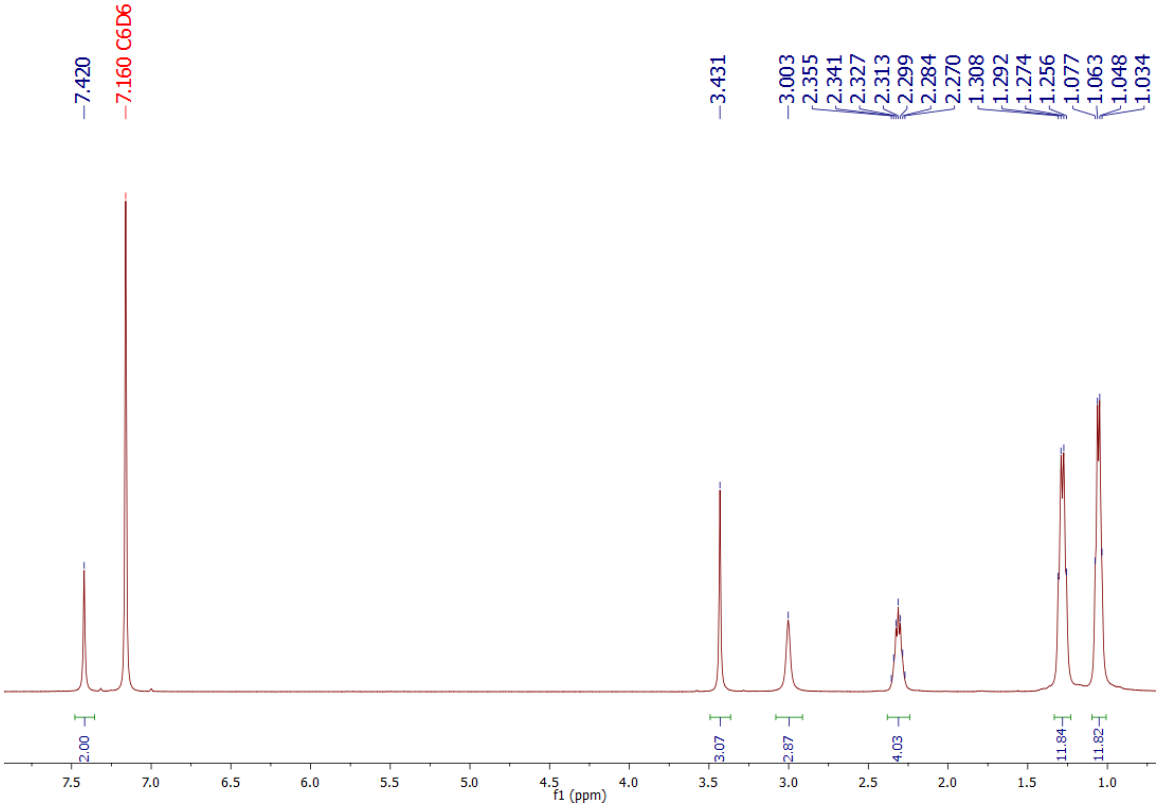

Figure A3.25 ^{1}H NMR spectra (500 MHz) of complex **12** in C$_6$D$_6$.

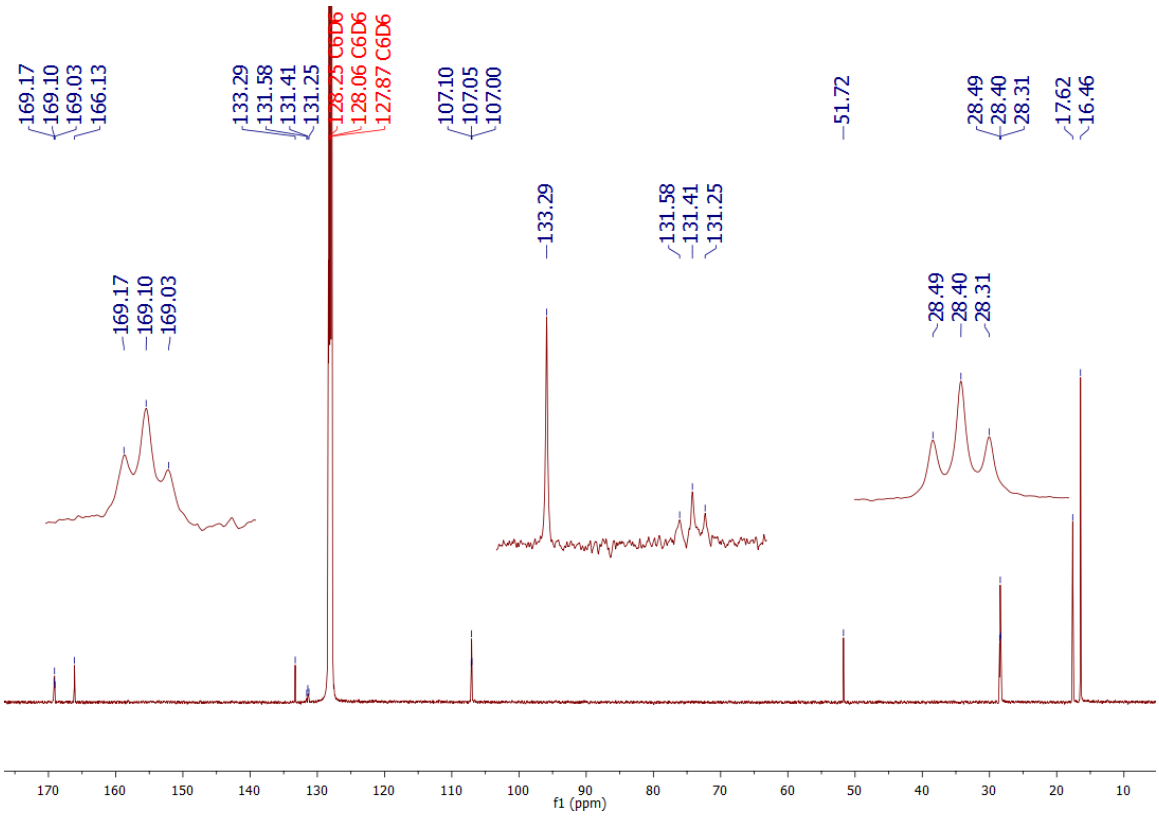

Figure A3.26 $^{13}C\{^{1}H\}$ NMR spectra (125 MHz) of complex **12** in C_6D_6.

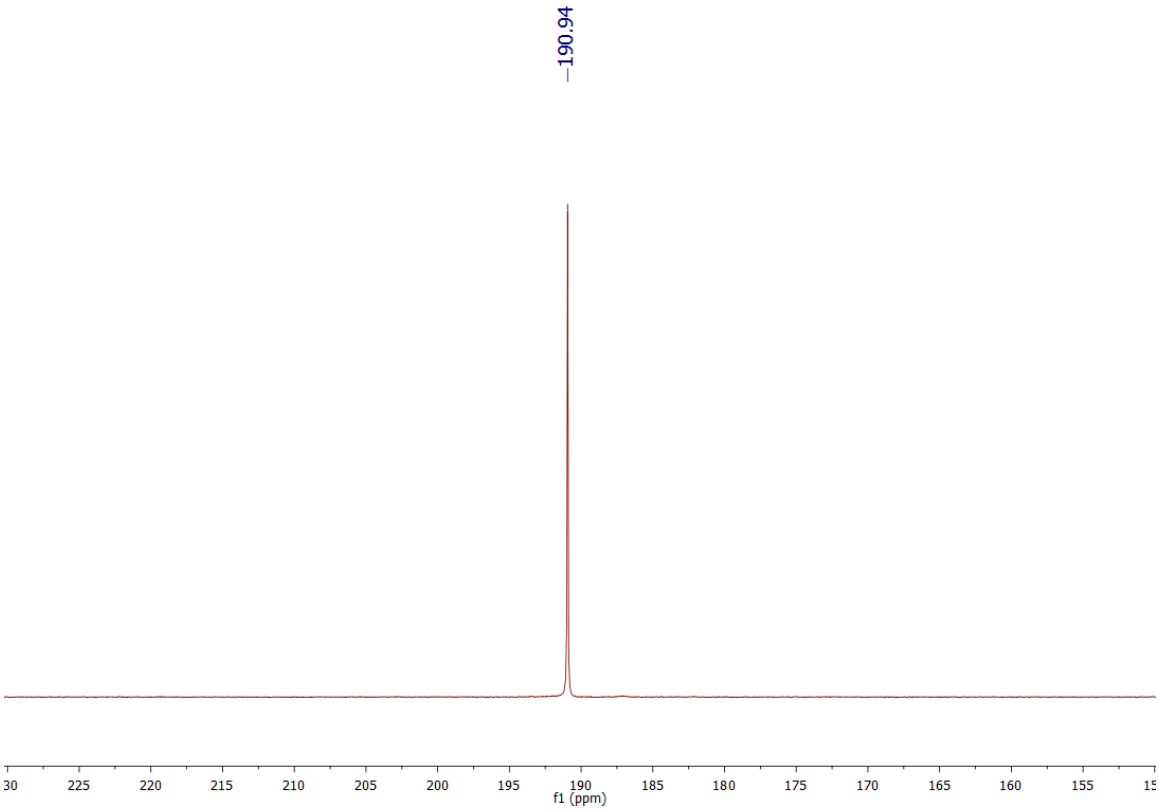

Figure A3.27 $^{31}P\{^{1}H\}$ NMR spectra (202 MHz) of complex **12** in C_6D_6.

Catalytic Tests

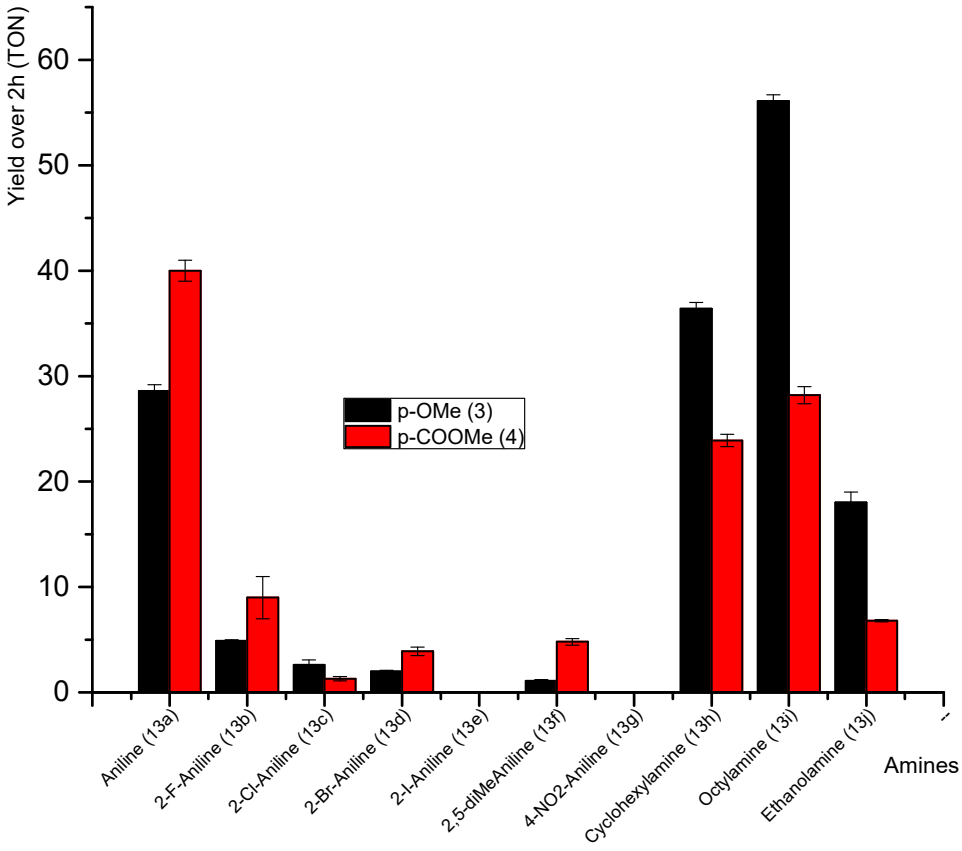

Figure A3.28 Plot of the yield (TON) for the hydroamination of crotonitrile (14a) catalyzed by **3** and **4** for the mono-addition product over 2 h.

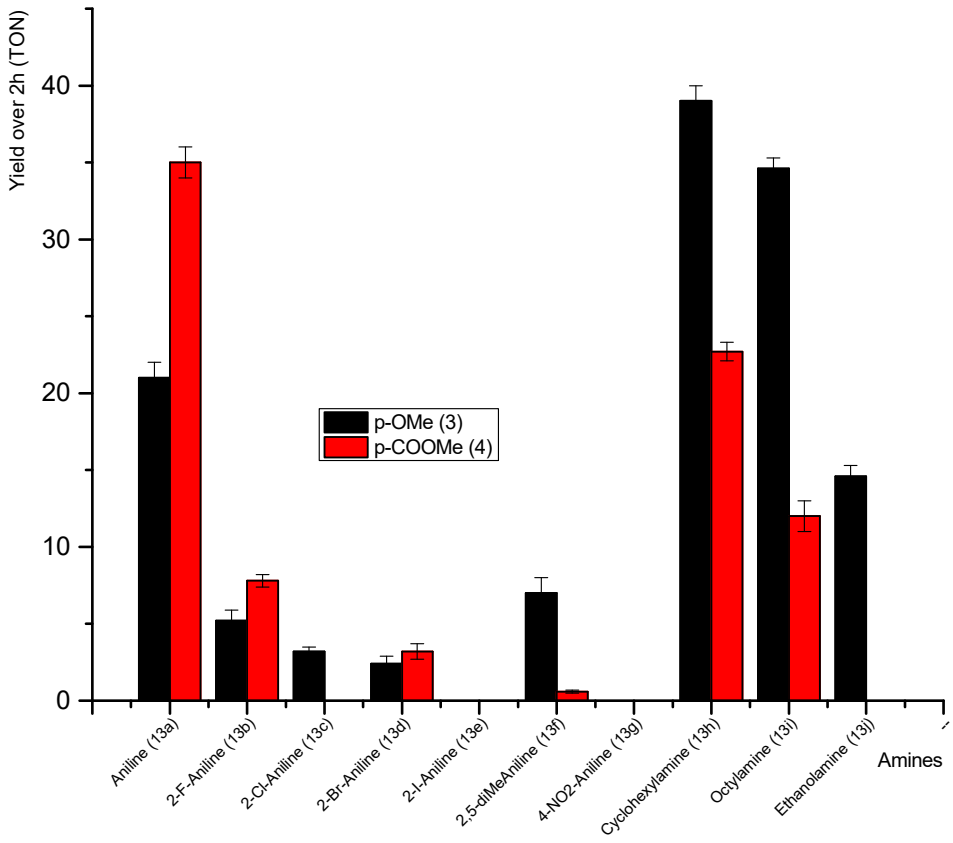

Figure A3.29 Plot of the yield (TON) for the hydroamination of methacrylonitrile (14b) catalyzed by **3** and **4** for the mono-addition product over 2 h.

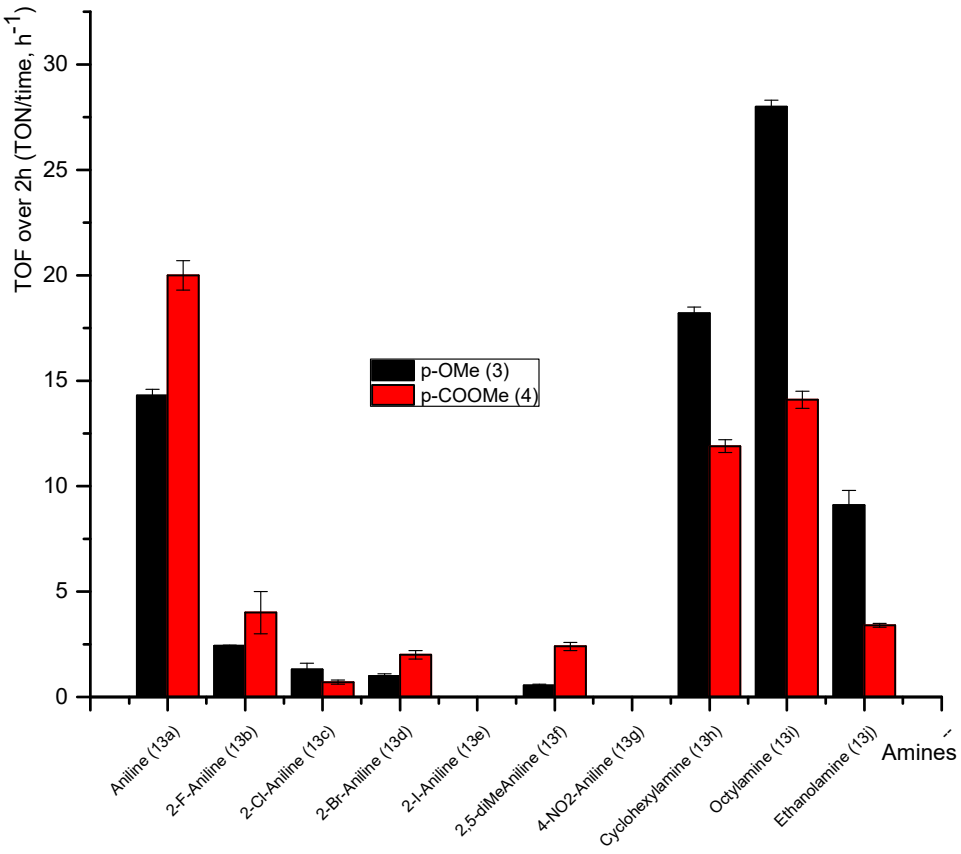

Figure A3.30 Plot of the TOF (TON/time, h^{-1}) for the hydroamination of crotonitrile (14a) catalyzed by **3** and **4** for the mono-addition product over 2 h.

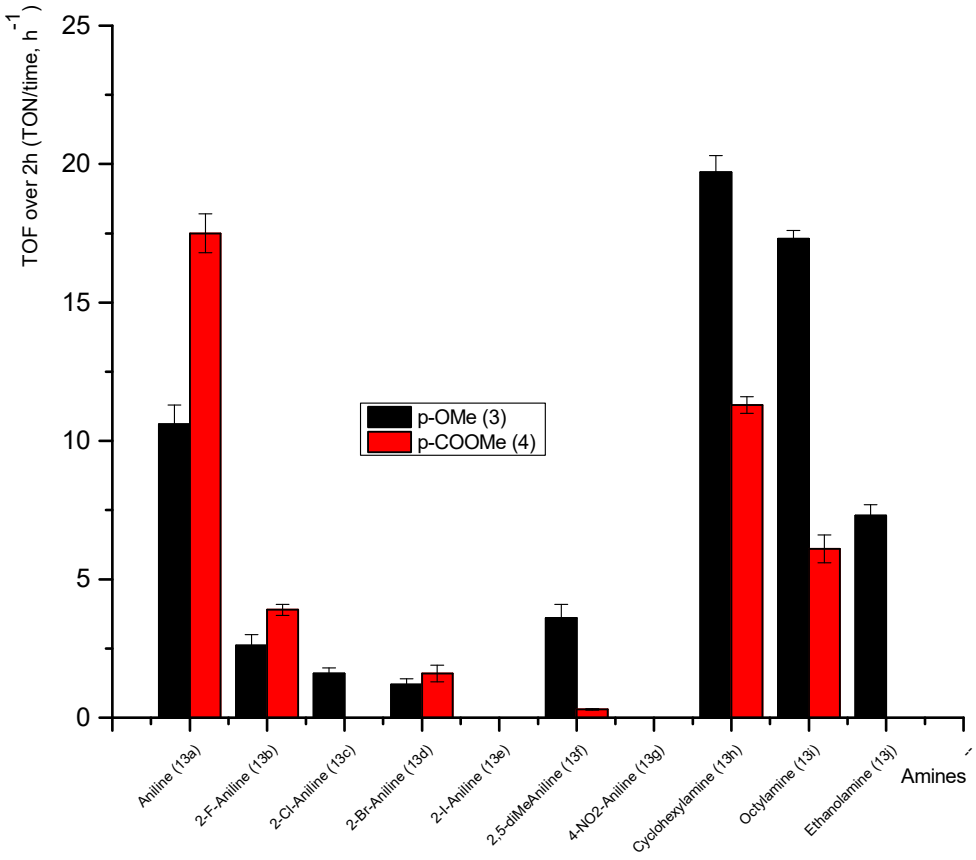

Figure A3.31 Plot of the TOF (TON/time, h^{-1}) for the hydroamination of methacrylonitrile (14b) catalyzed by **3** and **4** for the mono-addition product over 2 h.

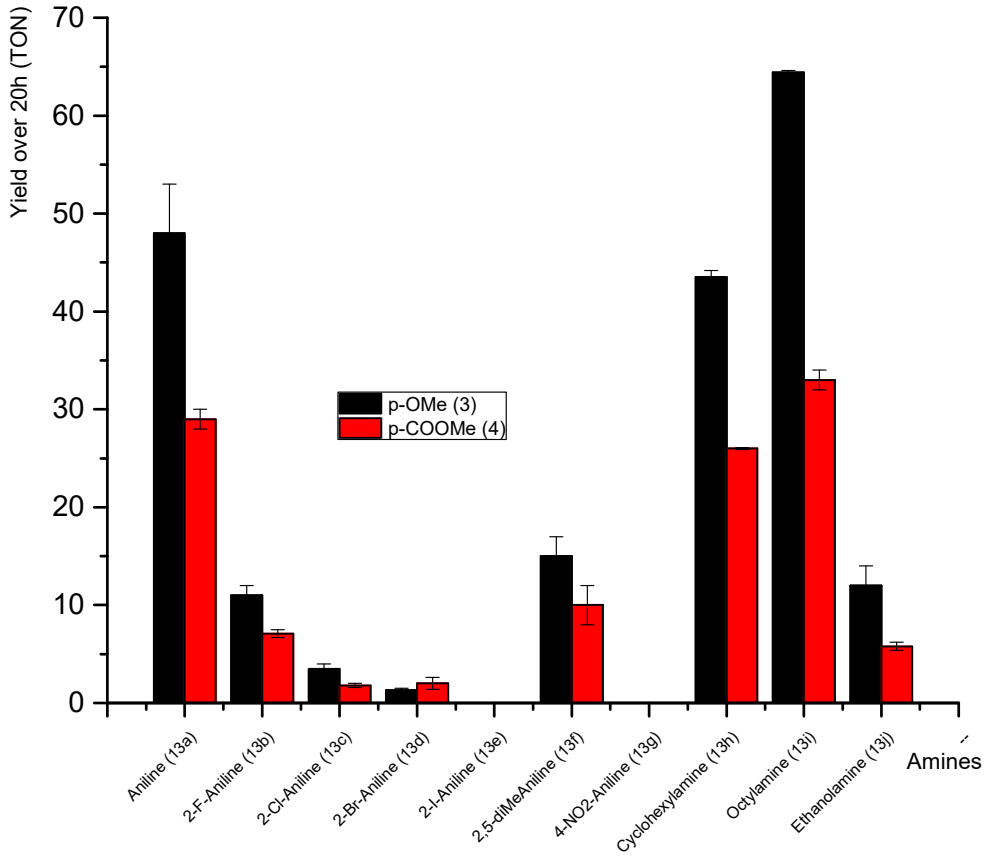

Figure A3.32 Plot of the yield (TON) for the hydroamination of crotonitrile (14a) catalyzed by **3** and **4** for the mono-addition product over 20 h.

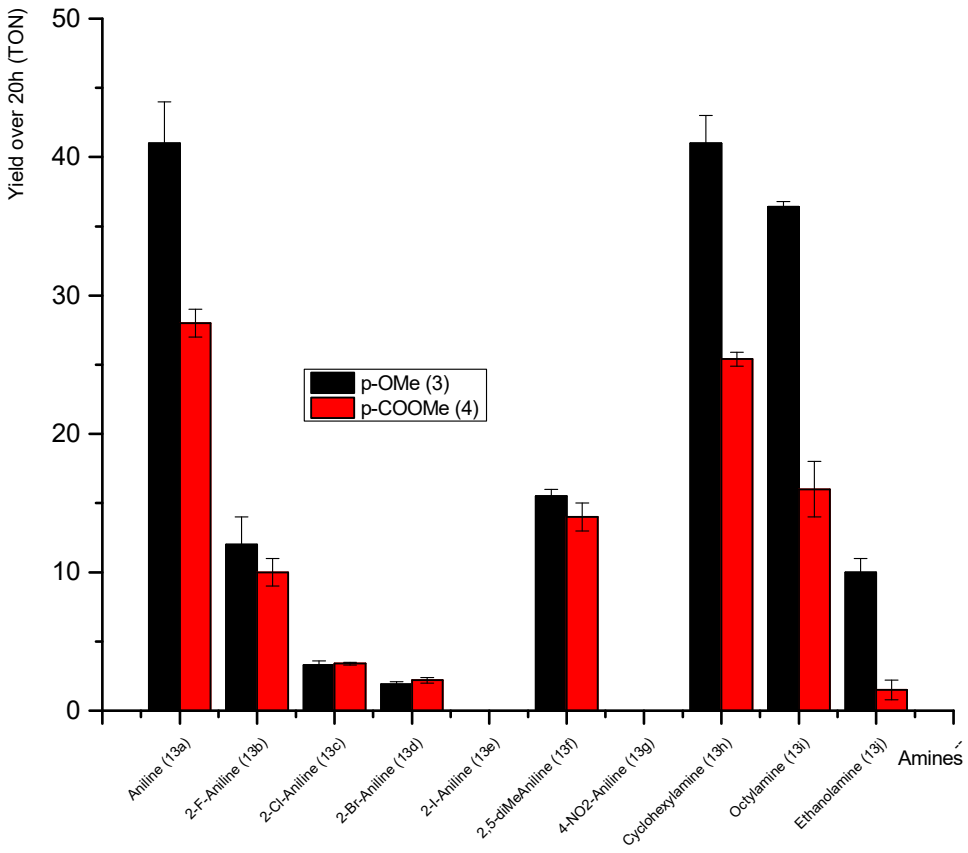

Figure A3.33 Plot of the yield (TON) for the hydroamination of methacrylonitrile (14b) catalyzed by **3** and **4** for the mono-addition product over 20 h.

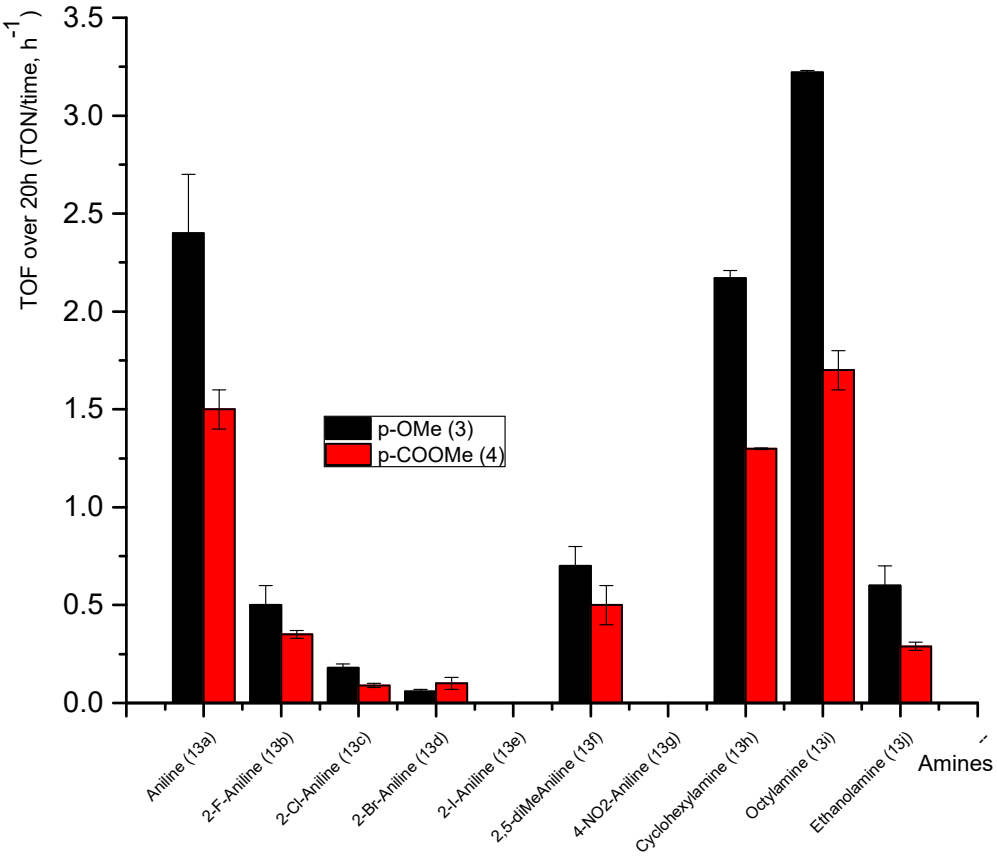

Figure A3.34 Plot of the TOF (TON/time, h^{-1}) for the hydroamination of crotonitrile (14a) catalyzed by **3** and **4** for the mono-addition product over 20 h.

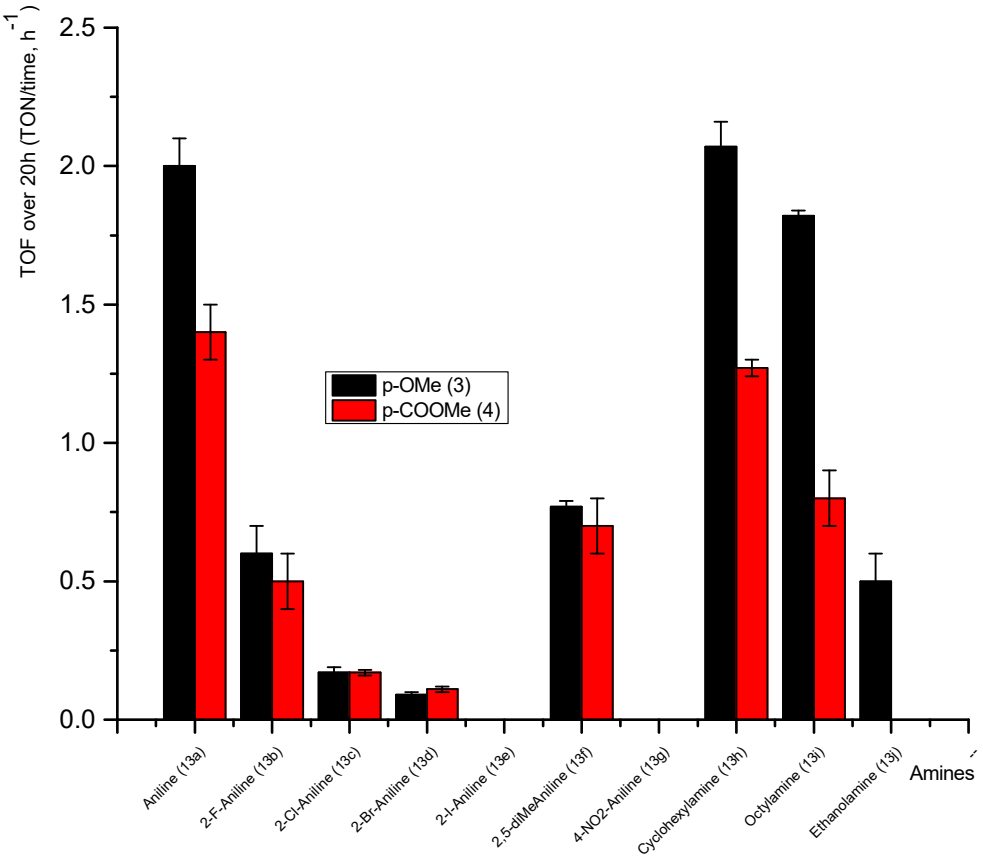

Figure A3.35 Plot of the TOF (TON/time, h^{-1}) for the hydroamination of methacrylonitrile (14b) catalyzed by **3** and **4** for the mono-addition product over 20 h.

Table A3.3 Results of the single addition product from the hydroamination reaction of crotonitrile (14a) catalyzed by complexes **3** and **4** over 2 h.

ENTRY	SUBSTRATE	PRODUCT	CATALYST	TON[a] (Yield, %)	TOF[a] [h^{-1}]
1	**13a**	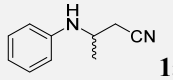 **15a**	**3**	28,6 ± 0,6	14,3 ± 0,3
2			**4**	40 ± 1	20,0 ± 0,7
3	**13b**	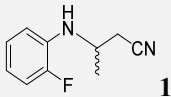 **15b**	**3**	4,9 ± 0,1	2,43 ± 0,03
4			**4**	9 ± 2	4 ± 1
5	**13c**	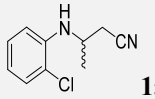 **15c**	**3**	2,6 ± 0,5	1,3 ± 0,3
6			**4**	1,3 ± 0,2	0,7 ± 0,1
7	**13d**	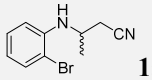 **15d**	**3**	2,0 ± 0,1	1,0 ± 0,1
8			**4**	3,9 ± 0,4	2,0 ± 0,2
9	**13e**	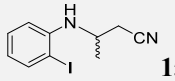 **15e**	**3**	0	0
10			**4**	0	0
11	**13f**	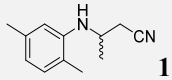 **15f**	**3**	1,1 ± 0,1	0,56 ± 0,04
12			**4**	4,8 ± 0,3	2,4 ± 0,2
13	**13g**	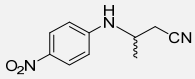 **15g**	**3**	0	0
14			**4**	0	0
15	**13h**	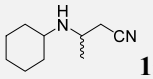 **15h**	**3**	36,4 ± 0,6	18,2 ± 0,3
16			**4**	23,9 ± 0,6	11,9 ± 0,3
17	**13i**	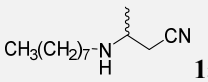 **15i**	**3**	56,1 ± 0,6	28,0 ± 0,3
18			**4**	28,2 ± 0,8	14,1 ± 0,4
19	**13j**	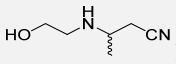 **15j**	**3**	18 ± 1	9,1 ± 0,7
20			**4**	6,8 ± 0,1	3,4 ± 0,1

a) TON and TOF are the average of three experiments under the same conditions.

Table A3.4 Results of the single addition product from the hydroamination reaction of crotonitrile (14a) catalyzed by complexes **3** and **4** over 20 h.

ENTRY	SUBSTRATE	PRODUCT	CATALYST	TON[a] (Yield, %)	TOF[a] [h^{-1}]
1	13a	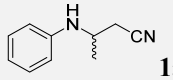 15a	3	48 ± 5	2,4 ± 0,3
2			4	29 ± 1	1,5 ± 0,1
3	13b	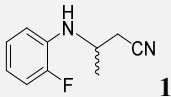 15b	3	11 ± 1	0,5 ± 0,1
4			4	7,1 ± 0,4	0,35 ± 0,02
5	13c	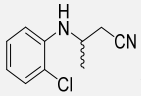 15c	3	3,5 ± 0,5	0,18 ± 0,02
6			4	1,8 ± 0,2	0,09 ± 0,01
7	13d	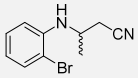 15d	3	1,3 ± 0,2	0,06 ± 0,01
8			4	2,0 ± 0,6	0,09 ± 0,03
9	13e	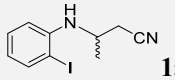 15e	3	0	0
10			4	0	0
11	13f	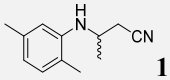 15f	3	15 ± 2	0,7 ± 0,1
12			4	10 ± 2	0,5 ± 0,1
13	13g	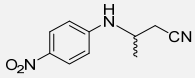 15g	3	0	0
14			4	0	0
15	13h	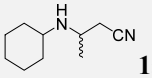 15h	3	43,5 ± 0,7	2,17 ± 0,04
16			4	26 ± 0,1	1,299 ± 0,004
17	13i	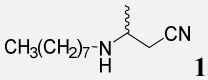 15i	3	64,4 ± 0,2	3,22 ± 0,01
18			4	33 ± 1	1,7 ± 0,1
19	13j	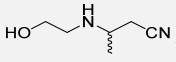 15j	3	12 ± 2	0,6 ± 0,1
20			4	5,8 ± 0,4	0,29 ± 0,02

a) TON and TOF are the average of three experiments under the same conditions.

Table A3.5 Formation of the double addition products from the hydroamination reaction of crotonitrile (14a) catalyzed by complexes **3** and **4** over 2 h.

ENTRY	SUBSTRATE	PRODUCT	CATALYST	TON[a] (Yield, %)	TOF[a] [h^{-1}]
1	13a	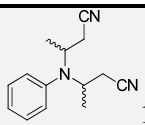 **15k**	3	0	0
2			4	0	0
3	13b	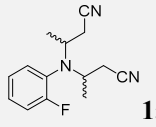 **15l**	3	0	0
4			4	0	0
5	13c	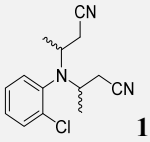 **15m**	3	0	0
6			4	0	0
7	13d	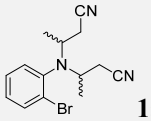 **15n**	3	0	0
8			4	0	0
9	13e	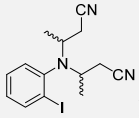 **15o**	3	0	0
10			4	0	0
11	13f	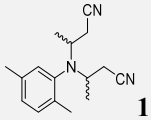 **15p**	3	0	0
12			4	0	0
13	13g	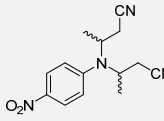 **15q**	3	0	0
14			4	0	0
15	13h	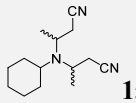 **15r**	3	0	0
16			4	0	0
17	13i	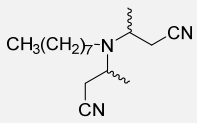 **15s**	3	3,5 ± 0,1	1,73 ± 0,03
18			4	0	0
19	13j	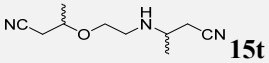 **15t**	3	0	0
20			4	0	0

a) TON and TOF are the average of three experiments under the same conditions.

Table A3.6 Formation of the double addition products from the hydroamination reaction of crotonitrile (14a) catalyzed by complexes **3** and **4** over 20 h.

ENTRY	SUBSTRATE	PRODUCT	CATALYST	TON[a] (Yield, %)	TOF[a] [h^{-1}]
1	13a	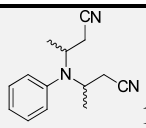 **15k**	3	0	0
2			4	0	0
3	13b	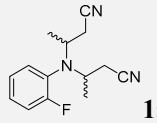 **15l**	3	0	0
4			4	0	0
5	13c	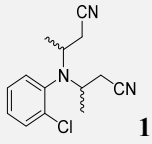 **15m**	3	0	0
6			4	0	0
7	13d	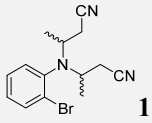 **15n**	3	0	0
8			4	0	0
9	13e	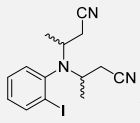 **15o**	3	0	0
10			4	0	0
11	13f	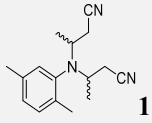 **15p**	3	0	0
12			4	0	0
13	13g	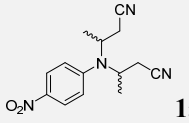 **15q**	3	0	0
14			4	0	0
15	13h	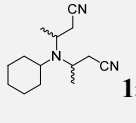 **15r**	3	0	0
16			4	0	0
17	13i	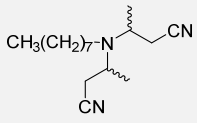 **15s**	3	3,6 ± 0,1	0,178 ± 0,005
18			4	0	0
19	13j	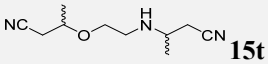 **15t**	3	0	0
20			4	0	0

a) TON and TOF are the average of three experiments under the same conditions.

Table A3.7 Results of the single addition product from the hydroamination reaction of methacrylonitrile (14b) catalyzed by complexes **3** and **4** over 2 h.

ENTRY	SUBSTRATE	PRODUCT	CATALYST	TON[a] (Yield, %)	TOF[a] [h^{-1}]
1	**13a**	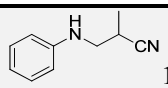 **16a**	**3**	21 ± 1	10,6 ± 0,7
2			**4**	35 ± 1	17,5 ± 0,7
3				38 ± 2 *	19 ± 1 *
4	**13b**	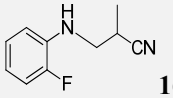 **16b**	**3**	5,2 ± 0,7	2,6 ± 0,4
5			**4**	7,8 ± 0,4	3,9 ± 0,2
6	**13c**	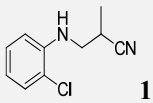 **16c**	**3**	3,2 ± 0,3	1,6 ± 0,2
7			**4**	0	0
8	**13d**	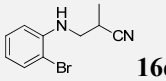 **16d**	**3**	2,4 ± 0,5	1,2 ± 0,2
9			**4**	3,2 ± 0,5	1,6 ± 0,3
10	**13e**	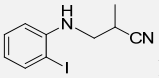 **16e**	**3**	0	0
11			**4**	0	0
12	**13f**	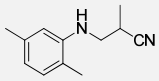 **16f**	**3**	7 ± 1	3,6 ± 0,5
13			**4**	0,6 ± 0,1	0,30 ± 0,03
14	**13g**	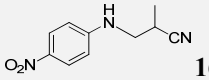 **16g**	**3**	0	0
15			**4**	0	0
16	**13h**	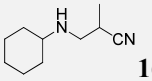 **16h**	**3**	39 ± 1	19,7 ± 0,6
17			**4**	22,7 ± 0,6	11,3 ± 0,3
18	**13i**	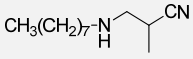 **16i**	**3**	34,6 ± 0,7	17,3 ± 0,3
19			**4**	12 ± 1	6,1 ± 0,5
20	**13j**	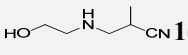 **16j**	**3**	14,6 ± 0,7	7,3 ± 0,4
21			**4**	0	0

a) TON and TOF are the average of three experiments under the same conditions. * In this experiment, 5 mmol of amine was used instead of 1 mmol

Table A3.8 Results of the single addition product from the hydroamination reaction of methacrylonitrile (14b) catalyzed by complexes **3** and **4** over 20 h.

ENTRY	SUBSTRATE	PRODUCT	CATALYST	TON[a] (Yield, %)	TOF[a] [h^{-1}]
1	**13a**	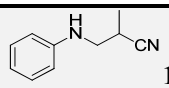 **16a**	**3**	41 ± 3	2,0 ± 0,1
2			**4**	28 ± 1	1,38 ± 0,05
3	**13b**	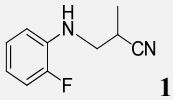 **16b**	**3**	12 ± 2	0,6 ± 0,1
4			**4**	10 ± 1	0,5 ± 0,1
5	**13c**	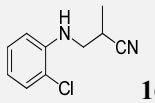 **16c**	**3**	3,3 ± 0,3	0,17 ± 0,02
6			**4**	3,4 ± 0,1	0,17 ± 0,01
7	**13d**	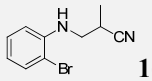 **16d**	**3**	1,9 ± 0,2	0,09 ± 0,01
8			**4**	2,2 ± 0,2	0,11 ± 0,01
9	**13e**	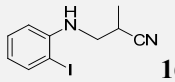 **16e**	**3**	0	0
10			**4**	0	0
11	**13f**	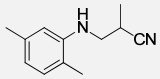 **16f**	**3**	15,5 ± 0,5	0,77 ± 0,02
12			**4**	14 ± 1	0,7 ± 0,1
13	**13g**	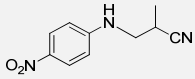 **16g**	**3**	0	0
14			**4**	0	0
15	**13h**	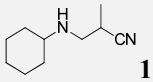 **16h**	**3**	41 ± 2	2,07 ± 0,09
16			**4**	25,4 ± 0,5	1,27 ± 0,03
17	**13i**	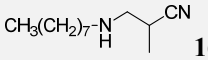 **16i**	**3**	36,4 ± 0,4	1,82 ± 0,02
18			**4**	16 ± 2	0,8 ± 0,1
19	**13j**	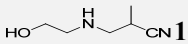 **16j**	**3**	10 ± 1	0,5 ± 0,1
20			**4**	1,5 ± 0,7	0.08 ± 0.04

a) TON and TOF are the average of three experiments under the same conditions.

TableA3.9 Formation of the double addition products from the hydroamination reaction of methacrylonitrile (14b) catalyzed by complexes **3** and **4** over 2 h.

ENTRY	SUBSTRATE	PRODUCT	CATALYST	TON[a] (Yield, %)	TOF[a] [h^{-1}]
1	13a	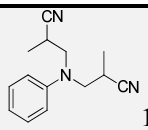 **16k**	3	4,7 ± 0,8	2,3 ± 0,4
2			4	0	0
3	13b	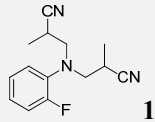 **16l**	3	0	0
4			4	0	0
5	13c	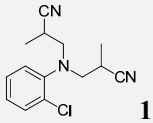 **16m**	3	0	0
6			4	0	0
7	13d	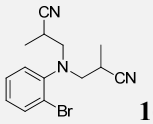 **16n**	3	0	0
8			4	0	0
9	13e	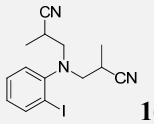 **16o**	3	0	0
10			4	0	0
11	13f	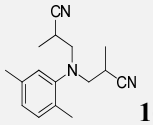 **16p**	3	0	0
12			4	0	0
13	13g	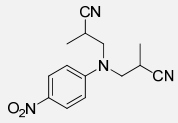 **16q**	3	0	0
14			4	0	0
15	13h	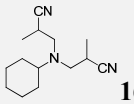 **16r**	3	0	0
16			4	0	0
17	13i	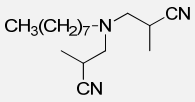 **16s**	3	2,1 ± 0,1	1,04 ± 0,06
18			4	0	0
19	13j	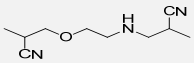 **16t**	3	0	0
20			4	0	0

a) TON and TOF are the average of three experiments under the same conditions.

Table A3.10 Formation of the double addition products from the hydroamination reaction of methacrylonitrile (14b) catalyzed by complexes **3** and **4** over 20 h.

ENTRY	SUBSTRATE	PRODUCT	CATALYST	TON[a] (Yield, %)	TOF[a] [h^{-1}]
1	13a	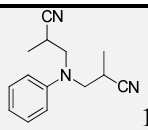 **16k**	3	5 ± 1	0,2 ± 0,1
2			4	0	0
3	13b	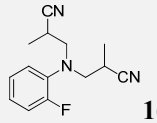 **16l**	3	0	0
4			4	0	0
5	13c	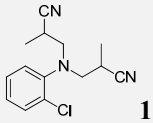 **16m**	3	0	0
6			4	0	0
7	13d	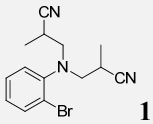 **16n**	3	0	0
8			4	0	0
9	13e	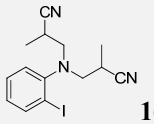 **16o**	3	0	0
10			4	0	0
11	13f	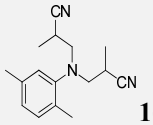 **16p**	3	0	0
12			4	0	0
13	13g	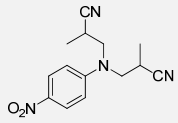 **16q**	3	0	0
14			4	0	0
15	13h	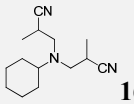 **16r**	3	0	0
16			4	0	0
17	13i	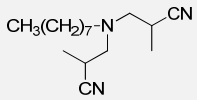 **16s**	3	2.0 ± 0,2	0,101 ± 0,01
18			4	0	0
19	13j	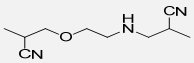 **16t**	3	0	0
20			4	0	0

a) TON and TOF are the average of three experiments under the same conditions.

Table A3.11 Testing the formation of the hydroamination product in the presence of either 14a or 14b and in the absence of catalyst over 2 h.

ENTRY	SUBSTRATE	PRODUCT	NITRILE	TON[a] (Yield, %)	TOF[a] [h^{-1}]
1	13a	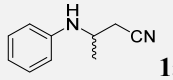 15a	14a	0	0
2			14b	0	0
3	13b	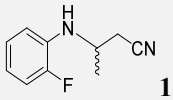 15b	14a	0	0
4			14b	0	0
5	13c	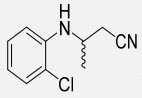 15c	14a	0	0
6			14b	0	0
7	13d	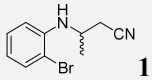 15d	14a	0	0
8			14b	0	0
9	13e	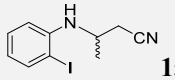 15e	14a	0	0
10			14b	0	0
11	13f	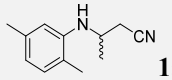 15f	14a	0	0
12			14b	0	0
13	13g	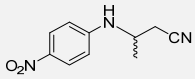 15g	14a	0	0
14			14b	0	0
15	13h	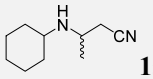 15h	14a	0	0
16			14b	0	0
17	13i	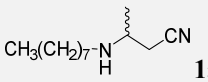 15i	14a	0	0
18			14b	0	0
19	13j	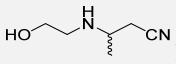 15j	14a	0	0
20			14b	0	0

a) TON and TOF are the average of three experiments under the same conditions.

A3 Annexe du chapitre 4

General procedure for catalytic runs

In a sealable vial was placed the amine or alcohol substrate (1 mmol), the nitrile (1 mmol), NEt_3 (1 mmol), the internal standard (dodecane, 0.1 mmol), and 0.5 mL of a 0.02 M solution of the Ni catalyst (**1-6**) in THF (0.01 mmol), and the resulting mixture was heated at 50 °C for the designated time. A small aliquot of the final mixture was diluted with acetone (~100x) and analyzed by GC/MS. The conversion and yield were determined based on a calibration curve prepared using authentic samples of the anticipated products.

Results of the catalytic experiments

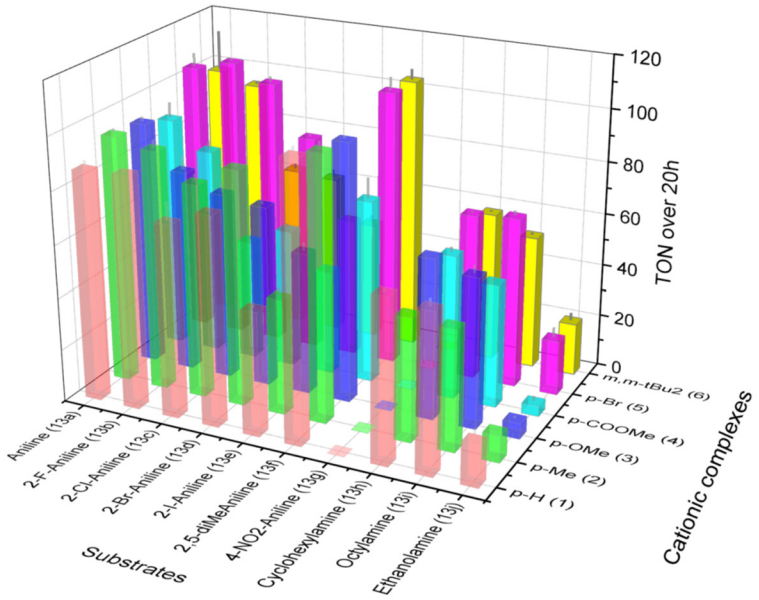

Figure A4.1 Plot of the yield (TON) for the hydroamination of acrylonitrile (14c) catalyzed by **1-6** for the mono-addition product over 20 h.

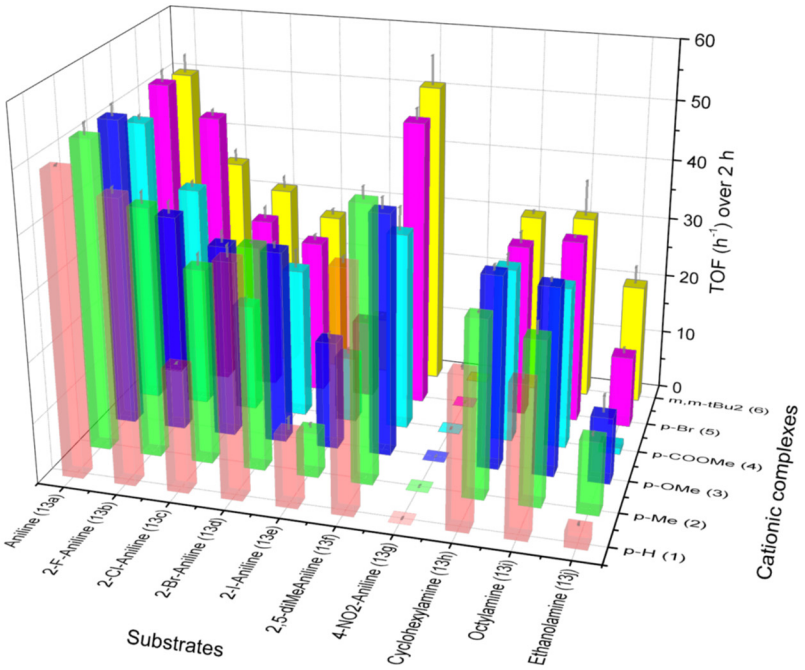

Figure A4.2 Plot of the TOF (TON/time, h^{-1})) for the hydroamination of acrylonitrile (14c) catalyzed by **1-6** for the mono-addition product over 2 h.

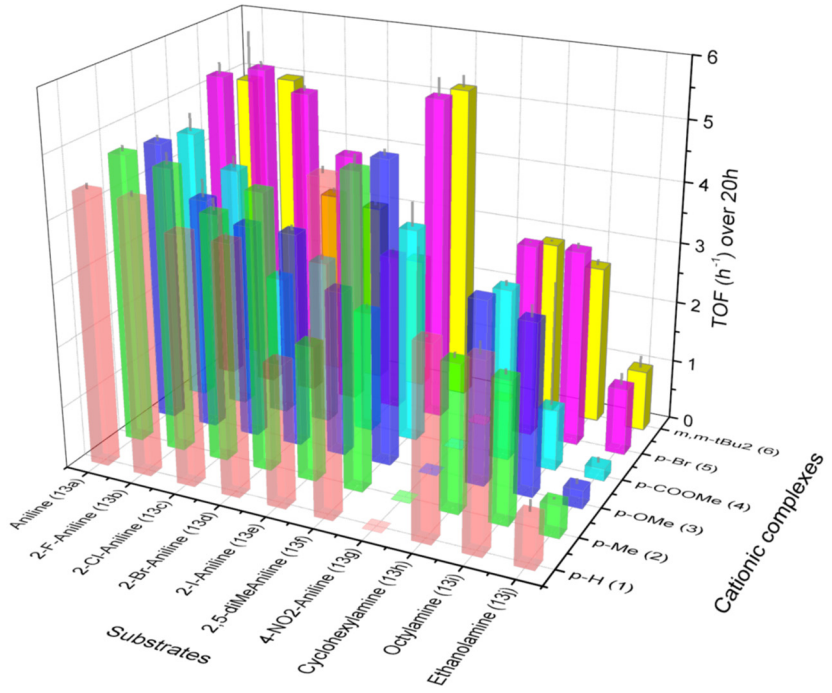

Figure A4.3 Plot of the TOF (TON/time, h^{-1})) for the hydroamination of acrylonitrile (14c) catalyzed by **1-6** for the mono-addition product over 20 h.

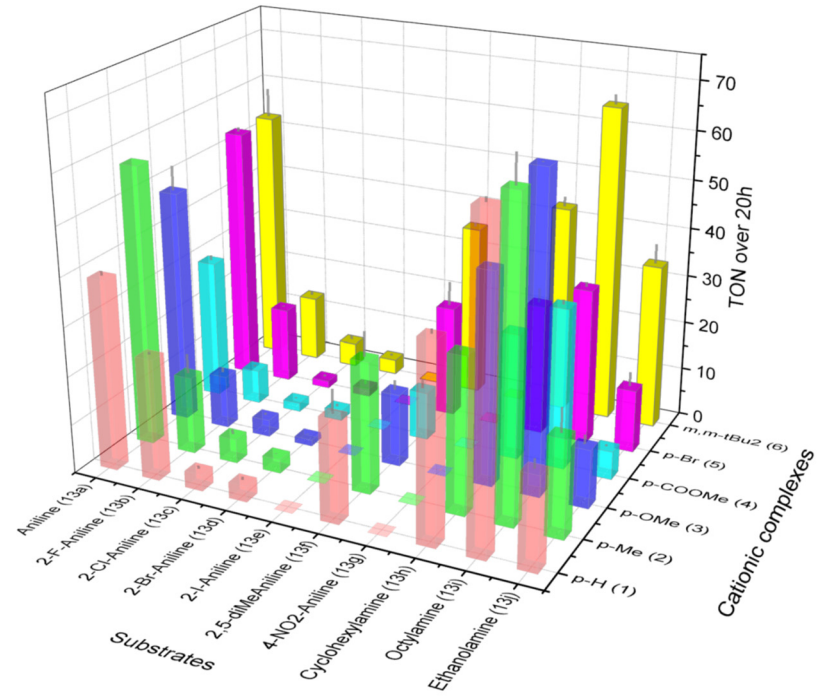

Figure A4.4 Plot of the yield (TON) for the hydroamination of crotonitrile (14a) catalyzed by **1-6** for the mono-addition product over 20 h.

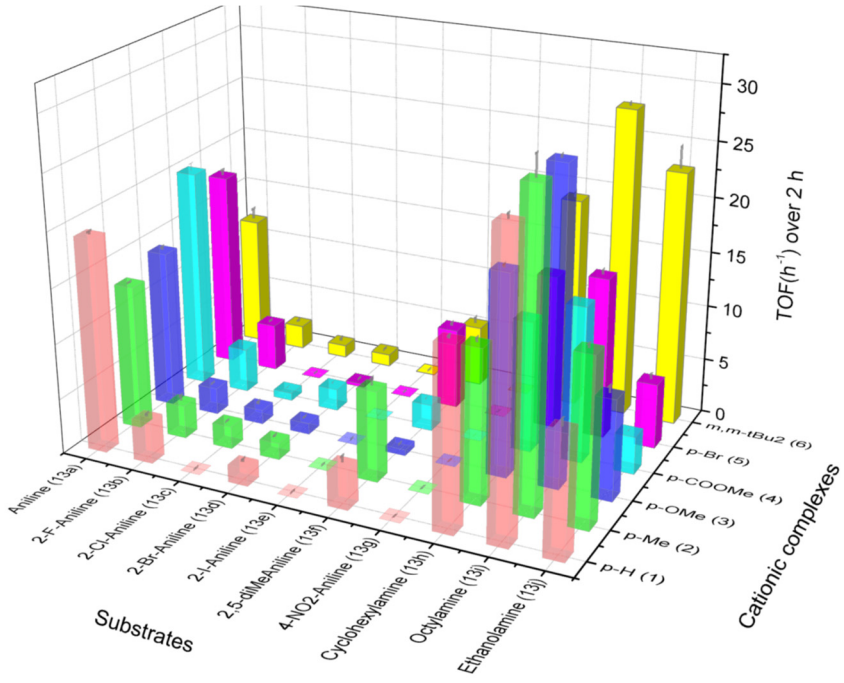

Figure A4.5 Plot of the TOF (TON/time, h^{-1})) for the hydroamination of crotonitrile (14a) catalyzed by **1-6** for the mono-addition product over 2 h.

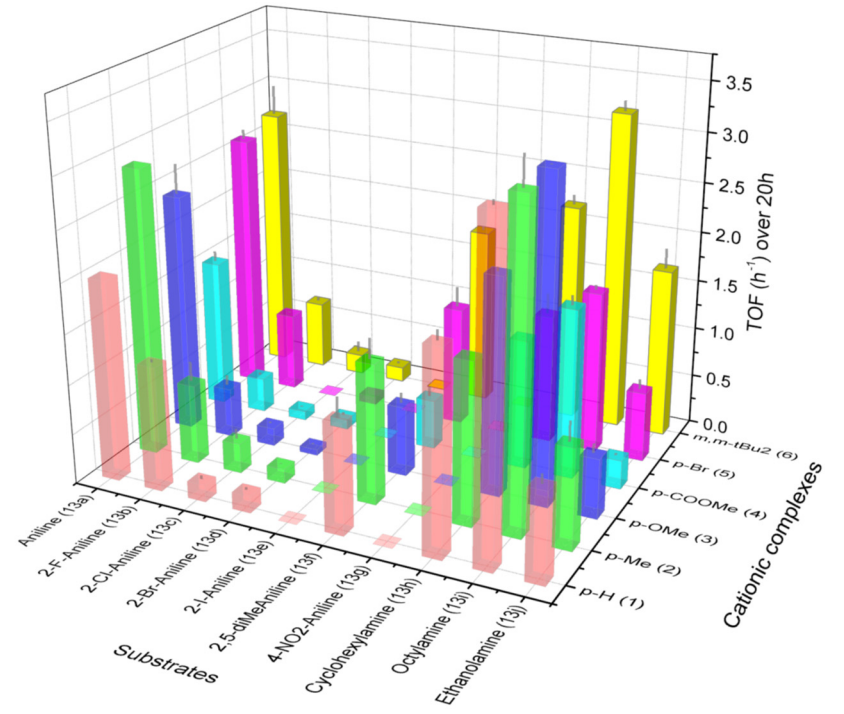

Figure A4.6 Plot of the TOF (TON/time, h^{-1})) for the hydroamination of crotonitrile (14a) catalyzed by **1-6** for the mono-addition product over 20 h.

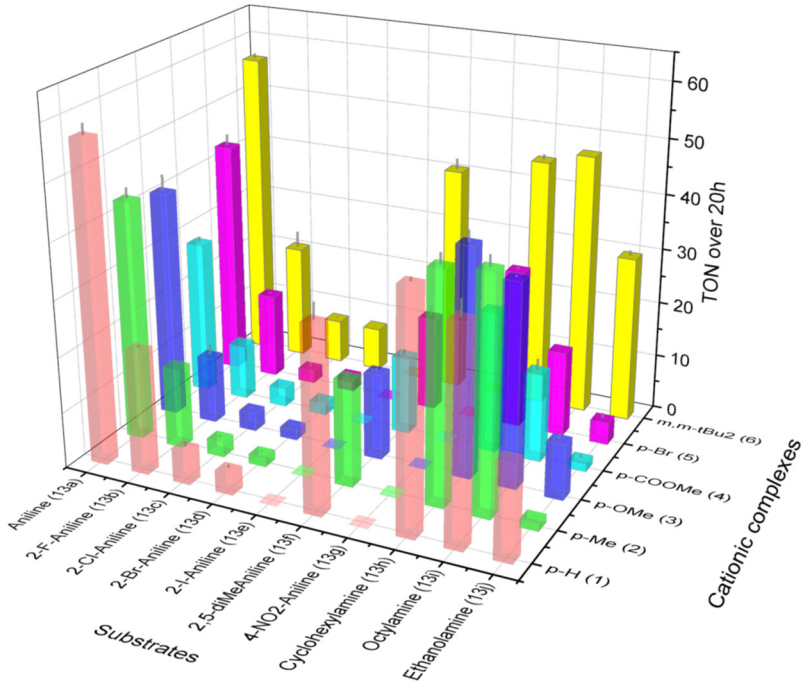

Figure A4.7 Plot of the yield (TON) for the hydroamination of methacrylonitrile (14b) catalyzed by **1-6** for the mono-addition product over 20 h.

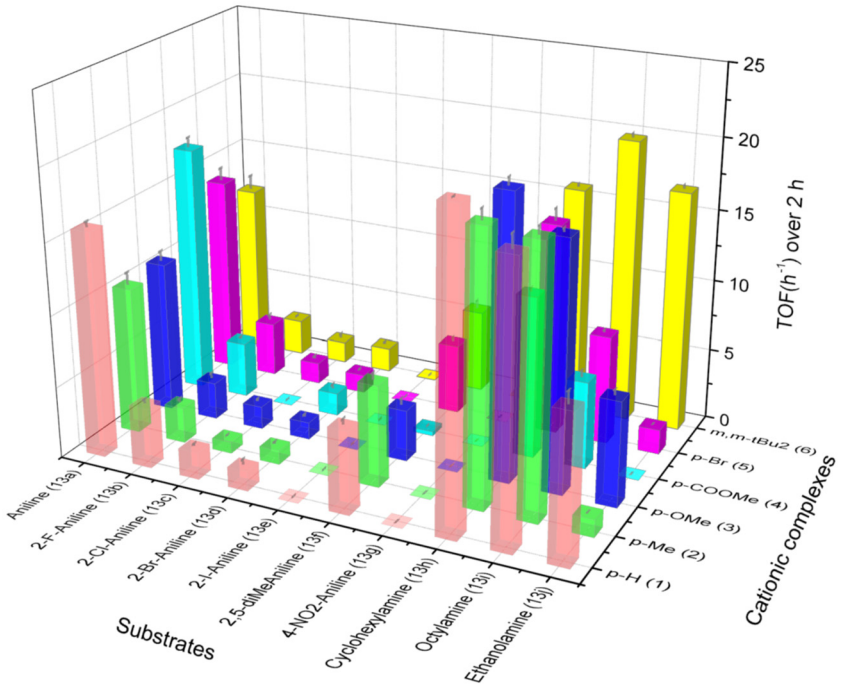

Figure A4.8 Plot of the TOF (TON/time, h^{-1})) for the hydroamination of methacrylonitrile (14b) catalyzed by **1-6** for the mono-addition product over 2 h.

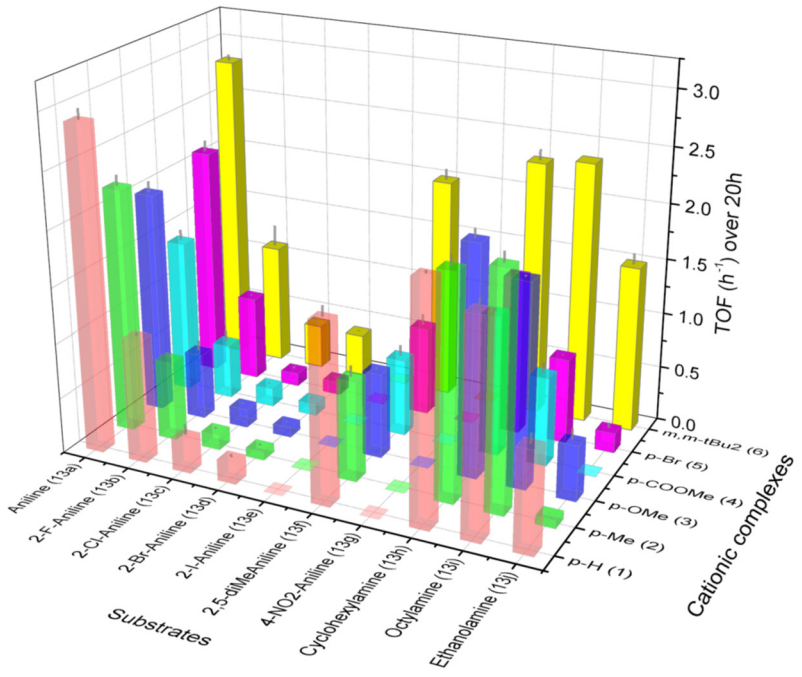

Figure A4.9 Plot of the TOF (TON/time, h^{-1})) for the hydroamination of methacrylonitrile (14b) catalyzed by **1-6** for the mono-addition product over 20 h.

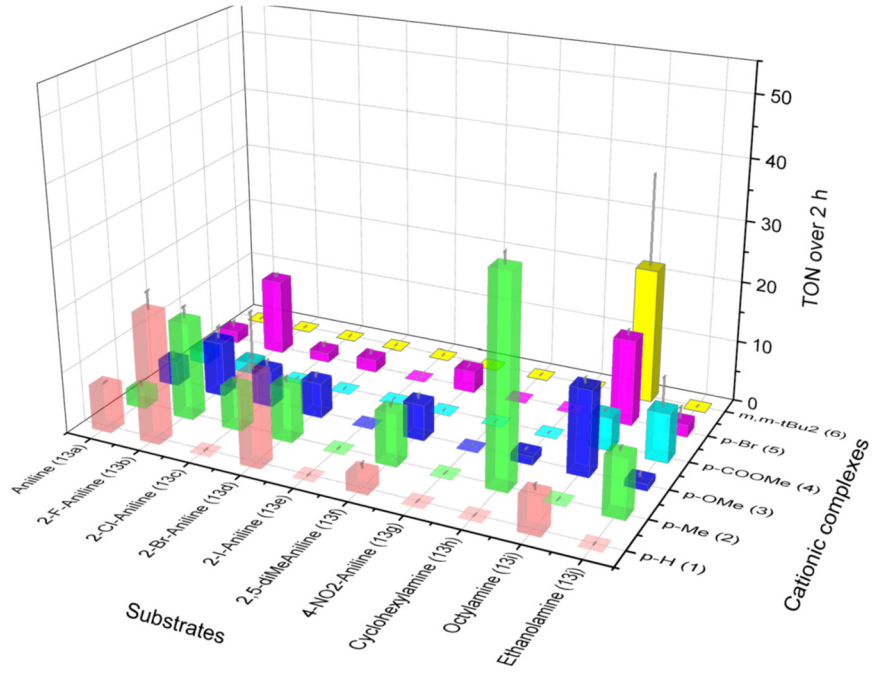

Figure A4.10 Plot of the yield (TON) for the hydroamination of acrylonitrile (14c) catalyzed by **1-6** for the double-addition product over 2 h.

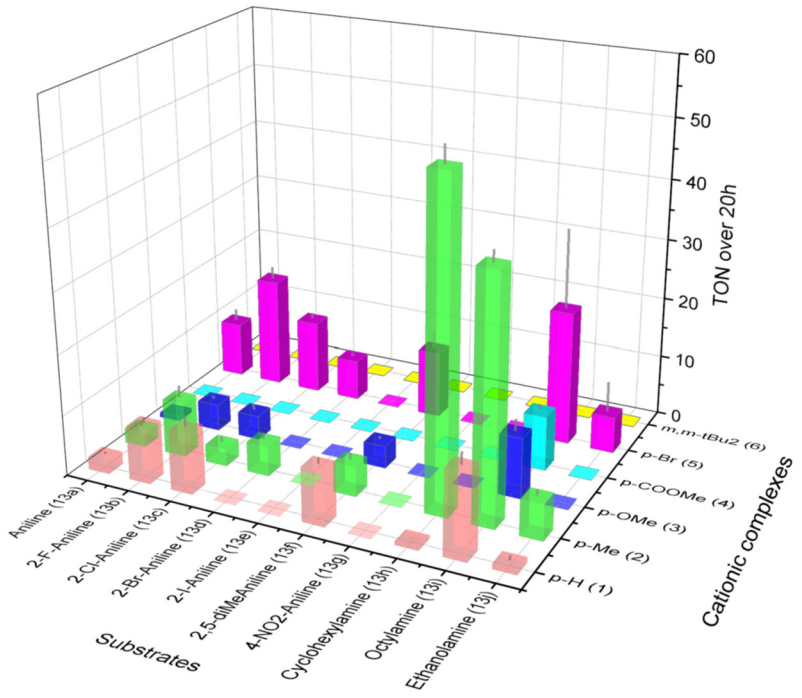

Figure A4.11 Plot of the yield (TON) for the hydroamination of acrylonitrile (14c) catalyzed by **1-6** for the double-addition product over 20 h.

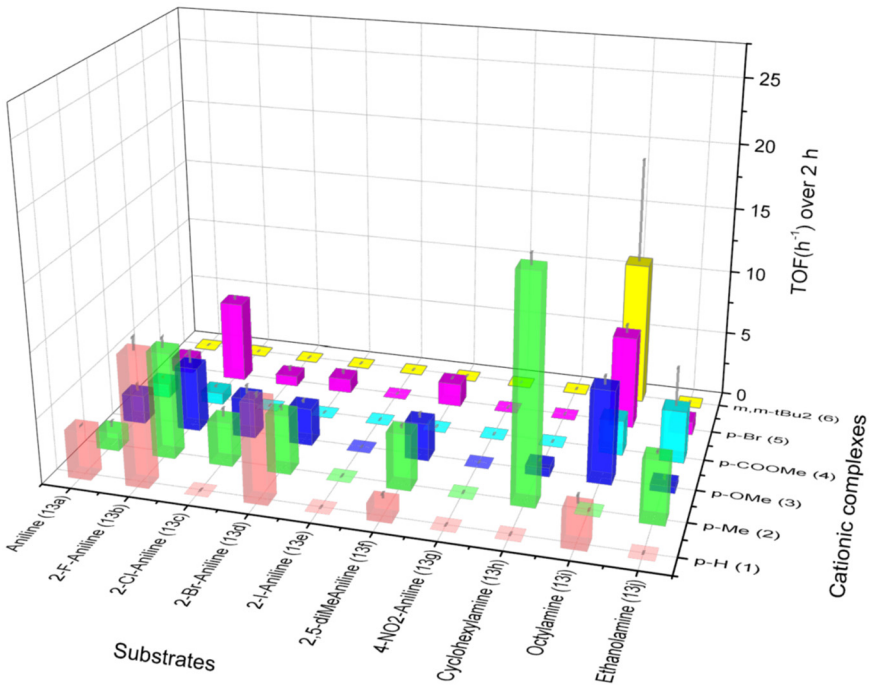

Figure A4.12 Plot of the TOF (TON/time, h^{-1})) for the hydroamination of acrylonitrile (14c) catalyzed by **1-6** for the double-addition product over 2 h.

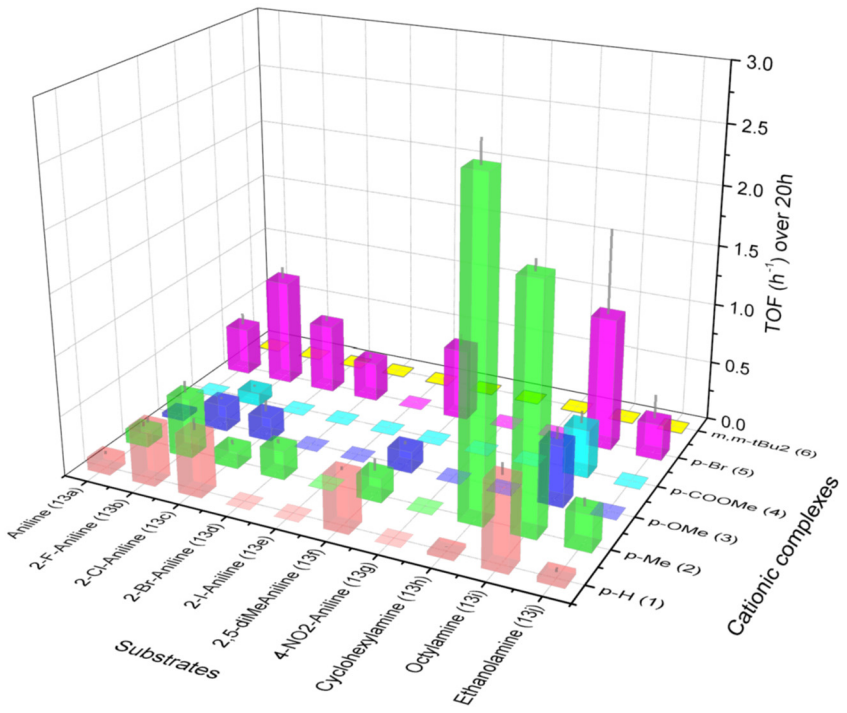

Figure A4.13 Plot of the TOF (TON/time, h^{-1})) for the hydroamination of acrylonitrile (14c) catalyzed by **1-6** for the double-addition product over 20 h.

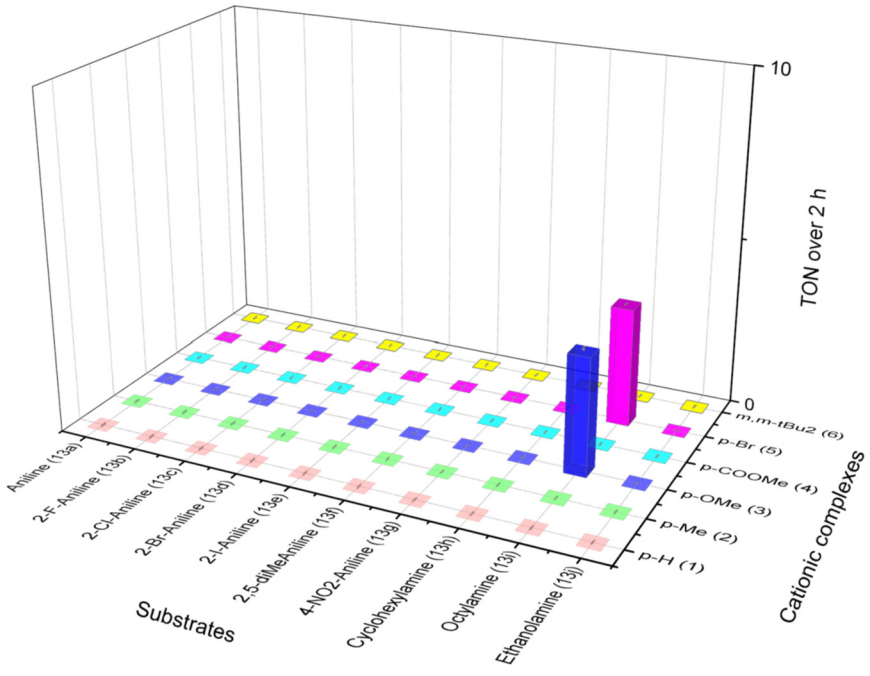

Figure A4.14 Plot of the yield (TON) for the hydroamination of crotonitrile (14a) catalyzed by **1-6** for the double-addition product over 2 h.

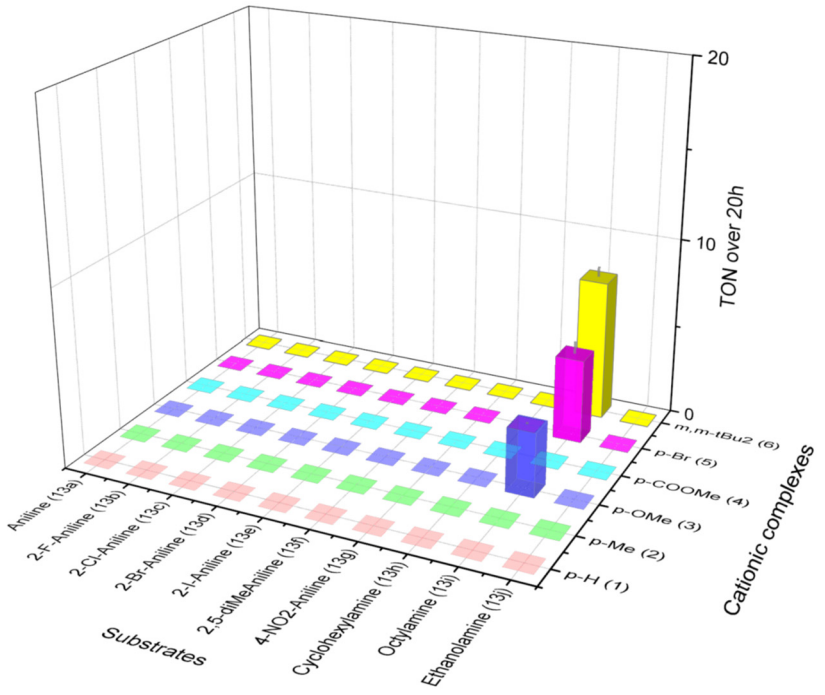

Figure A4.15 Plot of the yield (TON) for the hydroamination of crotonitrile (14a) catalyzed by **1-6** for the double-addition product over 20 h.

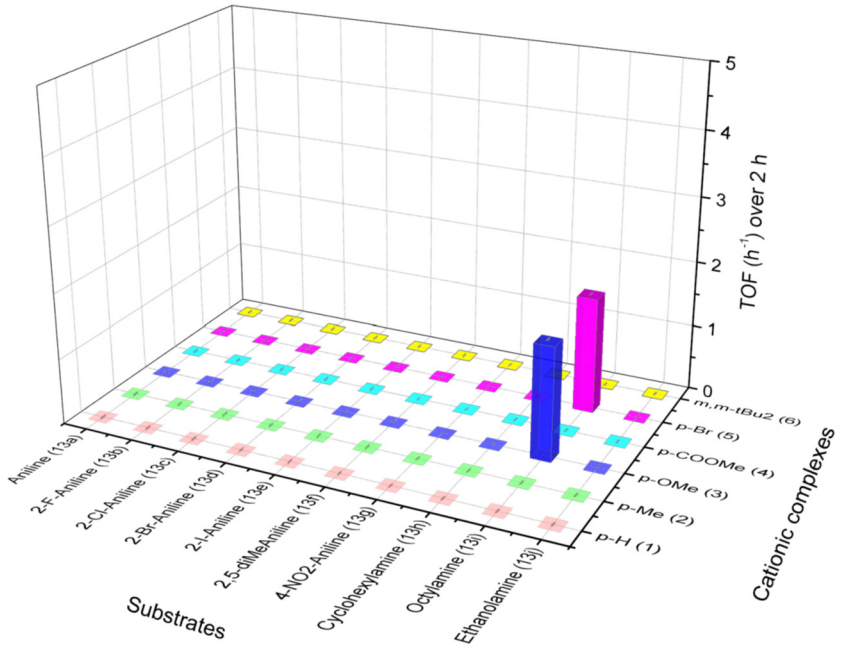

Figure A4.16 Plot of the TOF (TON/time, h^{-1})) for the hydroamination of crotonitrile (14a) catalyzed by **1-6** for the double-addition product over 2 h.

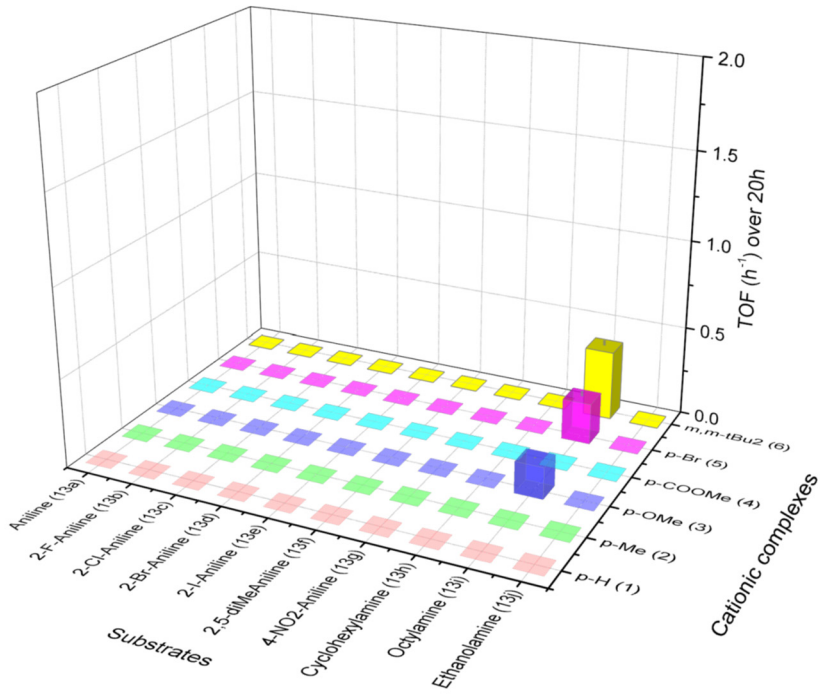

Figure A4.17 Plot of the TOF (TON/time, h^{-1})) for the hydroamination of crotonitrile (14a) catalyzed by **1-6** for the double-addition product over 20 h.

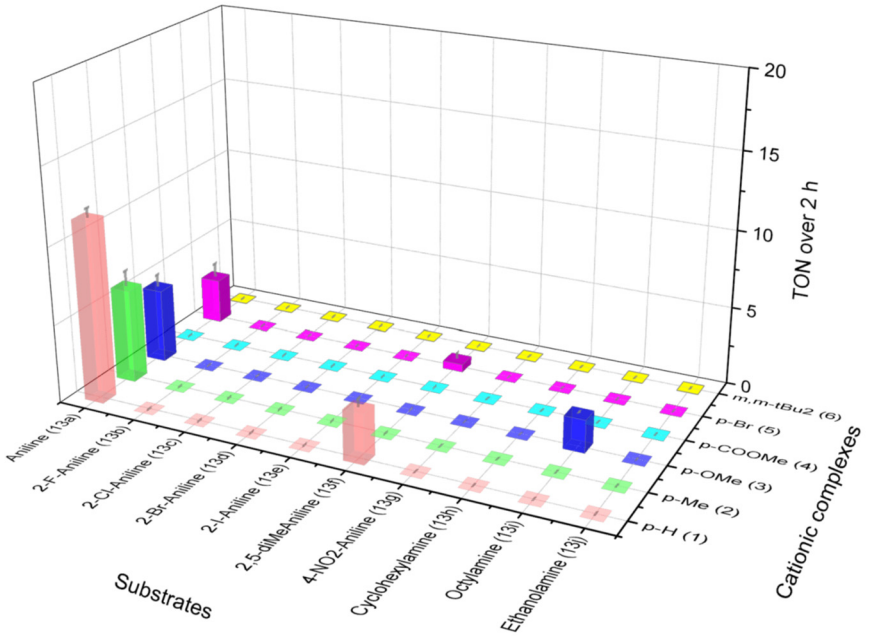

Figure A4.18 Plot of the yield (TON) for the hydroamination of methacrylonitrile (14b) catalyzed by **1-6** for the double-addition product over 2 h.

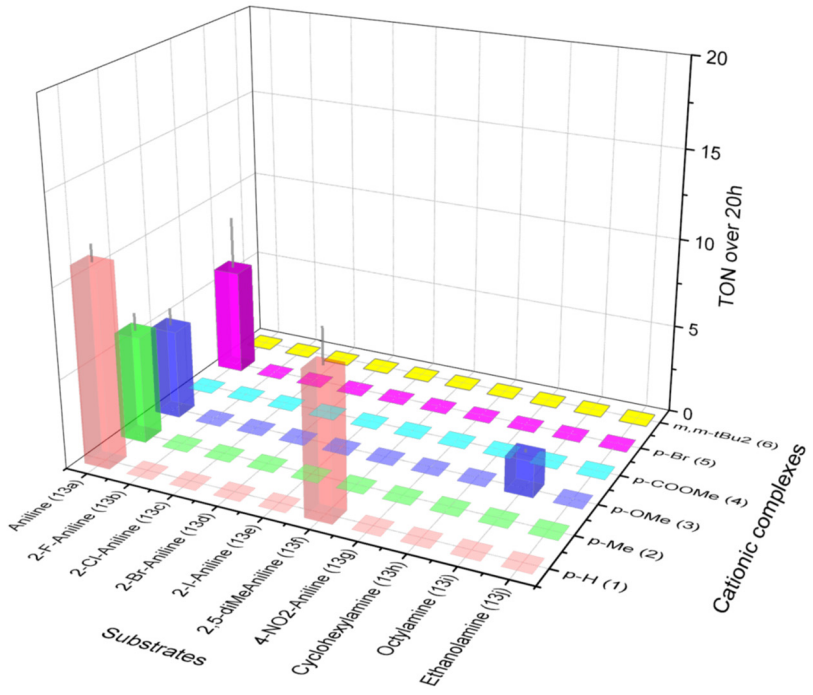

Figure A4.19 Plot of the yield (TON) for the hydroamination of methacrylonitrile (14b) catalyzed by **1-6** for the double-addition product over 20 h.

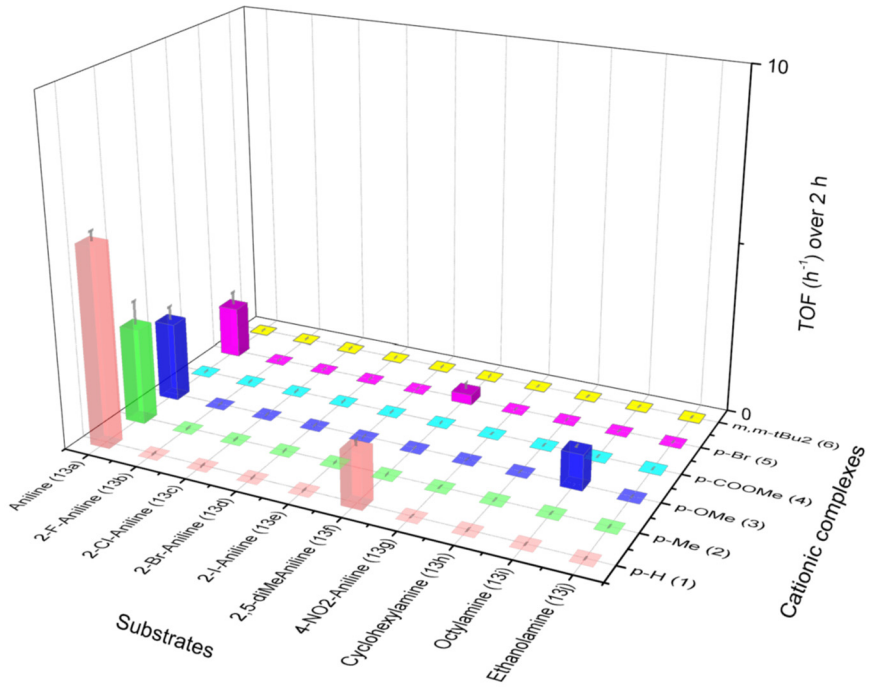

Figure A4.20 Plot of the TOF (TON/time, h^{-1})) for the hydroamination of methacrylonitrile (14b) catalyzed by **1-6** for the double-addition product over 2 h.

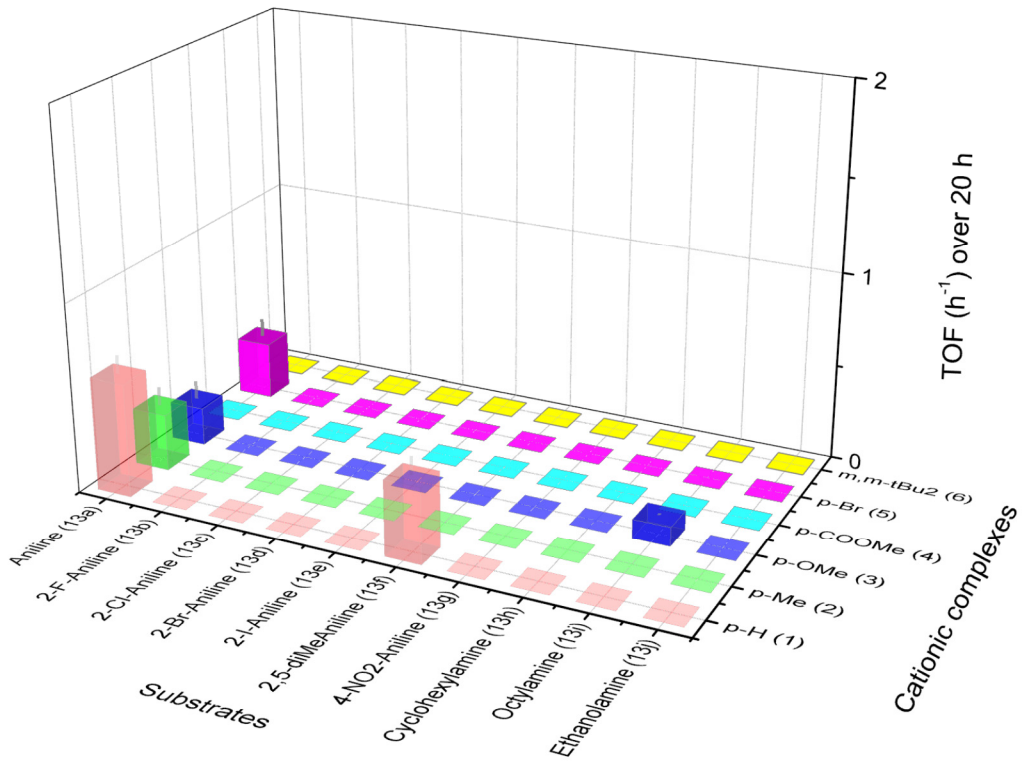

Figure A4.21 Plot of the TOF (TON/time, h^{-1})) for the hydroamination of methacrylonitrile (14b) catalyzed by **1-6** for the double-addition product over 20 h.

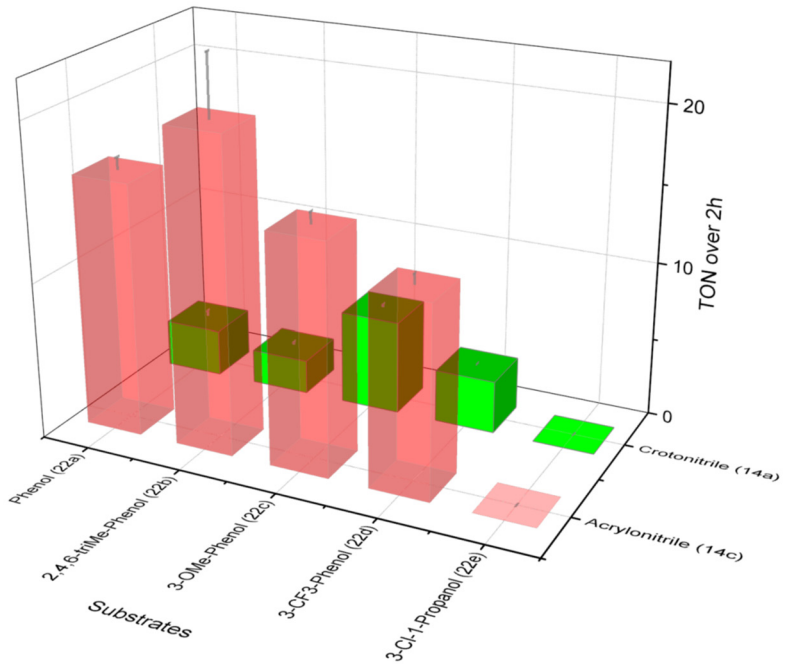

Figure A4.22 Plot of the yield (TON) for the hydroalkoxylation of 14c and 14a catalyzed by complex **2** for mono-addition product over 2 h.

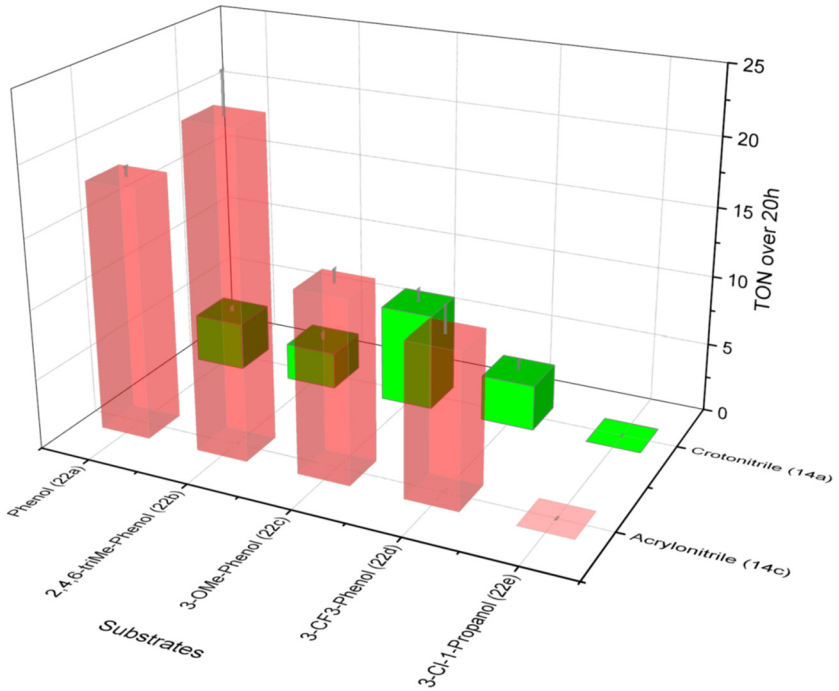

Figure A4.23 Plot of the yield (TON) for the hydroalkoxylation of 14c and 14a catalyzed by complex **2** for mono-addition product over 20 h.

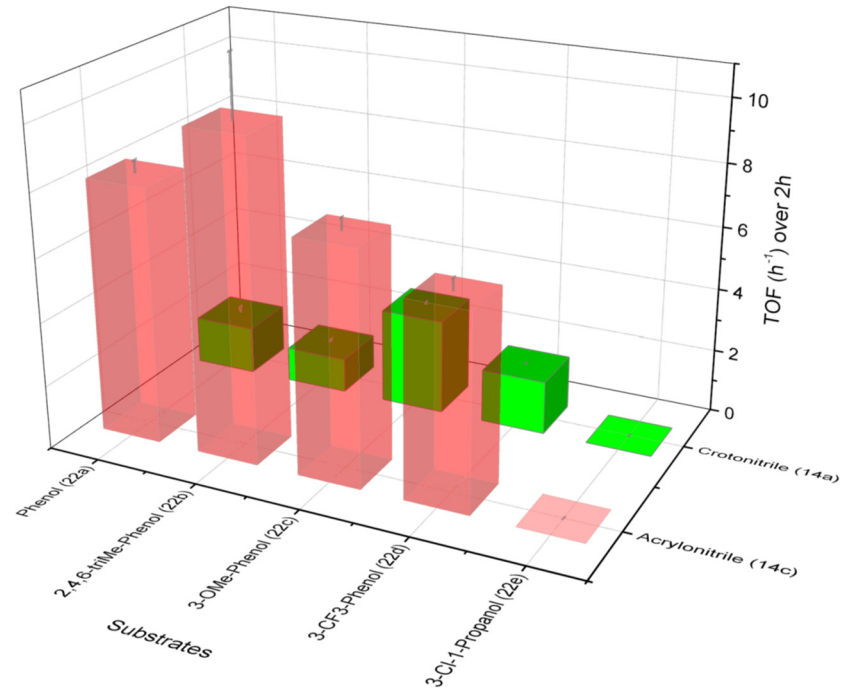

Figure A4.24 Plot of the TOF (TON/time, h^{-1})) for the hydroalkoxylation of 14c and 14a catalyzed by complex **2** for mono-addition product over 2h

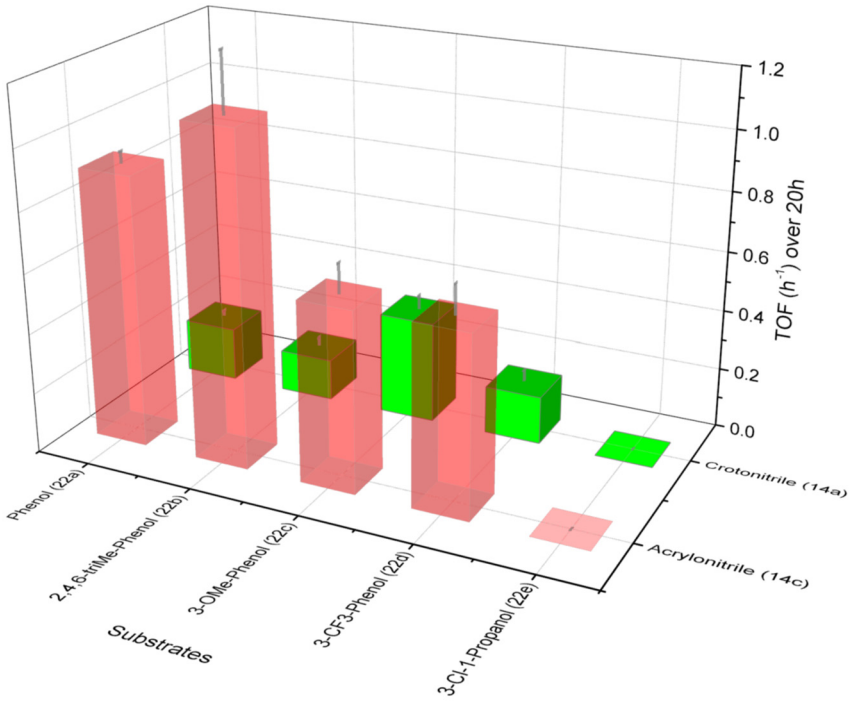

Figure A4.25 Plot of the TOF (TON/time, h^{-1})) for the hydroalkoxylation of 14c and 14a catalyzed by complex **2** for mono-addition product over 20 h.

Table A4.1 Results of the hydroamination of acrylonitrile (14c) catalyzed by complexes **1-6** over 2 h.

Entry	Substrate	Product	Catalyst	Catalyst loading[a] [mol%]	Time	TON[a]	TOF [a] [h^{-1}]
1	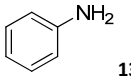 **13a**	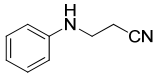 **15a**	**1**	1		98,6 ± 0,6	49,3 ± 0,3
2			**2**			102 ± 3	51 ± 2
3			**3**			103 ± 5	51 ± 2
4			**4**			95 ± 2	47,5 ± 0,8
5			**5**			102 ± 4	51 ± 2
6			**6**			99 ± 6	50 ± 3
7			**4**		5 mins	84 ± 2	1013 ± 26
8			**4**		15 mins	100 ± 2	400 ± 7
9			**4**		30 mins	108 ± 13	215 ± 25
10			**4**		1 h	115 ± 4	115 ± 4
11			**4**	0,5	2 h (20h)	199,3 ± 0,5 (207 ± 4)	99,7 ± 0,2 (10,4 ± 0,2)
12			**4**	0,05	2 h (20h)	13 ± 2 (95 ± 6)	6,5 ± 0,9 (4,8 ± 0,3)
13	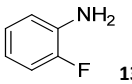 **13b**	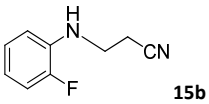 **15b**	**1**	1	2 h	93 ± 3	46 ± 1
14			**2**			81 ± 5	41 ± 2
15			**3**			71 ± 3	36 ± 2
16			**4**			75 ± 2	37 ± 1
17			**5**			91 ± 2	46 ± 1
18			**6**			70 ± 3	35 ± 2
19	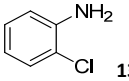 **13c**	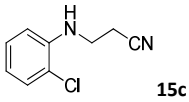 **15c**	**1**	1	2 h	40,5 ± 0,5	20,3 ± 0,3
20			**2**			65 ± 4	32 ± 2
21			**3**			64 ± 5	32 ± 2
22			**4**			35 ± 2	18 ± 1
23			**5**			58 ± 4	29 ± 2
24			**6**			62 ± 4	31 ± 2

25	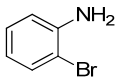 **13d**	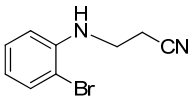 **15d**	**1**	1	2 h	76 ± 3	38 ± 2
26			**2**			72,9 ± 0,8	36,4 ± 0,4
27			**3**			65 ± 3	32 ± 1
28			**4**			50 ± 5	25 ± 3
29			**5**			52 ± 2	26 ± 1
30			**6**			54 ± 3	27 ± 1
31	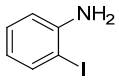 **13e**	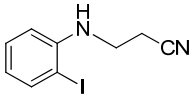 **15e**	**1**	1	2 h	24 ± 4	12 ± 2
32			**2**			15 ± 2	7,4 ± 0,8
33			**3**			36 ± 3	18 ± 1
34			**4**			22 ± 2	11 ± 1
35			**5**			26 ± 1	12,9 ± 0,5
36			**6**			18,7 ± 0,3	9,3 ± 0,2
37	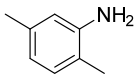 **13f**	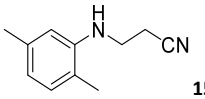 **15f**	**1**	1	2 h	77 ± 3	39 ± 1
38			**2**			91 ± 5	45 ± 2
39			**3**			80 ± 3	40 ± 2
40			**4**			65 ± 7	33 ± 4
41			**5**			96 ± 4	48 ± 2
42			**6**			102 ± 10	51 ± 5
43	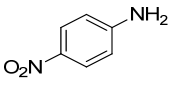 **13g**	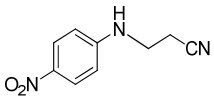 **15g**	**1**	1	2 h	0	0
44			**2**			0	0
45			**3**			0	0
46			**4**			0	0
47			**5**			0	0
48			**6**			0	0
49	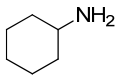 **13h**	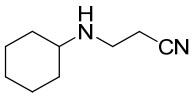 **15h**	**1**	1	2 h	50 ± 1	24,9 ± 0,7
50			**2**			58 ± 1	29,2 ± 0,5
51			**3**			64 ± 3	32 ± 1
52			**4**			59 ± 3	29 ± 2
53			**5**			58 ± 4	29 ± 2
54			**6**			61 ± 1	30,4 ± 0,7

55			**1**			49 ± 3	24,6 ± 0,8
56			**2**			54 ± 2	27 ± 1
57	$CH_3(CH_2)_7NH_2$ **13i**	$CH_3(CH_2)_7$-N(H)-CH_2CH_2CN **15i**	**3**	1	2 h	62 ± 1	31,1 ± 0,7
58			**4**			54 ± 1	26,9 ± 0,9
59			**5**			61,4 ± 0,8	30,7 ± 0,4
60			**6**			62 ± 12	31 ± 6
61			**1**			5 ± 1	2,7 ± 0,5
62			**2**			24 ± 1	12,0 ± 0,6
63	HO-$CH_2CH_2NH_2$ **13j**	HO-CH_2CH_2-N(H)-CH_2CH_2CN **15j**	**3**	1	2 h	21 ± 5	11 ± 3
64			**4**			2,3 ± 0,6	1,1 ± 0,3
65			**5**			24 ± 3	12 ± 1
66			**6**			41 ± 5	20 ± 3

a) TON and TOF are the average of three experiments under the same conditions.

Table A4.2 Results of the hydroamination of acrylonitrile (14c) catalyzed by 1mol% of complexes **1-6** over 20 h.

Entry	Substrate	Product	Catalyst	TON[a] [Yield, %]	TOF [a] [h^{-1}]
1	**13a**	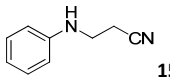 **15a**	**1**	87 ± 3	4,4 ± 0,1
2			**2**	94 ± 2	4,7 ± 0,1
3			**3**	93 ± 2	4,6 ± 0,1
4			**4**	89 ± 6	4,5 ± 0,3
5			**5**	104 ± 5	5,2 ± 0,2
6			**6**	98 ± 15	4,9 ± 0,8
7	**13b**	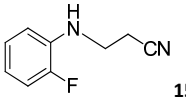 **15b**	**1**	88 ± 1	4,4 ± 0,1
8			**2**	91 ± 3	4,6 ± 0,2
9			**3**	77 ± 5	3,8 ± 0,3
10			**4**	79 ± 3	4,0 ± 0,2
11			**5**	108 ± 1	5,4 ± 0,1
12			**6**	94 ± 1	5,00 ± 0,05
13	**13c**	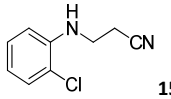 **15c**	**1**	73 ± 7	4,0 ± 0,4
14			**2**	81 ± 3	4 ± 0,2
15			**3**	71 ± 4	3,5 ± 0,2
16			**4**	46 ± 1	2,3 ± 0,1
17			**5**	102 ± 2	5,1 ± 0,1
18			**6**	62 ± 2	3,1 ± 0,1
19	**13d**	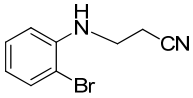 **15d**	**1**	79 ± 2	4 ± 0,1
20			**2**	89 ± 1	4,46 ± 0,05
21			**3**	69 ± 1	3,5 ± 0,1
22			**4**	53 ± 2	2,7 ± 0,1
23			**5**	83,0 ± 0,9	4,17 ± 0,05
24			**6**	61 ± 3	3 ± 0,1
25	**13e**	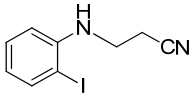 **15e**	**1**	47 ± 2	2,3 ± 0,1
26			**2**	44 ± 3	2,2 ± 0,2
27			**3**	54 ± 3	2,7 ± 0,1
28			**4**	40 ± 1	2 ± 0,1
29			**5**	53 ± 2	2,6 ± 0,1
30			**6**	45 ± 3	2,2 ± 0,2

31			**1**	104 ± 3	5,2 ± 0,1
32			**2**	100 ± 3	5 ± 0,2
33	**13f**	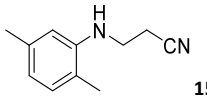 **15f**	**3**	98 ± 1	4,9 ± 0,1
34			**4**	70 ± 8	3,5 ± 0,4
35			**5**	105 ± 5	5,3 ± 0,3
36			**6**	104 ± 4	5,2 ± 0,2
37			**1**	0 ± 0	0 ± 0
38			**2**	0 ± 0	0 ± 0
39	**13g**	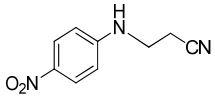 **15g**	**3**	0 ± 0	0 ± 0
40			**4**	0 ± 0	0 ± 0
41			**5**	0 ± 0	0 ± 0
42			**6**	0 ± 0	0 ± 0
43			**1**	62 ± 1	3,09 ± 0,05
44			**2**	47 ± 1	2,4 ± 0,1
45	**13h**	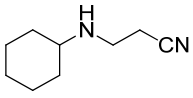 **15h**	**3**	60,7 ± 0,1	3,036 ± 0,004
46			**4**	55 ± 2	2,8 ± 0,1
47			**5**	63,5 ± 0,6	3,17 ± 0,03
48			**6**	57,4 ± 0,7	2,87 ± 0,03
49			**1**	60 ± 3	3,0 ± 0,2
50			**2**	46 ± 1	2,3 ± 0,1
51	**13i**	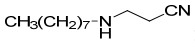 **15i**	**3**	57 ± 3	2,8 ± 0,2
52			**4**	48 ± 1	2,4 ± 0,2
053			**5**	65 ± 2	3,2 ± 0,1
54			**6**	51 ± 1	2,6 ± 0,1
55			**1**	16 ± 4	0,8 ± 0,2
56			**2**	10,3 ± 0,8	0,52 ± 0,04
57	**13j**	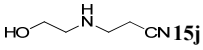 **15j**	**3**	6 ± 1	0,3 ± 0,1
58			**4**	4 ± 2	0,2 ± 0,1
59			**5**	21 ± 4	1,1 ± 0,2
60			**6**	20 ± 3	1,0 ± 0,2

a) TON and TOF are the average of three experiments under the same conditions.

Table A4.3 Results of the hydroamination of crotonitrile (14a) catalyzed by 1mol% of complexes **1-6** over 2 h.

Entry	Substrate	Product	Catalyst	TON [a] [Yield, %]	TOF [a] [h^{-1}]
1	**13a**	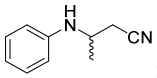 **16a**	**1**	38,7 ± 0,6	19,3 ± 0,3
2			**2**	26,3 ± 0,3	13,1 ± 0,1
3			**3** [b]	28,6 ± 0,6	14,3 ± 0,3
4			**4** [b]	40 ± 1	20,0 ± 0,7
5			**5**	36 ± 1	18,0 ± 0,5
6			**6**	24 ± 2	12 ± 1
7	**13b**	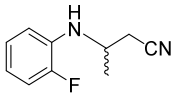 **16b**	**1**	7,6 ± 0,5	3,8 ± 0,3
8			**2**	6,1 ± 0,9	3,0 ± 0,5
9			**3** [b]	4,9 ± 0,1	2,43 ± 0,03
10			**4** [b]	9 ± 2	4 ± 1
11			**5**	8,5 ± 0,2	4,3 ± 0,1
12			**6**	4,5 ± 0,3	2,2 ± 0,2
13	**13c**	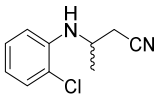 **16c**	**1**	0	0
14			**2**	4,1 ± 0,1	2,04 ± 0,03
15			**3** [b]	2,6 ± 0,5	1,3 ± 0,3
16			**4** [b]	1,3 ± 0,2	0,7 ± 0,1
17			**5**	0,9 ± 0,2	0,4 ± 0,1
18			**6**	2,2 ± 0,5	1,1 ± 0,3
19	**13d**	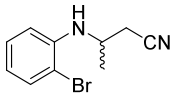 **16d**	**1**	3,2 ± 0,5	1,6 ± 0,3
20			**2**	3,0 ± 0,3	1,5 ± 0,2
21			**3** [b]	2,0 ± 0,1	1,0 ± 0,1
22			**4** [b]	3,9 ± 0,4	2,0 ± 0,2
23			**5**	0,6 ± 0,1	0,3 ± 0,1
24			**6**	2,2 ± 0,2	1,1 ± 0,1
25	**13e**	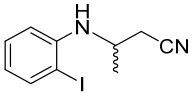 **16e**	**1**	0	0
26			**2**	0	0
27			**3** [b]	0	0
28			**4** [b]	0	0
29			**5**	0	0
30			**6**	0	0

31	**13f**	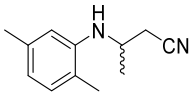 **16f**	**1**	7 ± 1	3,7 ± 0,6
32			**2**	16 ± 1	8,2 ± 0,7
33			**3** [b]	1,1 ± 0,1	0,56 ± 0,04
34			**4** [b]	4,8 ± 0,3	2,4 ± 0,2
35			**5**	14,6 ± 0,7	7,3 ± 0,3
36			**6**	11 ± 1	5,5 ± 0,6
37	**13g**	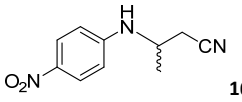 **16g**	**1**	0	0
38			**2**	0	0
39			**3** [b]	0	0
40			**4** [b]	0	0
41			**5**	0	0
42			**6**	0	0
43	**13h**	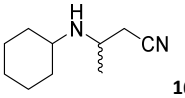 **16h**	**1**	32,5 ± 0,7	16,2 ± 0,3
44			**2**	27,6 ± 0,8	13,8 ± 0,4
45			**3** [b]	36,4 ± 0,6	18,2 ± 0,3
46			**4** [b]	23,9 ± 0,6	11,9 ± 0,3
47			**5**	28,1 ± 0,4	14,0 ± 0,2
48			**6**	38 ± 1	19,1 ± 0,5
49	**13i**	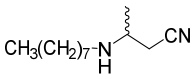 **16i**	**1**	52,9 ± 0,9	26,5 ± 0,5
50			**2**	57 ± 4	28 ± 2
51			**3** [b]	56,1 ± 0,6	28,0 ± 0,3
52			**4** [b]	28,2 ± 0,8	14,1 ± 0,4
53			**5**	29,1 ± 0,8	14,6 ± 0,4
54			**6**	55,7 ± 0,7	27,9 ± 0,3
55	**13j**	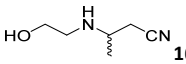 **16j**	**1**	22 ± 1	10,9 ± 0,7
56			**2**	30,3 ± 0,9	15,1 ± 0,4
57			**3** [b]	18 ± 1	9,1 ± 0,7
58			**4** [b]	6,8 ± 0,1	3,4 ± 0,1
59			**5**	12,0 ± 0,9	5,9 ± 0,5
60			**6**	45 ± 4	23 ± 2

a) TON and TOF are the average of three experiments under the same conditions. b) Results for catalysts **3** and **4** have been reported.[99]

Table A4.4 Results of the hydroamination of crotonitrile (14a) catalyzed by 1mol% of complexes **1-6** over 20 h.

Entry	Substrate	Product	Catalyst	TON[a] (Yield, %)	TOF[a] [h^{-1}]
1	**13a**	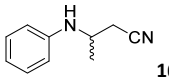 **16a**	**1**	39 ± 1	2,0 ± 0,1
2			**2**	57,4 ± 0,3	2,870 ± 0,002
3			**3**[b]	48 ± 5	2,4 ± 0,3
4			**4**[b]	29 ± 1	1,5 ± 0,1
5			**5**	53 ± 1	2,6 ± 0,1
6			**6**	53 ± 6	2,7 ± 0,3
7	**13b**	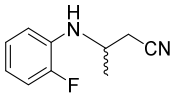 **16b**	**1**	25 ± 0,6	1,25 ± 0,03
8			**2**	16 ± 4	0,8 ± 0,2
9			**3**[b]	11 ± 1	0,5 ± 0,1
10			**4**[b]	7,1 ± 0,4	0,35 ± 0,02
11			**5**	15,7 ± 0,2	0,79 ± 0,01
12			**6**	13,7 ± 0,8	0,69 ± 0,04
13	**13c**	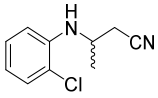 **16c**	**1**	3,4 ± 0,7	0,17 ± 0,04
14			**2**	5 ± 1	0,3 ± 0,1
15			**3**[b]	3,5 ± 0,5	0,18 ± 0,02
16			**4**[b]	1,8 ± 0,2	0,09 ± 0,01
17			**5**	1,5 ± 0,4	0 ± 0
18			**6**	5 ± 1	0,2 ± 0,1
19	**13d**	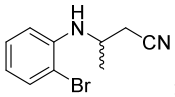 **16d**	**1**	3,3 ± 0,7	0,17 ± 0,03
20			**2**	2,9 ± 0,1	0,143 ± 0,004
21			**3**[b]	1,3 ± 0,2	0,06 ± 0,01
22			**4**[b]	2,0 ± 0,6	0,09 ± 0,03
23			**5**	1,63 ± 0,94	0,082 ± 0,001
24			**6**	3,1 ± 0,5	0,15 ± 0,02
25	**13e**	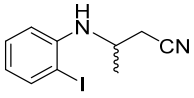 **16e**	**1**	0 ± 0	0 ± 0
26			**2**	0 ± 0	0 ± 0
27			**3**[b]	0 ± 0	0 ± 0
28			**4**[b]	0 ± 0	0 ± 0
29			**5**	0 ± 0	0 ± 0
30			**6**	0 ± 0	0 ± 0

31	**13f**	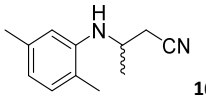 **16f**	**1**	21 ± 5	1,1 ± 0,2
32			**2**	27 ± 5	1,4 ± 0,2
33			**3** [b]	15 ± 2	0,7 ± 0,1
34			**4** [b]	10 ± 2	0,5 ± 0,1
35			**5**	23 ± 5	1,2 ± 0,2
36			**6**	35,7 ± 0,9	1,79 ± 0,04
37	**13g**	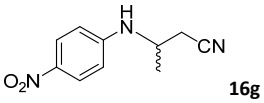 **16g**	**1**	0 ± 0	0 ± 0
38			**2**	0 ± 0	0 ± 0
39			**3** [b]	0 ± 0	0 ± 0
40			**4** [b]	0 ± 0	0 ± 0
41			**5**	0 ± 0	0 ± 0
42			**6**	0 ± 0	0 ± 0
43	**13h**	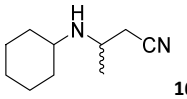 **16h**	**1**	40 ± 1	2,0 ± 0,1
44			**2**	32 ± 0,9	1,62 ± 0,05
45			**3** [b]	43,5 ± 0,7	2,17 ± 0,04
46			**4** [b]	26 ± 0,1	1,299 ± 0,004
47			**5**	27 ± 3	1,3 ± 0,2
48			**6**	43 ± 2	2,2 ± 0,1
49	**13i**	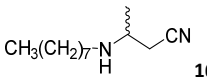 **16i**	**1**	65 ± 1	3,25 ± 0,05
50			**2**	64 ± 6	3,2 ± 0,3
51			**3** [b]	64,4 ± 0,2	3,22 ± 0,01
52			**4** [b]	33 ± 1	1,7 ± 0,1
53			**5**	32 ± 1	1,62 ± 0,05
54			**6**	65 ± 2	3,2 ± 0,1
55	**13j**	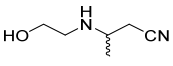 **16j**	**1**	19 ± 2	0,9 ± 0,1
56			**2**	20 ± 5	1,0 ± 0,2
57			**3** [b]	12 ± 2	0,6 ± 0,1
58			**4** [b]	5,8 ± 0,4	0,29 ± 0,02
59			**5**	13 ± 3	0,7 ± 0,1
60			**6**	34 ± 4	1,7 ± 0,2

a) TON and TOF are the average of three experiments under the same conditions. b) Results for catalysts **3** and **4** have been reported.[99]

Table A4.5 Results of the hydroamination of methacrylonitrile (14b) catalyzed by 1mol% of complexes **1-6** over 2 h.

Entry	Substrate	Product	Catalyst	TON [a] (Yield, %)	TOF [a] [h^{-1}]
1	**13a**	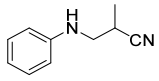 **17a**	**1**	31,4 ± 0,8	15,7 ± 0,4
2			**2**	21 ± 2	10,3 ± 0,9
3			**3** [c]	21 ± 1	10,6 ± 0,7
4			**4** [c]	35 ± 1	17,5 ± 0,7
5			**4** [b]	38 ± 2	19 ± 1
6			**5**	28 ± 2	13,9 ± 0,9
7			**6**	23 ± 2	12 ± 1
8	**13b**	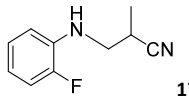 **17b**	**1**	8,4 ± 0,6	4,2 ± 0,3
9			**2**	5,0 ± 0,6	2,5 ± 0,3
10			**3** [c]	5,2 ± 0,7	2,6 ± 0,4
11			**4** [c]	7,8 ± 0,4	3,9 ± 0,2
12			**5**	7,6 ± 0,7	3,8 ± 0,4
13			**6**	5,0 ± 0,3	2,5 ± 0,1
14	**13c**	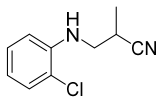 **17c**	**1**	3,7 ± 0,3	1,9 ± 0,2
15			**2**	1,6 ± 0,3	0,8 ± 0,1
16			**3** [c]	3,2 ± 0,3	1,6 ± 0,2
17			**4** [c]	0	0
18			**5**	3,0 ± 0,5	1,5 ± 0,2
19			**6**	3,0 ± 0,7	1,5 ± 0,3
20	**13d**	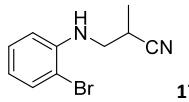 **17d**	**1**	2,8 ± 0,7	1,4 ± 0,4
21			**2**	2,1 ± 0,5	1,0 ± 0,2
22			**3** [c]	2,4 ± 0,5	1,2 ± 0,2
23			**4** [c]	3,2 ± 0,5	1,6 ± 0,3
24			**5**	2,5 ± 0,3	1,3 ± 0,1
25			**6**	3,4 ± 0,4	1,7 ± 0,2
26	**13e**	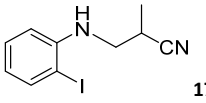 **17e**	**1**	0	0
27			**2**	0	0
28			**3** [c]	0	0
29			**4** [c]	0	0
30			**5**	0	0
31			**6**	0	0

32	**13f**	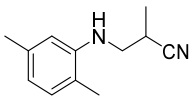 **17f**	**1**	11,7 ± 0,7	5,8 ± 0,4
33			**2**	14 ± 1	7,1 ± 0,5
34			**3** [c]	7 ± 1	3,6 ± 0,5
35			**4** [c]	0,6 ± 0,1	0,30 ± 0,03
36			**5**	9,8 ± 0,7	4,9 ± 0,3
37			**6**	12 ± 1	5,8 ± 0,6
38	**13g**	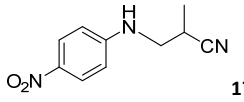 **17g**	**1**	0	0
39			**2**	0	0
40			**3** [c]	0	0
41			**4** [c]	0	0
42			**5**	0	0
43			**6**	0	0
44	**13h**	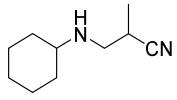 **17h**	**1**	43,0 ± 0,2	21,5 ± 0,1
45			**2**	38 ± 2	18,8 ± 0,8
46			**3** [c]	39 ± 1	19,7 ± 0,6
47			**4** [c]	22,7 ± 0,6	11,3 ± 0,3
48			**5**	30 ± 2	14,8 ± 0,9
49			**6**	31,9 ± 0,5	15,9 ± 0,2
50	**13i**	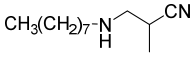 **17i**	**1**	39 ± 2	19 ± 1
51			**2**	37 ± 1	18,5 ± 0,6
52			**3** [c]	34,6 ± 0,7	17,3 ± 0,3
53			**4** [c]	12 ± 1	6,1 ± 0,5
54			**5**	15,5 ± 0,5	7,6 ± 0,2
55			**6**	39,7 ± 0,6	19,8 ± 0,3
56	**13j**	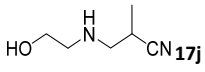 **17j**	**1**	20 ± 2	10,2 ± 0,9
57			**2**	2,4 ± 0,1	1,22 ± 0,04
58			**3** [c]	14,6 ± 0,7	7,3 ± 0,4
59			**4** [c]	0	0
60			**5**	3,4 ± 0,1	1,72 ± 0,04
61			**6**	33,5 ± 0,5	16,8 ± 0,3

a) TON and TOF are the average of three experiments under the same conditions. b) In this experiment, 5 mmol of amine is used. c) Results for catalysts **3** and **4** have been reported.[99]

Table A4.6 Results of the hydroamination of methacrylonitrile (14b) catalyzed by 1mol% of complexes **1-6** over 20 h.

Entry	Substrate	Product	Catalyst	TON[a] (Yield, %)	TOF [a] [h^{-1}]
1	**13a**	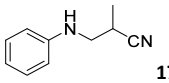 **17a**	**1**	57 ± 2	2,9 ± 0,1
2			**2**	43 ± 2	2,2 ± 0,1
3			**3** [b]	41 ± 3	2,0 ± 0,1
4			**4** [b]	28 ± 1	1,38 ± 0,05
5			**5**	43 ± 2	2,1 ± 0,1
6			**6**	56,6 ± 0,9	2,83 ± 0,05
7	**13b**	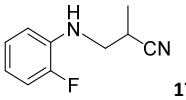 **17b**	**1**	22,1 ± 0,5	1,11 ± 0,03
8			**2**	14,5 ± 0,5	0,72 ± 0,03
9			**3** [b]	12 ± 2	0,6 ± 0,1
10			**4** [b]	10 ± 1	0,5 ± 0,1
11			**5**	15,5 ± 0,2	0,77 ± 0,01
12			**6**	21 ± 3	1,1 ± 0,2
13	**13c**	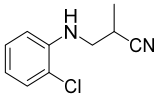 **17c**	**1**	6 ± 1	0,3 ± 0,1
14			**2**	2,8 ± 0,3	0,14 ± 0,02
15			**3** [b]	3,3 ± 0,3	0,17 ± 0,02
16			**4** [b]	3,4 ± 0,1	0,17 ± 0,01
17			**5**	2,4 ± 0,7	0,12 ± 0,03
18			**6**	7,9 ± 0,2	0,40 ± 0,01
19	**13d**	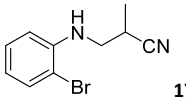 **17d**	**1**	3,9 ± 0,6	0,193 ± 0,03
20			**2**	1,7 ± 0,3	0,08 ± 0,02
21			**3** [b]	1,9 ± 0,2	0,09 ± 0,01
22			**4** [b]	2,2 ± 0,2	0,11 ± 0,01
23			**5**	2,5 ± 0,2	0,12 ± 0,01
24			**6**	7,8 ± 0,1	0,39 ± 0,01
25	**13e**	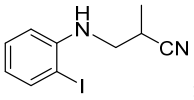 **17e**	**1**	0	0
26			**2**	0	0
27			**3** [b]	0	0
28			**4** [b]	0	0
29			**5**	0	0
30			**6**	0	0

31	**13f**	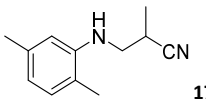 **17f**	**1**	33 ± 3	1,6 ± 0,1
32			**2**	19 ± 1	0,9 ± 0,1
33			**3** [b]	15,5 ± 0,5	0,77 ± 0,02
34			**4** [b]	14 ± 1	0,7 ± 0,1
35			**5**	17 ± 2	0,8 ± 0,1
36			**6**	41 ± 2	2.1 ± 0,1
37	**13g**	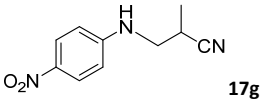 **17g**	**1**	0	0
38			**2**	0	0
39			**3** [b]	0	0
40			**4** [b]	0	0
41			**5**	0	0
42			**6**	0	0
43	**13h**	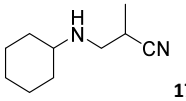 **17h**	**1**	42,2 ± 0,7	2,11 ± 0,03
44			**2**	41 ± 2	2.1 ± 0,1
45			**3** [b]	41 ± 2	2,07 ± 0,09
46			**4** [b]	25,4 ± 0,5	1,27 ± 0,03
47			**5**	28,6 ± 0,4	1,43 ± 0,02
48			**6**	45 ± 1	2,3 ± 0,1
49	**13i**	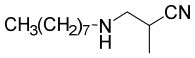 **17i**	**1**	38 ± 3	1,9 ± 0,1
50			**2**	42 ± 2	2,1 ± 0,1
51			**3** [b]	36,4 ± 0,4	1,82 ± 0,02
52			**4** [b]	16 ± 2	0,8 ± 0,1
53			**5**	15,4 ± 0,1	0,77 ± 0,01
54			**6**	47,2 ± 0,1	2,362 ± 0,003
55	**13j**	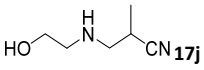 **17j**	**1**	17 ± 1	0,9 ± 0,1
56			**2**	1,5 ± 0,1	0,074 ± 0,003
57			**3** [b]	10 ± 1	0,5 ± 0,1
58			**4** [b]	1,5 ± 0,7	0.08 ± 0.04
59			**5**	4 ± 1	0,18 ± 0,05
60			**6**	30 ± 1	1,5 ± 0,1

a) TON and TOF are the average of three experiments under the same conditions. b) Results for catalysts **3** and **4** have been reported.[99]

Table A4.7 Formation of the double and triple addition products from the hydroamination reaction of 14c catalyzed by 1mol% of complexes **1-6** over 2 h.

Entry	Substrate	Product	Catalyst	TON[a] (Yield, %)	TOF[a] [h^{-1}]
1	**13a**	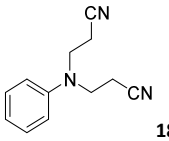 **18a**	**1**	7,4 ± 0,1	3,7 ± 0,1
2			**2**	2,8 ± 0,9	1,4 ± 0,5
3			**3**	4 ± 1	2,2 ± 0,6
4			**4**	2 ± 1	1,1 ± 0,2
5			**5**	2 ± 1	1,14 ± 0,03
6			**6**	0	0
7	**13b**	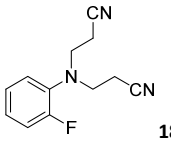 **18b**	**1**	21 ± 3	10 ± 1
8			**2**	16 ± 2	8,2 ± 0,8
9			**3**	9 ± 2	5 ± 1
10			**4**	1,8 ± 0,4	0,9 ± 0,2
11			**5**	12,6 ± 0,6	6,3 ± 0,3
12			**6**	0	0
13	**13c**	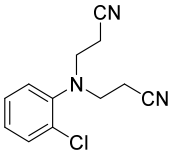 **18c**	**1**	0	0
14			**2**	7 ± 1	3,4 ± 0,7
15			**3**	6 ± 1	3,1 ± 0,7
16			**4**	0	0
17			**5**	1,6 ± 0,8	0,8 ± 0,4
18			**6**	0	0
19	**13d**	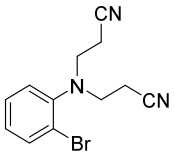 **18d**	**1**	15 ± 9	7,6 ± 0,4
20			**2**	9 ± 0,9	4,5 ± 0,4
21			**3**	5,8 ± 0,7	2,9 ± 0,3
22			**4**	0	0
23			**5**	2,1 ± 0,6	1,1 ± 0,3
24			**6**	0	0
25	**13e**	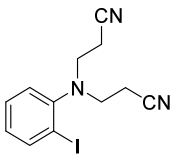 **18e**	**1**	0	0
26			**2**	0	0
27			**3**	0	0
28			**4**	0	0
29			**5**	0	0
30			**6**	0	0

31			**1**	3 ± 1	1,3 ± 0,4
32			**2**	8,6 ± 0,7	4,3 ± 0,3
33	**13f**	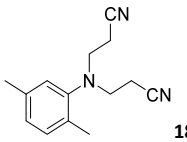 **18f**	**3**	5,9 ± 0,8	2,9 ± 0,4
34			**4**	0	0
35			**5**	3,6 ± 0,2	1,8 ± 0,1
36			**6**	0	0
37			**1**	0	0
38			**2**	0	0
39	**13g**	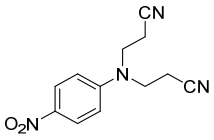 **18g**	**3**	0	0
40			**4**	0	0
41			**5**	0	0
42			**6**	0	0
43			**1**	0	0
44			**2**	34 ± 2	17,2 ± 0,9
45	**13h**	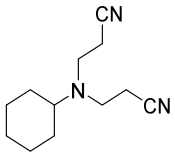 **18h**	**3**	1,4 ± 0,2	0,7 ± 0,1
46			**4**	0	0
47			**5**	0	0
48			**6**	0	0
49			**1**	6 ± 1	2,9 ± 0,7
50			**2**	0	0
51	**13i**	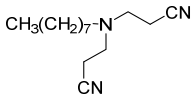 **18i**	**3**	14 ± 1	7,2 ± 0,7
52			**4**	5,4 ± 0,3	2,7 ± 0,2
53			**5**	14 ± 1	7,1 ± 0,7
54			**6**	22 ± 15	11 ± 8
55			**1**	0	0
56			**2**	9,6 ± 0,7	4,8 ± 0,3
57	**13j**	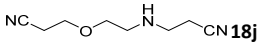 **18j**	**3**	1,1 ± 0,6	0,5 ± 0,3
58			**4**	8 ± 5	4 ± 3
59			**5**	2 ± 2	1 ± 1
60			**6**	0	0
61	**13j**	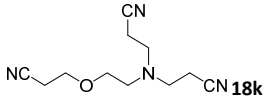 **18k**	**2**	0,6 ± 0,1	0,30 ± 0,06
62			**3**	0,51 ± 0,06	0,26 ± 0,03

a) TON and TOF are the average of three experiments under the same conditions.

Table A4.8 Formation of the double and triple addition products from the hydroamination reaction of 14c catalyzed by 1mol% of complexes **1-6** over 20 h.

Entry	Substrate	Product	Catalyst	TON[a] (Yield, %)	TOF[a] [h^{-1}]
1	**13a**	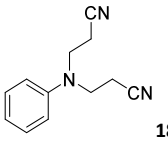 **18a**	**1**	2,1 ± 0,5	0,11 ± 0,03
2			**2**	2,4 ± 0,9	0,12 ± 0,04
3			**3**	0,74 ± 0,02	0,037 ± 0,001
4			**4**	0	0
5			**5**	9 ± 2	0,4 ± 0,1
6			**6**	0	0
7	**13b**	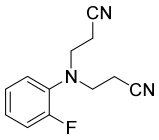 **18b**	**1**	9 ± 1	0,47 ± 0,05
8			**2**	9 ± 2	0,5 ± 0,1
9			**3**	4,4 ± 0,5	0,22 ± 0,02
10			**4**	0	0,11 ± 0,02
11			**5**	18 ± 2	0,9 ± 0,1
12			**6**	0	0
13	**13c**	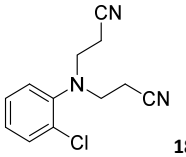 **18c**	**1**	10 ± 2	0,5 ± 0,1
14			**2**	2,9 ± 0,9	0,14 ± 0,04
15			**3**	4 ± 1	0,2 ± 0,1
16			**4**	0	0
17			**5**	12 ± 1	0,58 ± 0,05
18			**6**	0	0
19	**13d**	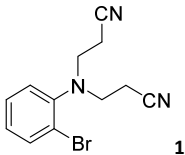 **18d**	**1**	0	0
20			**2**	5 ± 1	0,24 ± 0,04
21			**3**	0	0
22			**4**	0	0
23			**5**	6,7 ± 0,6	0,33 ± 0,03
24			**6**	0	0
25	**13e**	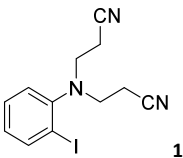 **18e**	**1**	0	0
26			**2**	0	0
27			**3**	0	0
28			**4**	0	0
29			**5**	0	0
30			**6**	0	0

31			**1**	9 ± 1	0,45 ± 0,03
32			**2**	5 ± 1	0,2 ± 0,1
33	**13f**	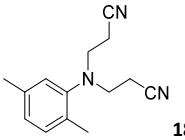 **18f**	**3**	3,7 ± 0,6	0,18 ± 0,03
34			**4**	0	0
35			**5**	11 ± 3	0,6 ± 0,1
36			**6**	0	0
37			**1**	0	0
38			**2**	0	0
39	**13g**	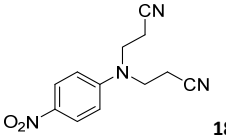 **18g**	**3**	0	0
40			**4**	0	0
41			**5**	0	0
42			**6**	0	0
43			**1**	0,6 ± 0,1	0,031 ± 0,005
44			**2**	53 ± 3	2,7 ± 0,2
45	**13h**	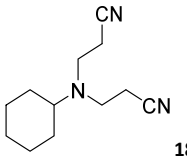 **18h**	**3**	0	0
46			**4**	0	0
47			**5**	0	0
48			**6**	0	0
49			**1**	14 ± 2	0,7 ± 0,1
50			**2**	40 ± 2	2 ± 0,1
51	**13i**	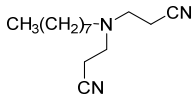 **18i**	**3**	10 ± 2	0,5 ± 0,1
52			**4**	9 ± 1	0,4 ± 0,1
53			**5**	22 ± 13	1,1 ± 0,7
54			**6**	0	0
55			**1**	0,9 ± 0,8	0,047 ± 0,04
56			**2**	6 ± 1	0,3 ± 0,07
57	**13j**	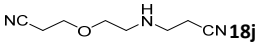 **18j**	**3**	0	0
58			**4**	0	0
59			**5**	6 ± 5	0,3 ± 0,2
60			**6**	0	0
61	**13j**	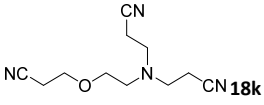 **18k**	**2**	0,35 ± 0,1	0,018 ± 0,005
62			**3**	0,219 ± 0,007	0,0110 ± 0,0003

a) TON and TOF are the average of three experiments under the same conditions.

Table A4.9 Formation of the double addition products from the hydroamination reaction of 14a catalyzed by 1 mol% of complexes **1-6** over 2 h.

Entry	Substrate	Product	Catalyst	TON[a] (Yield, %)	TOF [a] [h^{-1}]
1	13a	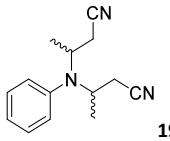 19a	1	0	0
2			2	0	0
3			3 [b]	0	0
4			4 [b]	0	0
5			5	0	0
6			6	0	0
7	13b	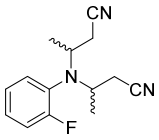 19b	1	0	0
8			2	0	0
9			3 [b]	0	0
10			4 [b]	0	0
11			5	0	0
12			6	0	0
13	13c	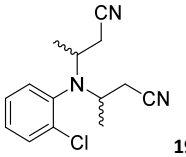 19c	1	0	0
14			2	0	0
15			3 [b]	0	0
16			4 [b]	0	0
17			5	0	0
18			6	0	0
19	13d	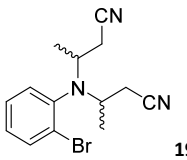 19d	1	0	0
20			2	0	0
21			3 [b]	0	0
22			4 [b]	0	0
23			5	0	0
24			6	0	0
25	13e	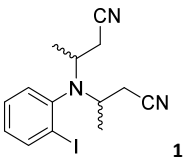 19e	1	0	0
26			2	0	0
27			3 [b]	0	0
28			4 [b]	0	0
29			5	0	0
30			6	0	0

31			**1**	0	0
32			**2**	0	0
33	**13f**	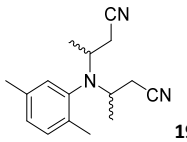 **19f**	**3** [b]	0	0
34			**4** [b]	0	0
35			**5**	0	0
36			**6**	0	0
37			**1**	0	0
38			**2**	0	0
39	**13g**	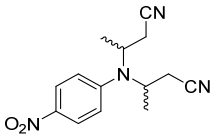 **19g**	**3** [b]	0	0
40			**4** [b]	0	0
41			**5**	0	0
42			**6**	0	0
43			**1**	0	0
44			**2**	0	0
45	**13h**	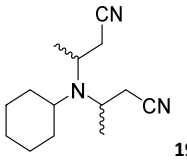 **19h**	**3** [b]	0	0
46			**4** [b]	0	0
47			**5**	0	0
48			**6**	0	0
49			**1**	0	0
50			**2**	0	0
51	**13i**	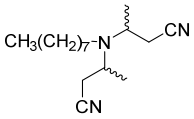 **19i**	**3** [b]	3,5 ± 0,1	1,73 ± 0,03
52			**4** [b]	0	0
53			**5**	3,52 ± 0,02	1,76 ± 0,01
54			**6**	0	0
55			**1**	0	0
56			**2**	0	0
57	**13j**	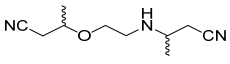 **19j**	**3** [b]	0	0
58			**4** [b]	0	0
59			**5**	0	0
60			**6**	0	0

a) TON and TOF are the average of three experiments under the same conditions. b) Results for catalysts **3** and **4** have been reported.[99]

Table A4.10 Formation of the double addition products from the hydroamination reaction of 14a catalyzed by 1 mol% of complexes **1-6** over 20 h.

Entry	Substrate	Product	Catalyst	TON[a] (Yield, %)	TOF[a] [h^{-1}]
1	13a	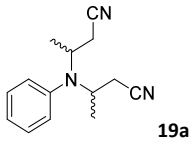 19a	1	0	0
2			2	0	0
3			3[b]	0	0
4			4[b]	0	0
5			5	0	0
6			6	0	0
7	13b	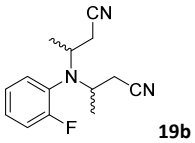 19b	1	0	0
8			2	0	0
9			3[b]	0	0
10			4[b]	0	0
11			5	0	0
12			6	0	0
13	13c	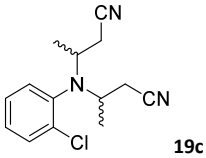 19c	1	0	0
14			2	0	0
15			3[b]	0	0
16			4[b]	0	0
17			5	0	0
18			6	0	0
19	13d	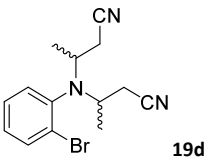 19d	1	0	0
20			2	0	0
21			3[b]	0	0
22			4[b]	0	0
23			5	0	0
24			6	0	0
25	13e	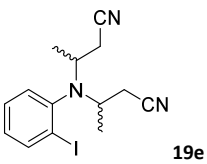 19e	1	0	0
26			2	0	0
27			3[b]	0	0
28			4[b]	0	0
29			5	0	0
30			6	0	0

31			**1**	0	0
32			**2**	0	0
33	**13f**	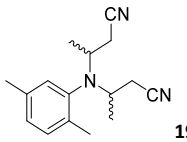 **19f**	**3** [b]	0	0
34			**4** [b]	0	0
35			**5**	0	0
36			**6**	0	0
37			**1**	0	0
38			**2**	0	0
39	**13g**	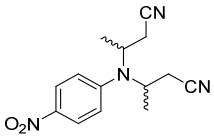 **19g**	**3** [b]	0	0
40			**4** [b]	0	0
41			**5**	0	0
42			**6**	0	0
43			**1**	0	0
44			**2**	0	0
45	**13h**	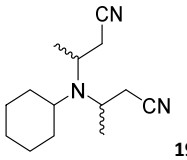 **19h**	**3** [b]	0	0
46			**4** [b]	0	0
47			**5**	0	0
48			**6**	0	0
49			**1**	0	0
50			**2**	0	0
51	**13i**	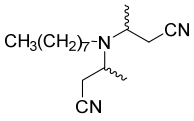 **19i**	**3** [b]	3,6 ± 0,1	0,178 ± 0,005
52			**4** [b]	0	0
53			**5**	4,7 ± 0,7	0,23 ± 0,03
54			**6**	7,8 ± 0,6	0,39 ± 0,03
55			**1**	0	0
56			**2**	0	0
57	**13j**	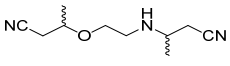 **19j**	**3** [b]	0	0
58			**4** [b]	0	0
59			**5**	0	0
60			**6**	0	0

a) TON and TOF are the average of three experiments under the same conditions. b) Results for catalysts **3** and **4** have been reported.[99]

Table A4.11 Formation of the double addition product from the hydroamination of 14b catalyzed by 1 mol% of complexes **1-6** over 2 h.

Entry	Substrate	Product	Catalyst	TON[a] (Yield, %)	TOF[a] [h^{-1}]
1	13a	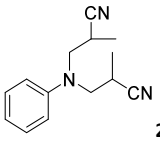 **20a**	1	11,6 ± 0,6	5,8 ± 0,3
2			2	6 ± 1	2,8 ± 0,7
3			3[b]	4,7 ± 0,8	2,3 ± 0,4
4			4[b]	0	0
5			5	2,9 ± 0,9	1,5 ± 0,4
6			6	0	0
7	13b	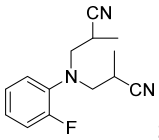 **20b**	1	0	0
8			2	0	0
9			3[b]	0	0
10			4[b]	0	0
11			5	0	0
12			6	0	0
13	13c	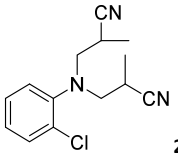 **20c**	1	0	0
14			2	0	0
15			3[b]	0	0
16			4[b]	0	0
17			5	0	0
18			6	0	0
19	13d	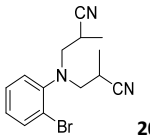 **20d**	1	0	0
20			2	0	0
21			3[b]	0	0
22			4[b]	0	0
23			5	0	0
24			6	0	0
25	13e	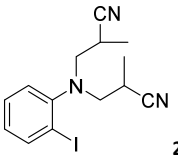 **20e**	1	0	0
26			2	0	0
27			3[b]	0	0
28			4[b]	0	0
29			5	0	0
30			6	0	0

31	**13f**	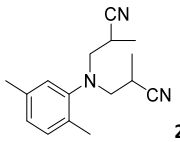 **20f**	**1**	3,2 ± 0,5	1,6 ± 0,2
32			**2**	0	0
33			**3** *b*	0	0
34			**4** *b*	0	0
35			**5**	0,5 ± 0,4	0,3 ± 0,2
36			**6**	0	0
37	**13g**	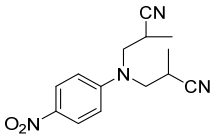 **20g**	**1**	0	0
38			**2**	0	0
39			**3** *b*	0	0
40			**4** *b*	0	0
41			**5**	0	0
42			**6**	0	0
43	**13h**	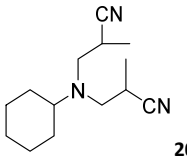 **20h**	**1**	0	0
44			**2**	0	0
45			**3** *b*	0	0
46			**4** *b*	0	0
47			**5**	0	0
48			**6**	0	0
49	**13i**	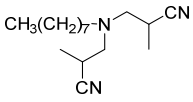 **20i**	**1**	0	0
50			**2**	0	0
51			**3** *b*	2,1 ± 0,1	1,04 ± 0,06
52			**4** *b*	0	0
53			**5**	0	0
54			**6**	0	0
55	**13j**	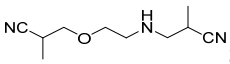 **20j**	**1**	0	0
56			**2**	0	0
57			**3** *b*	0	0
58			**4** *b*	0	0
59			**5**	0	0
60			**6**	0	0

a) TON and TOF are the average of three experiments under the same conditions. b) Results for catalysts **3** and **4** have been reported.[99]

Table A4.12 Formation of the double addition product from the hydroamination of 14b catalyzed by 1 mol% of complexes **1-6** over 20 h.

Entry	Substrate	Product	Catalyst	TON[a] (Yield, %)	TOF[a] [h^{-1}]
1	**13a**	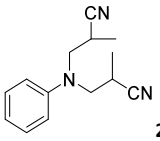 **20a**	**1**	11 ± 1	0,6 ± 0,1
2			**2**	6 ± 1	0,3 ± 0,1
3			**3** [b]	5 ± 1	0,2 ± 0,1
4			**4** [b]	0	0
5			**5**	6 ± 3	0,3 ± 0,1
6			**6**	0	0
7	**13b**	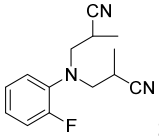 **20b**	**1**	0	0
8			**2**	0	0
9			**3** [b]	0	0
10			**4** [b]	0	0
11			**5**	0	0
12			**6**	0	0
13	**13c**	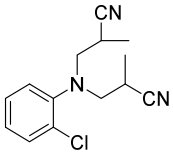 **20c**	**1**	0	0
14			**2**	0	0
15			**3** [b]	0	0
16			**4** [b]	0	0
17			**5**	0	0
18			**6**	0	0
19	**13d**	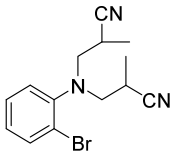 **20d**	**1**	0	0
20			**2**	0	0
21			**3** [b]	0	0
22			**4** [b]	0	0
23			**5**	0	0
24			**6**	0	0
25	**13e**	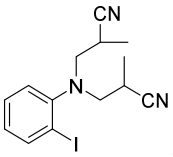 **20e**	**1**	0	0
26			**2**	0	0
27			**3** [b]	0	0
28			**4** [b]	0	0
29			**5**	0	0
30			**6**	0	0

31			**1**	8 ± 2	0,4 ± 0,1
32			**2**	0	0
33	**13f**	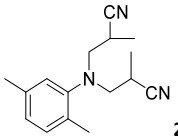 **20f**	**3** [b]	0	0
34			**4** [b]	0	0
35			**5**	0	0
36			**6**	0	0
37			**1**	0	0
38			**2**	0	0
39	**13g**	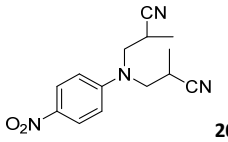 **20g**	**3** [b]	0	0
40			**4** [b]	0	0
41			**5**	0	0
42			**6**	0	0
43			**1**	0	0
44			**2**	0	0
45	**13h**	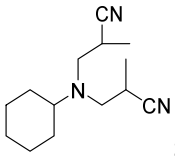 **20h**	**3** [b]	0	0
46			**4** [b]	0	0
47			**5**	0	0
48			**6**	0	0
49			**1**	0	0
50			**2**	0	0
51	**13i**	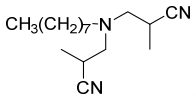 **20i**	**3** [b]	2 ± 0,2	0,101 ± 0,01
52			**4** [b]	0	0
53			**5**	0	0
54			**6**	0	0
55			**1**	0	0
56			**2**	0	0
57			**3** [b]	0	0
58	**13j**	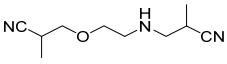 **20j**	**4** [b]	0	0
59			**5**	0	0
60			**6**	0	0

a) TON and TOF are the average of three experiments under the same conditions. b) Results for catalysts **3** and **4** have been reported.[99]

Table A4.13 Results of hydroamination in the absence and presence of catalysts for different amines, and acrylonitrile (14c), crotonitrile (14a), methacrylonitrile (14b) or cinnamonitrile (14d).

Entry	Substrate	Product	Nitrile	Time [h]	Catalyst	TON[a] (Yield, %)	TOF[a] [h^{-1}]
1	**13a**	**15a**	14c	2 (20)	**None**	0	N/A
2	**13b**	**15b**				0	N/A
3	**13c**	**15c**				0	N/A
4	**13d**	**15d**				0	N/A
5	**13e**	**15e**				0	N/A
6	**13f**	**15f**				0	N/A
7	**13g**	**15g**				0	N/A
8	**13h**	**15h**				16 % (26 %)	N/A
9	**13i**	**15i**				5% (45 %)	N/A
10	**13j**	**15j**				0	N/A
11	**13a**	**16a**	14a	2	**None**	0	N/A
12	**13b**	**16b**				0	N/A
13	**13c**	**16c**				0	N/A
14	**13d**	**16d**				0	N/A
15	**13e**	**16e**				0	N/A
16	**13f**	**16f**				0	N/A
17	**13g**	**16g**				0	N/A
18	**13h**	**16h**				0	N/A
19	**13i**	**16i**				0	N/A
20	**13j**	**16j**				0	N/A
21	**13a**	**17a**	14b	2	**None**	0	N/A
22	**13b**	**17b**				0	N/A
23	**13c**	**17c**				0	N/A
24	**13d**	**17d**				0	N/A
25	**13e**	**17e**				0	N/A
26	**13f**	**17f**				0	N/A
27	**13g**	**17g**				0	N/A
28	**13h**	**17h**				0	N/A
29	**13i**	**17i**				0	N/A
30	**13j**	**17j**				0	N/A

31	 **13k**	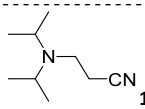 **15k**	14c	2	**None**	0	N/A
32					**3**	3,3 ± 0,8	1,6 ± 0,4
33	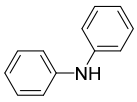 **13l**	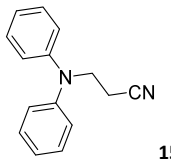 **15l**	14c	2	**None**	0	N/A
34					**1**	0	0
35					**2**	0	0
36					**4**	0	0
37	 **13m**	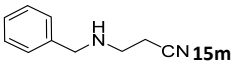 **15m**	14c	2 (20)	**None**	30 ± 1	15.5 ± 0.1
38					**3**	101.7 ± 0.6	50.9 ± 0.3
39						(99 ± 3)	(4.9 ± 0.1)
40	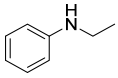 **13n**	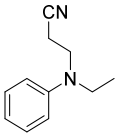 **15n**	14c	2 (20)	**None**	30 ± 5	15 ± 3
41					**3**	54 ± 1	26,8 ± 0,7
42						(71 ± 3)	(3.5 ± 0.2)
43	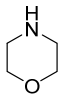 **13o**	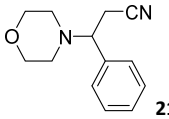 **21o**	14d	2	**None**	0	N/A
44					**4**	22 ± 1	10,9 ± 0,6

a) TOF and TON are the average of three experiments under the same conditions.

Table A4.14 Results of hydroalkoxylation 14c and 14a catalyzed by 1 mol% of complex **2** and without catalyst over 2 h for the mono-addition product.

Entry	Substrate	Product	Nitrile	Catalyst	TON[a] (Yield, %)	TOF[a] [h^{-1}]
1	 **22a**	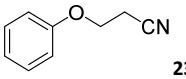 **23a**	14c	**None**	0	0
2				**2**	16,1 ± 0,8	8,0 ± 0,4
3	**22a**	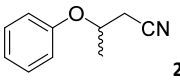 **24a**	14a	**2**	3,0 ± 0,4	1,5 ± 0,2
4	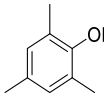 **22b**	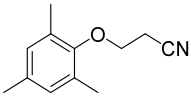 **23b**	14c	**None**	0	0
5				**2**	20 ± 4	10 ± 2
6	**22b**	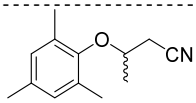 **24b**	14a	**2**	2,2 ± 0,2	1,1 ± 0,1
7	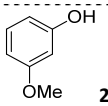 **22c**	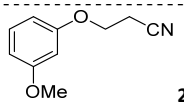 **23c**	14c	**None**	0	0
8				**2**	14,7 ± 0,8	7,3 ± 0,4
9	**22c**	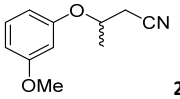 **24c**	14a	**2**	6,0 ± 0,2	3,0 ± 0,1
10	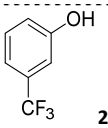 **22d**	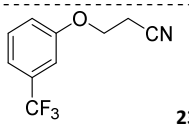 **23d**	14c	**None**	0	0
11				**2**	12,2 ± 0,7	6,1 ± 0,4
12	**22d**	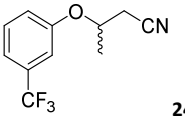 **24d**	14a	**2**	3,38 ± 0,04	1,69 ± 0,02
13	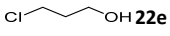 **22e**	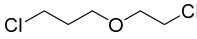 **23e**	14c	**None**	0	0
14				**2**	0	0
15	**22e**	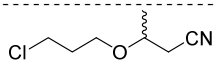 **24e**	14a	**2**	0	0

a) TOF and TON are the average of three experiments under the same conditions.

Table A4.15 Results of hydroalkoxylation 11a and 11b catalyzed by 1 mol% of complex **2** over 20 h.

Entry	Substrate	Product	Nitrile	TON[a] (Yield, %)	TOF[a] [h^{-1}]
1	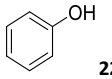 **22a**	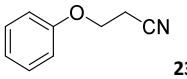 **23a**	14c	17.9 ± 0.7	0.90 ± 0.04
2	**22a**	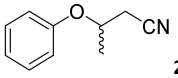 **24a**	14a	3.5 ± 0.3	0.18 ± 0.02
3	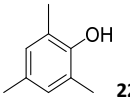 **22b**	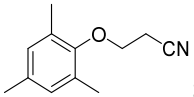 **23b**	14c	23 ± 3	1.1 ± 0.2
4	**22b**	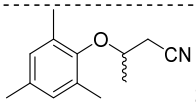 **24b**	14a	2.7 ± 0.5	0.14 ± 0.03
5	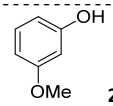 **22c**	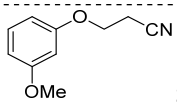 **23c**	14c	13 ± 1	0.0.16 ± 0.1
6	**22c**	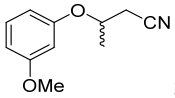 **24c**	14a	7 ± 1	0.34 ± 0.05
7	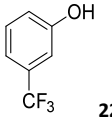 **22d**	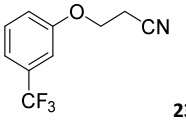 **23d**	14c	11 ± 2	0.6 ± 0.1
8	**22d**	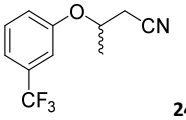 **24d**	14a	3.3 ± 0.8	0.16 ± 0.04
9	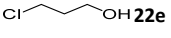 **22e**	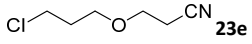 **23e**	14c	0	0
10	**122e**	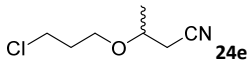 **24e**	14a	0	0

a) TOF and TON are the average of three experiments under the same conditions.

Mechanistic analyses

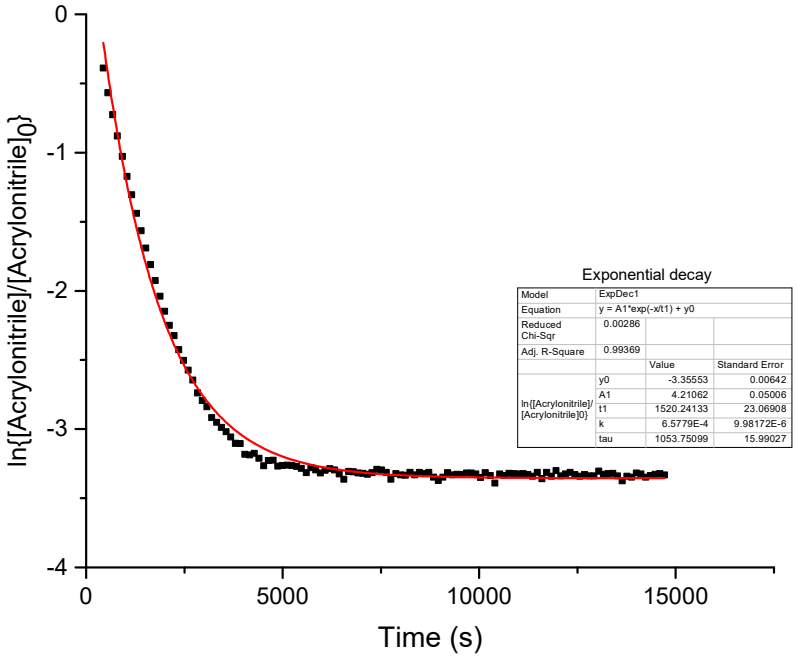

Figure A4.26 ln{[Acrylonitrile]/[Acrylonitrile]$_0$} vs. Time plot for the hydroamination of acrylonitrile catalyzed by **1** under pseudo-first order conditions**.**

An exponential decay fit was done on the data, using the equation $y = A1e^{(-x/t1)} + y0$, with the following parameters: y0 = -3.356; A1 = 4.21; t1 = 15x10^2; R^2 = 0.994. Experimental conditions: an NMR tube was charged with aniline (5 mmol), acrylonitrile (0.5 mmol), Et_3N (0.5 mmol), dodecane (internal standard, 0.3 mmol) and the appropriate catalyst (0.005 mmol) in 0.5 mL of C_6D_6 and agitated for a few seconds. Spectrums were then taken every two minutes for two hours and the concentration of acrylonitrile was determined by comparing the integration ratio of the acrylonitrile and dodecane signals to a calibration curve prepared from pure acrylonitrile samples in dodecane and C_6D_6. Linear fit of the first part of the curve did not show good agreement or R^2 factor.

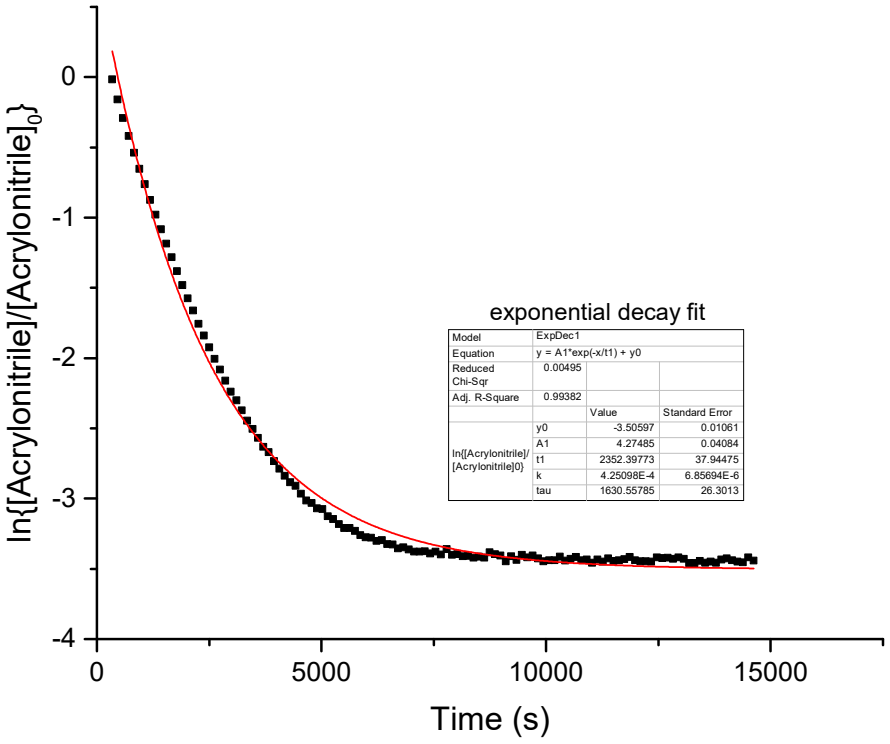

Figure A4.27 ln{[Acrylonitrile]/[Acrylonitrile]$_0$} vs. Time plot for the hydroamination of acrylonitrile catalyzed by **2** under pseudo-first order conditions.

An exponential decay fit was done on the data, using the equation $y = A1*e^{(-x/t1)} + y0$, with the following parameters: y0 = -3.51; A1 = 4.27; t1 = 24x10^2; R^2 = 0.994. See caption of **Figure A4.26** for the experimental conditions. Linear fit of the first part of the curve did not show good agreement or R^2 factor.

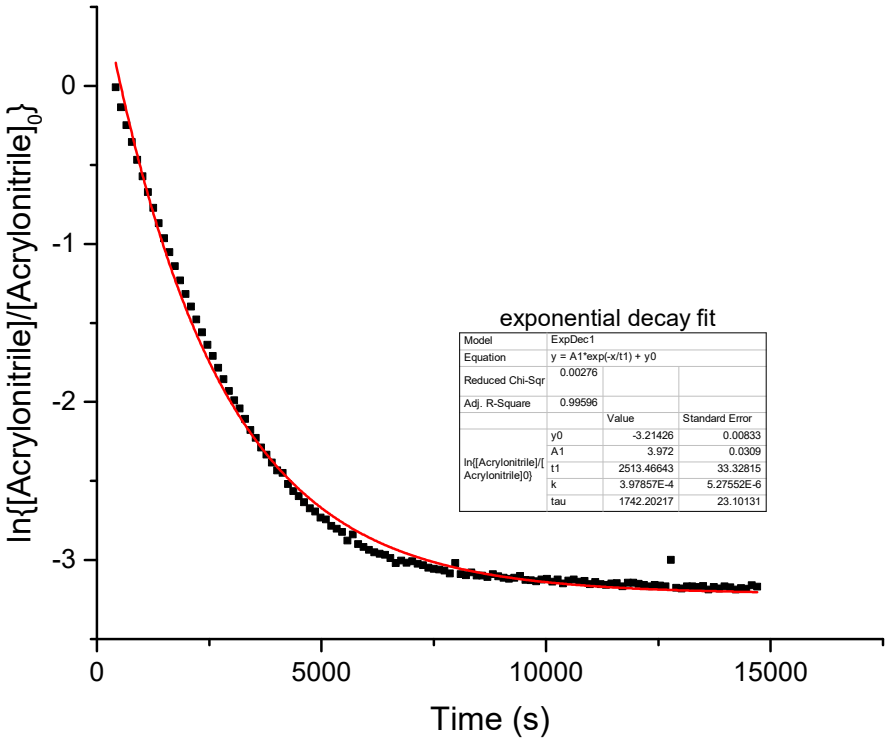

Figure A4.28 ln{[Acrylonitrile]/[Acrylonitrile]$_0$} vs. Time plot for the hydroamination of acrylonitrile catalyzed by **3** under pseudo-first order conditions**.**

An exponential decay fit was done on the data, using the equation $y = A1*e^{(-x/t1)} + y0$, with the following parameters: y0 = -3.214; A1 = 3.97; t1 = 25x10^2; R^2 = 0.996. See caption of **Figure A4.26** for the experimental conditions. Linear fit of the first part of the curve did not show good agreement or R^2 factor.

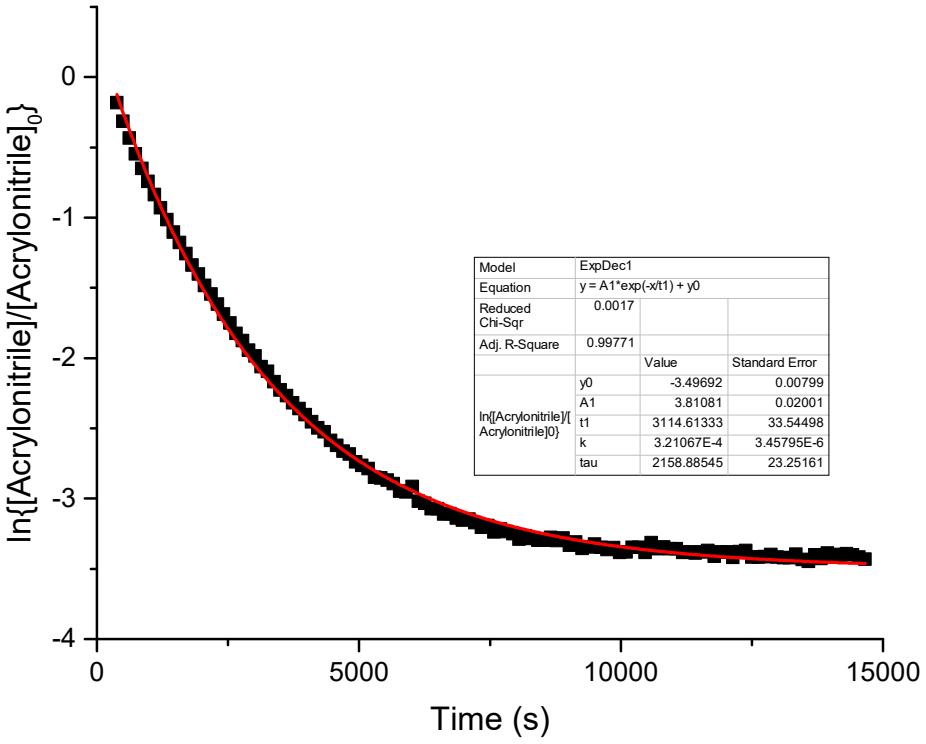

Figure A4.29 ln{[Acrylonitrile]/[Acrylonitrile]$_0$} vs. Time plot for the hydroamination of acrylonitrile catalyzed by **4** under pseudo-first order conditions**.**

An exponential decay fit was done on the data, using the equation $y = A1*e^{(-x/t1)} + y0$, with the following parameters: y0 = -3.497; A1 = 3.81; t1 = $31x10^3$; $R^2 = 0.998$. See caption of **Figure A4.26** for the experimental conditions. Linear fit of the first part of the curve did not show good agreement or R^2 factor.

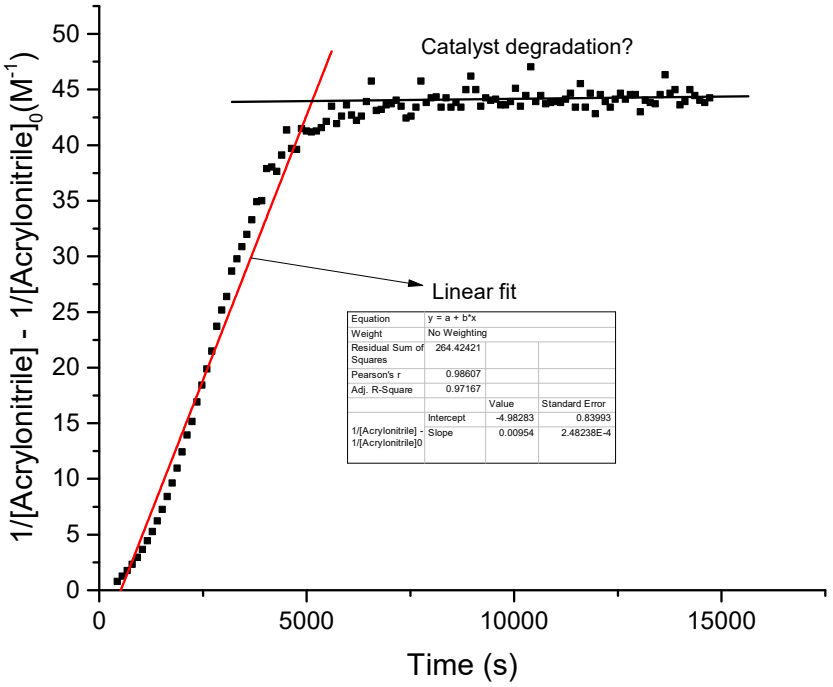

Figure A4.30 1/[Acrylonitrile] – 1/[Acrylonitrile]$_0$ vs Time plot for the hydroamination of acrylonitrile catalyzed by **1** under pseudo-first order conditions**.**

A linear fit was done on part of the data to see the possible 2nd order dependency followed by a possible contribution of the catalyst degradation which shows a plateau. The linear fit was done using the equation y = a + bx, where a = -5.0, b = 0.0095 and R^2 = 0.9717. See caption of **Figure A4.26** for the experimental conditions.

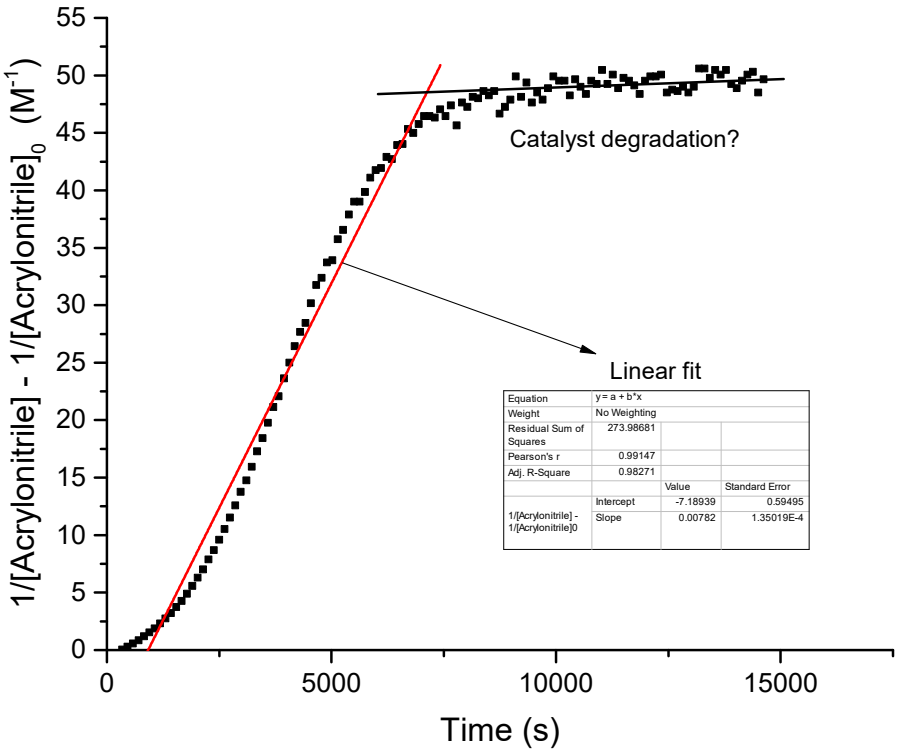

Figure A4.31 1/[Acrylonitrile] – 1/[Acrylonitrile]$_0$ vs Time plot for the hydroamination of acrylonitrile catalyzed by **2** under pseudo-first order conditions**.**

A linear fit was done on part of the data to see the possible 2nd order dependency followed by a possible contribution of the catalyst degradation which shows a plateau. The linear fit was done using the equation y = a + bx, where a = -7.2, b = 0.0078 and R^2 = 0.9827. See caption of **Figure A4.26** for the experimental conditions.

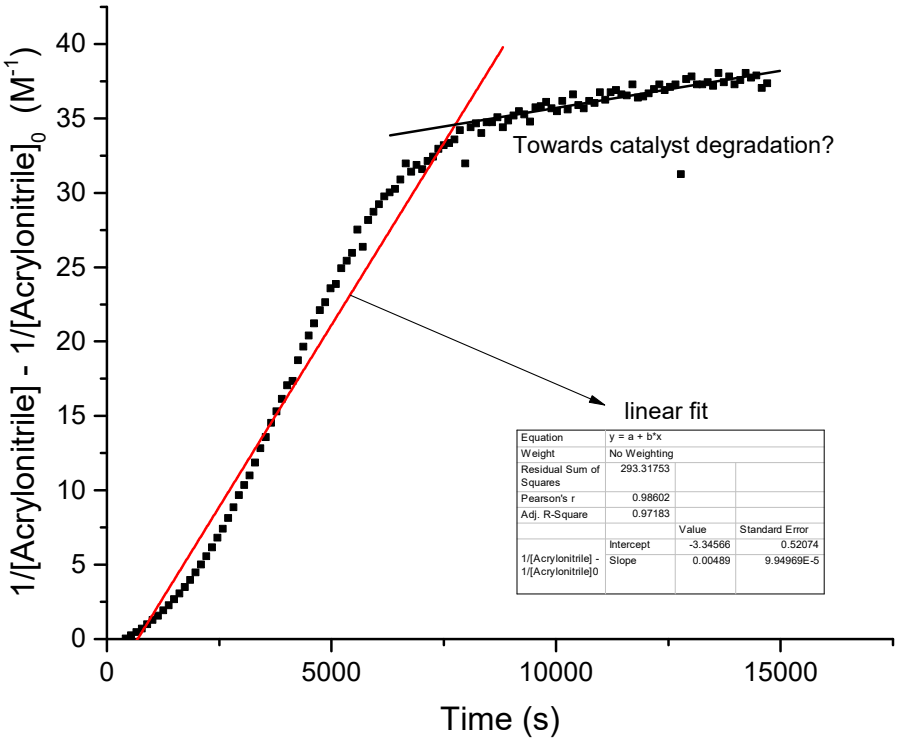

Figure A4.32 1/[Acrylonitrile] – 1/[Acrylonitrile]$_0$ vs Time plot for the hydroamination of acrylonitrile catalyzed by **3** under pseudo-first order conditions**.**

A linear fit was done on part of the data to see the possible 2nd order dependency followed by a possible contribution of the catalyst degradation which shows a plateau. The linear fit was done using the equation y = a + bx, where a = -3.3, b = 0.00489 and R^2 = 0.9718. See caption of **Figure A4.26** for the experimental conditions.

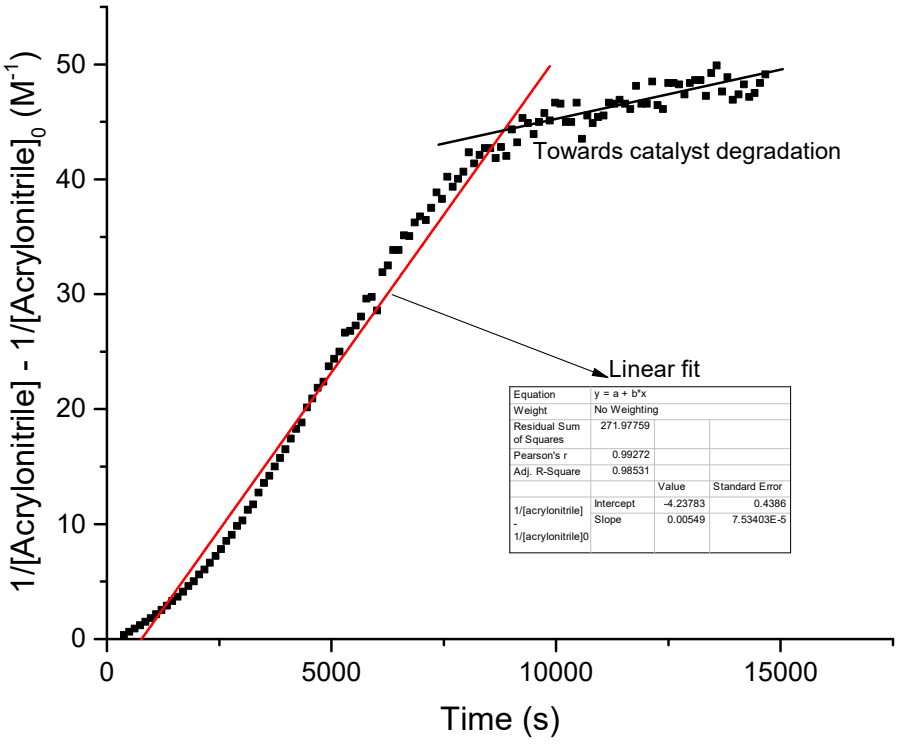

Figure A4.33 1/[Acrylonitrile] – 1/[Acrylonitrile]$_0$ vs Time plot for the hydroamination of acrylonitrile catalyzed by **2** under pseudo-first order conditions**.**

A linear fit was done on part of the data to see the possible 2nd order dependency followed by a possible contribution of the catalyst degradation which shows a plateau. The linear fit was done using the equation y = a + bx, where a = -4.2, b = 0.00549 and R^2 = 0.9853. See caption of **Figure A4.26** for the experimental conditions.

Table A4.16 Kinetic of the product inhibition of **3** by **15a**

[**3**] (M)	[**15a**] (M)	Exchange rate V_{ex} (M s^{-1})	Obsvd. rate constant, K_{obs} (s^{-1})
4,46 x 10^{-2}	4,46 x 10^{-3}	2,03 x 10^{5}	
4,40 x 10^{-2}	8,79 x 10^{-3}	4,08 x 10^{5}	
4,34 x 10^{-2}	1,30 x 10^{-2}	6,31 x 10^{5}	1.2 x 10^{8}
4,29 x 10^{-2}	1,71 x 10^{-2}	9,52 x 10^{5}	
4,23 x 10^{-2}	2,12 x 10^{-2}	1,41 x 10^{6}	
4,18 x 10^{-2}	2,51 x 10^{-2}	2,06 x 10^{6}	
4,13 x 10^{-2}	2,89 x 10^{-2}	2,95 x 10^{6}	

$4{,}08 \times 10^{-2}$	$3{,}26 \times 10^{-2}$	$3{,}98 \times 10^{6}$	
$4{,}03 \times 10^{-2}$	$3{,}63 \times 10^{-2}$	$6{,}13 \times 10^{6}$	
$3{,}98 \times 10^{-2}$	$3{,}98 \times 10^{-2}$	$8{,}18 \times 10^{6}$	
$3{,}76 \times 10^{-2}$	$5{,}64 \times 10^{-2}$	$2{,}85 \times 10^{7}$	7.9×10^{11}
$3{,}56 \times 10^{-2}$	$7{,}13 \times 10^{-2}$	$8{,}84 \times 10^{7}$	
$3{,}22 \times 10^{-2}$	$9{,}67 \times 10^{-2}$	$2{,}17 \times 10^{8}$	
$2{,}71 \times 10^{-2}$	$1{,}35 \times 10^{-1}$	$1{,}33 \times 10^{9}$	
$1{,}93 \times 10^{-2}$	$1{,}93 \times 10^{-1}$	$1{,}45 \times 10^{9}$	

Table A4.17 Kinetic of the product inhibition of **4** by **15a**

[**4**] (M)	[**15a**] (M)	Exchange rate, V_{ex} ($M\ s^{-1}$)	Obsvd. Rate constant K_{obs} (s^{-1})
$4{,}06 \times 10^{-2}$	$4{,}06 \times 10^{-3}$	$5{,}32 \times 10^{5}$	
$4{,}01 \times 10^{-2}$	$8{,}01 \times 10^{-3}$	$9{,}40 \times 10^{5}$	1.0×10^{8}
$3{,}96 \times 10^{-2}$	$1{,}19 \times 10^{-2}$	$1{,}51 \times 10^{6}$	
$3{,}91 \times 10^{-2}$	$1{,}56 \times 10^{-2}$	$1{,}88 \times 10^{6}$	
$3{,}86 \times 10^{-2}$	$1{,}93 \times 10^{-2}$	$3{,}10 \times 10^{6}$	
$3{,}81 \times 10^{-2}$	$2{,}29 \times 10^{-2}$	$4{,}50 \times 10^{6}$	
$3{,}76 \times 10^{-2}$	$2{,}63 \times 10^{-2}$	$6{,}53 \times 10^{6}$	3.2×10^{10}
$3{,}72 \times 10^{-2}$	$2{,}97 \times 10^{-2}$	$8{,}83 \times 10^{6}$	
$3{,}67 \times 10^{-2}$	$3{,}31 \times 10^{-2}$	$1{,}07 \times 10^{7}$	
$3{,}63 \times 10^{-2}$	$3{,}63 \times 10^{-2}$	$2{,}03 \times 10^{7}$	
$3{,}25 \times 10^{-2}$	$6{,}49 \times 10^{-2}$	$3{,}59 \times 10^{7}$	
$2{,}94 \times 10^{-2}$	$8{,}81 \times 10^{-2}$	$5{,}97 \times 10^{7}$	1.0×10^{9}
$2{,}47 \times 10^{-2}$	$1{,}23 \times 10^{-1}$	$1{,}06 \times 10^{8}$	
$1{,}76 \times 10^{-2}$	$1{,}76 \times 10^{-1}$	$1{,}16 \times 10^{8}$	

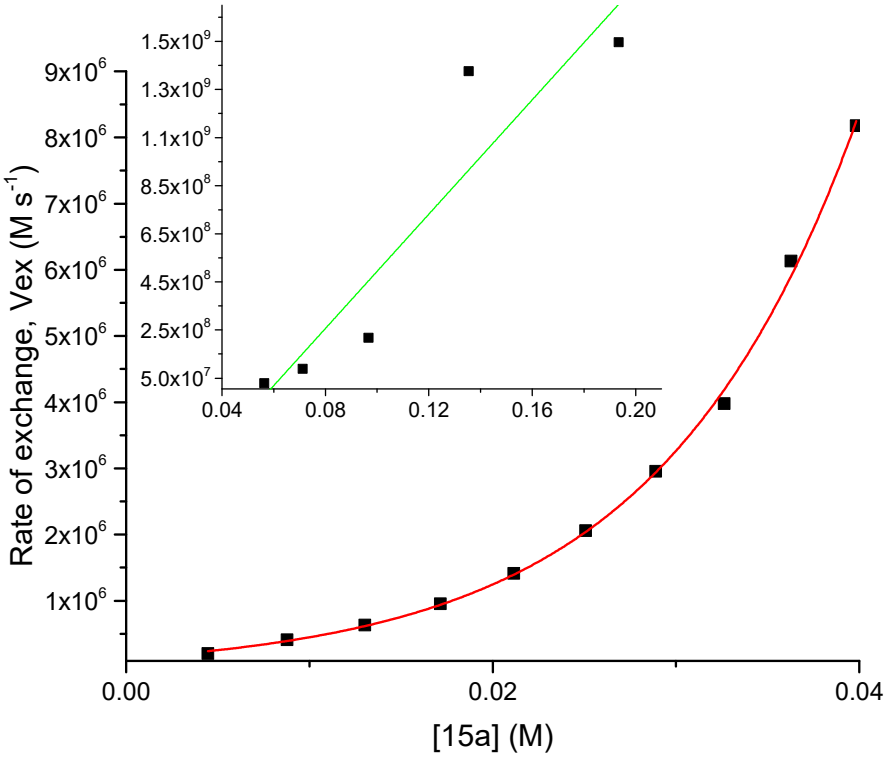

Figure A4.34 Variation of the rate of exchange (V_{ex}) vs. concentration of 15a with catalyst **3.**

The exchange rate constant (K_{ex}) was determined by ^{31}P NMR lineshape analysis of samples containing increasing amounts (0.1 to 10 equivs.) of the pure mono-addition product (3-anilinopropionitrile, **15a**) in C_6D_6 at 298 K. An exponential growth function was fitted to the data (red line), with the formula $y = y0 + A1*\exp^{(x/t1)}$, where $y0 = -8x10^5$; $A1 = 2.0x10^6$; $t1 = 0.0108$; $R^2 = 0.9979$. A linear fit was applied at [**15a**] > 0.04 M (green line) with the formula $y = 1.2x10^{10}\ x - 7x10^8$ ($R^2 = 0.8259$). K_{ex} was determined experimentally for each concentration by applying formula (1) found in the text. Experimental conditions: To a NMR tube containing a 0.041 M solution of catalyst **3** in C_6D_6 was added increasing amounts (from 0.1 to 10 equivs.) of the pure mono-addition product (**15a**, 3-anilinopropionitrile), which was followed by a thorough agitation between each addition and a ^{31}P NMR spectra was taken after each addition.

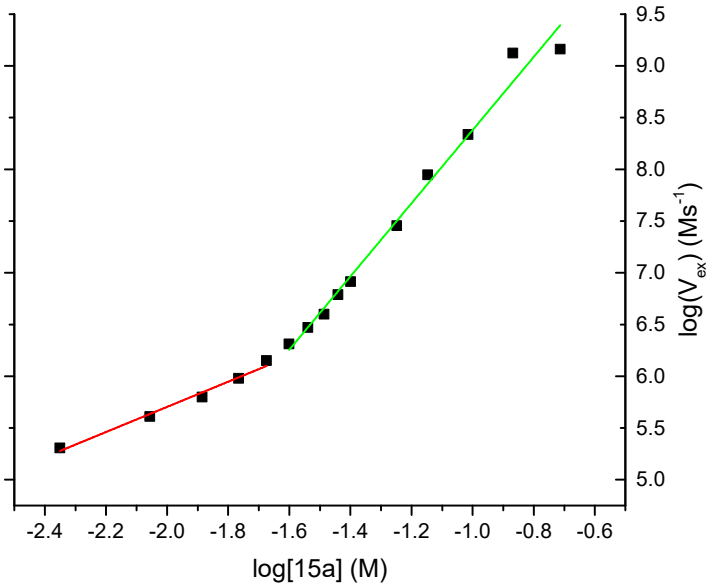

Figure A4.35 Plot of the logarithm of the reaction rate (V_{ex}) vs the logarithm for the concentration of **15a** with catalyst **3.**

Two linear regressions were performed on the data to fit the equation $\log(V_{ex}) = \log(K_{obs}) + m \log[\mathbf{15a}]$. The first, at low concentrations of **15a** (green line, [**15a**] < 2.12 x 10^{-2} M), has the formula y = 1.22x + 8.1 (R^2 =0.9816). The second, at medium to high concentrations of **15a** (red line, [**15a**] > 2.51 x 10^{-2} M), has the formula y = 3.5x + 11.9 (R^2 = 0.9836). See **Figure A4.34** for more details and experimental conditions

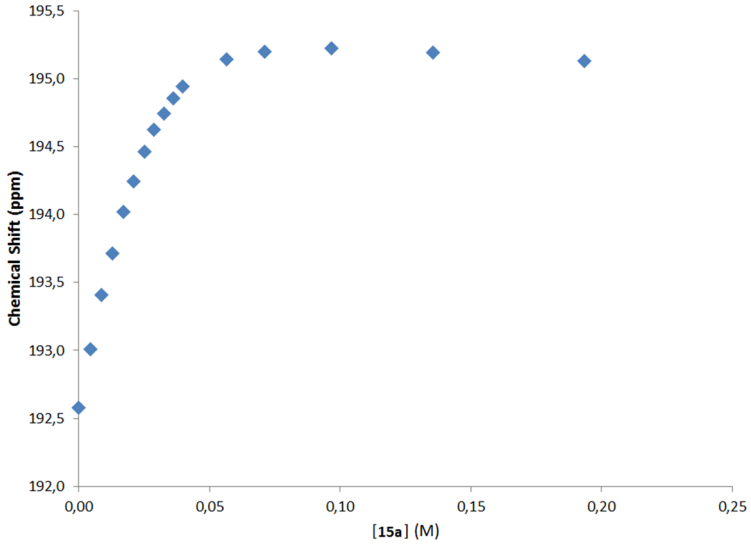

Figure A4.36 ^{31}P NMR titration curve of complex **3** with **15a** (161 MHz, C_6D_6, 298 K).

See caption of **Figure A4.34** for experimental conditions

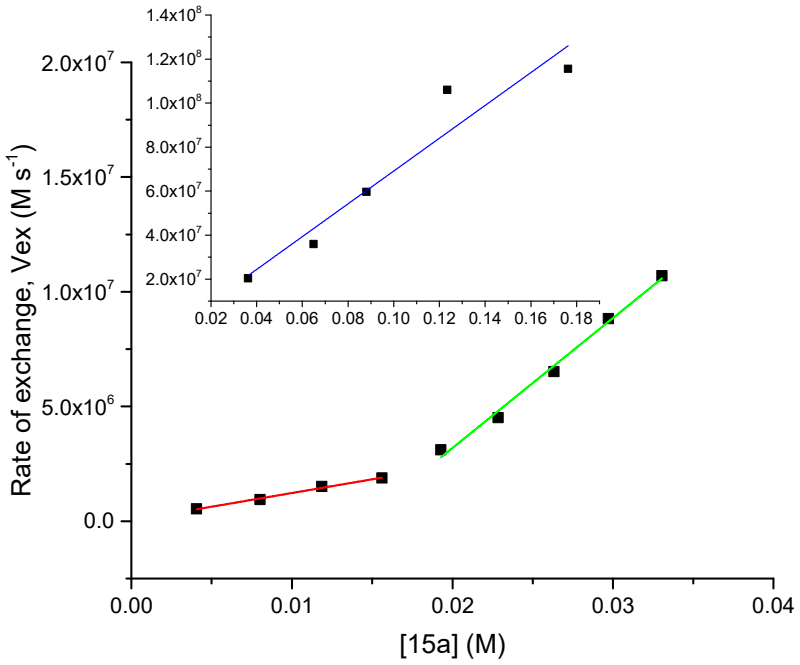

Figure A4.37 Variation of the rate of exchange (V_{ex}) vs. concentration of **15a** with catalyst **4.**

The exchange rate constant (K_{ex}) was determined by ^{31}P NMR lineshape analysis of samples containing increasing amounts (0.1 to 10 equivs.) of the pure mono-addition product (3-anilinopropionitrile, **15a**) in C_6D_6 at 298 K. Three linear fits were done on the data. The first, for the data between 0 and ~ 0.015 M (red line), has the formula $y = 1.19x10^8x + 3x10^5$ ($R^2 = 0.9906$). The second fit was done on the data between ~0.02M and ~0.035M (green line) with the formula $y = 5.7x10^8x - 8x10^6$ ($R^2 = 0.9900$). The third, for the data > 0.035M, has the formula $y = 7.5x10^8 x - 5x10^6$ ($R^2 = 0.8986$). K_{ex} was determined experimentally for each concentration by applying formula (1) found in the text. Experimental conditions: To a NMR tube containing a 0.043 M solution of catalyst **4** in C_6D_6 was added increasing amounts (from 0.1 to 10 equivs.) of the pure mono-addition product (**15a**, 3-anilinopropionitrile), which was followed by a thorough agitation between each addition and a ^{31}P NMR spectra was taken after each addition

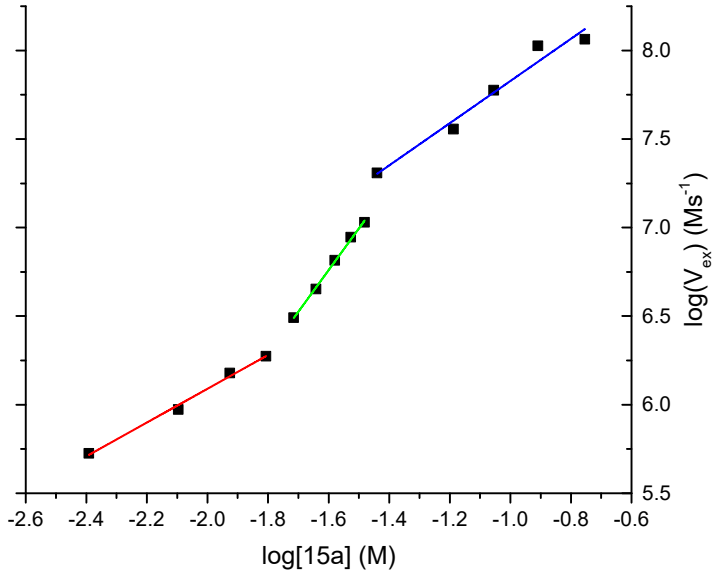

Figure A4.38 Plot of the logarithm of the reaction rate (V_{ex}) vs the logarithm for the concentration of **15a** with catalyst **4.**

Three linear regressions were performed on the data to fit the equation $\log(V_{ex}) = \log(K_{obs}) + m \log[\mathbf{15a}]$. The first, at low concentrations of **15a** (red line), has the formula y = 0.95x + 8.0 (R^2 =0.9912). The second, at medium concentrations of **15a** (green line), has the formula y = 2.35x + 10.5 (R^2 = 0.9969). The third, at high concentrations of **15a** (blue line) has the formula y = 1.2x + 9.0 (R^2 = 0.9546). See **Figure A4.37** for more details and experimental conditions

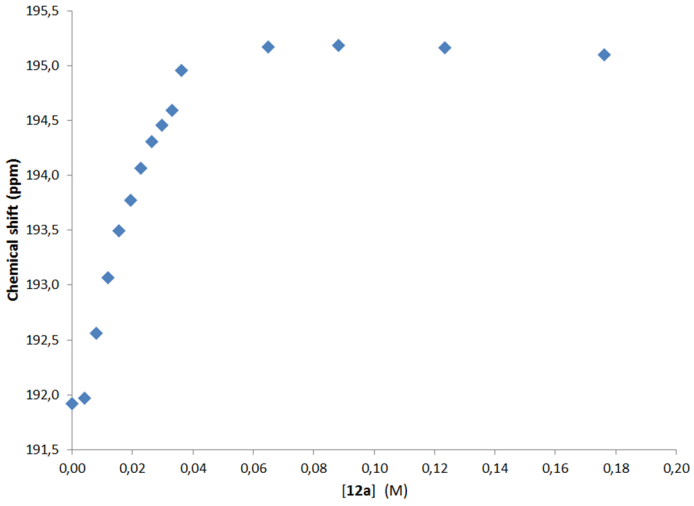

Figure A4.39 ^{31}P NMR titration curve of complex **4** with **15a** (161 MHz, C_6D_6, 298 K**).**

See caption of **Figure A4.37** for experimental conditions.

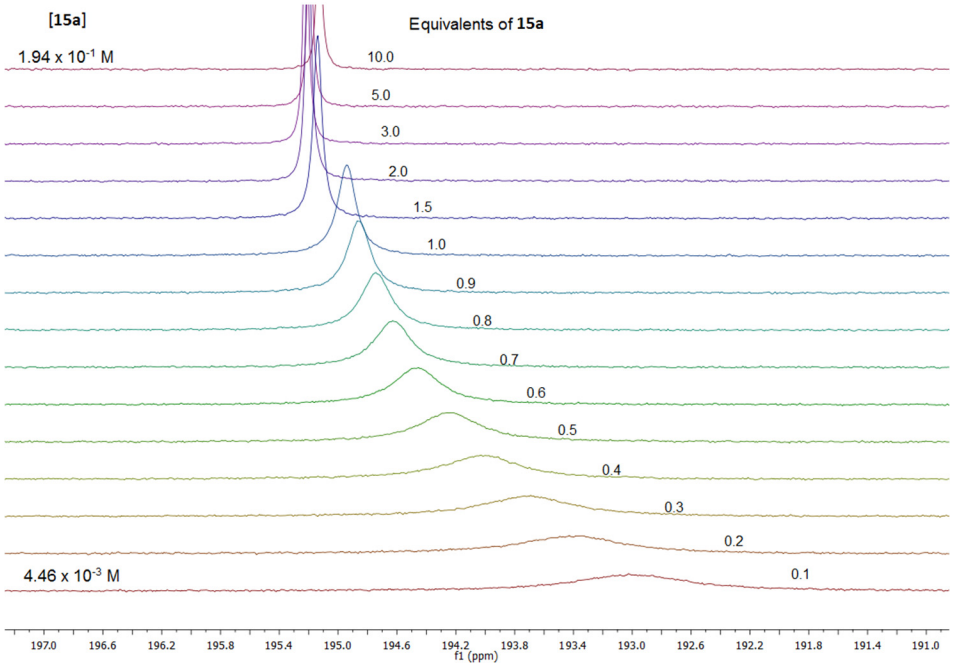

Figure A4.40 Stacked ^{31}P NMR spectra showing the change in both chemical shift and $LW_{1/2}$ with the addition of **15a** in the presence of **4.**

See caption of **Figure A4.37** for experimental conditions.

Table A4.18 Kinetic of the product inhibition of 4 by 15h

[**4**] (M)	[**15h**] (M)	Exchange rate, V_{ex} (s^{-1})	Obsvd. Rate constant K_{obs} (s^{-1})
4.01×10^{-2}	4.01×10^{-3}	4.29×10^{5}	3.09×10^{8}
3.91×10^{-2}	7.81×10^{-3}	8.75×10^{5}	
3.81×10^{-2}	1.14×10^{-2}	1.46×10^{6}	
3.72×10^{-2}	1.49×10^{-2}	2.21×10^{6}	
3.55×10^{-2}	2.13×10^{-2}	3.27×10^{6}	
3.47×10^{-2}	2.43×10^{-2}	3.72×10^{6}	
3.39×10^{-2}	2.71×10^{-2}	4.06×10^{6}	
3.32×10^{-2}	2.99×10^{-2}	4.51×10^{6}	
3.25×10^{-2}	3.25×10^{-2}	4.98×10^{6}	
2.94×10^{-2}	5.88×10^{-2}	6.63×10^{6}	8.51×10^{6}
2.68×10^{-2}	8.05×10^{-2}	6.68×10^{6}	
2.29×10^{-2}	1.14×10^{-1}	7.19×10^{6}	
1.76×10^{-2}	1.76×10^{-1}	7.27×10^{6}	

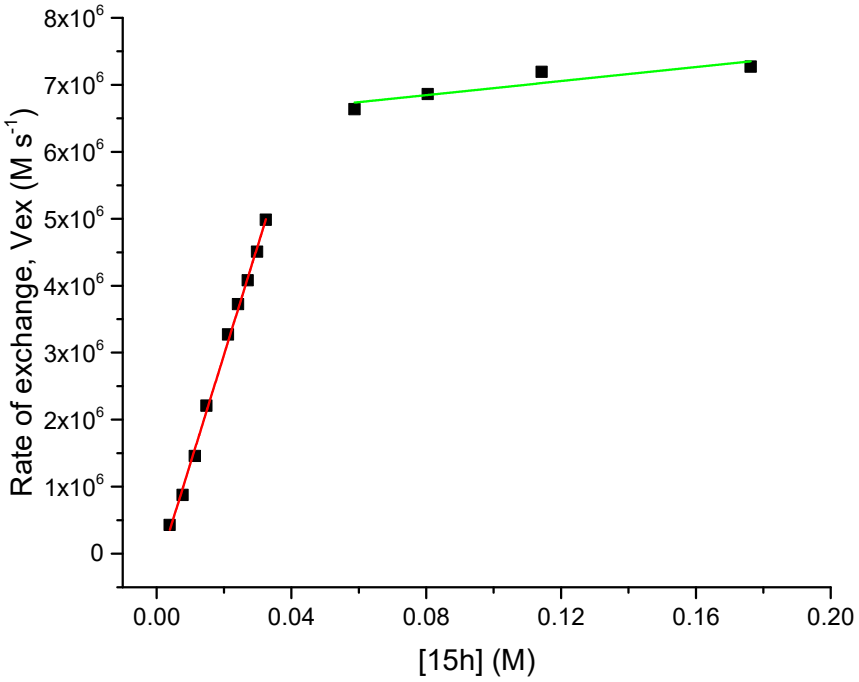

Figure A4.41 Variation of the rate of exchange (V_{ex}) vs. concentration of **15h** with catalyst **4.**

The exchange rate constant (K_{ex}) was determined by ^{31}P NMR lineshape analysis of samples containing increasing amounts (0.1 to 10 equivs.) of the pure mono-addition product (**15h**, (3-cyclohexylamino)propanenitrile) in C_6D_6 at 298 K. A one-phase exponential growth function with time constant parameter fit was used for the principal plot ([**15h**] between 0.004 and 0.18 M) with the equation $y = A1*e^{(-x/t1)} + y0$ and with the following parameters: y0 = 7.4E6; A1 =-8.5E6; t1 =-0.029; R^2 =0.9918. It is also possible to fit the data with two linear regressions. The first linear regression (blue line) for the region of 0.004 M < [**15h**] < 0.04 M has the formula y = 1.63E8x -3E6 (R^2 = 0.9971). The second linear regression was applied to the region 0.04 M > [**15h**] < 0.2 M with the formula y = 5.3E6 + 6E6 (R^2 = 0.7443). K_{ex} was determined experimentally for each concentration by applying formula (1) found in the text. Experimental conditions: To a NMR tube containing a 0.043 M solution of catalyst **4** in C_6D_6 was added increasing amounts (from 0.1 to 10 equivs.) of the pure mono-addition product (**15h**, (3-cyclohexylamino)propanenitrile), which was followed by a thorough agitation between each addition and a ^{31}P NMR spectra was taken after each addition

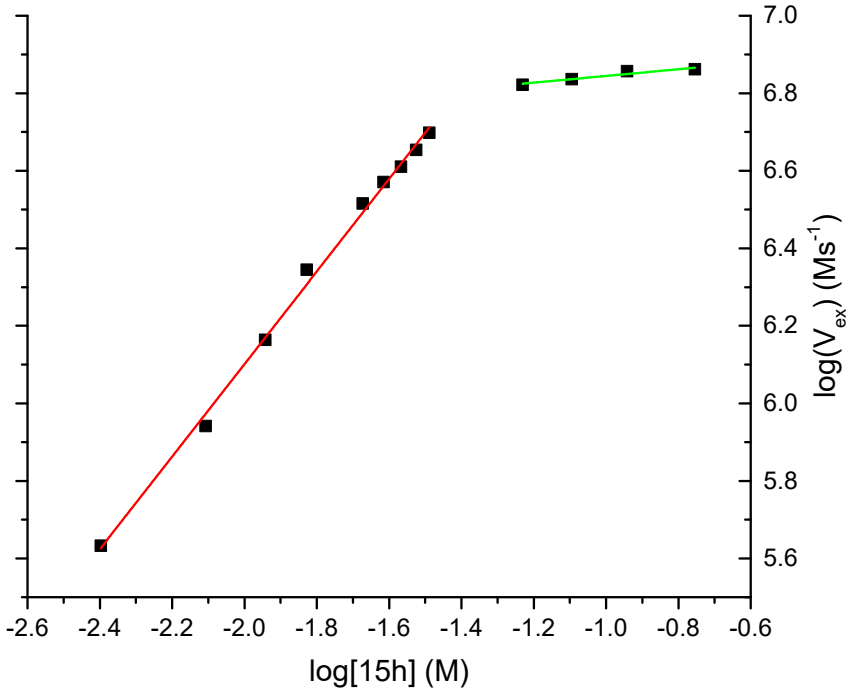

Figure A4.42 Plot of the logarithm of the reaction rate, V_{ex}, vs the logarithm for the concentration of **15h** with catalyst **4.**

Two linear regressions were performed on the data to fit the equation $\log(V_{ex}) = \log(K_{obs}) + m \log[\mathbf{15h}]$. The first, at low concentrations of **15h** (red line), has the formula y = 1.19 x + 8.49 (R^2 =0.9962). The second, at medium to high concentrations of **15h** (green line), has the formula y = 0.09x + 6.93 (R^2 =0.8827). See **Figure A4.41** for more details and experimental conditions

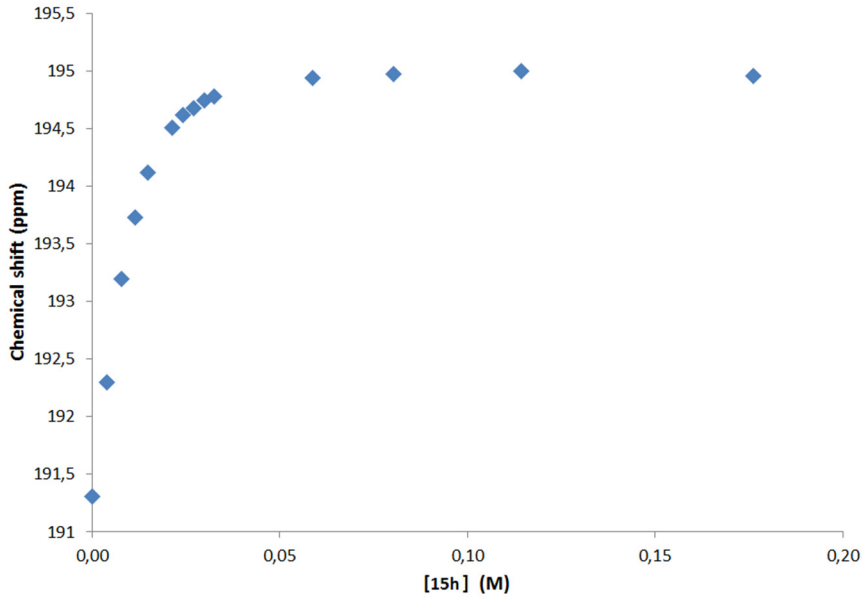

Figure A4.43 ^{31}P NMR Titration curve of complex **4** with **15h** (161 MHz, C_6D_6, 298 K).

See caption of **Figure A4.41** for experimental conditions.

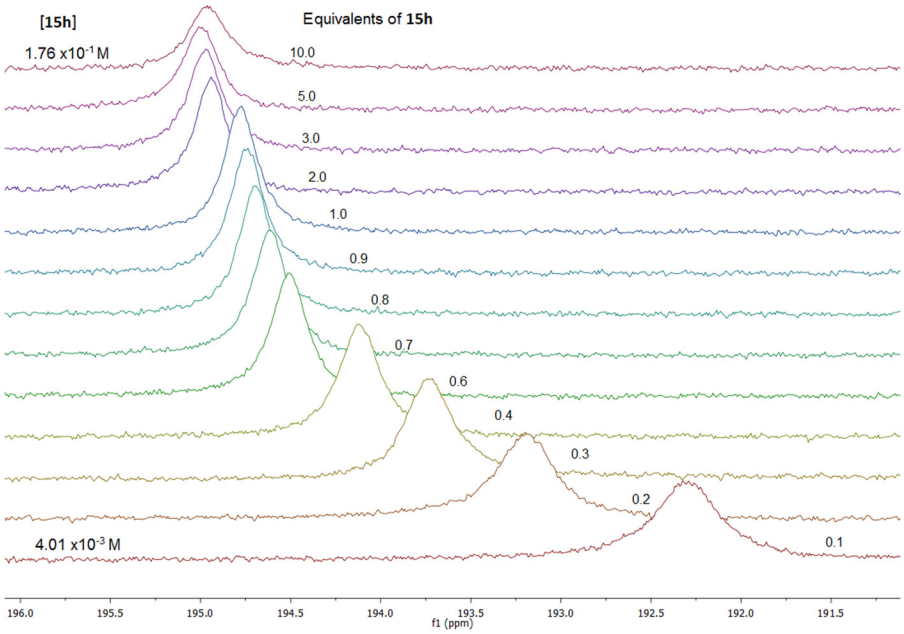

Figure A4.44 Stacked ^{31}P NMR spectra showing the change in both chemical shift and $LW_{1/2}$ with the addition of **15h** in the presence of **4.**

See caption of **Figure A4.41** for experimental conditions